# Thermal Performance of Unloaded Spiral Strand and Locked-Coil Cables for Bridge Infrastructure

Benjamin Nicoletta

A thesis submitted to the Faculty of Graduate Studies in partial fulfillment of the degree requirements for the degree of Master of Applied Science

Graduate Program in Civil Engineering, York University

Toronto, Ontario

August 2020

# ABSTRACT

This thesis presents significant context to the topic of bridge fire safety engineering and contributes experimental work on the thermal performance of steel stay-cables for bridge infrastructure. The goal of this work is to ultimately develop the fire resilience of critical infrastructure like bridges, as currently there are no contemporary code requirements for the fire resistance of bridge infrastructure, nor is there significant guidance available for practitioners who wish to design bridges or cable-supported structures for the fire load case. The thesis is divided into, first, an introduction to the practice of structural fire engineering which presents fundamental information on how materials are affected by fires, how fires are considered in structural engineering applications, and how the methodology of fire safety engineering is undertaken in contemporary standards. Next, a literature review of bridge fire research provides a comprehensive summary of the state of bridge fire safety research in terms of the assessment of fire risks and hazards, the modelling of bridge fire scenarios, and the thermo-structural response of steel, composite steel-concrete, concrete, cable-supported, and polymer-reinforced bridges. The deficiencies of bridge fire safety engineering explicitly affect cable-supported bridges which have been seldom tested experimentally for fire scenarios. A study examining the use of pool fire exposure to fire test structural members is presented in the context of glass-fibre reinforced polymer stay-in-place formwork which found a deterioration in GFRP-concrete bond with increasing temperature. This thesis then applies this pool fire exposure methodology and further seeks to develop an understanding of the thermal response of steel stay-cables under exposure to a non-standard fire. Herein, multiple varieties of stay-cable are instrumented with thermocouples and heated by a methanol pool fire. Novel imaging techniques observe the cables' surface during heating and cooling and enable the calculation of thermal strains and deformations. Results indicate a diminished occurrence of extreme temperature development with increasing cable diameter, a normalization of cross-sectional temperatures outside of the localized heating region for all cables, and multiple deformational behaviours attributed to cable uncoiling, thermal bowing, and rotational wire effects. The Eurocode thermal strain equations are useful in approximating the thermal elongation of the cable members in some cases. Additionally, the role of lubricating blocking agents in the fire performance of cable members has been shown to render current fire protection guidance for cable members unconservative. Further discussion towards the application of the experimental results is presented in this thesis, as well as topics to be considered for future research.

# ACKNOWLEDGMENTS

My warmest thanks are extended primarily to my supervisor Professor John Gales whose support and encouragement throughout this project and earlier made this journey never feel like a job. Additionally, the mentorship provided by Joshua Woods, Matthew Smith, and Panos Kotsovinos is immensely appreciated and served to motivate and refine my research. The accommodation and assistance provided by Professor Weckman and her team at the University of Waterloo throughout this and other research programs is thanked greatly. The diligent feedback provided by my examination committee, including Professor Khan, Professor Tomlinson, and Professor Pantazopoulou, is further acknowledged. I am thankful for the enjoyable laboratory experiences and discussions with Riad Rajab as well as the other members of the research team, including Bronwyn, Chloe, Georgette, Tim, Danielle, Ginelle, Julia, and Ariel, never once produced a dull moment. The exceptional and caring work conducted by Sindy Mahal to benefit York University students such as myself is admirable  Finally, my parents, friends, family, and Jenny are thanked beyond expression for their kindness, support, and love throughout this process. The Natural Sciences and Engineering Research Council of Canada and the government of Ontario are acknowledged for their financial support. ARUP Fire is also acknowledged for their in-kind and monetary support towards this project.

# DECLARATION

The chapters of this thesis have been modified from existing publications written by the author but were influenced by several colleagues. For all cases pertaining to these publications, the author has conducted the experimental and analytical research, as well as drafted the majority of the documents. Input from colleagues has contributed to the overall development of conclusions and the higher-level of focus of the studies. Publications that do not fit this criterion are cited as secondary sources.

Chapter 3 is based on:

Nicoletta, B., Kotsovinos, P., and Gales, J. 2020a. Review of the Fire Risk, Hazard, and Thermomechanical Response of Bridges in Fire. Canadian Journal of Civil Engineering, 47(4), 363-381. DOI: 10.1139/cjce-2018-0767.

Nicoletta, B., Smith, M., and Gales, J. 2018. Toward Fire Resilience in Canadian Bridge Infrastructure. CSCE Conference for Short and Medium Span Bridges, Quebec City, Que., Canada.

Chapter 4 is based on:

Nicoletta, B., Woods, J., Gales, J., and Fam, A. 2019a Postfire Performance of GFRP Stay-in-Place Formwork for Concrete Bridge Decks. J. Compos. for Constr., 23(3), DOI: 10.1061/(ASCE)CC.1943-5614.0000941.

Chapter 5 is partially based on:

Nicoletta, B., P. Kotsovinos, and J. Gales. 2019b. Experimental thermal Performance of structural steel stay-cables in fire: Preliminary progress. 15th Interflam. Egham, UK: Royal Holloway College.

Nicoletta, B., Gales, J., Kotsovinos, P. 2020b. The York-Arup Cable Experiments: Implications for the Fire Design of Cable-supported Bridges. IABSE 2020 Conference. New Zealand. 6pp.

Nicoletta, B., Gales, J., Kotsovinos, P. 2020c. Experimental Fire Performance of Unloaded stay-cables for Bridge Infrastructure. IABSE 2020 Conference. New Zealand. 6pp.

and was modified and submitted to the Structural Engineering International journal in August 2020 under:

Nicoletta, B., Gales, J., Kotsovinos, P. 2020. Experimental Thermal Performance of Unloaded Steel Stay-Cables for Bridge Infrastructure Subject to Pool Fires. Structural Engineering International. Submitted (Manuscript No. X2526.20.08).

# TABLE OF CONTENTS

# LIST OF TABLES

# LIST OF FIGURES

# NOTATION

$A_f$ = pool fire pan area available for burning ($m^2$)

$A_t$ = total area of enclosure ($m^2$)

$A_v$ = total area of vertical openings ($m^2$)

$b$ = thermal absorptivity for the total fire enclosure ($Ws^{1/2}$ / mK)

$c$ = material heat capacity (J/K)

$D_{f,\,\mathrm{eff}}$ = effective fire diameter of a rectangular pool fire pan (m)

$h$ = coefficient of convective heat transfer ($W/m^2K$)

$h$ = height above pool fire pan base (mm)

$h_{eq}$ = weight average window height (m)

$k$ = pool fire extinction coefficient ($m^{-1}$)

$L_f$ = longest dimension of a rectangular pool fire pan (m)

$\dot{m}''$ = mass burning rate per unit area ($kg/m^2s$)

$\dot{m}''_{\infty}$ = theoretical maximum mass burning rate per unit area ($kg/m^2s$)

$O$ = open factor of the fire compartment

$\dot{q}''_{conduction}$ = conductive heat flux ($W/m^2$)

$\dot{q}''_{convection}$ = convective heat flux ($W/m^2$)

$\dot{Q}_{f,\,max}$ = theoretical maximum heat release rate (kW)

$\dot{q}''_{radiation}$ = radiative heat flux ($W/m^2$)

$T$ = temperature of the radiative surface (K)

$t$ = time (minutes)

$t^*$ = time adjusted for parametric fire determination (minutes)

$W_f$ = shortest dimension of a rectangular pool fire pan (m)

$x$ = refers to the horizontal coordinate used in digital image correlation (positive is taken as to the right relative to the camera)

$x_{1,0}$ = the horizontal coordinate of the first point of interest in digital image correlation analyses for the reference photo number (px)

$x_{1,i}$ = the horizontal coordinate of the first point of interest in digital image correlation analyses for photo number *i* (px)

$x_{2,0}$ = the horizontal coordinate of the second point of interest in digital image correlation analyses for the reference photo number (px)

$x_{2,i}$ = the horizontal coordinate of the second point of interest in digital image correlation analyses for photo number *i* (px)

$y$ = refers to the vertical coordinate used in digital image correlation (positive is taken as down relative to the camera)

$\beta$ = pool fire mean beam length corrector (unitless)

$\Gamma$ = parametric fire time factor function of the opening parameter, $O$, and a given thermal absorptivity, $b$ (unitless)

$\Delta Hc$ = heat of combustion (kJ/kg)

$\varepsilon$ = emissivity (unitless)

$\varepsilon_{x,i}$ = the longitudinal strain calculation at photo number *i* (unitless)

$\varepsilon_{th}$ = thermal strain (unitless)

$\varepsilon_{slip}$ = strain discontinuity from loss of composite action between concrete and GFRP

$\theta$ = steel temperature for calculating thermal strains (°C)

$\theta_g$ = fire gas temperature (°C)

$\lambda$ = thermal conductivity (W/mK)

$\rho$ = material density (kg/m$^3$)

$\sigma$ = Stefan-Boltzmann constant taken as 5.67 x 10$^{-8}$ W/m$^2$K$^4$

$\varphi$ = radiation view factor (unitless)

# Chapter 1: Introduction

## 1.1 Introduction

Bridges are critical infrastructure and vital to the communities they serve. Bridges are also robust structures and are designed for a wide variety of loading conditions including snow, wind, earthquake, flooding, and even ship impacts. Yet, bridges are rarely, if ever, designed against the fire load case which can arguably introduce more severe loading conditions than the scenarios listed above. It is well-cited in the literature and apparent in bridge design standards such as the CAN/CSA-S6-14, AASHTO LRFD Bridge Design Specifications, and Eurocode 1 Part 1-2 and Part 2 that there are no enforced fire endurance requirements in contemporary bridge design (Kodur et al. 2010, Garlock et al. 2012 , CSA 2014a, AASHTO 2015, CEN 2002, CEN 2003). The only guidance provided by a national standard is the National Fire Protection Association (NFPA) Standard 502 which specifies a high-level method to select design fires for highway bridges over 300 metres in length (NFPA 2014) but does not provide procedures to perform a comprehensive analysis and design. Woodworth (2013) corroborates this lack of bridge fire guidance through bridge collapse survey data from the New York Department of Transportation (NYDOT) which indicated fires are responsible for more bridge collapses than earthquakes. Ultimately, the lack of fire resistance requirements for bridge structures means most types of bridges are either inherently vulnerable to fire exposure or have an unquantified thermal response.

Bridge fires are uncommon events often resulting from vehicle collisions beneath overpasses and, as such, it is expected that the occurrence of these events will become more frequent with increasing urbanization (Garlock et al. 2012). Other recent bridge fire events have also involved ruptured natural gas lines, arson, construction material fires, and electrical fires. Garlock et al. (2012) recount major bridge fire events from 1995-2009 while Kotsovinos et al. (2020a) recount specific fire events that have affected cable-supported bridges; Table 1.1 summarizes these bridge fire events and presents more events not originally included.

Table 1.1. Recent bridge fire events (supplemented from Garlock et al. 2012 and Kotsovinos et al. 2020a).

| Bridge/Location | Date | Cause of Fire | Bridge Material | Damage Extent |
|---|---|---|---|---|
| Ladner Creek Trestle Bridge | May 27th 2018 | Ignition from a lit cigarette | Timber trestle | Minor structural damage: flaming debris ignited a bushfire below the bridge |
| I-85 Overpass, Georgia | March 30th 2017 | Ignition of stored construction materials | Steel girders with concrete deck | Collapse of a 28 m span |
| CN Trestle Bridge, Alberta | April 26th 2016 | Arson | Timber trestle | Complete collapse of the rail bridge |

| Bridge/Location | Date | Cause of Fire | Bridge Material | Damage Extent |
|---|---|---|---|---|
| Lazienkowski Bridge, Poland | February 14th 2015 | Ignition of stored construction materials | Steel girder bridge | Replacement of entire bridge |
| Chishi Bridge, China | October 29th, 2014 | Fire originating in hollow bridge tower during constructions | Cable-stayed Bridge | Nine cables were lost over a period of 85 minutes. Temporary cables were installed to correct the excessive deflections. One girder experienced large torsional forces and severe cracks were observed in the deck and girders webs in the affected region. |
| Zakim Boston Bridge, USA | April 21st, 2014 | Heavy goods truck fire | Cable-stayed bridge | Fire was not located near to any cables and so damage was limited however charring was observed on a cable sheath |
| New Little Belt Bridge, Denmark | March 2013 | Heavy goods truck fire | Suspension bridge | No significant damage was done to the main cable however the zinc coating of a cable band was observed to have melted and one cable required replacement |
| Beaver River Trestle Bridge, Alberta | June 22nd 2012 | Arson involving a car fire at bridge base | Timber trestle | Significant damage to timber frame |
| Russky Island Bridge, Russia | December 12th, 2011 | Ignition of wooden construction materials from welding | Cable-stayed bridge | No significant damage was reported to the cable system however 38 firetrucks were required to battle the blaze |
| Hazel Park I-75 overpass, Michigan | July 15th 2009 | Gasoline tanker collision | Steel girders with concrete deck | Complete bridge collapse |
| Big Four Bridge, Kentucky | May 7th 2008 | Electrical fire of lighting system | Steel truss bridge | Minor structural damage and debris |
| Stop Thirty Road, Tennessee | June 20th 2007 | Gasoline tanker collision | Hollow concrete box girder | Very minor damage requiring some repairs |
| Mezcala Bridge, Mexico | March 17th 2007 | Heavy goods truck and school bus fire | Cable-stayed bridge with steel superstructure | Ignition of a high-density polyethylene sheath resulted in the loss of one cable-stay and minor damage on an adjacent cable |
| MacArthur Maze Interchange, California | April 29th 2007 | Gasoline tanker collision | Steel girders with concrete deck | Collapse of two spans totalling 160 m |

| Bridge/Location | Date | Cause of Fire | Bridge Material | Damage Extent |
|---|---|---|---|---|
| Bill Williams River Bridge, Arizona | July 28th 2007 | Gasoline tanker collision | Precast prestressed concrete I-girders with concrete deck | Concrete girders were damaged and required repairs, but none were replaced |
| Belle Isle Bridge, Oklahoma | January 28th 2006 | Heavy goods truck collision | Precast prestressed concrete I-girders with concrete deck | Concrete girders were slightly damaged |
| Rio-Antirio Bridge, Greece | January 28th, 2005 | Fire initiated from a lightning strike | Cable-stayed bridge | Lightning strike initiated a fire at the pylon-cable connection which resulted in the failure of one cable which damaged an adjacent cable |
| Wiehltalbridge, Germany | August 26th 2004 | Gasoline tanker collision | Orthotropic steel duck on concrete piers | Web buckling in a main girder and plastic deformation in deck cantilever |
| Norwalk River Bridge, Connecticut | July 12th 2005 | Gasoline tanker collision | Precast prestressed concrete box girders with concrete deck | Deck replacement was required |
| I-95 Overpass, Connecticut | March 26th 2003 | Car and gasoline tanker collision | Steel girders with concrete deck | Collapse and partial collapse of two bridge spans |
| I-20/I-59/I-65 Interchange, Alabama | January 5th 2002 | Gasoline tanker collision | Steel girders | Main bridge span deflected over 3 m |
| I-80W/I-580E Ramp, California | February 5th 1995 | Gasoline tanker collision | Steel girders with concrete deck | Minor damage to deck and other facilities |
| Vivegnis Bridge, Belgium | August 14th 1985 | Rupture of a natural gas pipeline | Steel tied-arch bridge | Complete collapse of the bridge |

Although the events in Table 1 represent some of the most severe recent fire events, this table is not exhaustive, nor does it necessarily describe the frequency or severity of bridge fire events, especially for rural bridges, highway on-ramps, or other seemingly "minor" bridge structures that do not receive significant media attention and/or go unreported. For example, a brief internet search returned that, in June 2020 alone, two timber railway bridges, a 150 m long trestle in Montgomery County, Kansas, and the Fred Meijer Heartland Trail Bridge in Michigan were destroyed by fire from suspected arson. Similarly, the Gardiner Expressway in downtown Toronto, Ontario, experienced at least five fires resulting from homeless persons' settlements between February and May of 2020 (see Figure 1.1).

Figure 1.1. Aftermath of a settlement fire under the Gardiner Expressway in Toronto.

Although these settlement fires may have been relatively minor in severity, each fire occurrence requires a structural assessment which, in many jurisdictions, is not easily attained due to the lack of knowledge available pertaining to the thermo-structural response or the post-fire assessment of bridges. There exists great intersection between many research topics, especially those of settlement fires, timber bridge fires, and aging/disrepaired bridges (see again Figure 1.1 – note the proximity of the fire to the exposed rebar on the pier), under the overarching scope of bridge fire safety research, and these multi-disciplinary areas have not been identified nor mentioned in the literature (Nicoletta et al. 2020a). Bridge fire safety is an ongoing yet nascent field of fire safety engineering and there is immense room for development and exploration that has, so far, begun only with the thermo-structural response of steel and concrete bridges, and, to a much lesser extent, fibre-reinforced polymer (FRP) and cable-supported bridges. A quantification of the true number of bridge fire events has yet to be established due to the lack of event reporting, especially internationally beyond North America and Europe, although recently a database for bridge fire events has been created by Peris-Sayol and Payá-Zaforteza (2017).

## 1.2 Motivation

Traditionally, life safety has been a primary motivation in fire protection engineering which was manifested in the structural fire avenue through the term “fire resistance”. Fire resistance has historically referred to the ability for a structural member (the distinction between *structural member* and *structure* is important here) to resist a fire, defined by a standardized time-temperature history, for a certain duration. For example in Canada, fire resistance ratings (FRRs) define the ability of a structural element to maintain a set of predefined thermal performance criteria for, generally, a one-, two-, or three-hour time period (see the broader discussion in Chapter 2 for more background into the state of fire protection engineering). The

intention of these fire resistance ratings is to enable a structure's occupant to safely egress, hence the emphasis on life safety. What this approach fails to consider is the fire performance of a global structure which may not be reflected by the piecewise fire protection of members on an element-by-element basis, nor does it often allow tailored solutions for complex structural systems for which the generalized and standardized fire resistance ratings may not apply. Further, the heavy consideration for life safety limits the scope of fire protection to *only* ensure life safety and often fails to consider economic impacts associated with operational continuity after damage is inflicted as is done in earthquake engineering, for example. This extension of fire resistance beyond life safety to consider also the potential structural damage and repair time associated with a fire has recently taken the name of *fire resilience*. Resilience involves understanding of a structure's role in the economic and social fabric of the area it serves and designing to ensure these functions are maintained after significant damage. Fire resilience is achieved through performance-based fire design (PBFD) approaches and must consider the potential fire hazards, risks, thermo-structural responses, acceptable damage levels, and acceptable return times to maximum operational capacity. Not only do PBFDs enable design for fire resilience, they are also necessary for the fire protection of complex, non-standard structures, a category that bridge structures often fall under.

The determination of fire risk is an important step in the fire design of bridges because it is not economical to fire protect all bridges. Care must be taken to ensure the potential fire risk a bridge may face warrants the resource cost associated with providing fire protection. In general, the fire risk of a structure is a function of the probability of a potential fire hazard occurring and the consequence of the potential fire event. Therefore, in order to quantify risk, the probability of a fire event and the expected damage level of a bridge must be determined for the given fire hazard. This in part requires specific knowledge of the structure's thermo-mechanical which is main contribution of this thesis and thereby establishes the relevance of the work herein.

Bridge infrastructure falls into a unique category as the common structural systems found in bridges vary significantly from those in buildings for which current prescriptive fire protection methods have been created. In many cases, life safety in bridge fire scenarios, if considered at all, is assumed to be readily achieved as bridges are open structures and egress can occur unabated. These two factors yield that bridge fire safety has been developed very little and the knowledge transfer from the fire protection of buildings to that of bridges is not widely applicable or is unquantified. This lack of consideration for bridge fire safety has yielded that no contemporary bridge design standards specify fire performance metrics for bridges. Although contemporary code requirements do not specify fire resistance requirements for bridges, advancements in structural engineering tools, the rise of PBFDs for other structures in Canada and internationally, and the desire of stakeholders to produce more robust structures has provided bridge

designers with the opportunity to create fire-resilient bridge infrastructure. The state of bridge fire research is accelerating to provide the knowledge required to facilitate bridge PBFDs, however, many knowledge gaps persist that still limit the ability of practitioners to create fire-resilient bridges. The work presented in this thesis targets persisting knowledge gaps pertaining to the fire performance of cable-supported bridges and, specifically, the response of steel cables to localised fire exposure.

## 1.3 Scope of Project

This thesis contributes to the overall bridge fire safety engineering field by first presenting a review of contemporary bridge fire research on topics ranging from bridge fire hazard and risk assessment, bridge fire modelling, and the thermo-structural response of various bridge systems.

This first experimental program in this thesis studies the use of pool fires to inflict fire damage to bridge structural components. In this test series, a glass-fibre reinforced polymer (GFRP) stay-in-place formwork beam is exposed to a pool fire at midspan and tested in flexure to study the residual strength following a fire. The fire-damaged beam is compared to several similar beams with simulated fire damaged applied. These types of GFRP-concrete bridge members have rarely been studied for their fire performance and this portion of the thesis serves to shed light on their thermo-mechanical behaviour. Ultimately, the fire exposure methodology applied in this series serves to inform the fire exposure used in the later experimental tests.

Limited experimental research has examined the fire performance of steel stay-cables used in bridges or other cable-supported structures. These elements may be particularly susceptible to fire exposure if unprotected given their typical high-load applications and relatively small cross-section when compared to other structural members (see Figure 1.2 for two structural applications of steel cable members). The relatively small cross-section of cable members provides little inherent resistance to heating and ultimately results in a poor or unquantified response to effects like material strength/elasticity degradation, thermal expansion, and thermal creep effects, for example.

Figure 1.2. (Left) A cable-supported bridge in Alberta, Canada with an inset photo of a steel cable member; (right) a cable-supported structure in Manitoba, Canada.

Although the subject of prestressing strands exposed to fire has been studied (see Gales et al. 2016a for example) and hold some similarities to stay-cables in terms of wire configurations and the use of high-strength cold-drawn steel, larger diameter ( >80 mm) strand members have not been studied despite their use in many contemporary bridges or other structures (Kotsovinos et al. 2020a). The experimental research herein targets the fire performance of a variety of steel stay-cables, including those of diameter greater than 80 mm and up to a diameter of 140 mm. Of particular interest in the fire performance of these elements and herein is the development of thermal strains during heating and cooling, the occurrence of secondary deformations relating to non-uniform heating, the effect of cable lubricants and other manufacturing treatments, and the evolution of heat transfer throughout the cable structure. To address these topics, a total of nine stay-cables of varying diameter, coil configuration, and steel type were exposed to a localised methanol pool fire and instrumented to record temperature and deformation. Further, this research presents the use of a novel application optical measuring technique that involves a combination of digital image correlation (DIC) and narrow-spectrum illumination to observe surface deformations without optical interference from flames. Based on the experimental results, suggestions for the future modelling of stay-cable elements are discussed.

This research does not consider the behaviour of stay-cables simultaneously exposed to fire and under tension to avoid introducing complicating factors before a basic understanding of the unloaded thermal response is obtained. However, this thesis can be used to direct future studies that consider simultaneously heating and loading of stay-cables.

## 1.4 Research Objectives and Thesis Outline

The objectives of the research presented herein are as follows:

1) Present a review of bridge fire research literature and identify knowledge gaps in the current state-of-the-art;

2) Examine the use of pool fire exposure on bridge structural members in the context of GFRP stay-in-place formwork;

3) Better understand how non-uniform heating influences the thermal deformational behaviour of stay-cable elements;

4) Provide data on and conclusions about the heat transfer in stay-cables with respect to cable diameter, coil configuration, and steel type; and

5) Discuss and review factors critical to the thermo-structural modelling of stay-cable members.

The structure of the thesis is divided into seven chapters presented below in brief abstracts:

**Chapter 2: Review of structural fire engineering practice** presents introductory information on the topic of structural fire engineering to provide an unfamiliar reader with a brief background into key aspects of the field. This chapter is intended for an audience with some familiarity in structural engineering and considers three sections: the effect of fire on the microstructural and material properties of steel as addressed in contemporary standards, the determination of thermal boundary conditions or design fires for use in structural fire engineering designs, and the methodology of structural fire engineering design. This chapter is intended to provide a reader with sufficient information on the topic to later engage with subsequent chapters of this thesis.

**Chapter 3: Review of the fire risk, hazard, and thermo-mechanical response of bridges in fire** reviews multiple aspects of existing literature pertaining to the bridge fire safety engineering. A literature review compares studies from six significant areas in effort to summarize key findings and make available the most relevant information for researcher and practitioner use. Literature is categorized into the modelling of bridge fire scenarios, the determination of bridge fire hazard and risk, and the thermo-structural response of composite steel-concrete bridges, cable-supported bridges, concrete bridges, and fibre-reinforced polymer (FRP) reinforced bridges. The chapter concludes with a general discussion that identifies knowledge gaps and suggests priority research topics for each category.

**Chapter 4: Postfire performance of GFRP stay-in-place formwork for concrete bridge decks** presents experimental tests of the postfire flexural performance of beams reinforced with glass-fibre reinforced polymer (GFRP) stay-in-place formwork (Nicoletta et al. 2019a). The GFRP stay-in-place formwork is intended to serve as both formwork and a structural reinforcement for concrete bridge decks. This configuration leaves the soffit of a bridge deck exposed to fire which prompts concerns for the fire performance of this system. This study compares a fire-damaged beam reinforced with GFRP stay-in-place formwork to identical beams with simulated fire damage to assess the role of the exposed GFRP reinforcement and its response to damage. Results indicate some inherent fire resistance for this system for the scale of fire studied in this program. A small-scale test series concluded a degradation of GFRP-concrete bond strength with increasing temperature exposures. This work is relevant in the scope of the thesis as it served to initially develop the fire exposure methodology applied in Chapter 5 in the context of bridge structural elements.

**Chapter 5: The fire performance of unloaded steel stay-cables for bridge infrastructure subject to pool fires** presents experimental research on the unloaded thermal response of steel stay-cables exposed to a localised pool fire. Relevant literature pertaining to the fire performance of steel cables, specifically bridge cables and other larger-diameter strands, is reviewed in this chapter. Nine manufacturer-provided steel stay-cables of varying diameter, coil configuration, and steel type are exposed to a 30-minute methanol pool fire

while instrumented with thermocouples and observed with a combination of digital image correlation (DIC) and narrow-spectrum illumination. The thermocouples collect temperature data throughout the cable cross-section and along the cable length to quantify heat transfer in these domains. The optical imaging provided by DIC enables a determination of thermal strains and deformations on the cable surface during heating and cooling. Results describe the role of increasing cable diameter, coil configuration, and steel type on the heat transfer in the cable structure. The thermal strain behaviour is also quantified based on the same categories and compared to relevant code equations. A deformational behaviour named thermal torsion is presented and characterized.

**Chapter 6: Implications for the thermal modelling of steel stay-cables** reviews critical literature pertaining to the thermo-mechanical modelling of steel stay-cable members and individual steel members in general. The experimental results from Chapter 5 are discussed in the context of developing models to better understand the thermo-structural performance of cable members. This sections considers four areas for which future modelling or experimental work could target: the fire behaviour of full locked-coil cables, the longitudinal heat transfer in cable members, the thermal deformations and interwire friction of cables, and other general topics such as the role of manufacturing compounds in cable fire performance.

**Chapter 7: Conclusions and recommendations** provides the major conclusions and the novelty of the thesis presented herein. The practical considerations yielded from this work are presented based on the experimental and analytical results discussed. Areas of future consideration under the topic of bridge fire safety research and the fire performance of cable-supported structures are proposed.

# Chapter 2: Review of Structural Fire Engineering Practice

## 2.1 Introduction

This chapter aims to provide high-level information to the reader on the topic of structural fire safety engineering, particularly in the context of steel structures and cable-supported bridges. Considered herein is the material response of steel to fire, the fire dynamics considered in structural fire engineering applications, and the methods and methodology of structural fire engineering practice. While not exhaustive by any means, the material in this chapter is intended to provide sufficient information to allow a reader with existing structural engineering knowledge to engage with the fire-related material presented in the body of this thesis. The content discussed herein is largely based on the guidance for the design of steel structures provided by Eurocode 1 Part 1-2: Actions on Structures Exposed to Fire (CEN 2002), Eurocode 4 Part 1-2: Design of Composite Steel and Concrete Structures, Structural Fire Design (CEN 2005), and CSA S16-14: Design of Steel Structures, Annex K: Structural Design for Fire Conditions by Analysis (CSA 2014b) which references Eurocode procedures, in addition to some of the author's commentary.

### 2.1.1 Heat Transfer from Fire

This subsection will provide a basic background as to what constitutes a fire and how the associated heat transfer mechanisms are described. As a foreword, the scope of this section is to introduce the topics of combustion and the ensuing radiative, convective, and conductive heat transfer mechanisms to an unfamiliar reader. This discussion will, unless otherwise specified, consider only flames from premixed sources whereas, for more advanced topics such as diffusion flame combustion, the reader is directed to appropriate literature (Drysdale 2011).

Open-air fires are perhaps best described as the hot gases released through the exothermic chemical action of combustion, given below for the stoichiometric incomplete combustion of liquid methanol ($CH_3OH$) fuel:

$$4\ CH_3OH + 3\ O_2 \rightarrow CO_2 + 8\ H_2O + 3\ C \qquad [2.1]$$

where the methanol oxidizes to produce carbon dioxide, water, and soot (solid carbon) through incomplete combustion. This reaction releases energy primarily as heat through radiative and convective means. The energy released by combustion is dependent on the fuel's heat of combustion, $\Delta Hc$ [J/kg], and the degree of incomplete combustion in the process which, in turn, is dependent on the proportion of oxygen and fuel available to the reaction. If the mass burning rate per unit area, $\dot{m}''$ [kg/m$^2$s], the heat of combustion, the area of the fire, $A_f$ [m$^2$], and the quality of combustion are known, the heat release rate (HRR), $\dot{Q}_f$,, [W] can be determined. The HRR of a fire indicates the quantity of energy released from the combustion reaction

per unit of time and is transmitted through either convection or radiation. The HRR is the most important factor in characterizing a fire as it allows an absolute comparison of a fire's energy (Drysdale 2011). The portion of the total HRR transmitted through convection or radiation is dependent on the fuel, fire geometry, and quality of combustion. In general, radiation-dominated fires undergo less complete combustion and therefore produce more soot which is heated to red-hot incandescence and radiates energy to the surroundings; it is the incandescence of soot (or other non-combusted fuel or solids) that provides the archetypical fire with its characteristic orange color. This radiative mechanism sacrifices some of the hot combustion gas temperature to heat the soot and other particulates and therefore loses some convective heat transfer ability in the process. If the flame temperatures of a fire are known, the radiation flux released to a target, $\dot{q}_{radiation}''$, can be determined by equation 2.2:

$$\dot{q}_{radiation}'' = \varphi\, \varepsilon\, \sigma\, T^4 \qquad [2.2]$$

where $\varepsilon$ is the emissivity of the radiator (a measure of the efficiency of the radiation surface – a perfect emitter has an emissivity of unity), $T$ is the temperature of the radiator, $\sigma$ is the Stefan-Boltzmann constant, and $\varphi$ is a configuration or view factor that considers the geometry between the emitter and receiver (such as the angle of incidence). For a convection-dominated fire, less radiation is emitted through particulate incandescence and gas temperatures are generally higher, thus increasing the convective heat transfer received by a target, as described by equation 2.3:

$$\dot{q}_{convection}'' = h\, \Delta T \qquad [2.3]$$

where $\dot{q}_{convection}''$ is the convective heat flux to a target, $\Delta T$ is the difference in gas and target surface temperature at the location of heat transfer, and $h$ is the convective heat transfer coefficient for the target surface which is dependent on geometry, fluid interaction, temperature, and the material of the target. Equation 2.2 and 2.3 express the two basic mechanisms through which fires transmit energy. Conduction is the third mode of heat transfer and occurs once a temperature gradient has been established in a solid, as per equation 2.4 for one-dimensional conduction:

$$\dot{q}_{conduction}'' = -\lambda\, dT/dx \qquad [2.4]$$

where $\dot{q}_{conduction}''$ is the conductive heat flux through the solid, $\lambda$ is the thermal conductivity of the solid and $dT/dx$ represents the thermal gradient of temperature in the x-coordinate. Although greatly simplified herein, equations 2.2 – 2.4 provide the basis of the heat transfer mechanisms that will be discussed in this thesis and serve to introduce the common parameters that will be discussed.

## 2.2 Steel Material Response to Fire

This section will examine the thermo-mechanical response of steel to fire as it is the primary structural material examined in this thesis and serves as a good learning medium to convey structural fire engineering

concepts. Although focus is given to steel, note that the generalized structural fire engineering approach holds many similarities between all structural materials, such as the temperature-dependent degradation of material properties.

### 2.2.1 Microstructural Changes to Steel at Elevated Temperatures

Fire exposure affects steel by initiating changes in the microstructure which result in mechanical performance loss. In general, the microstructure of structural steel at ambient conditions consists of α-ferrite and iron carbide ($Fe_3C$). The proportion of carbon content in the steel determines the formation of grain structures where, at the eutectoid level of C = 0.77%, pearlite is developed which consists of both α-ferrite and iron carbide and forms thin plates (Mamlouk and Zaniewski 2016). For C < 0.77%, as steel cools below the eutectoid temperature (727°C), grains of austenite form and α-ferrite accumulates at the resulting grain boundaries. As the steel cools further, the austenite is transformed into pearlite which is now surrounded by a skeleton of α-ferrite (Mamlouk and Zaniewski 2016). The relative presence of ferrite, pearlite, and iron carbide have important effects on the properties of the steel. For example, ferrite has low strength and high ductility, while iron carbide has high strength and limited ductility, therefore combining these minerals in various proportions will result in different steel properties (Mamlouk and Zaniewski 2016). Similarly, increasing the carbon content of steel increases strength but decreases ductility. The cooling process used in steel manufacturing also has implications on the steel grain structure and therefore the material properties. Moderate cooling rates will develop fine-grained pearlite called bainite while quenching will produce martensite, both of which increase steel strength at the cost of ductility. Heat treating steel allows some grain restructuring to occur by promoting the growth and recrystallization of grains. This restructuring will vary depending on the heat-treatment temperatures, where steel heated to above the eutectoid temperature (727°C), for example, will promote the development of austenite and, under appropriate cooling rates, will reform the pearlite and α-ferrite found in mild steel (Mamlouk and Zaniewski 2016). This is important in the context of structural fire engineering as the grain structural changes that occur due to heating can 1) be observed in the microstructure post-fire, for example if bainite, martensite, or more-coarse pearlite are present, then steel temperatures above 727°C must have been reached (see Robertson and Gales 2016), and 2) affect high-temperature material properties based on microstructure. Additionally, steel heat treatments can resolve residual strains developed as a result of manufacturing or grain structure development; cold-drawn high-strength steel tends to lose the benefits gained from cold-drawing at temperatures above 600°C (Wright et al. 2013). The specific steel alloy has effects on the fire performance of the material as well. For example, the addition of chromium and molybdenum in steel alloys are known to improve fire performance by altering microstructural changes at elevated temperatures (Mamlouk and Zaniewski 2016).

The above description of steel microstructure is relevant in the discussion of the fire performance of steel cables, as these members are typically cold-formed manufactured and are of high-strength and low-relaxation (cables can also be normal relaxation depending on stress relief measures applied after manufacturing – the distinction between low and normal-relaxation is often found in context of prestressing cables). Therefore, not only do fire-induced microstructural changes occur in the steel affect material properties, strength gain from cold-drawing may also be lost if sufficient temperatures are reached (Robertson and Gales 2016). This implies there are many factors to consider when assessing the high-temperature material properties of steel cable members and that a simple temperature-dependent reduction factor approach, as discussed in the following section, may not be appropriate for some scenarios.

### 2.2.2. Mechanical Performance Changes to Steel at Elevated Temperatures

While specific or non-standard steel configurations may require specific attention from relevant code guidance or research literature, the general procedure for considering the material behaviour of steel in fire is to apply temperature-specific reduction factors to relevant mechanical properties. Therefore, as steel temperatures increase, the effective material stress-strain curve is reduced based on code-suggested reduction factors. Figure 2.1 demonstrates the stress-strain curve for a generic structural steel at various elevated temperatures based on the reduction factors given in Eurocode 4 Part 1-2 (these reduction factors are also adopted in Annex K of CSA S16-14) (CEN 2005, CSA 2014b).

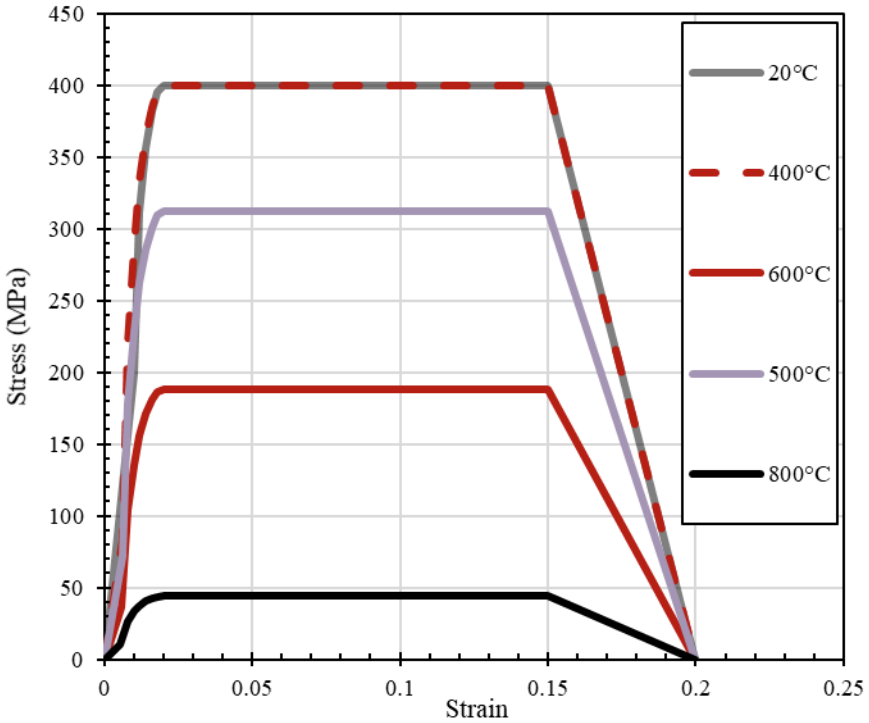


Figure 2.1. Reduction of steel stress-strain material properties with temperature. Strain hardening is not considered in this demonstration but is permitted in some cases (CEN 2005).

For example, standard structural carbon steel at a temperature of 400°C will experience a 30% reduction in the modulus of elasticity for structural design purposes but no decrease in yield or ultimate tensile strength (CEN 2005). At 600°C, the modulus of elasticity has decreased by almost 70%, and the yield strength is now below 50% of the original ambient value; at 1200°C no more structural capacity is present (CEN 2005). The implication of the loss of material properties with elevated temperatures for steel members is that, in the majority of cases, irreversible plastic strains are created under standard loading levels once sufficiently high temperatures are achieved in a fire scenario. Although this does not necessarily indicate a member initiate could initiate a collapse during a fire (although it could fail based on other criteria as will be discussed later), it does mean that unprotected steel members could likely require replacement or repair if excessive plastic strains are developed. One solution is to adopt the design philosophy preventing plastic deformations from occurring in fire scenarios altogether (Jeanneret et al. 2019).

The above discussion greatly simplifies the process of material strength degradation as a result of extreme temperatures. While the information relating to Figure 2.1 is useful for providing a basic understanding of the degradation of steel and how such processes are accounted for in structural design, further context must be given to establish the complexities and uncertainties surrounding such a simplification. The consensus among researchers is that the plastic and elastic phases of steel performance become increasingly challenging to distinguish at elevated temperatures, and that a true estimation of the plastic failure phase is very difficult to achieve (Gales et al. 2016b). This is in part due to the phenomenon of thermal creep which results in steel grain dislocations at high temperatures and induces additional permanent strains on a member. The issues with developing high temperature material reduction factors arise in part due to the material testing methods used to determine such values which either, induce a load, then heat the member (transient testing), or heat the member, then apply a load (steady state testing). Both testing methods have effects on the high temperature mechanical performance of the material as the heating rate and loading rate used in these tests can influence the failure point by limiting or exacerbating the onset of thermal creep (Gales et al. 2016b). Therefore, although the steel material reduction factors presented in current code guidance are informed experimentally, the true behaviour of steel at elevated temperatures is more difficult to accurately encompass. There are further complexities associated with thermal creep phenomenon however the associated discussions are beyond the scope of this introductory chapter.

The degradation of material properties may be the primary effect of fire on structural members, however so-called “indirect fire actions”, such as thermal expansion, deformation, or creep (CEN 2005) can also have critical implications on a structure by inducing severe loads on restraining connections or adjacent members. Values for the thermal expansion of structural members are provided in relevant structural design standards (CEN 2005, CSA 2014b). These indirect fire actions are not typically fully accounted for by

prescriptive fire design methods which typically only consider the performance of a single element. To illustrate, Flint et al. (2013) reported that a temperature rise of only 100-200°C in a steel member is sufficient to cause local buckling of a connection through thermal expansion where, for reference, typical fire protection on steel members serves only to prevent an upper-limit of temperature from being reached (typically over 500°C per these authors), not to account for these secondary effects. Additionally, Smith and Gales (2018a), in a case study of a composite building in Canada, indicated that compression due to the thermal expansion of a steel member exceeded 1700 kN in connections designed for maximum seismic or wind loads of 200 kN. For a similar reason, the cooling phase of a fire is also critical as thermal contraction occurs and any plastic deformations incurred during heating now create similar excessive tensile forces on connections (Smith and Gales 2018a). These critical loads are induced proportionally to the degree of restraint in a member's connections where, traditionally, a designer must select whether a member is specifically "restrained" or "unrestrained" (LaMalva et al. 2020). This discussion is continued by LaMalva et al. (2020) who consider the origins of restrained and unrestrained terminology in structural fire engineering and highlight the arbitrary nature of the code guidance provided by ASTM E119: Standard Test Methods for Fire Tests of Building Construction and Materials (ASTM 2016) and other codes that have adopted this standard. This topic hosts another challenge in the structural fire engineering community in that the definitions of restrained and unrestrained – shown to have immediately critical effects in terms of fire design as per Smith and Gales (2018a) – is largely dependent on the tests done to quantify the fire performance of an assembly (ie the restraint conditions of the test apparatus used in determination of the fire performance) (LaMalva et al. 2020). This is a fallacy of the prescriptive fire design method, as standardized fire resistance tests for members rarely incorporate similar boundary conditions in situ structural members (LaMalva et al. 2020), and therefore a restrained fire test may completely fail to represent a restrained member in a building frame, for example. Additionally, the degree of restraint cannot be so easily discretized into "restrained" and "unrestrained" with binary fire resistance requirements for either, a spectrum of restraint conditions must be considered at the designer's discretion with fire performance guidance to suit. So again, as to not downplay the complexity of the structural fire engineering topic, secondary fire effects like thermal expansion can be critical to the fire performance of a structure, however there is little consensus to the procedures through which these effects are accounted in design through prescriptive means, at least.

In the context of steel cable members, a similar concern for the degradation of material properties in fire is intuitive and has been considered in the literature, however many indirect fire actions have yet to be established by modelling or research efforts. For example, the load-carrying capacity of cables is a non-linear function of span length, tensile forces, and ultimately sag, all of which become transient in a fire scenario where cable stiffness changes and elongation occurs. Additionally, as described in Chapters 5 and

6 of this thesis, research into local effects at the member level associated with the fire performance of cable members is still nascent.

## 2.3 Fire Dynamics for Structural Fire Engineering Purposes

To account for fire scenarios in structures, structural elements are generally assigned temperature-dependent reduction factors which require that the inputs into a thermo-structural model or analysis must include a time-temperature history (a function of temperature versus time) or a maximum temperature for a structural member. The thermal boundary condition can also be represented by a fire's heat release rate and the corresponding heat transfer to the structural element in question. This section will briefly review the topic of fire dynamics for use in structural fire engineering applications which serves to provide this input for thermo-structural models. While material properties and other direct structural implications resulting from fires may be intuitive for a structural engineer, incorporating fire dynamics into structural engineering solutions often proves more difficult as many structural engineers do not receive formal education into fire science which is a challenging and complex discipline with little in common to structural engineering.

For the purposes of structural fire engineering and barring more complex scenarios, tools have been developed for practitioner use that simplify the fire science portion into so called "design fires" which are intended to represent the worst-case scenario fires that a structure may experience. These design fires typically only provide a time-temperature history that represents the thermal boundary a structural assembly is exposed to, which is, in turn, generally applied in a heat transfer analysis to determine a corresponding time-temperature history for the structural member. More advanced solutions for structural fire design exist however and can instead consider a thermal boundary condition such as a heat flux, or an entire thermal analysis where a fire scenario is modelled computationally and a heat transfer analysis is performed for a structural member. Advanced analyses are typically performed for highly complex scenarios. Simplified design fires are the most commonly used and facilitate the determination of structural thermal boundary conditions but have limited applicability in that, in many cases, the design fires are not truly representative of a plausible fire a structure could experience. This is especially true for non-standard structures for which fire behaviour is difficult or impossible to generalize to a single time-temperature history. Eurocode 1 Part 1-2 outlines potential design fires to be considered (CEN 2002):

1. The standard fire (also referred to as CAN/ULC S101, ASTM E119, ISO 834 for Canadian, American, and international standards respectively): the standard fire is the pioneering design fire and was implemented in the early 20$^{th}$ century as a worst-case scenario fire for a building (Ingberg 1916). This fire has been the basis for the vast majority of structural fire protection testing to present. It provides a

logarithmic temperature development with no cooling phase. The standard fire is given by the following equation:

$$\theta_g = 20 + 345 \log_{10}(8t + 1) \quad [2.5]$$

where $\theta_g$ is the fire gas temperature (°C) and $t$ is the time in minutes.

2. The Eurocode hydrocarbon fire: the hydrocarbon fire is similar to the standard fire in that it features no cooling phase but has a faster temperature growth time and a constant maximum temperature. It is intended to represent hydrocarbon fuel loads in a compartment. Equation 2.6 gives the time-temperature function for the hydrocarbon fire:

$$\theta_g = 1080 (1 - 0.325 e^{-0.167t} - 0.675 e^{-2.9t}) + 20 \quad [2.6]$$

3. The Eurocode parametric fires: the parametric fires provide an alternative solution to the previous two standard fires and allow for the specific consideration of fuel loads and quantities, in addition to ventilation and other fire parameters. The parametric fires allow for more specific and realistic compartment fire scenarios to be adopted and are overall more robust than the previous design fires. Equations 2.7 to 2.11 demonstrate the inputs considered by a parametric fire:

$$\theta_g = 20 + 1325 (1 - 0.324 e^{-0.2t^*} - 0.204 e^{-1.7t^*} - 0.472 e^{-19t^*}) \quad [2.7]$$

where $t^*$ is given by the following equations:

$$t^* = t \Gamma \quad [2.8]$$

and:

$$\Gamma = (O/b)^2 / (0.04/1160)^2 \quad [2.9]$$

where $O$ is the opening factor determined by the total area of vertical openings, $A_v$, the weighted average window height, $h_{eq}$, and the total area of the enclosure, $A_t$:

$$O = A_v h_{eq}^{1/2} / A_t \quad [2.10]$$

and:

$$b = (\rho c \lambda)^{1/2} \quad [2.11]$$

where $\rho$ is the density of the enclosure boundary, $c$ is the specific heat of the enclosure boundary, and $\lambda$ is the thermal conductivity of the enclosure boundary.

Figure 2.2 demonstrates the three Eurocode building design fires discussed above. Note how the parametric fire allows for a more specific response based on the fire dynamics properties of the situation considered. In Figure 2.2, the sample parametric fire curve represents a very fast growth rate that self-extinguishes after approximately 20 minutes. Compared to the standard fire curve, a structural member experiencing the severity of fire shown by the parametric fire curve may behave much differently. Note that the time-temperature histories of two fires are not always comparable, as another important parameter controlling

the heat transfer to a structural member is the HRR which may not correlate proportionately with gas temperatures as shown in Figure 2.2. However, for the scope of this chapter, Figure 2.2 serves only to illustrate some differences between the thermal boundaries specified in contemporary design standards.

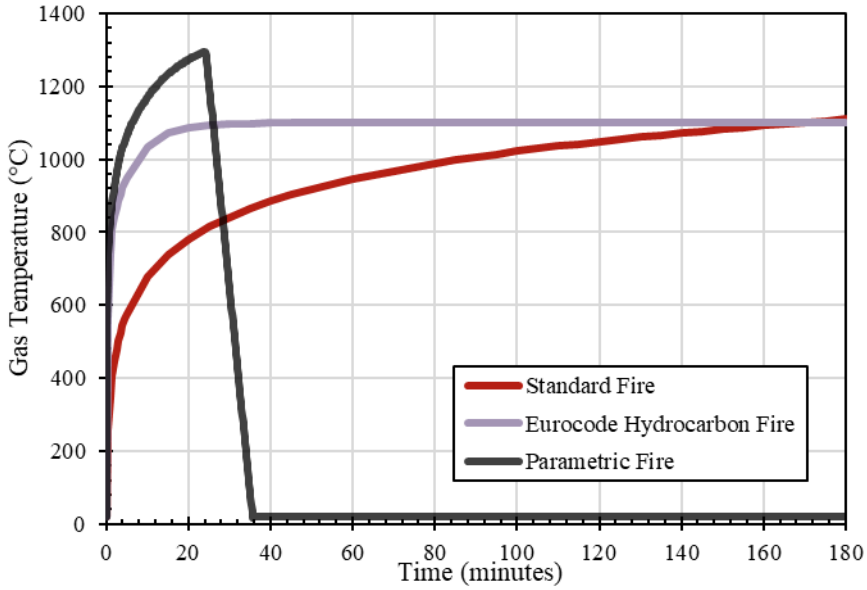


Figure 2.2. Time-temperature histories for compartment fires used in building design (CEN 2002).

These three design fires presented by Eurocode 1 (CEN 2002) have a critical underlying assumption accompanying their use in that they are intended specifically for compartment fires. The lack of generalization presented by the above design fires arises from the goal of these fires to replicate a compartment fire where flashover will occur. A compartment refers to an enclosure within a structure with an intersecting floor, ceiling, and walls with or without natural or mechanical ventilation or openings (ASCE 2018). This definition is broad but, for the purposes of applying design fires, a compartment is defined exclusively by the Eurocode through the requirement that localized fire models (also provided in Eurocode 1 Appendix C) be applied "where flashover is unlikely to occur" (CEN 2002). Therefore, a compartment may refer to a location within a structure where flashover is likely to occur. Flashover is the near-instantaneous combustion of all combustible materials in a compartment which produces extremely high temperatures consistently throughout a room. The phenomenon of flashover is complicated and beyond the scope of this chapter, but in general can occur in smaller sized compartments and is unlikely to occur on large, open floor plates or in atria, for example.

The applicability of these design fires is limited to their intended use which creates complications for more complex structures with open floor plans or other non-compartmentalized features. This motivated the development of "travelling fires" which were observed in larger compartments where flashover was less probable and would consume areas of fuel on floor plate, propagate to additional fuel sources, and self-extinguish where fuel was exhausted (Stern-Gottfried and Rein 2012). These fires were found to be much

more applicable for a variety of building types and represent the fourth fire type considered in this chapter. Travelling fires begin to move beyond the previous distinction of compartment fires by recognizing the ability for structural fires to operate in dynamics more akin to an open space.

4. Travelling Fires: Developed by (Stern-Gottfried and Rein 2012) and later improved upon by Rackauskaite et al. (2016), travelling fires consider a near-field and a far-field of heat transfer to structural elements. The near-field represents regions directly exposed by flames that undergo severe heating for a short period of time. The far-field represents regions away from the main fire that undergo pre-heating through radiation and hot gas accumulation on the ceiling; the far-field undergoes mild heating for a long period of time. The near-field and far-field move across a floor plate together based on the fuel accumulation and assumed burning rate.

As mentioned, many of the simplified design fires are not applicable for non-standard structures where flashover will not occur. The Eurocode parametric fires allow more detailed consideration of potential design fires but are non-standard in North America where prescriptive methods based on the original standard fire persist. This becomes an issue as prescriptive fire protection methods are provided by standards for specific member types exposed to the standard fire in assembly fire-testing, so the applicability of these prescriptive methods becomes questionable for non-standard fire exposures. Travelling fires represent an improvement in the understanding the variable nature of structural fire scenarios and accounting for such in design, but do not provide solutions for structures that have evaded definition as compartmentalized or non-compartmentalized. The conclusion to be made here is that fires are highly variable phenomena which cannot be easily generalized; there are many structural fire engineering applications that have yet to be quantified in terms of an appropriate thermal boundary.

The fifth design fire considered herein is the alternative solution which allows a designer to propose a non-standard thermal boundary on the basis of proving equivalence to the appropriate fire resistance requirements. This procedure is allowed under the National Building Code of Canada (NBCC) if the alternative solution meets the same functional statements required in prescriptive design, as will be discussed in the next section.

5. Alternative solutions: the Eurocode and NBCC allows alternative methods to be applied in designs which can include more advanced computational or experimental solutions to determine the thermal boundary of a structure. In the context of bridge fire safety engineering, alternative solutions are the most utilized as researchers have dismissed the applicability of the previous design fires to represent bridge fire scenarios, as will be discussed in Chapter 3 (consider an open-air hydrocarbon pool fire from a tanker truck compared to a potential fire in a building structure, for example).

In the context of bridge fires, alternative solutions to providing thermal boundary conditions generally involve computational fire models as little experimental research has yet quantified the large-scale fires a bridge could be exposed to. This poses a problem as the variability of the most commonly applied bridge fire exposure, that of a gasoline tanker truck fire, considered in the literature is quite large, as shown in Figure 2.3 which compares heat release rates per unit area (HRRPUA) of gasoline tanker fires from a number of authors. One challenge still facing researchers in bridge fire safety engineering is the quantification of bridge fire exposures to establish consistency between such models.

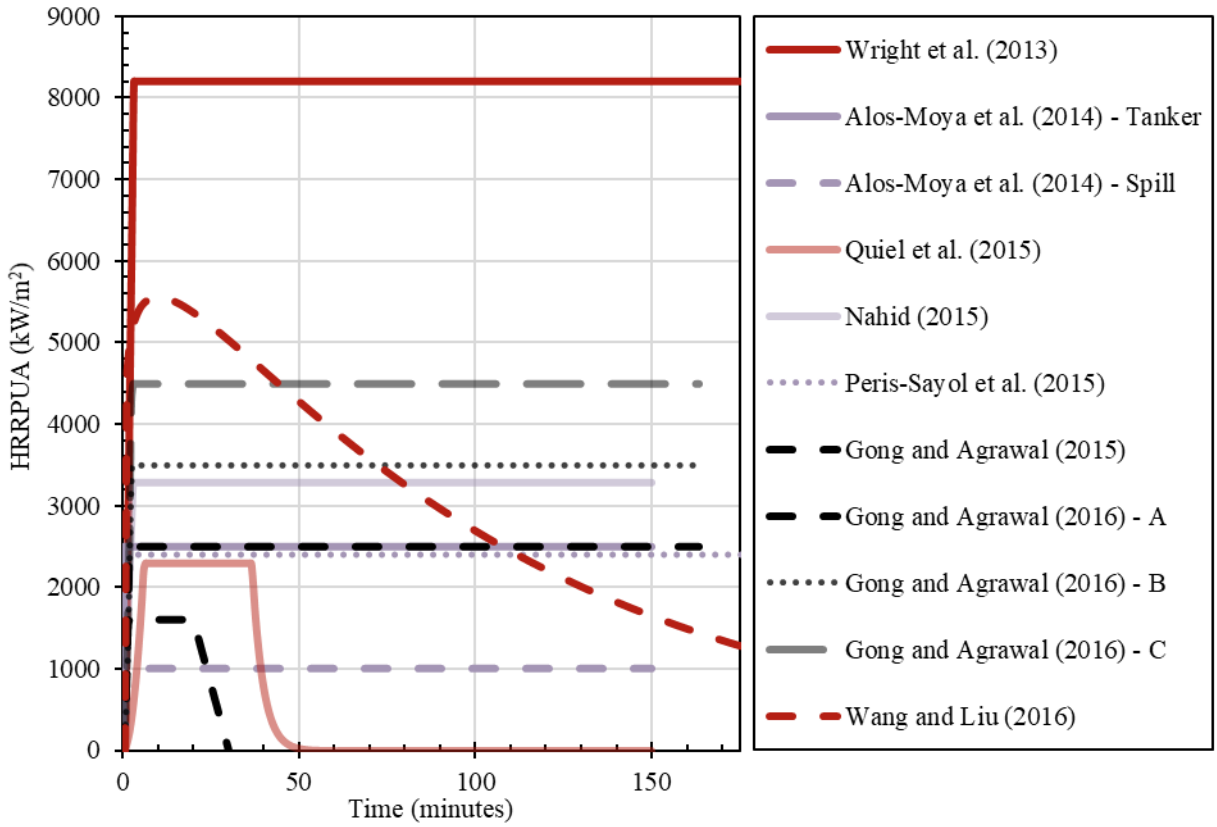


Figure 2.3. Variation of heat release rates per unit area for tanker truck fires considered in bridge fire scenarios.

Performance-based fire designs (PBFD) are becoming more popular internationally (and gaining attention in Canada with addition of Annex K to CSA S16-14 which is objective-based) but some structural fire applications are exceptionally delayed in this transition such as that of bridge fire safety engineering. This is partially due to the fact that bridges have rarely, if ever, had fire protection requirements in structural design standards. Additionally, in cases where bridges were to be designed for the fire load case, insufficient research on the thermo-mechanical response of bridge structural types has hindered the design and only limited knowledge transfer from the field of building fire safety could occur due to a number of dissimilarities between the fields. These dissimilarities are beyond the scope of this chapter but at a high

level include great differences between structural systems as well as the expected fire dynamics in each scenario.

## 2.4 Structural Fire Methodology

The Eurocode allows the most detailed contemporary fire designs in that it establishes the alternative fire curves discussed previously and allows for acceptable performance-based solutions which typically require a higher form of analysis (CEN 2002). Canadian standards for steel construction (CSA 2014b) have recently included Annex K which offers objective-based solutions that enable structural fire designs beyond that of traditional prescriptive methods (Smith and Gales 2018b) and applies content from Eurocode 1 Part 1-2 and Eurocode 4 Part 1-2. This section will briefly describe the methodology of fire safety engineering from a traditional prescriptive approach compared to a more advanced PBFD.

Prescriptive fire protection approaches, such as those used in Canada, function on the basis of assigning a fire resistance rating (FRR) to predetermined structural and architectural assemblies. An FRR represents a time duration for which an assembly has been experimentally shown to resist fire based on stability, integrity, and insulation. Stability refers to structural stability and requires that a member not collapse locally or globally for the duration of its FRR; generally, this is determined by limiting deflection, rate of deflection, and ensuring connection strength during fire. Integrity is achieved by limiting the transmission of hot flames and gases through an assembly. Insulation is achieved by limiting the temperatures of unexposed surfaces to acceptable values. These three criteria are intended to enhance the life safety of occupants by ensuring safe egress of a structure in a fire scenario. As described, prescriptive methods are generally informed by experimentation where furnace tests applying the standard fire curve are performed to assess if a structural assembly can meet the requirements for stability, integrity, and insulation. If so, this assembly is fire rated for the appropriate fire resistance duration and can be selected by designers where fire protection is required. Therefore, the generalized prescriptive fire design process is as follows:

1. A specific fire resistance rating is required per the relevant building code specification; and
2. A fire-rated assembly is chosen from a list of available fire-rated assemblies to meet the specified requirement.

Little consideration for the type of fire exposure or global structural system is considered in this approach. Objective or performance-based fire designs generally require an understanding of the possible fire exposures a structure could face. As they are intended to be alternate solutions to the prescriptive methods above, the same performance metrics of stability, integrity, and insulation are required to be met, however the means of establishing these are to be determined by the designer. Non-prescriptive design methods required approval from the authority having jurisdiction (AHJ) in the region. This can create problems in

jurisdictions where performance-based approaches are not common and the AHJs may not have the technical knowledge to approve such a design. This is an issue acknowledged by Canadian fire researchers and practitioners and is discussed thoroughly by Quiquero et al. (2018). The general procedure for undertaking a PBFD could be as follows:

1. A range of possible design fires are chosen based on available fuel types and other risk factors;
2. The thermal boundary is established through alternative means if appropriate;
3. A thermo-structural analysis is conducted to assess the structural response based on the thermal boundary. In some cases, finite elemental models will be applied to demonstrate the performance of more complex systems.
4. If performance is unacceptable, means of fire protection are specified such as the application of passive or active fire protection or the design is altered to improve fire performance and the analysis is repeated.

In situations where the requirement of fire resistance is not necessarily specified, such as in bridge structures, the procedure above could be preceded by a risk analysis to determine if the plausible fire hazards, coupled with the knowledge of the structure, create sufficient risk to warrant a PBFD. This could include a cost-benefit analysis as a PBFD can sometimes allow for the reduction of fire protection that would otherwise be specified through prescriptive methods. As described in the previous section, performance-based approaches are typically used for bridge fire designs as the thermal boundaries and thermo-structural guidance available in contemporary standards are applicable largely for buildings only where fire scenarios and structural systems vary. Therefore, advanced models are required for bridge structures to establish both non-standard and severe thermal boundaries and later demonstrate acceptable thermo-mechanical performance for complex systems.

## 2.5 Summary

This chapter was intended to provide a brief introduction to the practice of structural fire engineering for the reader. The content herein is simplified greatly but it is believed by the author to be sufficient such that the topics considered in this thesis can be engaged with. This chapter examined the material response of steel exposed to fire to establish the general approach for considering thermal effects in structural members. This was followed by a brief introduction into how fire dynamics are considered in structural fire engineering and the implications of the various methods of simplification currently adopted in design. Finally, this chapter was concluded with a comparison between prescriptive and performance-based structural fire design approaches. Commentary with respect to the topic of bridge fire safety engineering was included throughout to provide context to the following thesis chapters. In general, the information

herein applies largely to building fires for which research and existing design methods have been tailored. Structures such as bridges require more complex analyses to determine fire performance metrics which are not always possible due to a relative lack of research. It is for this reason that research such as that presented in this thesis is necessary and valuable to a practitioner.

# Chapter 3: Review of the Fire Risk, Hazard, and Thermo-Mechanical Response of Bridges in Fire

## 3.1 Introduction

Resilient fire design aims to limit potential fire damage and ultimately ensure a return to peak operational capacity in a reduced timeframe following a fire. The acceptable period required for a bridge to return to its original operational capacity is highly dependent on the nature of the bridge and the requirements of the relevant stakeholders (Kotsovinos et al. 2016a). Resilient design requires information about a structure's response to a variety of exposures such that systems can be implemented to prevent unacceptable losses (Smith and Gales 2017). For the case of critical infrastructure like bridges, costs associated with operational time lost due to structural repairs, structural damage, and traffic closures can be substantial. There can often be economic incentive to develop the fire resilience of bridge infrastructure. For example, Chung et al. (2008) reported that the daily indirect traffic losses associated with the fire-induced MacArthur Maze overpass collapse in California were approximately $6 million USD. It took 26 days for the MacArthur Maze interchange to reopen to traffic (Chung et al. 2008). Despite this, there are no specific code requirements for bridge fire safety in different national jurisdictions, particularly in North America and Europe, and only minimal guidance available for establishing potential design fires for bridges which is provided by the National Fire Protection Association (NFPA) Standard 502 (NFPA 2014). Research into bridge fires is ongoing but knowledge gaps persist that limit the research users' and practitioners' ability to conduct performance-based fire designs that apply existing research.

This chapter provides a review of research conducted on bridge fire risk and hazard assessment and the thermo-mechanical response of bridges to fires. The goal is to summarize key findings from research conducted to date and make the most relevant information available for researcher and practitioner use. Additionally, the information reviewed herein will be used to inform priority research areas and identify knowledge gaps in the literature. Of specific note in the literature is the work of Garlock et al. (2012) whom conduct the first major literature review in this field of study and reviewed past bridge fire events, summarized best-practice post-fire assessment and repair strategies for bridges, and identified potential research areas and knowledge gaps. The work herein could be considered an extension of the literature review by Garlock et al. (2012) but it is recommended by the authors that the interested reader should also review the work of Garlock et al. (2012) as it is still relevant and the key reference in the literature of bridge fire safety. This work does not provide a comprehensive lessons-learned through case studies as this has been performed by Garlock et al. (2012) and others before (Kodur et al. 2010; Peris-Sayol et al. 2017).

The key research themes consider subdivisions as follows: bridge fire hazard and risk assessment, bridge fire scenario modelling, as well as the structural response of steel, concrete, composite steel-concrete, cable-supported, and polymer bridges to fire. These topics have been determined by the author as areas in which research needs have been identified. This chapter concludes with a discussion of bridge fire experimentation and presents knowledge gaps that the research community could consider targeting. The author tabulates research publications and includes some discussion pertaining to major studies under each category when relevant. Only publications available in the English language are considered.

## 3.2 Review of Bridge Fire Literature

### 3.2.1 Fire Hazard and Risk Assessment Framework

Bridges can range in span and provide varying levels of service to the surrounding community, ranging from redundant (with no or limited impact associated with closure) to critical (with detrimental effects on traffic operations in the case of closure). Life safety due to fire-induced collapse could also be of relevance for certain types of bridge however the life safety of users or staff due to a fire that is not related to a fire-induced structural failure is outside the scope of this work. It is not economic or feasible to provide fire resistance to all bridges against the threat of fire (Naser and Kodur 2015). Further, if a bridge is deemed to require fire resistance, care has to be taken to assess the possible fire hazards it may experience in its lifetime and the subsequent design must respond accordingly.

The literature studied in this section represents the initial considerations that are taken to consider the fire risk and hazards in bridge infrastructure. Table 3.1 presents a summary of past research efforts and the conclusions presented by each, followed by more detailed summaries of substantial studies.

Table 3.1. Relevant literature on bridge fire hazard and risk assessment framework.

| Study Title | Author(s) (Year) | Research Topic | Summary |
|---|---|---|---|
| Review and Assessment of Fire Hazard in Bridges | Kodur et al. (2010) | Overview of the potential hazards created by fires and considerations for design | The document details bridge fire hazards and significant case studies. Issues and knowledge gaps in literature and a design methodology are presented. |
| Vulnerability of Bridges to Fire | Giuliani et al. (2012) | Discussion of the necessity of bridge specific code requirements and a review of case studies | The authors differentiate between bridge and building fires. Case study analysis concludes that the majority of bridge fires are caused by gasoline tankers and most bridges do not collapse. Authors speculate more bridge fires occur than are reported especially outside of the US. |

| Study Title | Author(s) (Year) | Research Topic | Summary |
|---|---|---|---|
| Fire Hazard in Bridges: Review, Assessment and Repair Strategies | Garlock et al. (2012) | A detailed overview of significant bridge fire events, bridge fire literature, best practices post-fire repair and assessment strategies, and research gaps in the field | This document is the first and key reference publication that provides significant context to the issue of bridge fire safety. Details of real bridge fire incidents and relevant research studies are discussed. Best practice post-fire assessment and repair techniques with respect to concrete and steel bridges are presented to inform practitioners and researchers. A series of lessons learned through case studies is also presented. |
| Fire Hazard Assessment for Highway Bridges with Thermal Mechanical Modelling | Woodworth (2013) | A dissertation concerning bridge fire hazard assessment through statistical analysis and thermo-structural modelling of a bridge fire with FDS and ABAQUS | A review of statistical data found wild and trash fires occur frequently when compared to vehicles fires on bridges but are typically small in severity and not reported. Interstate highway bridges have the largest fire risk and more vehicle fires occur in rural areas where accident rates are larger. |
| Highway Bridge Fire Assessment Report | Wright et al. (2013) | A significant report on bridge fire hazards based on case study review and scenario modelling | The main risk to consider is loss of bridge service. It is reasonable to expect one bridge to permanently lose service from a fire per year in the US. Improving highway safety on/near bridges reduces crash and fire risk. The fire response of steel bridges is governed by the presence of redundant unexposed girders. |
| A Probabilistic Assessment for Classification of Bridges Against Fire Hazard | Naser and Kodur (2015) | Presents a rational method for assessing bridge fire risk and vulnerability to potential fire hazards | The proposed assessment provides a framework to identify critically vulnerable bridges based on bridge and traffic characteristics. Importance factors are assigned to inform design. |
| Re-testing of a Fire Damaged Bridge | Au (2016) | Post-fire assessment, repair, and long-term testing of a fire-damaged concrete overpass. | Load tests conducted 6 years after initial post-fire repairs found little deterioration in strength. The post-fire retrofitting techniques were deemed successful. |
| Resilient Bridge Design Framework to Extreme Fire Loading | Mueller et al. (2016) | Methodology for designing fire resistant bridges applied to a case study. | The proposed framework successfully established the maximum fire exposure threat and informed design decisions in the case study considered. A resilient design approach is adopted which considers potential acceptable damage states as opposed to strictly designing against collapse. |

| Study Title | Author(s) (Year) | Research Topic | Summary |
|---|---|---|---|
| Qualitative Assessment of the Fire Hazards Beneath Bridges | Kotsovinos et al. (2016a) | The paper presents a hazard assessment process for the characterization of the threat to a bridge from potential fires beneath it. | The hazard assessment facilitates an understanding of any necessary mitigation measures/restrictions that need to be imposed by the operators of the region below the bridge and/or the amount of fire protection to be provided to the bridge structure. |
| Detailed Analysis of the Causes of Bridge Fires and Their Associated Damage Levels | Peris-Sayol et al. (2017) | Data review and analysis of more than 150 bridge fire scenarios | The analysis shows tanker truck fires are the most damaging fire type a bridge can experience. Gasoline fires were responsible for most bridge damage with typical fuel volumes ranging from 30-35 $m^3$. |
| Quantified Fire Risk Assessment for the Design of Bridges Against Fire | Flint et al. (2017) | Methodology for the characterization of fire hazards in bridges | The authors present a risk-based methodology that utilizes quantified risk assessment as part of the decision making process for the design of bridges. A case study of a cable stayed bridge is presented. |
| Performance-Based Design of Bridge Structures under Vehicle-Induced Fire Accidents: Basic Framework and a Case Study | Ma et al. (2019) | Framework for the performance-based design of bridges applied to a case study | The study presents a framework to undertake a performance-based fire design for bridge infrastructure by setting performance targets, determining evaluation methods, conducting a fire safety analysis, calculating economic consequences, and proposing fire resistance strategies. The authors discuss plausible fire scenarios, thermo-structural analyses, fire resistance levels, and a risk-based cost estimate approach to facilitate bridge design. The authors conclude by applying the proposed framework to a case study of a cable-supported bridge. |
| Semiquantitative Fire Risk Grade Model and Response Plans on a National Highway Bridge | Ann et al. (2019) | Bridge fire risk model based on numerical modelling to inform response times | The authors propose a framework to assess the fire risk level of a bridge and involves determining risk factors, creating a fire model in FDS, determining the maximum bridge surface temperature to establish a risk grade, using satellite information modelling to asses fire suppression response times, and outlining a response plan. This methodology is applied to existing bridges to determine fire risk grades and potential response plans. |

| Study Title | Author(s) (Year) | Research Topic | Summary |
|---|---|---|---|
| Fire Risk Assessment of Cable Bridges for Installation of Firefighting Facilities | Kim et al. (2020) | Risk assessment methodology for the placement of fire hydrants and standpipes | The authors present factors to consider the fire likelihood and response scenarios, bridge vulnerability, and bridge importance in a risk analysis. The main risk components to consider are fog occurrence, heavy vehicle use, firefighter response time, effective bridge deck width, bridge materials, cable spacing and type, span, cable layout, traffic density, repair cost, and bridge span. The choice of either fire hydrant or standpipe installation is governed by the final risk level. |

It is well-cited in the literature and apparent after reviewing bridge design standards such as the CAN/CSA-S6-14, AASHTO LRFD Bridge Design Specifications, and Eurocode 1 Part 1-2 and Part 2 that there are no specific fire resistance requirements in contemporary bridge design (Kodur et al. 2010, Garlock et al. 2012, Peris-Sayol et al. 2017, CSA 2014a, AASHTO 2015, CEN 2002, CEN 2003). In practice, fire resistance specifications are beginning to be considered on the basis of owner requirements that are driven by property protection and operational continuity goals rather than legislative requirements (see Kotsovinos et al. 2016a). The only guidance provided by a national standard is the National Fire Protection Association (NFPA) Standard 502, which specifies a high-level method to select design fires for highway bridges over 300 m in length but does not provide procedures to undertake a computational fluid dynamics (CFD) model of a vehicle fire or the means to apply a fire in a thermo-structural model (NFPA 2014). Fire modelling and design of buildings vary greatly from bridges due to dissimilar and irredundant structural systems, well-ventilated potential fire scenarios in open air, and different consequences associated with structural failure (Kodur et al. 2010; Garlock et al. 2012; Giuliani et al. 2012; Wright et al. 2013). Therefore, a specific framework is needed to facilitate the design of bridges in the event of fires on or around the bridge. Research efforts discussed herein have established the base tools necessary to conduct fire hazard assessments, determine and characterize fire scenarios, apply thermal conditions to bridge structures, and assess structural response.

Loss of bridge service is the primary factor in dictating fire risk and can be a result of moderate to severe fires which have mainly occurred due to vehicle collisions in previous fire incidents (Wright et al. 2013). Past experience has shown that more typically it is the most severe vehicle fires, such as fully loaded heavy goods vehicles (HGVs) and tanker trucks, which can cause permanent loss of bridge service. It is reasonable to expect one bridge in North America to permanently lose service as a result of a fire per year; however this metric is based on survey data from the New York State Department of Transportation (NYDOT) cited in Garlock et al. (2012) and Wright et al. (2013) which considers also small and rural timber bridges that may be more susceptible to fire. One of the most effective methods in reducing bridge fire hazards may be

to increase highway safety near bridges which can reduce the number of vehicle fires from collisions (Woodworth 2013; Wright et al. 2013; Liu and Lou 2016). It is unlikely vehicle collisions could be completely prevented in any given highway segment, but proper road safety design can be applied to reduce bridge fire risk from vehicles. In cases where fire risk is greater than acceptable, bridge structural design coupled with active and passive fire protection systems can be relied on to protect assets. Kotsovinos et al. (2016b) have identified a lack of experimental data on the open-air fires of HGVs and gasoline tankers and that the majority of cited data in bridge fire literature is based on tunnel fire experiments where the fire dynamics are different.

Woodworth (2013) presents statistical data on the occurrence of bridge fires in the US. Of specific note is the rate of bridge-threatening hydrocarbon fires which is approximately one per year based on data from 1994-2013 (Woodworth 2013). Of bridge-threatening hydrocarbon truck fires from 1994 to 2013, the majority have been gasoline tanker fires (Woodworth 2013). However, for a given bridge, the most common fuel loads being transported in the region should be considered in a bridge fire design. For example, in their study of a cable stayed bridge, Kotsovinos et al. (2016b) consider a liquefied natural gas (LNG) truck fire that could occur on the bridge due to the position of an LNG terminal in the surrounding area. To provide more context to the threat of bridge fires, Woodworth (2013) compares bridge failures due to fires to other sources of failure as reported in the NYDOT survey. The most prevalent categories of bridge collapse in descending order are: hydraulic events (assumed to refer to events like scour, debris flow, and flooding), collisions, overloading, deterioration, miscellaneous, fire, nature (assumed to refer to natural disasters outside of earthquakes and flooding), and earthquakes, among some other more minor categories (Woodworth 2013). Woodworth (2013) also reports that, of bridge collapses documented in the NYDOT survey, many of the fire-induced collapses were in small rural location bridges, most of which were timber bridges exposed to wildfires. Therefore, the risk posed by wildfires is largely directed to smaller timber bridge infrastructure and the risk to the non-timber bridge types considered in this chapter is not yet quantified in the literature.

Naser and Kodur (2015) provide a comprehensive framework for assessing the vulnerability of bridges to fire. Despite an overall increase in frequency in recent years (Garlock et al. 2012), bridge fires are low-probability events and it is not economically reasonable to conduct intensive performance-based fire designs for all bridges. The most critical bridges in terms of vulnerability to fire should be provided with adequate fire resistance on the basis of protecting life safety and minimizing potential economic disruptions. Using available statistical data (Wardhana and Hadipriono 2003, NFPA 2008, Scheer 2010), Naser and Kodur (2015) found the probability for a single bridge in the US to experience a vehicle fire in a given year to be 2.27% and the probability of one fire-induced bridge collapse to occur in a given year to be 3.1%.

These values are low when compared to those for multi-storey buildings, for which the probability of one building in the US experiencing a fire is 29.5% and the probability of one fire-induced collapse occurring is 12.1% (Naser and Kodur 2015). Note that these values may be different in other jurisdictions such as those where there is less transport by heavy goods or fuel transport vehicles. Although the probability for fire occurrence and fire-induced collapse is much higher in multi-storey buildings, the likelihood of vehicle fires affecting bridges is still high enough to be classified as a probable risk by the National Fire Protection Association (NFPA) (NFPA 2007). This is because the consequence of structural failure in bridges can be high, in particular for long span bridges that are critical infrastructure. The low probability of bridge fire events compared to building fires is a main factor that has and continues to inhibit the development and implementation of fire resistance requirements for bridge infrastructure. This is contrary to other low probability accidental events such as ship impacts or explosion that are often considered in the design of long span bridges. Flint et al. (2017) have proposed the use of quantified risk assessment (QRA) to derive probabilities and consequences for the design of bridges as discussed. Moreover, since safe egress can be readily achieved in the majority of bridge infrastructure, life safety is not often a concern in bridge fire design. It should be noted that for long-span infrastructure such as cable-supported bridges, life safety could also be a concern as evacuation times may be long and the fire may be difficult to reach by the fire service (Kotsovinos et al. 2016a). The value in protecting bridges against fire is in developing resilient transportation networks that are easily repairable in the event of a fire. As a note, literature on the growing concerns of wildfires is limited, however it is foreseeable that these transportation networks will play a critical role in community evacuation events that will ultimately rely on the existing fire resilience of bridge infrastructure.

Naser and Kodur (2015) consider two factors in determining the fire hazard level for a bridge: the structural vulnerability and critical nature with respect to the traffic network. Naser and Kodur (2015) propose importance factors that can be applied to each structural member type to account for fire scenarios. These importance factors assign a weight to five classes, considered briefly in Table 3.2 where the most critically vulnerable bridge will have a weighted score of unity.

Table 3.2. Weighted classes to assess bridge fire hazard (adapted from Naser and Kodur 2015).

| | Class | Parameter | Weight |
|---|---|---|---|
| 1. | Geometric Features, Materials, Design Characteristics | Structural system, material and components; lanes; current condition | 0.47 |
| 2. | Fire Hazard Likelihood | Firefighter response time; historical/architectural significance; potential fire scenario | 0.22 |
| 3. | Traffic Demands | Average daily traffic; location | 0.11 |
| 4. | Economic Impact | Vicinity to alternate routes; predicted repair time; predicted repair cost | 0.12 |
| 5. | Expected Losses Due to Fire | Potential life and property loss; environmental damage | 0.08 |

Peris-Sayol et al. (2017) compiled data from over 150 bridge fire events and present correlations between bridge damage levels and bridge and fire characteristics. Fires from tanker truck collisions are the most damaging events and gasoline is the most damaging (and common) type of hydrocarbon fuel; typical tanker fuel volumes were found to be between 30 and 35 $m^3$ (Peris-Sayol et al. 2017). From a strictly statistical perspective, the bridge site, structural system, and geometry do not have a significant effect on the bridge damage level (Peris-Sayol et al. 2017). It must be noted, however, that the observations made by Peris-Sayol et al. (2017) may be heavily skewed by the large number of steel girder highway bridges which represented the majority of collapsed bridges from tanker truck collisions. This may imply that, due to the severity of tanker truck fires, these factors make little difference on the bridge damage extent when faced with such extreme conditions. Peris-Sayol et al. (2017) identify the importance of the fire load position (the position of the combustible fuel) with respect to the structural elements of the bridge. For example, a tanker fire on the deck of a girder bridge may not pose a threat to the bridge structure unless large amounts of fuel spills below and ignites. Conversely, a fire on the deck of a cable-supported bridge may be the most critical fire position based on the proximity to the cables. The potential fire load positions are critical in determining fire risk. If it is not possible for a fuel load to accumulate in the worst-case scenario locations, it is less likely a fire that will cause major structural damage and the overall risk is reduced. The criticality of each fire scenario will depend on the type and use of the bridge and the surrounding site as discussed by Kotsovinos et al. (2016a). Peris-Sayol et al. (2017) recommend ensuring adequate fuel drainage from the bridge deck and limiting storing flammable materials below bridges to reduce fire risk. The database of bridge fire information used in the statistical analysis by Peris-Sayol et al. (2017) is openly accessible online and can be updated with contributions from the bridge fire community or downloaded by the interested reader (see Peris-Sayol and Payá-Zaforteza 2017).

Fire hazards may be more complex to establish for large and complicated structures. Kotsovinos et al. (2016a) have carried out a qualitative assessment of the fire hazards beneath a cable-stayed bridge. A number of fire hazards were identified as posing a threat to the bridge and its users such as: 1) an HGV (including gasoline tankers) fire on a road or in an industrial yard beneath the bridge; 2) a train (locomotive and/or cargo) fire under the bridge; 3) a ship fire (including fuel spill) on the river or in the docks below the bridge; 4) an industrial loading vehicle fire under the bridge; 5) a timber storage yard fire beneath the bridge; and 6) a wildfire under the bridge. The qualitative assessment by Kotsovinos et al. (2016a) for each of the fire hazards identified that the worst-case fires are unlikely and therefore the severity of the consequences requires that the likelihood of the event be considered. The probability/frequency of the identified fire hazards can be assessed so that the bridge owners can determine whether the risk is sufficiently great to require the implementation of restrictions or mitigating measures.

Flint et al. (2017) continues the work from Kotsovinos et al. (2016a) and presents a risk-based methodology using quantified fire risk assessment as part of the decision-making process for the design of bridges. As a case study, all fire hazards identified by Kotsovinos et al. (2016a) are adopted to determine the probability of an event and its potential consequences. The study was based on relevant statistics collected from local authorities, national authorities, and international organizations.

### 3.2.2 Bridge Fire Scenario Modeling

If the fire risk for a given bridge is unacceptable, measures must be taken to decrease risk through sufficient design, see for example the restriction and mitigation measures suggested by Kotsovinos et al. (2016a). Where the potential of a fire cannot be mitigated, characterizing potential fire scenarios is an important step in creating fire-resistant bridges since subsequent structural design relies on the outputs generated by fire models. The majority of severe highway bridge fires are initiated through vehicle collisions but other circumstances such as construction materials being stored beneath a bridge must also be considered. Other fire hazards may also be likely such as those described in the previous section and Kotsovinos et al. (2016a). This section discusses the research efforts made in modelling various bridge fires as presented in Table 3.3.

Table 3.3. Relevant literature on bridge fire modelling and fire scenarios.

| Study Title | Author(s) (Year) | Research Topic | Summary |
|---|---|---|---|
| Thermal Structural Analysis of the MacArthur Maze Freeway Collapse | Noble et al. (2008) | Early modelling endeavor of the MacArthur Maze collapse using Lawrence Livermore National Laboratory (LLNL) finite element software | The developed numerical model is approximate in nature but provided a simple method to estimate bridge failure times. |
| Integrated Fire Dynamics and Thermo-mechanical Modelling of a Bridge Under Fire | Choi et al. (2012) | Framework for bridge fire analysis using FDS and ABAQUS was developed and applied to the MacArthur Maze case study | A numerical model was validated using existing data from RC beams exposed to fire. The overall behaviour of the MacArthur Maze collapse was recreated. |
| Analysis of a Bridge Failure due to Fire Using Computational Fluid Dynamics and Finite Element Models | Alos-Moya et al. (2014) | FDS and ABAQUS modelling of a tanker fire below a steel girder bridge and the thermo-structural response with emphasis on various fire parameters | The numerical models were in agreement with observations of the case study considered. The Eurocode standard and hydrocarbon fires were found to not accurately represent bridge fire scenarios. Uniform bridge heating is only reasonable for short span bridges. |

| Study Title | Author(s) (Year) | Research Topic | Summary |
|---|---|---|---|
| Protection of Cable-Stay Bridges from Accidental and Man-Made Fire Hazards: A Rational Physics-Based Approach to Analysing Vulnerabilities and Mitigation | Woodworth et al. (2015) | Presents an approach to consider potential fire threats through fuel containment, drainage, and burning rates | The rational method proves useful for the performance-based design of bridge deck drainage systems. The relationship between deck drainage spacing and fire size is approximately linear. Overall risk assessment is improved. |
| Analysis of the Influence of Geometric, Modelling, and Environmental Parameters on the Fire Response of Steel Bridges Subjected to Realistic Fire Scenarios | Peris-Sayol et al. (2015) | This parametric study considering the effect fire position, structural boundary conditions, model scale, vertical clearance, span type, and wind on a steel bridge using FDS and ABAQUS | The modelled behaviour of the most exposed girder is representative of the full structure when appropriate boundary conditions are used. Fires close to abutments produced higher temperatures and had shorter times to failure. Faster wind speeds reduced the effect of the fire. |
| A Streamlined Framework for Calculating the Response of Steel-Supported Bridges to Open-Air Tanker Truck Fires | Quiel et al. (2015) | Structural bridge fire modelling framework for analysing members exposed to fires | The proposed modelling framework was efficient in recreating bridge fire responses over a variety of fire parameters. Authors note the inadequacy of standard fires in the context of bridge fire design and develop a simplified fire model to be used in design. |
| Performance-Based Prioritization of Fire Mitigation for Highway Bridges | Quiel et al. (2016) | Development of a tool to identify and prioritize application of fire protection | Proposed tool creates an envelope for a variety of fire exposures that can be used to identify structural elements where fire protection is required. |
| Analysis of the Factors that Influence the Maximum Adiabatic Temperatures in I-girder Bridges | Peris-Sayol et al. (2016) | Parametric study using fires modelled in FDS and statistical analysis to determine influential factors | Six parameters - four geometric and two fire - are varied to determine the influence on gas temperatures near structural elements. Fire load position, fuel type, and vertical clearance factors have the largest impact on steel girder flange temperatures. Steel web temperatures are also heavily affected by bridge substructure. |

| Study Title | Author(s) (Year) | Research Topic | Summary |
|---|---|---|---|
| New Design Fires for Performance Based Engineering of Highway Bridges | Hu et al. (2016) | Development of potential bridge fires for use in design and applied to a case study | Classification of potential bridge fires was shown to enable more realistic estimates of bridge response. |
| Thermal Fluid-Structure Interaction and Coupled Thermal-Stress Analysis in a Cable-Stayed Bridge Exposed to Fire | Nariman (2018) | Applying a model to determine vortex, drag, lift, and vibration responses to a bridge exposed to the standard fire | The developed model is adequate in determining vibration, vortex lock-in regions, and deck fatigue resulting from fire scenarios. |
| Valencia Bridge Fire Tests: Validation of Simplified and Advanced Numerical Approaches to Model Bridge Fire Scenarios | Alos-Moya et al. (2019) | Application and evaluation of a simplified fire correlation and FDS to model a large experimental bridge fire scenario | Heskestad and Hamada's analytical correlation for predicting gas temperatures was found to be representative in recreating experimental values for three of the four test scenarios with HRRs ranging from 361 to 1130 kW and flame length to ceiling height ratios of less than 2.0. Despite some deficiencies, the authors recommend using Heskestad and Hamada's correlation for the preliminary design of future bridge fire tests and indicate its potential as a starting point in real bridge fire analyses. FDS was found to be representative of all fire scenarios examined. |

Alos-Moya et al. (2014) apply a Fire Dynamics Simulator (FDS) model of a tanker truck fire compared with the Eurocode standard and hydrocarbon fires below a steel girder overpass to determine the influence of fire discretization, code-suggested fire curves, and live loading on the thermo-structural response. The Eurocode standard and hydrocarbon fires applied uniformly were found to not accurately represent realistic fires in medium and long-span bridges where large longitudinal temperature gradients are present (Alos-Moya et al. 2014). The Eurocode fires are better suited for short-span bridge fire models where longitudinal temperatures are relatively constant (Alos-Moya et al. 2014).

Quiel et al. (2015) propose four general steps to determine the structural response of a bridge exposed to fire:

1. Determine fire characteristics like burning area, flame height, duration, and heat release rate;

2. Calculate the heat transfer to structural members;

3. Calculate structural member temperature increase based on heat exposure and duration; and

4. Apply material degradation factors at elevated temperatures and conduct a structural analysis.

Many bridge fire studies make use of simplified fire models like the standard hydrocarbon fire or parametric fires which are over-conservative and not representative of real fires resulting from large open-air hydrocarbon fires (Quiel et al. 2015). Detailed solutions involve CFD modelling of potential fire events which is intensive and often not practical due to a lack of input parameters, especially for forensic analyses where observations of a fire may not have been possible. Intermediate solutions are less intensive and can estimate a single fire parameter like temperature or heat release rate (HRR) for use in a thermo-structural model to determine a response. The framework proposed by Quiel et al. (2015) considers a pool fire as a solid shape that outputs calculated radiation values. This solid model is discretized into a luminous and a smoke obscured region (with varying emissivity) that is further discretized into individually modifiable rectangular elements (Quiel et al. 2015). This model can consider fire non-uniformity due to geometric or environmental factors and can efficiently approximate realistic bridge fire scenarios.

Elsewhere in the literature, efforts from Alos-Moya et al. (2019) have validated the use of simplified bridge fire models by comparing Heskestad and Hamada's (1993) analytical ceiling jet temperature correlation to experimental results from the gasoline pool fires used in bridge fire testing by Alos-Moya et al. (2017). Heskestad and Hamada's (1993) correlations were found to underpredict peak temperatures by just over 30% but were otherwise representative in reproducing temperature profiles in shape and magnitude along the soffit of the exposed bridge deck (Alos-Moya et al. 2019). The authors indicate this correlation has potential in conducting preliminary designs of future bridge fire experiments where medium-scale pool fires are applied (found accurate for HRRs of 361-1130 kW and flame-to-ceiling height ratios less than 2.0) (Alos-Moya et al. 2019). The authors also indicate the potential for Heskestad and Hamada's (1993) correlations to be used as a starting point for a simplified model to estimate full-scale bridge fire temperatures.

### 3.2.3 Structural Fire Response of Steel and Composite Steel-Concrete Bridges

As discussed, steel bridges make up the largest portion of collapsed bridges due to fire (Peris-Sayol et al. 2017) and have been the key focus of the research community following the MacArthur Maze collapse in California. This section presents research detailing the fire response of steel and composite concrete-steel bridges in Table 3.4 with more detailed discussions following.

Table 3.4. Relevant literature on the effect of fire on steel and composite steel-concrete bridges.

| Study Title | Author(s) (Year) | Research Topic | Summary |
|---|---|---|---|
| Failure of a Tied-Arch Bridge Submitted to a Severe Localized Fire | Dotreppe et al. (2005) | Modelling of the response and collapse of a steel tied-arch bridge exposed to a hydrocarbon fire using SAFIR | The qualitative response and failure mode of the bridge was replicated with good agreement to observations of the event. |
| A Numerical Investigation of the Fire Response of a Steel Girder Bridge | Paya-Zaforteza and Garlock (2012) | Parametric study examining effects of deck restraint, structural steel type, constitutive relationships, live loading, and fire scenario | Results showed the presence of live loading had little effect on bridge behaviour, thermal expansion will routinely be larger than expansion joint widths and should be accounted for in models, and stainless performed better than carbon steel, among others. Specific local behaviours for each parameter studied are described. |
| Evaluating Fire Resistance of Steel Girders in Bridges | Kodur et al. (2012) | Thermo-structural analysis of a steel bridge girder exposed to a hydrocarbon fire in ANSYS | Authors review the major differences between bridge and building fire exposures. The developed model was validated and successfully applied to a case study. It was found the inclusion of steel-concrete composite action significantly increased fire resistance. |
| Post-Fire Strength Assessment of Steel Bridges Based on Residual Out-of-Plane Web Deformations | Glassman and Garlock (2014) | Parametric study of to determine the post-buckling shear strength of fire damaged steel bridge girders | Factors influencing the web shear response of steel girders were varied to assess the shear strength reserve in fire damaged steel girders based on post-fire observations. Steel webs that were loaded to shear buckling capacity at varying elevated temperatures and reloaded at ambient showed little reduction in post-buckling shear strength. |
| Diagnosis, Assessment and Repair of the Mathilde Bridge Close to Collapse during a Fire | Godart et al. (2015) | Review of the response and management techniques taken by municipalities surrounding the Mathilde Bridge in France after a large fire | A steel girder bridge was exposed to a large fire. The authors consider the assessment, analysis, and repair process undertaken by engineers to restore bridge operation. Post-fire assessment test and modelling methods are discussed. Good initial design was attributed in preventing significant economic loss. |
| Behaviour of Steel Bridge Girders under Fire Conditions | Aziz et al. (2014) | Experimental tests and subsequent ANSYS modelling of three composite concrete-steel bridge girders exposed to the ASTM standard fire | The experimental time to failure under standard fire exposure was between 30 and 40 minutes in bottom flange yielding in girders with web slenderness of 50 and web shear buckling for web slenderness exceeding 100. Closer stiffener spacing was found to increase girder fire resistance. |

| Study Title | Author(s) (Year) | Research Topic | Summary |
|---|---|---|---|
| Response of Fire Exposed Steel Bridge Girders | Aziz (2015) | Dissertation detailing the material and structural behaviour of composite steel-concrete bridge girders exposed to a standard fire | This study covers multiple research topics involving experimental and material tests of AASHTO designed composite bridge girders as well as modelling efforts to estimate girder post-fire residual capacity and determine the most influential structural parameters on fire resistance. |
| Computational Study of Highway Bridges Structural Response Exposed to a Large Fire Exposure | Nahid (2015) | Dissertation involving the numerical modelling of composite steel-concrete bridges with varying geometries and fire exposures | The modelling procedure and methods of reducing computational time are described in detail. A range of structural element heights were determined for which permanent damage would not be sustained for a variety of fire exposures. Localized fires were shown to cause failure via excessive material degradation while uniform heat exposures cause failure via excessive deflection. |
| Preliminary Investigation of Composite Steel Box Girder Bridges in Fire | Braxtan et al. (2015) | Uncoupled thermal and structural modelling of a weathering-steel box girder under hydrocarbon fire exposure | The max displacement was achieved after 11 minutes and failure occurred after 13 minutes of Eurocode hydrocarbon fire exposure at midspan. The girder appeared to fail in web shear buckling when heated next to the support. Authors highlight a need for understanding local effects of steel box girders in fire. |
| Numerical Simulation of Fire to a Long Span Truss Bridge | Gong and Agrawal (2015) | Forensic FDS and ABAQUS modelling of steel bridge stringers exposed to an HGV fire applied to a case study | The developed fire and thermo-structural models showed good agreement with the damage modes and measured deformations of the actual event. |
| Lazienkowski Bridge Fire in Warsaw – Structural Damage and Restoration Method | Zobel et al. (2016) | Review of the assessment and analysis of bridge fire that occurred on a steel girder bridge in Poland | A variety of qualitative damage descriptions of the concrete deck, steel girders, bearing supports, and other structural members are provided. Post-fire material property tests are also discussed. The authors note that the majority of residual bridge deformations are a result of post-fire thermal contraction. |
| Buckling Instability Behaviour of Steel Bridge Under Fire Hazard | Wang and Liu (2016) | Numerical modelling in FDS and ANSYS of a steel box girder bridge exposed to a variety of vehicle fires at midspan | The developed model shows that the critical shear buckling stress in the box girder web is exceeded after 17 minutes of exposure to a tanker truck fire. Shear buckling failure occurs before midspan deflection limits are reached. After 15 minutes of fire exposure, web temperatures are shown to accelerate rapidly. |

| Study Title | Author(s) (Year) | Research Topic | Summary |
|---|---|---|---|
| Safety Evaluation of a Large-Span Double-Deck Cable-Stayed Steel Bridge Under Fire | Liu and Lou (2016) | Full fire, heat transfer, and structural analysis of fire scenarios on the bottom deck of a double-deck steel bridge | Under a variety of fire scenarios modelled in FDS, transverse steel truss members were found to be adequate except in the case of a tanker truck fire. The authors suggest several traffic management recommendations to limit the risk of fires as a result of vehicle collisions. |
| Thermo-Structural Response of Highway Bridge Structures with Tub Girders and Plate Girders | Nahid et al. (2017) | FDS and ABAQUS modelling of steel plate girder and steel tub girder bridges exposed to an HGV fire at midspan are compared | The fire exposure used in this study was intended to fail the steel plate girder so the response of the tub girder could be compared. As expected, the plate girder bridge failed under the given fire exposure while bridges with single and multiple tub girders did not. Adding a flame shield between flanges of the plate girders did not prevent failure. The tub girders were found to have superior moment capacity compared to the plate girders. |
| Strategies for Enhancing Fire Performance of Steel Bridges | Kodur et al. (2017) | Methodology to determine fire risk and mitigate fire hazard in bridge infrastructure | A procedure is presented to evaluate the fire risk of a given bridge by determining an importance factor. This importance factor gives information on the critical nature of the bridge which can be used in deciding fire hazard mitigation methods. A fire resistance of 60-120 minutes for bridges is suggested. |
| Valencia Bridge Fire Tests: Experimental Study of a Composite Bridge in Fire | Alos-Moya et al. (2017) | Experimental tests of a composite steel-concrete bridge exposed to a real gasoline pool fire | Experiment provided information on the accuracy of using small-scale pool fires to represent bridge fire scenarios as well as data to be used in model validation. The structural and material responses are documented in addition to the effects of varying fire locations and environmental conditions. |
| Fire Safety of Bridges – Methodology Supporting Design and Forensic Evaluation | Yanagisawa et al. (2017) | Analytical and numerical investigation of a composite steel girder overpass applied to a case study | The authors present a methodology to determine heat transfer to steel girders using SOFiSTiK FEM software. Based on time-dependent material properties, the collapse of the 9-Mile overpass is modelled analytically and fire protection methods are suggested. |

| Study Title | Author(s) (Year) | Research Topic | Summary |
|---|---|---|---|
| Recommendations for Improving Fire Performance of Steel Bridge Girders | Whitney et al. (2018) | ABAQUS modelling of a composite steel-concrete bridge girder exposed to standard and hydrocarbon fires to examine varying girder parameters | Bridge section factor, girder flange and web thickness, steel material properties, concrete slab width and thickness, and applied fire protection properties were varied to examine the effect on cross-section temperatures. Increasing girder web thickness and introducing intumescent or sprayed fire protection were the most effective parameters in reducing member temperatures. |
| Fire Resistance of Composite Steel and Concrete Highway Bridges | Hu et al. (2018) | Modelling the effect of bridge skewness and abutment restraint on a composite bridge exposed uniformly to the Eurocode hydrocarbon fire | Skew bridges were found to retain greater stiffness during fire exposure than non-skew bridges. The Eurocode hydrocarbon fire is thought to be too demanding especially during initial heating. |
| Behaviour of Composite Box Bridge Girders under Localized Fire Exposure Conditions | Zhang et al. (2019) | Experimental and numerical analyses of steel-concrete composite box girders exposed to localised fire | The authors present experimental results of simply-supported and continuous steel-concrete box girders exposed to a localised fire. Results show simply-supported girders fail in deflection while continuous girders fail in web and flange flexural buckling. Longitudinal stiffeners were found to improve fire resistance based on numerical modelling. Transverse stiffeners were found to have a negligible effect on fire performance. Continuous girder fire performance can be improved by protecting the hogging moment region. |
| Effectiveness of Stiffeners on Steel Plate Shear Buckling at Ambient and Elevated Temperatures | Glassman et al. (2019) | Finite element modelling study of steel stiffener role in slender plate shear behaviour at ambient and elevated temperatures | The authors use non-linear FEM modelling to study the role of stiffeners in the shear buckling and ultimate shear capacity of slender steel plates. Stiffeners were found to be more effective when oriented to reinforce the compression field, but this effect diminishes at elevated temperatures. Vertical stiffeners contribute the most to shear buckling and ultimate shear strength by providing lateral restraint to the plate. At elevated temperatures, stiffeners were found to be less effective in providing lateral support and carry more axial force. |

| Study Title | Author(s) (Year) | Research Topic | Summary |
|---|---|---|---|
| A Numerical Model for Evaluating Fire Performance of Composite Box Bridge Girders | Zhang et al. (2020a) | Numerical modelling in ANSYS of composite box girders exposed to the ISO hydrocarbon and standard fires | The authors present numerical results of thermo-mechanical modelling of composite steel-concrete box girders exposed to uniform hydrocarbon and standard fire heating. Results found the presence of longitudinal stiffeners can significantly slow deflection rates and prevent sudden collapse in late stages of the fire. The use of inclined box girder webs can also slow the rate of deflection and provides better fire resistance than vertical webs. |

Paya-Zaforteza and Garlock (2012) examined the effect of varying deck axial restraint, constitutive relationships for carbon steel, live loading, and fire scenarios on the response of a steel girder bridge (both carbon and stainless-steel models are considered). The Eurocode standard and hydrocarbon fires (CEN 2002) as well as a large hydrocarbon fire proposed by Stoddard (2004) were applied uniformly to the bridge structure in ABAQUS (Paya-Zaforteza and Garlock 2012). Stainless steel structural models experienced lower temperatures than carbon steel models due to lower thermal conductivity and increased time to failure by over 80%, which was attributed to superior high-temperature mechanical properties (as opposed to superior thermal properties) (Paya-Zaforteza and Garlock 2012). Thermal expansion was found to be greater than is permitted by typical expansion joints and should be accounted for in modelling (Paya-Zaforteza and Garlock 2012). This is corroborated by Alos-Moya et al. (2014) where it is noted that longitudinal thermal expansion routinely exceeds the width of expansion joints. Paya-Zaforteza and Garlock (2012) also conclude that the inclusion of live-loading has negligible influence on the bridge response to fire, which was again confirmed by Alos-Moya et al. (2014). When considering axial restraint to replicate the effect of excessive thermal expansion, deflections were reduced, and failure occurred through excessive strains due to buckling (Paya-Zaforteza and Garlock 2012). Conversely, in an axially unrestrained model, larger deflections were observed, and failure occurred through excessive deflections (Paya-Zaforteza and Garlock 2012). The real fire scenario presented by Stoddard (2004) yielded a longer time to failure than the Eurocode hydrocarbon fire (Paya-Zaforteza and Garlock 2012). This indicates the Eurocode hydrocarbon fire may be too severe when uniform heating is considered.

Braxtan et al. (2015) conducted a preliminary analysis of a multi-span composite weathering steel box girder exposed to the Eurocode hydrocarbon fire. The largest noted difference between carbon and weathering steel properties was the loss of yield strength with temperature increase above 400°C for traditional steel and above ambient for weathering steel (Braxtan et al. 2015). The Eurocode hydrocarbon fire was considered in the midspan of the centre span and adjacent to a pier in an outer span; the effects of localization were considered by applying the fire intensity gradient created by Alos-Moya et al. (2014)

which decreased the fire intensity every five metres from the fire source (Braxtan et al. 2015). The midspan fire caused large deflections and stresses in the bottom flange while the fire close to the pier caused large stresses in the girder web and concrete slab (Braxtan et al. 2015).

Based on the steel girders modelled by Paya-Zaforteza and Garlock (2012), Peris-Sayol et al. (2015) use FDS modelling of a gasoline tanker truck fire and a thermo-structural model in ABAQUS to consider the effects of fire load position, structural boundary conditions, model scale (single element representation versus full bridge structure), vertical clearance, span configuration, and wind effects. It was found modelling the single most fire-exposed girder can approximate the full bridge response in terms of failure modes, critical temperatures, and time to failures (Peris-Sayol et al. 2015). Large axial forces were developed in the girders when longitudinal restraint was applied (Peris-Sayol et al. 2015); this is representative of the typical bridge response when expansion joint width is exceeded. A fire load in close proximity to the abutment increased member temperatures and reduced failure time when compared to fire at midspan due to reduced ventilation (especially in single-span bridges with abutments that can retain hot gases) and the Coandă effect (Peris-Sayol et al. 2015). Wind was found to reduce the effect of the fire but can also direct flames onto structural members depending on the fire load location (Peris-Sayol et al. 2015).

Aziz (2015) experimentally and numerically characterizes the response of steel bridge girders exposed to the ASTM E119 standard fire. Three ASSHTO-compliant steel bridge girders were simultaneously heated in a furnace recreating ASTM E119 and loaded by an actuator (Aziz 2015). The girders were found to fail after 30-35 minutes of heating with a rolled steel girder with web slenderness near 50 failing in flexural yielding and a steel plate girder with web slenderness greater than 100 failing in web shear buckling (Aziz 2015). Material tests informed reduction factors for the strength, modulus of elasticity, and post-heated strength, and guidance for high-temperature creep is suggested (Aziz 2015). Aziz (2015) proposed a methodology to determine the residual capacity of steel bridge girders exposed to fire that consists of:

1. Determining the ambient capacity of the girder using FEM modelling;
2. Exposing the girder to a fire scenario under appropriate loading and boundary conditions with elevated-temperature material properties; and
3. Allowing the girder to cool then loading incrementally until failure.

A parametric study by Aziz (2015) found that steel girders fail in under 20 minutes during exposure to hydrocarbon fires where failure is in flexural yielding or web shear buckling for web slenderness ratios of less than 40 or greater than 50, respectively. The presence of stiffeners does not enhance the fire resistance, however increasing axial restraint improves high-temperature flexural behaviour; including fire insulation is the most effective way to increase girder fire resistance (Aziz 2015).

Alos-Moya et al. (2017) present experimental results of a large-scale composite steel-concrete bridge with two abutments supporting a composite steel deck with girders on bearings exposed to a real open-air gasoline pool fire. Fire exposure was characterized through a series of preliminary test fires that measured temperatures at varying heights above the fire, measured the fuel mass loss rates, and concluded winds above 2 m/s affected flame behaviour substantially (Alos-Moya et al. 2017). The bridge was exposed to varying fire sizes at the midspan and adjacent to an abutment (Alos-Moya et al. 2017). Although the fire load considered in this study is smaller than that of a tanker truck fire (upwards of 72 MW per Babrauskas 2016), Alos-Moya et al. (2017) report that the severity of fire is acceptable since:

1. The bridge was required to withstand multiple tests without significant damage;

2. The steel girder temperatures were found to be similar to those of real fire events;

3. The fire load was sufficient to impinge a flame on the bridge deck; and

4. Safety concerns rendered a large fire unfeasible.

The mass loss rate was similar to predicted values, however the effect of moving the fuel pan closer to the bridge deck increased the mass loss rate due to an increase of heat radiating back into the pan, while moving the pan closer to the abutment decreased the mass loss rate (Alos-Moya et al. 2017). There was little difference between the web and bottom flange temperatures of the steel girders in any fire scenario, but the top flange was significantly cooler (Alos-Moya et al. 2017). Both gas and steel temperatures varied significantly in the longitudinal direction (Alos-Moya et al. 2017). Non-negligible wind speeds reduced observed deflections and decreasing the distance between the fire source and the bottom steel flange increased deflections (Alos-Moya et al. 2017).

Hu et al. (2018) used ABAQUS modelling of a two-span steel bridge to examine the effect of bridge skewness and abutment restraint of the fire response of the structure. A fire duration of 20 minutes was chosen on the basis that failure is typically induced within this period (Kodur et al. 2012) and it was assumed a fire under one span would not influence the adjacent span (Hu et al. 2018). In general, skew bridges yield a stiffer response to fire as a result of two-way action developed by the varying stiffness in girder members (Hu et al. 2018).

Whitney et al. (2018) conducted a two-dimensional parametric study of the girder properties in a steel bridge exposed to ASTM E119 in ABAQUS. The influence of global girder section factor, steel flange and web thicknesses, steel material properties, concrete slab width and thickness, applied intumescent paint, and spray-applied insulation thickness on the heat transfer through the bridge cross-section was studied (Whitney et al. 2018). Increasing girder web thickness and introducing either intumescent paint or spray-applied fire insulation were the most effective parameters in reducing cross-sectional temperature while the

influence of alternative carbon steel material properties and increasing concrete slab thickness had little benefit (Whitney et al. 2018).

### 3.2.4 Structural Fire Response of Cable-Supported Bridges

Cable-supported bridges often have a primary function in the surrounding community and their stability can also have important life safety consequences to users and staff (Kotsovinos et al. 2016a). Naturally the most susceptible to a fire on the deck of the bridge members for cable supported bridges are the pre-tensioned structural cables. Although the fire performance of cables would be similar to that of the cables used in other structures such as stadia or Ferris wheels, limited research has been undertaken to date to describe their thermo-mechanical behaviour. This section presents relevant research on the topic of cable supported bridges in Table 3.5 followed by a more detailed discussion of significant literature. The detailed thermo-mechanical response of structural cables at component level (Atalioti et al. 2017) is outside the scope of this chapter and is reviewed more specifically in Chapter 5 of this thesis.

Table 3.5. Relevant literature on the effect of fire on cable-supported bridges.

| Study Title | Author(s) (Year) | Research Topic | Summary |
|---|---|---|---|
| Evaluation of the Impact of Potential Fire Scenarios on Structural Elements of a Cable-Stayed Bridge | Bennetts and Moinuddin (2009) | Heat transfer modelling of various fire exposures to insulated and uninsulated steel stay-cables | Developed heat transfer models found the presence of a thin mineral wool insulation would likely protect the stay-cables from extreme temperatures for the duration of the fire scenarios considered. Uninsulated cables reach high temperatures quickly. |
| Study on Thermal and Structural Behaviour of a Cable-Stayed Bridge | Liu et al. (2012) | Heat transfer and structural analysis of a cable-stayed bridge in ANSYS | The cable-stayed bridge was found to be vulnerable to a variety of fire scenarios. The authors note a difficulty in characterizing the fires produced from gasoline trucks. |
| Safety of Cable-Supported Bridges During Fire Hazards | Gong and Agrawal (2016) | Structural response to a fire scenario was studied for cable-stay, anchored suspension, and self-anchored suspension bridges using non-linear FEA. | Vulnerability was dependent on fire location and level of existing axial force. Self-anchored suspension bridges were most vulnerable due to large thermally-induced axial forces in the deck. Cable-stayed bridges had longitudinally-varying induced axial forces. |
| Assessing the Fires on the Deck of Cable Stayed Bridges | Kotsovinos et al. (2016b) | A design-based approach to characterize fires for cable-stayed bridges | Authors present an approach to assess the fire hazard and risk on a cable-stayed bridge. Multiple vehicle design fires are discussed as well as goals of fire protection and constraining factors considered in the assessment. |

| Study Title | Author(s) (Year) | Research Topic | Summary |
|---|---|---|---|
| Experimental Study of Epoxy Coatings for Fire Protection of Bridge Cables | Tolstrup et al. (2019) | Material testing of fire protection materials for cable members | Cone calorimetry tests of various intumescent epoxy coatings provided information about the development of char and the role of elastomer membranes in the system. |
| Heat Transfer on a Disk: A Closed-Form Solution for Suspension Bridge's Main Cables Exposed to Fire | Sloane and Betti (2019) | Development of an analytical mathematical solution for the heat transfer in a suspension cable | The authors present a normalization and non-dimensionalization procedure for the case of a main suspension cable exposed to a hydrocarbon fire and develop a closed-form solution for the heat transfer of the member. |
| Static Performance of a Long-Span Concrete Cable-Stayed Bridge Subjected to Multiple-Cable Loss during Construction | Zhang et al. (2020b) | ABAQUS modelling of a bridge fire event on a cable-supported bridge | The authors review the fire incident on the Chishi bridge which resulted in the gradual loss of nine consecutive cable members. Using ABAQUS, the authors use measured deflections and field notes from the fire event to recreate a structural model of the bridge. The observed structural responses of the bridge deck, girder, cables, and pylon are matched well by the model. Torsion and biaxial bending resulted in severe cracking in the slab and web of some concrete girders. The undamaged cables were found to not have undergone any plastic deformation but approached 93% of the wire yield strength. The concrete girders approached 84% of the crushing stress. Tension redistribution from ruptured cables was found to occur predominately to adjacent cables in the same plane. Opposing movement of pylon legs was observed before repairs which resulted in cracking of the transverse pylon beams. Of 23 cable pairs used on either side of the pylon, the loss of nine individual cables was insufficient to cause progressive collapse of the structure. |
| Stability Assessment of a Suspension Bridge Considering the Tanker Fire Nearby Steel-Pylon | Cui et al. (2020) | Fire modelling in FDS of a tanker truck fire coupled with thermo-structural modelling in ANSYS of a suspension bridge | The authors model a tanker fire using FDS and consider other fire scenarios in a thermo-structural model of a suspension bridge pylon tower. Results show the maximum stress values in pylon areas with temperatures between 300 and 400°C, with reduced stresses in hotter regions near 800°C. A critical fire suppression time of 30 minutes was determined which coincides with a significant drop in the stability coefficient of the tower. |

| Study Title | Author(s) (Year) | Research Topic | Summary |
|---|---|---|---|
| Fire Protection of Bridge Cables | Kragh et al. (2020) | Development of passive fire protection for suspension bridge cables | The authors use heat transfer modelling of suspension bridge main cables to determine potential cable temperatures. A passive fire protection retrofitting system is developed and tested in furnace conditions for a resistance rating of 50 minutes. A cost-benefit analysis determined passive fire protection is optimized on the lower 10 m of cable members. |
| Fire Performance of Structural Cables: Current Understanding, Knowledge Gaps, and Proposed Research Agenda | Kotsovinos et al. (2020a) | Literature review on the topic of the fire performance of structural cables | Considering structural cables specifically as an element, the authors review experimental and numerical literature on the fire performance of these elements. Future research topics are presented and include fire scenarios for cable-supported bridges, thermo-mechanical properties for large-diameter cable members, failure criteria, thermal deformations, cable terminal fire performance, material properties, fire protection products, and the role of sheathing and blocking agents. |

Bennetts and Moinuddin (2009) reviewed the potential fire scenarios a cable-stayed bridge may experience based on vehicle fires on the bridge deck. Three major fire cases are considered in their work:

1. HGV fire close to main support (towers) or cables;

2. Oil/flammable liquids tanker fire in same regions; and

3. Gas jet fire from a pipe fracture in a liquid natural gas (LNG) tanker impinging a cable.

Each fire case was applied in a 2-D thermal analysis of both a steel stay-cable and a welded steel box structure (representing a stay-cable tower). Fire properties from Pettersson et al. (1976), Shokri and Beyler (1989), and Beyler (2002), were used to model each fire scenario respectively. All fire scenarios consider radiation and convection and are two hours in duration. Stay-cables were modelled as a square configuration of two or three layers of lumped masses for both an uninsulated and insulated case (Bennetts and Moinuddin 2009). The insulated strand case was protected by a 13 mm thick mineral fibre blanket that was modelled with and without an air gap to the adjacent cable surface. Cable geometric factors such as air gaps and contact areas between wires were not considered in the thermal analysis. Bennetts and Moinuddin (2009) concluded the presence of the insulation layer would likely protect the cables from severe temperatures in all cases until the fire is extinguished. The uninsulated cables experience rapid temperature rise and would experience severe material degradation.

There is limited literature related to the analysis of bridge cables under thermal loads. Bundled strand construction can be difficult to analyse especially when the inclusion of lubricants or stopping agents within cable voids can make thermal and structural analysis non-intuitive and continuum mechanics more challenging to apply (Wright et al. 2013). However, detailed analysis approaches have been presented in the literature (Atalioti et al. 2017). Furthermore, bridge cables can lose significant strength under thermal loads. Strength gain from the cold drawing process is lost typically when steel approaches 600°C (Wright et al. 2013). Wright et al. (2013) hypothesized that, despite the most exposed surface cables reaching critical temperatures first in a fire, the yield deformation will be delayed due to load shedding via differential thermal expansion; heated perimeter wires will tend to expand more than interior wires but some strain compatibility through friction will be present and result in a load transfer to the interior. Based on this, overall cable elongation is expected to be minimal until internal cable temperatures rise. Post-fire cable evaluation will be dependent on the temperatures reached in individual wires however the post-fire strength may be approximated by using the average post-fire strength of all individual wires in a cable cross-section (Wright et al. 2013).

Gong and Agrawal (2016) examined the effect of various fires on the response of cable-supported bridge decks. The main factors to consider with respect to bridge deck stability in fires are material degradation from heating, additional loading due to thermal expansion, and additional bending moment due to thermal bowing (Usmani et al. 2001). Three cable-supported bridges, a cable-stayed, anchored suspension, and self-anchored suspension, are considered in thermo-structural analysis. Of the three bridge types, the self-anchored suspension bridge deck has the largest pre-existing axial compression force, which increases its susceptibility to thermal strains. Cable-stayed bridges have a distributed axial force along the length of the deck but are usually less than half of the compression of a self-anchored suspension bridge (Gimsing and Georgakis 2011). FDS was used to model fire scenarios resulting from a ship fire below the deck and a truck fire above the deck. ABAQUS was applied for the thermo-structural analysis. Gong and Agrawal (2016) conclude the critical nature of pre-existing and thermally-induced axial forces in cable-supported bridge decks. Anchored suspension bridges were the least vulnerable of the cases studied due to having no existing axial compression. Fire scenarios near the tower involved critical secondary load (P-delta) effects, especially in self-anchored suspension bridges (Gong and Agrawal 2016).

Similar to Bennetts and Moinuddin (2009), Kotsovinos et al. (2016b) present a number of potential fire scenarios on a bridge deck that could affect the thermal and structural response of a cable-stayed bridge; namely:

1. An HGV fire;

2. A petrol tanker fire arising from the early ignition of the fuel at the release location following puncture of the tank containing the fuel;

3. A pool fire on the deck of the bridge arising from the delayed ignition of the fuel spilled from the location of the localized failure/puncture of the envelope of the tank of a petrol tanker; and

4. A tanker transporting LNG resulting in pool/jet fires.

The potential for structural collapse of the cable-stayed bridge is estimated by considering the potential severity of the fire scenarios in terms of peak heat release rate and duration which can affect metrics such as flame length and structural member temperatures. A similar methodology is followed by Kotsovinos et al. (2016a) for potential fire scenarios below the deck of a cable-stayed bridge that could affect the steel girders and structural cables.

Zhang et al. (2020b) present modelling results in ABAQUS of the Chishi bridge which lost nine cables on the same plane from a fire in the pylon during construction. The damage did not initiate progressive collapse, but significant cracking was observed in the bridge deck and girders near the affected region, the undamaged cables were found to have reached approximately 90% of the yield strength, and the girders approached almost 90% of the ultimate crushing load. These authors' structural model did not consider a thermal component but was able to accurately recreated observed deformations from the event.

Kotsovinos et al. (2020a) provide a review of existing literature relevant to the fire performance of structural cables. These authors review research beginning with the thermal response of prestressing steel strands which have received more attention than larger diameter strands used in bridge infrastructure. State-of-the art information is presented on the material properties, thermal expansion, wire load shedding, creep and relaxation, and connection terminals of steel cable members. Experimental and numerical literature on the fire performance of large-diameter cable members is also reviewed in addition to industry standards on the topic. Kotsovinos et al. (2020a) conclude by suggesting key topics for future research.

### 3.2.5 Structural Fire Response of Concrete Bridges

The fire response of concrete bridge structural members is a relatively under-researched topic, likely due to concrete's assumed inherent fire resistance capacity. This section presents relevant literature on the response of concrete bridge members exposed to fire in Table 3.6.

Table 3.6. Relevant literature on the effect of fire on concrete bridges.

| Study Title | Author(s) (Year) | Research Topic | Summary |
|---|---|---|---|
| Deflection for Pre-Stressing Concrete Thin-Wall Box Girders Under Action of Multi-Span Loads Exposed to Fire | Zhang et al. (2012) | Numerical modelling of a four-span prestressed concrete box girder bridge exposed to the ISO standard fire in varying regions | The general deflection response of the bridge is presented for each region of heating considered. |
| Damage Assessment of One Pre-Stressed Concrete Bridge after Fire | Xiang et al. (2013) | Damage assessment of a prestressed concrete bridge exposed to a vehicle fire | Application of qualitative observation-based post-fire damage assessment methods to determine concrete damage. An estimation of bridge residual capacity is presented. |
| Assessment and Repair of a Fire-Damaged Pre-stressed Concrete Bridge | de Melo et al. (2014) | Review of the damage assessment and repair of the Dean's Brook Viaduct prestressed concrete bridge | Four concurrent stages were undertaken to expedite the repair of the bridge. A recount of the detail damaged assessment tests conducted to assess post-fire material properties is presented. There was no significant loss in tendon prestress in areas where concrete cover remained. Exposed tendons had only localized prestress loss. |
| Post Fire Guidance for the Critical Temperature of Prestressing Steel | Robertson and Gales (2016) | High temperature experimental tests of prestressing steel for post-tensioned concrete are presented. | Residual steel strength tests over multiple high temperature ranges found conventional guidance for prestressing steel may not be conservative. Revisions to guidance are suggested. |
| Structural Fire Performance of Contemporary Post-Tensioned Concrete Construction | Gales et al. (2016a) | Detailed experimental study considering the fire performance of post-tensioned concrete members and prestressing strands | This project outlines procedures for testing post-tensioned concrete in fire, findings of structural fire experiments, and recommendations for designers. The article is the most up to date literature review of available testing in the public domain and addresses the performance of prestressed concrete bridge girders throughout. |
| Behaviour of Prestressed Concrete Box Bridge Girders under Hydrocarbon Fire Condition | Zhang et al. (2017) | ANSYS modelling of a prestressed concrete box girder exposed to the ASTM hydrocarbon pool fire | Modelling of the box girder bottom flange and web elements were shown to have very similar temperatures for all fire exposures. Girder deflection is characterized in four stages. Vertical deflections are found to decrease after a degree of heating due to prestressing tendons resisting thermal expansion of the concrete. The degree of prestressing is shown to have a significant role in deflection behaviour. |

| Study Title | Author(s) (Year) | Research Topic | Summary |
|---|---|---|---|
| Performance of Prestressed Concrete Box Bridge Girders under Hydrocarbon Fire Exposure | Song et al. (2020) | ANSYS modelling of a prestressed concrete box girder exposed to the ISO hydrocarbon pool fire | Numerical modelling validated by scaled furnace testing a box girder is able to replicate the response of the element exposed to a hydrocarbon fire. The degree of loading, concrete cover, and prestress were found to have significant effects on the fire response of the girder. Deflection-based and moment capacity-based failure criterion may be more applicable than a rate of deflection-based criteria. |

Gales et al. (2016a) reviewed contemporary issues with post-tensioned concrete in fire and specifically the behaviour of pre-stressing steel at elevated temperatures. Gales et al. (2016a) introduced a test program for analysing the fire behaviour of prestressing steel which is influenced from results of tests on girders used for informing bridge performance. Guidelines for practitioners in assessing post-tensioned concrete after fires are discussed. Although experiments were not specifically for bridge girder structures, they provide insight into load-induced thermal straining (LITS) and tendon performance. Robertson and Gales (2016) follow this with a comprehensive literature review of bridge fires of prestressed concrete and post-fire mechanical testing of prestressing wires exposed to a range of fire severities, noting spalling and current methodologies for post-fire material evaluation being insufficient and in need of further study.

Zhang et al. (2017) conducted modelling of a prestressed concrete box girder exposed to the ASTM E1529-14a large hydrocarbon pool fire (ASTM 2014) uniformly along its length in ANYSYS. Web and bottom flange elements were shown to have approximately the same temperatures for all fire durations considered and after 120 minutes of exposure web and bottom flange temperatures (included prestressing steel) exceed 450°C (Zhang et al. 2017). Zhang et al. (2017) found the vertical deflections of box girders take place in four distinct stages:

1. Linear increase in deflections due to thermal expansion (independent of applied loads);
2. Slight decrease in deflections as prestressing strands resist thermal expansion of bottom concrete flange;
3. Non-linear increase in deflections as material properties degrade; and
4. Rapid increase in deflections due to further material degradation and high-temperature creep in the prestressing strands.

The degree of prestressing has a significant role in high-temperature response. Zhang et al. (2017) associated lower prestressing with a more rapid deflection increase in the first stage, a longer duration for which downward deflection is reversed and reduced hogging rates in the second stage, more significant

creep and more rapid deflection increase in the third stage, and larger and more rapid deflections in the fourth stage.

### 3.2.6 Structural Fire Response of Polymer Bridges

Elevated temperatures are known to have severe effects on the performance of fibre reinforced polymer (FRP) members due to the effects of glass transition which compromises the structural properties of the polymer matrix and reduces composite action between glass, aramid, or carbon fibres with the resin. Similarly, fire can result in charring or combustion of timber members and, in the case of engineered timber members, adhesive degradation. Due to the lack of fire resistance requirements for bridge structural members, polymer members or reinforcements (including both timber and FRP) can be often applied in bridge infrastructure with little attention to the fire performance of the system. This section details the limited research studies conducted in examining the fire performance of polymer bridge members in Table 3.7 followed by a discussion of significant literature.

Table 3.7. Relevant literature on the effect of fire on FRP-reinforced bridges.

| Study Title | Author(s) (Year) | Research Topic | Summary |
|---|---|---|---|
| Temporal Thermal Behaviour and Damage Simulations of FRP Deck | Alnahhal et al. (2006) | ABAQUS modelling of a bridge consisting of FRP bridge deck exposed to an oil fire in varying regions | The worst-case scenario was determined to be a truck fire above the bridge deck which caused failure in under 7.5 minutes. The most critical factors for the fire performance of FRPs are thermal conductivity, coefficient of thermal expansion, resin type, and glass fibre type. |
| Numerical Study of FRP Reinforced Concrete Slabs at Elevated Temperature | Adelzadeh et al. (2014) | Modelling of concrete slabs reinforced with GFRP rebar exposed to the ASTM standard fire | The study found the concrete cover thickness has a significant effect on the fire resistance of the member. The temperature-domain method based on steel reinforced members in fire is not fully applicable to GFRP reinforced members. |
| Fire Test of FRP Members Applied to Railway Bridge | Cabova et al. (2016) | Experimental tests of FRP panels for use in railway bridge decks | Fire tests intended to simulate burning electrical cables were found to have negligible impact on the FRP. The majority of FRP panel configurations were able to support live loads post-fire. |
| Evaluating Fire-Damaged Components of Historic Covered Bridges | Kukay et al. (2016) | National technical report on the assessment and fire protection of heritage timber covered bridges. | The authors reviewed the thermal response of heritage timber in fire and discuss the analysis of fire damaged timber members. Post-fire assessment tests are reviewed in addition to rehabilitation procedures. Methods for fire protecting existing bridges are presented. |

| Study Title | Author(s) (Year) | Research Topic | Summary |
|---|---|---|---|
| Performance of CFRP-Strengthened Concrete Bridge Girders under Combined Live Load and Hydrocarbon Fire | Beneberu and Yazdani (2018) | Large-scale experimental study of a bridge span support by three prestressed concrete girders reinforced with varying CFRP wrapping and fire insulation | Authors distinguish the differences between standard and realistic fire testing in the context of bridge fire research experiments. The majority of concrete spalling was hypothesized to be a result of thermal shock via wind-induced fire temperature variations. |
| Residual Strength of CFRP Strengthened Prestressed Concrete Bridge Girders after Hydrocarbon Fire Exposure | Beneburu and Yazdani (2019) | Experimental structural testing of full-scale CFRP-reinforced prestressed concrete girders after exposure to a large hydrocarbon pool fire | The authors test three fire-damaged prestressed concrete girders to assess post-fire residual flexural strength. Two of three girders were reinforced with a CFRP wrap prior to fire exposure. One of these girders also included applied fire-protection material. The third girder was unreinforced and unprotected. The unprotected CFRP girder lost 59% of its theoretical flexural strength. The fire-protected CFRP girder did not experience any reduction in flexural capacity but failed in CFRP debonding, contrary to the predicted failure mode in relevant guidelines. |
| Post-Fire Performance of GFRP Stay-in-Place Formwork for Concrete Bridge Decks | Nicoletta et al. (2019) | Experimental study investigating the post-fire mechanical behaviour of GFRP stay-in-place formwork reinforced concrete beams following hydrocarbon pool fire exposure and simulated fire damage. | The GFRP-concrete beam experienced no loss in strength after a 14-minute heptane pool fire and moderate damage to the GFRP reinforcement. Evidence of thermally-induced non-linearities in structural performance are presented. |

Little research has examined the effect of fire on polymer bridge elements. Early numerical models of FRP bridge decks have shown the most influential material properties in determining fire performance are the thermal conductivity, coefficient of thermal expansion, polymer resin type, and glass fibre type (Alnahhal et al. 2006). Experimental tests of FRP and glass fibre reinforced polymer (GFRP) bridge decks (Alnahhal et al. 2006; Nicoletta et al. 2019a) have shown good fire resistance properties for small-scale fire exposures, however evidence of complex interactions between GFRP reinforcement and concrete as a result of heating have been identified by Nicoletta et al. (2019a) that require additional research.

Large-scale experimental fire tests on carbon fibre reinforced polymer (CFRP) reinforced prestressed concrete bridge girders by Beneberu and Yazdani (2018) provide information on the vulnerability of both adhered CFRP wrapping and prestressed concrete to realistic fire exposures. The test bridge consisted of three prestressed concrete girders reinforced: one control girder, one CFRP-wrapped girder, and one fire-

protected CFRP girder; the girders supported precast deck panels and a cast-in-place deck (Beneberu and Yazdani 2018). Fire was inflicted via a hydrocarbon pool fire in a 6.10 m by 3.05 m pan with a volume of 4.23 $m^3$ at a height of 1.2 m below the bottom of the concrete girders for a duration of one hour. Thermocouples recorded a peak fire temperature of over 1100°C with some wind-induced temperature variations exceeding 600°C between 2.3 and 3.3 minutes into the test (Beneberu and Yazdani 2018). The girders were significantly damaged by the fire exposure. Beneberu and Yazdani (2018) observed that the glass-transition temperature of CFRP epoxy was exceeded within 41 seconds of ignition and CFRP debonding occurred after 6 minutes. Approximately 25% of the concrete volume was lost due to spalling resulting from thermal shocking via large temperature fluctuations early in the test (Beneberu and Yazdani 2018). Multiple prestressing strands were found to be fractured and exposed; the fire protection was effective in keeping CFRP-concrete interface temperatures below the glass transition point and protecting concrete and steel elements (Beneberu and Yazdani 2018). In subsequent work, flexural testing of the prestressed concrete girders by Beneberu and Yazdani (2019) assessed the residual strength following the fire exposure. It was found that the unprotected CFRP-reinforced girder lost 59% of its theoretical flexural strength while the fire-protected CFRP-reinforced girder experienced no reduction in flexural capacity (Beneberu and Yazdani 2019). The fire-protected CFRP-reinforced girder did however experience CFRP debonding which is contrary to the American Concrete Institute (ACI) guidelines which predict a failure mode involving prestressing steel yielding and CFRP wrapping failing in tension (Beneberu and Yazdani 2019). Beneberu and Yazdani (2019) highlight the potential risk of failure facing prestressed concrete I-girders that are exposed to hydrocarbon pool fires.

While timber is considered a polymer alike to FRPs, there is limited fire research available regarding this type of infrastructure. The sole publication on the topic by Kukay et al. (2016) provides a comprehensive approach to assessing, rehabilitating, and designing small-scale covered timber bridges for fire scenarios and includes test procedures for fire-damaged timber members, but no work has been done to expand research on the topic to other timber bridge types such as trestles. For example, there is limited to no guidance available within the recently published Wood Bridge Reference Guide in Canada pertaining to the fire design of timber bridges (Woodworks 2019). The fire performance of timber bridges is a research need particularly within the context of vulnerable transportation networks for wildfire community evacuations where smaller timber bridges may be relied on. The author highlights potential flammability aspects where ember generation in a wildfire is a credible scenario for a loss of a timber bridge.

## 3.3 Implications for Bridge Fire Experimentation

Bridge fire experiments are rare due to high costs and safety and environmental concerns. Many institutions lack the size of fire testing and load-inducing equipment required to test bridge structural systems at a

meaningful and credible scale. Large-diameter hydrocarbon pool fires can be one of the most severe and realistic exposures a bridge may experience in its lifetime (Peris-Sayol et al. 2017). Fire experiments that make use of non-standard open-hydrocarbon pool fires are even rarer despite yielding results that would be otherwise unobtainable (Alos-Moya et al. 2017; Beneberu and Yazdani 2018). For example, experimental tests have shown that the natural variations in open-air hydrocarbon pool fire temperatures exacerbate the spalling of prestressed concrete as a result of thermal shocking (Beneberu and Yazdani 2018). There is contention among researchers working on the fire safety of bridges as to the applicability of furnace testing with standard fire curves (such as ASTM E119, ISO 834, and the Eurocode standard fires) and open-air fire testing with realistic (but less easily characterized) non-standard fires. Readily characterized furnace tests facilitate numerical modelling validation while non-standard fire tests replicate realistic structural responses that would not be realized in standard fire tests. Many researchers have emphasized the inapplicability of standard fire curves due to a failure of these curves to capture the cooling phase (Kodur et. al 2010; Paya-Zaforteza and Garlock 2012; Beneberu and Yazdani 2018), temperature variation (Alos-Moya et al. 2014; Alos-Moya et al. 2017; Beneberu and Yazdani 2018), maximum member temperatures (Wright et al. 2013), localized nature (Alos-Moya et al. 2014; Alos-Moya et al. 2017; Beneberu and Yazdani 2018; Hu et al. 2018), intensity (Paya-Zaforteza and Garlock 2012; Beneberu and Yazdani 2018), and rapid temperature increase (Beneberu and Yazdani 2018), created by large, open-air, hydrocarbon pool fires. Furnace tests also fail to consider the influence of fuel load position, vertical clearance, and longitudinal temperature gradients. The applicability of the Eurocode hydrocarbon fire has been questioned as well on the basis that it fails to represent the peak temperatures achieved in more realistic hydrocarbon fire curves such as that proposed by Stoddard (2004) (Paya-Zaforteza and Garlock 2012) but may be too severe when uniform heating is considered (Paya-Zaforteza and Garlock 2012; Hu et al. 2018). Alos-Moya et al. (2014) suggest Eurocode standard and hydrocarbon fires are only applicable in short-span bridges where fire localization is less critical. The use of localized fire exposures is critical in determining the structural response of medium and long-span bridges since bridge failure modes vary depending on if heating is uniform or localized. Under localized exposure, local failures from extreme heating have been shown to occur before global failures due to excessive deflection (Wang and Liu 2016) which may not be the general case under uniform heating. Axial elongation of bridge structural members has been identified as a critical effect since typical expansion joint widths are not sufficient to prevent contact with abutments or adjacent bridge spans in a fire (Giuliani et al. 2012; Paya-Zaforteza and Garlock 2012; Woodworth 2013; Wright et al. 2013; Gong and Agrawal 2016). This has also been reported in actual bridge fire events (Godart et al. 2015; Zobel et al. 2016). Furnaces can practically support limited spans of samples in the order of a few metres. Axial elongation is proportional to the length of heating along a bridge, therefore uniform heating will produce unrealistic thermal expansion value compared to localized fires.

Despite the limitations introduced by standard fire testing in bridge fire applications, high temperature data of bridge structural systems is still valuable in validating models and investigating controlled failure modes. Bisby et al. (2013) and Gales et al. (2012) make a similar argument with respect to building fire testing in which the applicability of standardized fires diminishes with increasing scale and complexity of experimentation. Based on Bisby et al. (2013), the opposite can be said where standardized fires gain applicability for smaller systems where specific behaviours such as flexural behaviour and material properties can be studied without complicating factors. The above limitations arise when standard fires are applied to large-scale bridge structural systems. This is known as "consistent crudeness" coined by Platt et al. (1994) and Buchanan (2001) where it is suggested researchers must strive for a consistent level of fidelity or reality in how structures and their respective fires are considered. As experimentation is rare, this methodology can be applied to modelling endeavors as well.

## 3.4 Knowledge Gaps and Future Research Targets

Further research to develop bridge fire resilience framework is needed. The author has addressed this need by proposing a framework in previous studies that has a basis for determining and ensuring operational resilience. This framework for improving the fire resilience of bridge infrastructure is as follows (Nicoletta et al. 2018):

1. Increase bridge inspection scope to determine the significance of individual bridges to the overall transportation network in the event of a fire induced structural failure;
2. Determine bridge vulnerability to potential fires following a detailed fire hazard identification process and engagement with all stakeholders;
3. Identify critically vulnerable bridges and the associated fire risk based on the performance requirements set by the relevant stakeholders; and
4. Make design and retrofit guidance on improving bridge fire resistance available to practitioners. Post-fire review requirements must also be established.

While the authors have focused specific attention into commonly used materials, there exists other material types that need further investigation as they are also considered in normal practice. Specifically based upon the literature review provided herein future research areas suggested by the authors are presented in Table 3.8.

Table 3.8. Required research for the development of bridge fire resilience framework.

| Topic | Suggested Research |
|---|---|
| Fire Hazard and Risk Assessment Framework | • Development of a robust incident reporting system to gather statistical data on bridge fires<br>• Analysis of the economic considerations of bridge fire resilience considering direct and indirect losses<br>• More sophisticated tools are needed to assist designers in establishing credible bridge fire scenarios<br>• Development of more robust residual strength assessment and repair strategies for bridge structural types |
| Bridge Fire Scenario Modelling | • Development of clear and consistent criteria to establish realistic fire exposures for bridge infrastructure<br>• Examination into what constitutes a localized fire for bridge structures |
| Steel Bridges | • Experimentation towards steel girder behaviour under hydrocarbon fire exposures to consider the effect of extreme localized heating, the global bridge response under non-uniform heating in the transverse direction, the post-fire strength, and the effect of rapid localized steel quenching from firefighters.<br>• Experimental research into the influence of varying structural steel types<br>• A study into the effects of localized fire in steel box girders |
| Cable-Supported Bridges | • Information is needed concerning the thermal expansion and other high-temperature responses of steel cables of varying configurations like locked-coil, parallel, and spiral structural strands<br>• Examination into the risk of cable uncoiling as a result of thermal expansion and loss of tension<br>• A study towards the influence of lubricants and stopping agents on the fire performance and resistance of cable members<br>• Analysis of the global structural response of cable-supported systems in terms of load shedding to adjacent unheated cables in fire scenarios |
| Concrete Bridges | • A study towards the fire response of aging and disrepaired concrete bridges<br>• Guidance development to assess prestressed concrete bridges postfire |

| Topic | Suggested Research |
|---|---|
| Polymer Bridges | • Examination of the high temperature interactions between FRP-reinforcements and concrete in bridge applications<br>• A study of the influence of exposed and flammable GFRP reinforcements contributing to fire severity<br>• Experimental research towards consider timber bridges which have had very little attention in the context of bridge fire safety |

## 3.5 Conclusions and Recommendations

This chapter provided a state of the art review of the research conducted to date on the topic of bridge fires in effort to summarize key findings and make available the most relevant information for practitioner and researcher use. The key research themes considered are the determination of bridge fire risk and hazard and the structural response of various bridge structural and material types. While this approach has generated a specific guide for priority areas of research focus the fire practitioner could consider, some limitations to the author's approach must be acknowledged. Material innovations are emerging that are being considered for this infrastructure type such as prestressed timber. These topics must be considered for fire research as well though, to the knowledge of the authors, have not been considered by the research community nor has the fire performance of timber trestles or other common timber bridge types. In addition, most fire design frameworks appear to be generated to deal with the concept of fire resistance. In the authors' opinion, this approach (originally coined for buildings and not infrastructure) has a degree of incompatibility to the expected function of bridge structures (for example, the expected thermal boundary that should be utilised). It is advisable that the fire practitioner community develop an agreed-upon consensus document on establishing a proper testing protocol for this infrastructure type as second-stage research. This should work towards establishing an experimental centre for research that can specifically procure the needed equipment to assess the fire hazard from an experimental view. Some labs are in existence that deal with scale at ambient temperatures, but they are not designed to handle the fire case. This may not be without difficulty giving the expense such an endeavour would have. While the author has reviewed articles available in the English language, non-English literature may also have valuable test and data that can be considered, and the reader is encouraged to explore these to build upon this research framework provided herein.

# Chapter 4: Postfire Exposure Performance of GFRP Stay-in-Place Formwork for Concrete Bridge Decks

## 4.1. Introduction

Bridges represent some of the most critical infrastructure in society, acting as vital transportation links for the movement of people and goods. The rapid development of transportation infrastructure, combined with an increasing volume of transported hazardous/ flammable materials, makes bridge fires a widespread concern (Garlock et al. 2012). Although rapid evacuations of bridge spans during fires allow life safety objectives to be met relatively easily, the materials and structural systems of bridges are rarely designed to limit economic losses, which can be substantial in the event of bridge closure or collapse.

In recent years, there has been a rise in the use of advanced composite materials such as glass fibre–reinforced polymers (GFRPs) in civil engineering applications. One innovative application of GFRP composites is the use of stay-in-place permanent formwork for reinforced concrete (RC) structural elements. The benefits of pultruded GFRP composite formwork include a high strength-to-weight ratio, resistance to corrosion, availability in a variety of configurations, and reduced construction time when compared to traditional formwork. Specifically, the corrosion resistance and reduced labor have made pultruded GFRP stay-in-place formwork popular in bridge deck construction where harsh environments will accelerate the corrosion of steel reinforcement (Nelson and Fam 2014a).

In past research, many GFRP stay-in-place cross sections have been studied for bridge deck applications, including protruding box sections, hollow cavities, and corrugated sheets (Nelson and Fam 2013, 2014a, b). This paper focuses on a GFRP stay-in-place form that features a base plate with T-shaped ribs protruding upward, aptly named T-Up formwork. The T-Up ribs in this variation span the deck transversely to traffic and between girders. Due to the limited width of forming dies in the pultrusion process, GFRP stay-in-place forms are designed to be spliced together with mechanical or adhesive fasteners. Figure 4.1 demonstrates a typical span of a bridge deck reinforced with the spliced GFRP formwork used in this study. GFRP stay-in-place forms are built in the same manner as traditional formwork but remain composite with the concrete as part of the structural member. In this configuration, the underside of the bridge deck and GFRP soffit is exposed to damage from fire or vandalism from below.

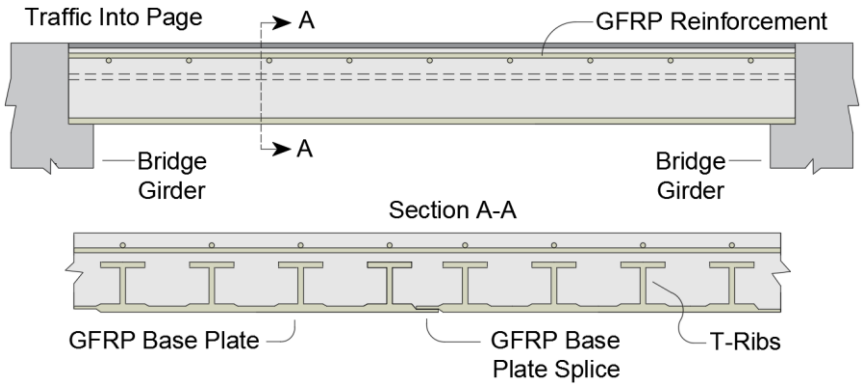

Figure 4.1. Typical configuration of GFRP stay-in-place T-up formwork.

Due to the variable nature of GFRP fabrication, there exists an extremely wide variety of structural applications, many of which have not yet been studied in terms of fire performance. Despite the numerous structural applications of GFRPs, previous studies investigated the mechanical behaviour, fire resistance, and modeling strategies of pultruded GFRP members including bridge decks, beams, and columns, among others (Correia et al. 2010, 2013, 2015; Gibson et al. 2006; Bai et al. 2010; Morgado et al. 2015, 2018a, b; Yanes- Armas et al. 2016, 2017). Little to no fire testing has been conducted in connection with GFRP stay-in-place formwork systems. In general, the lack of information affecting some GFRP applications' performance in fire is a major issue inhibiting their widespread use (Morgado et al. 2015). To the author's knowledge, this study is the first fire exposure test involving a concrete-GFRP stay-in-place formwork member, and for this reason, conducting an extreme in-fire test with no prior knowledge of the system's response to fire might be premature. Ultimately this study focuses on the mechanics of a fire-damaged GFRP system in order to provide direction for future studies that will consider a wider variety of in- and postfire testing with more severe damage and aim to establish fire resistance ratings for the system. This research aims to examine the structural contribution of GFRP stay-in-place formwork in a bridge deck that has been damaged by a small pool fire from below. Fire damage is also simulated in varying spans to allow for a direct analysis of the GFRP stay-in-place formwork's structural contribution.

## 4.2. Background and Motivation

In the context of this thesis, this test program serves to examine the use of a pool fire exposure to fire test bridge structural members. Although the fire exposure in this study is limited in scale, the methodology serves to inform future studies seeking to apply larger-scale tests.

The structural performance of GFRP stay-in-place formwork in applications for RC bridge decks has been studied in detail in the literature, and researchers have successfully examined failure modes, behavioural mechanics, the effect of form splicing, and the impact of freeze–thaw cycles (Nelson and Fam 2014a, b,

2013; Boles et al. 2015; Honickman et al. 2009). However, little to no large or small-scale testing has been done to quantify the structural impact of fire damage on GFRP stay-in-place forms.

In terms of mechanical performance, the material's glass fibres have been shown to retain strength at relatively high temperatures. The GFRP in this study uses E-glass fibres, which have a softening temperature of approximately 850°C (Correia et al. 2015). However, the GFRP's polymer resin is more sensitive to high temperatures than the glass fibres due to the effect of glass transition, an important parameter influencing the fire performance of GFRP composites. Glass transition temperature is the temperature at which a resin matrix transitions from a solid to a soft rubberlike consistency and loses its mechanical strength. For many GFRP composites this temperature is typically between 60°C and 140°C (Correia et al. 2013). After exceeding this temperature, composite action between the glass fibres and the epoxy resin is guaranteed to be lost if not already compromised before such a point, reducing the stiffness of the GFRP (Correia et al. 2015). If temperatures increase further and reach the decomposition temperature, the GFRP resin may ignite if it is exposed and has vaporized, potentially contributing to the growth of a fire under specific conditions (Gales et al. 2016c). While some more chemically advanced composites can yield strong performance in fire, these hazards can be especially prevalent in economical and chemically simple GFRPs.

In addition to the research needs on this topic, this research was preceded by a material study conducted by Gales et al. (2016c), which used a cone calorimeter to test several commercially available GFRP stay-in-place formwork samples and determine fire reaction characteristics. These parameters are of particular interest in bridge applications because the GFRP form makes up the soffit of the bridge deck and could be exposed to fire from below. Figure 4.2 below demonstrates the typical burning sequence of the GFRPs in the cone calorimeter tests. The underlying glass fibre structure can be seen as the GFRP resin decomposes, vaporizes, and ignites. After flame-out, a char layer was observed in all tests. Table 4.1 gives the material and fire reaction properties for the GFRPs used in the study (Gales et al. 2016c). Sample 1C is the GFRP material discussed herein and was tested by the author in accordance to the former test program. Samples 1A, 1B, and 1C were all specified to contain no fire retardants; however, a scanning electron microscope (SEM) microstructural analysis with energy dispersive spectroscopy indicated that Samples 1A and 1B may have contained an active fire retardant agent despite manufacturer specifications. This agent is hypothesized as an aluminum trihydroxide filler. A previous study using the same GFRP stay-in-place formwork as this program found the glass transition temperature of the material to be 109°C when tested in accordance with ASTM E1356-08 (Fam et al. 2016). As shown in Table 4.1 and as observed by Gales et al. (2016c), GFRP thickness plays an important role in the heat transfer, vaporization, and fire chemistry of a sample. A thermally thick sample demonstrates a longer time for the resin to decompose and ignite. Gales et al.

(2016c) hypothesized that, in the case of a thermally thick GFRP plate heated from below (a typical configuration for a GFRP stay-in-place formwork bridge deck), the resin is likely to decompose and fall off of the structure before igniting in place and influencing fire spread.

Table 4.1. GFRP stay-in-place formwork test configurations and selected fire reaction polymer test results with 50 kW/m$^2$ incident heat flux. Adapted from Gales et al. (2016c).

| Sample | Test Configuration | | | Test Results | | | |
|---|---|---|---|---|---|---|---|
| | Resin Type | Manufacturer Specified Fire Retardant | Thickness (mm) | Ignition Time (s) | Flameout Time (s) | Mass at Ignition (g) | Mass after Flameout (g) |
| 1A | Polyester | No** | 3.6 | 72 | 410 | 77.8 | 55.3 |
| | | | | 67 | 423 | 76.9 | 55.2 |
| 1B | | No** | 9.5 | 187 | 1091 | 180.0 | 129.2 |
| 1C* | | No | 13.7 | 91 | 1875 | 235.0 | 157.2 |
| | | | | 109 | 1880 | 235.0 | 161.0 |
| 2A | | Yes | 6.1 | 80 | 671 | 111.0 | 73.1 |
| | | | | 97 | 619 | 110.7 | 72.2 |
| 3A | Vinylester | Yes | 4.1 | 86 | 300 | 62.5 | 38.5 |
| | | | | 109 | 411 | 60.1 | 36.5 |

* GFRP stay-in-place formwork used in this study.
** may have contained an active fire retardant despite manufacturer specification.

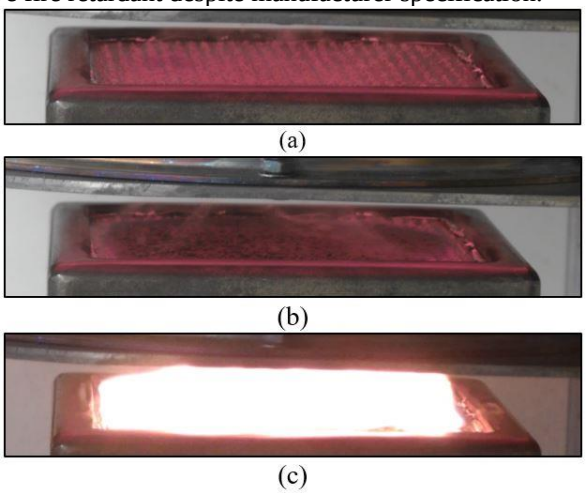


Figure 4.2. GFRP stay-in-place formwork cone calorimeter testing sequence: (a) decomposition of GFRP resin; (b) resin vaporization; and (c) ignition.

## 4.3. Experimental Program

### 4.3.1 Test Specimens and Fabrication

An experimental program was developed to quantify the structural contribution of damaged GFRP stay-in-place T-Up formwork in one-way bending. The test specimens represent strips of concrete bridge deck reinforced with GFRP formwork, created by dividing two full-sized, commercially available GFRP stay-in-place forms longitudinally along the span of the T-ribs. The two 1,675 × 840 mm GFRP forms used in this study each had four T-Up ribs spanning the full length of the forms spaced at 205 mm on centre. Gales

et al. (2016c) determined that the thermal thickness began to influence the samples at approximately 9.5 mm thickness. Thermal thickness has implications for the scalability of fire tests involving GFRPs because the fire resistance properties do not scale proportionally between a thermally thin and thermally thick sample. For this reason, a GFRP thickness greater than 9.5 mm was used in this study to make use of the fire resistance benefits associated with thermal thickness and select a GFRP structural form that was representative of a full-scale bridge deck in practice. The base plate has a maximum thickness of 19 mm, which tapered to 13.7 mm away from the ribs. The ribs protruded 96 mm from the interior of the base plate to the top of the rib flange. Mechanical testing by previous author measured the ultimate tensile strength and modulus of the GFRP in the longitudinal direction to be 203 MPa and 16.8 GPa, respectively, and the same properties in the transverse direction to be 126 MPa and 15.6 GPa, respectively (Nelson and Fam 2013).

A two-dimensional grid of 10-M GFRP V-ROD rebar was added to each specimen to better represent actual strips of a GFRP stay-in-place formwork bridge deck where a top rebar mesh would be used. The longitudinal rebar was placed 35 mm above each T-Up rib. The transverse bars were the lower rebar layer and spaced at 185 mm. The total beam height including the GFRP base plate was 186 mm. The specimen sizes are based on the dimensions from a full-scale comparison of a RC–steel composite bridge deck with a GFRP stay-in-place formwork–RC bridge deck (Nelson and Fam 2013). The GFRP formwork decks were designed to be comparable to a Canadian Highway Bridge Design Code (CAN/CSA-S6-14)– compliant RC–steel composite bridge deck, resulting in a GFRP member depth of 186 mm to achieve the same effective reinforcement depth as the traditional steel composite deck. However, the GFRP deck had a higher reinforcement ratio and additional vertical ribs compared with the traditional RC–steel deck (Nelson and Fam 2013). The concrete beam widths were chosen as the same spacing of the GFRP T-Up ribs to accommodate and centre one full rib per beam (with the exception of C2). The beams and test cylinders were covered by wet burlap for the curing duration. The 50-day concrete compressive strength was 45.7 ± 1.2 MPa based on six cylinders tested in accordance with ASTM C39. The 90-day concrete compressive strength was measured as 47.9 MPa. Figure 4.3 shows the strip specimens in the formwork prior to casting and the cured beams. No surface preparation of any kind was applied to the GFRP formwork prior to casting.

The control specimens, referred to as C1 and C2, were tested in their undamaged state and had one and two T-Up ribs along their length, respectively. The purpose behind varying the number of T-Up ribs along the width of the specimens was to determine whether downscaling the number of T-Up ribs had a proportional effect on the performance of the beam. The beam specimens with simulated fire damage are referred to as SD1, SD2, SD3, and SDF. Simulated damage was applied to these specimens by physically removing the

GFRP base plate in different regions of the beam. The T-Up ribs, which were fully embedded in concrete, remained undamaged. Figure 4.4 and f outline the dimensions and damage areas of each beam. The basis for the removal of the GFRP base plate originated from the material testing described in Gales et al. (2016c), where it was hypothesized that during a fire, a portion of the GFRP base plate would be damaged while the interior T-Up ribs would be protected by the concrete heat sink. This study assumed a worst-case scenario, where the entire thickness of the base plate loses structural capacity. This approach also assumed that the concrete directly adjacent to the base plate remains undamaged from the fire (this is proven valid for the fire scenario in this study). Even if overly conservative, this method of simulating fire damage allows controlled and precise removal of the GFRP base plate, which enabled a better understanding of its contribution to the load carrying capacity of the structural member. The fire-damaged specimen, referred to as FD, was exposed to a 14.5 min heptane pool fire between point loads to compare with Beam SD3, which had simulated damage in the same region. The heated region on Beam FD represented 33% of the beam's span. Two layers of gypsum board were provided outside of the heated zone to prevent flame spread and protect other regions of the beam. The gypsum board was CertainTeed Easi-Lite Lightweight gypsum and had a thickness of 12.7 mm, a weight of 6.4 kg=m2, and both a flame spread rating of 15 and smoke developed rating of 0 in accordance with ASTM E84. After testing and board removal there was no evidence of GFRP damage beneath the boards (no charring/discoloration). This method allowed a direct comparison of the flexural behaviours of Beams FD and SD3.

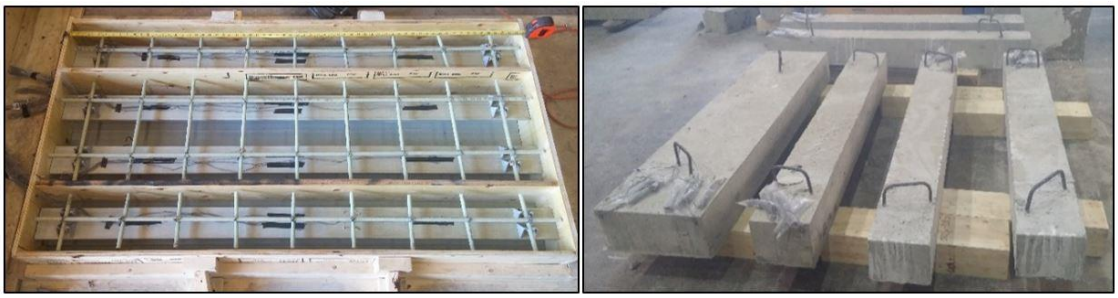

Figure 4.3. Beam fabrication and casting.

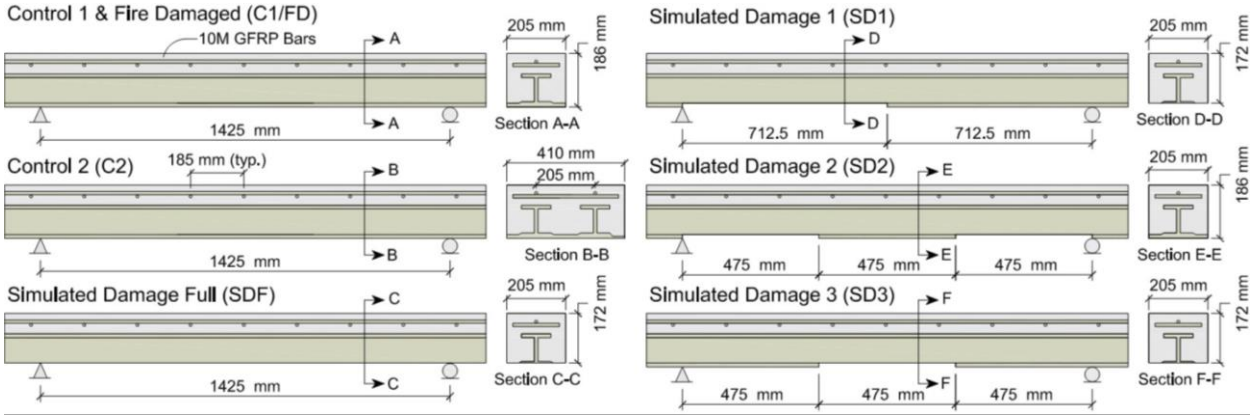


Figure 4.4. Control and simulated damage beam specimens.

Table 4.2. Test specimen design details.

| Beam | Dimensions (mm) | Damage Type |
|---|---|---|
| C1 | 1425 x 205 x 186 | None |
| C2 | 1425 x 410 x 186 | None |
| SD1 | 1425 x 205 x 186 | Left half of GFRP base plate removed |
| SD2 | 1425 x 205 x 186 | GFRP plate shear spans removed |
| SD3 | 1425 x 205 x 186 | GFRP plate removed between point loads |
| SDF | 1425 x 205 x 172 | Full span GFRP plate removed |
| FD | 1425 x 205 x 186 | Fire damaged between point loads |

Note: Beam dimensions are given in a c/c span x width x depth format.

### 4.3.2 Experimental Test Setup and Instrumentation

The most damaging bridge fires are commonly caused by tankers spilling flammable liquids near or below a bridge, with hydrocarbon fuels being the most relevant (Garlock et al. 2012; Peris-Sayol et al. 2017). The fire test described herein was intended to be experimental in nature to explore the appropriate GFRP–concrete response resulting from a fire-damaged state. The pool fire used to damage Beam FD had a pan diameter of 300 mm, burned 1.6 L of heptane at 0.11 L=min, and had a continuous flame height of approximately 0.5 m. The beam was supported 500 mm above the base of the fuel pan. See Drysdale (2011) for information on calculating thermal exposures from pool fires. A total burn time of approximately 15 min was used to inflict minor fire damage to the beam and study the underlying mechanics. The author acknowledges this is a relatively small fire exposure; however, the ultimate goal is to direct future tests where large-scale fires will be considered. A small fire exposure allows the GFRP response to be studied without the introduction of complicating factors, such as concrete degradation. Short-duration hydrocarbon pool fires for structural testing have been used by Byström et al. (2014). Elsewhere in the literature, modeling by Aziz and Kodur (2013) and by Kodur et al. (2017) of composite concrete-steel bridge decks and unprotected steel bridge girders, respectively, suggests failure times for hydrocarbon fires of under 25 min, albeit under more severe fire exposures. For the purpose of invoking a damage state, the small fire exposure described herein is assumed to be suitable.

Moreover, in Canada and many other jurisdictions where the GFRP stay-in-place formwork is marketed, there is no specific fire endurance requirement for bridges. European and American/ Canadian bridge design standards (Eurocode 1 Part 2 and AASHTO/ CSA, respectively) do not discuss bridge fires, and European fire design standards (Eurocode 1 Part 1-2) apply to buildings, not bridges, where typical spans and structural systems vary greatly (CSA 2014a, AASHTO 2015, CEN 2002, CEN 2003). This is a well-described issue that has been discussed by many researchers (Garlock et al. 2012; Peris-Sayol et al. 2017). As far as the author is aware, the only national standard that provides information on the fire endurance requirements of bridges is National Fire Protection Association (NFPA) 502: Standard for Road Tunnels,

Bridges, and Other Limited Highways, which specifies the general method to select design fires for bridges longer than 300 m (NFPA 2014). This standard recommends that design fires for bridges be chosen based on the potential fire produced by the types of vehicles passing under the bridge in question (NFPA 2014). Local authorities or bridge owners may specify fire resistance on a case-by-case basis, but this is not the international norm based on the information detailed earlier.

Based on NFPA 502's recommendation to consider the design fires of vehicle types that pass under a bridge, the fire scenario in this manuscript (although admittedly small) may be considered realistic depending on the scale of the bridge in question (NFPA 2014). More generally, a fast and hot fire should be in the range of considered design fires when carrying out a full performance-based design of a bridge.

Simulated fire damage to Specimens SD1, SD2, SD3, and SDF was applied in the laboratory over a month after casting by cutting on either side of the web-base joint and prying off the base plate. No concrete was damaged in the removal of the GFRP base plate. All specimens except Specimen FD were tested approximately 50 days after casting. Due to laboratory restrictions, the burning and testing of Specimen FD occurred approximately 3 months after the testing of all other specimens.

After the simulated and fire damage was applied to each beam, they were tested in simply supported, four-point monotonic bending. Figure 4.5 gives the typical load configuration for each test and the setup for the pool fire. This loading configuration was used to quantify the flexural performance of the GFRP stay-in-place formwork. The beams spanned 1,425 mm from support centres with 125 mm overhangs at either side. Point loads were spaced evenly along the span at 475 mm.

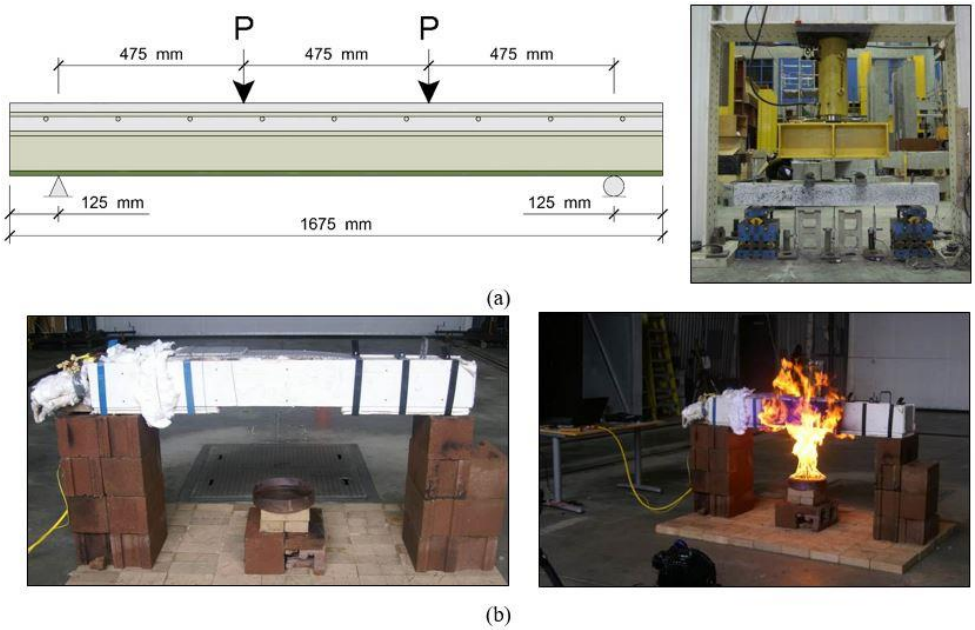


Figure 4.5. (a) Typical experimental test setup and loading configuration; (b) pool fire burn setup.

Specimen FD was tested at ambient temperature after the fire was exhausted to assess the residual capacity of the beam postfire. Heating while loading was beyond the scope of this paper; however, the author acknowledges its relevance, especially in the context of GFRP materials, where the effect of the glass transition temperature is critical (Gales and Green 2015; Del Prete et al. 2015).

A variety of instrumentation techniques were used in this study to monitor the responses of the test specimens. Three linear voltage displacement transducers (LVDTs) were used to measure the deflections along the length of each beam. GFRP-rated strain gauges were installed at the quarter spans and midspan of the T-Up rib flanges to monitor changes in rib strain relative to damage extents. In general, FRPs can be very susceptible to high temperatures, especially in the case of externally bonded FRP reinforcements where adhesion can be compromised by heating as described in Del Prete et al. (2015). Specimen FD was instrumented with two thermocouples placed on the interior side of the GFRP base plate at the midspan to record the GFRP–concrete bond temperature. Two additional thermocouples were used to monitor the ambient air temperature in the laboratory and the temperature of the GFRP soffit. All thermocouples were simple k-type gauges and only measured point temperatures and are illustrated in Figure 4.6 showing temperature versus time.

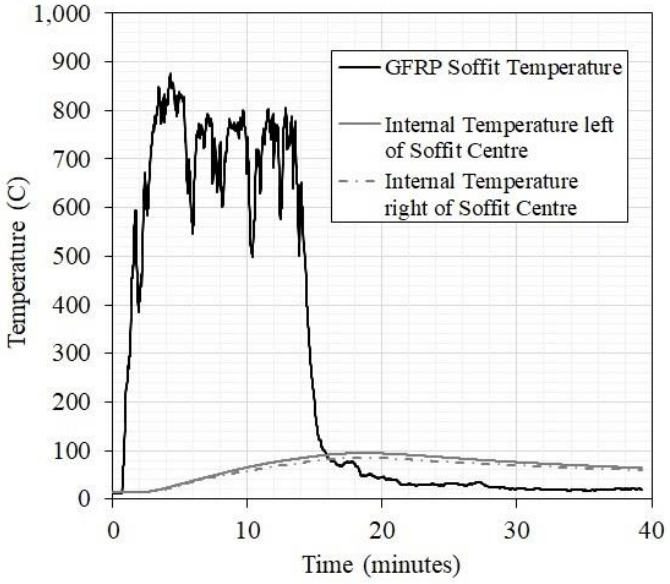


Figure 4.6. Time temperature history for beam FD.

Both thermocouples on the interior side of the GFRP base plate measured peak temperatures of less than 100°C, while the gas temperature at the exposed surface measured a peak of approximately 900°C. A numerical study would be useful to investigate the heat transfer across the GFRP–concrete interface and assess the degree of heating the concrete can sustain beyond this layer. Because the concrete temperature adjacent to the GFRP soffit was below 100°C, there exists negligible degradation of concrete strength due to heating at any point in the concrete and spalling could not have occurred. This result is important because

it validates the author's assumption that only the GFRP formwork would be damaged in a fire of this severity. This assumption was the basis for only removing sections of the GFRP forms and not damaging the adjacent concrete or the embedded GFRP rib. It should be noted that this method of simulated damage is only valid for pool fires of the extent and severity described. More severe fires will transfer additional heat to the concrete and cause severe material degradation, expansion, or spalling due to temperatures well beyond 100°C.

### 4.3.3 Direct Bond Shear Tests

The adhesive bond between the GFRP formwork and concrete is the main component of shear transfer between materials, with friction representing a secondary component. This shear transfer is vital to developing composite action between the concrete and the GFRP reinforcement. An experimental program was developed to test the GFRP–concrete bond shear strength after exposure to increasing bond temperatures, as observed in the previously described beam tests. This experimental program is intended to provide insight on potential GFRP resin post-curing or other localized bond-altering effects as a result of heating.

The direct shear test program consisted of 16 small-scale specimens of GFRP formwork samples cast between two concrete blocks to recreate the bond between the GFRP formwork and a concrete bridge deck. The concrete also provides a loading surface for the apparatus. The concrete mix design, strength, and moisture were consistent and verified with the ambient concrete properties of the beam tests. The samples were heated to a range of internal bond temperatures near those experienced by Beam FD tested herein, as recorded by thermocouples at the GFRP–concrete interface. The GFRP–concrete bond in Beam FD was measured to have a peak temperature of just under 100°C. Sample temperatures varied between 100°C and 200°C in increments of 25°C. This temperature range encompasses the bond temperatures recorded in Beam FD and beyond. Ambient tests were conducted to provide a baseline. Samples were heated at a rate of 5°C=min to the desired temperature in a laboratory oven and held for 2 h to ensure uniform temperature. Heated samples were allowed to cool to ambient temperature and tested in a direct shear apparatus using an Instron 5882 loading actuator at a loading rate of 0.25 mm=min. Figure 4.7 shows a typical GFRP–concrete sample in a direct shear apparatus. The author believes this loading configuration is more representative of the interaction between GFRP formwork and concrete in large-scale than a pullout test. In this study, the orientation of the GFRP fibres and their influence on the bond shear strength were studied by testing half the samples parallel to the GFRP fibre direction and the other half perpendicular to the GFRP fibre direction. The orientation seemed to show little difference in the results. Table 4.3 outlines the test variables considered.

### 4.3.4 Digital Image Correlation

Digital image correlation (DIC) was used to measure displacements and estimate slip at the concrete–GFRP interface. Figure 4.8 shows a typical DIC setup in this study. A series of photos are taken during each test at regular intervals with a high-resolution camera. By introducing a speckled paint pattern on the side of the specimen, the movement of points on the surface can be tracked between photos using computer software and deformation values can be obtained. In past studies, DIC proved to be a useful tool for determining displacements, relative movements of concrete and external reinforcements, and other surface deformations (Verbruggen et al. 2016; Destrebecq et al. 2011).

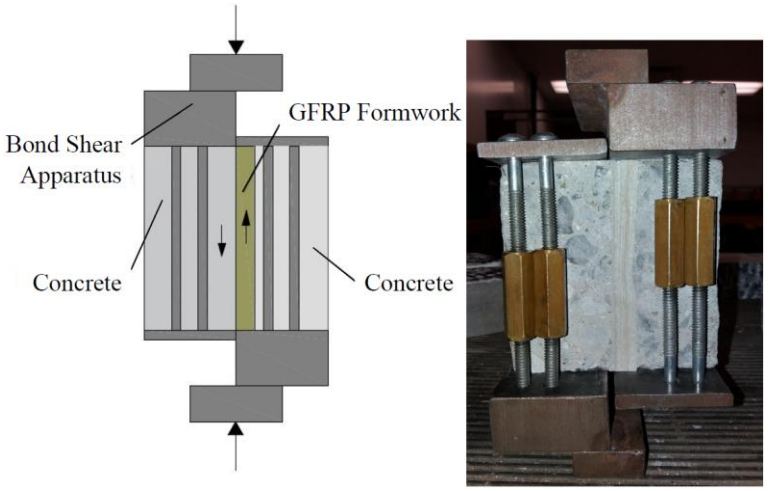


Figure 4.7. Direct bond shear test apparatus.

The camera used in this study was a 50-megapixel Canon 5Ds Mark III. The software used in analysis was GeoPIV-RG and MATLAB, which applies interpolation functions to track movement between points of interest in subsequent images. Gales and Green (2015) outline some qualitative errors associated with optical measuring and potential solutions to these issues. The measurement error associated with DIC is on the order of 0.0001 mm, arising from GeoPIV-RG's standard and rotational errors of 0.001 pixels (px) and 0.0001 px, respectively (Blaber et al. 2016). To validate the reliability of the DIC analysis, the calculated results of the vertical deflection at midspan for Beams C1 and FD were compared to the measured values from the LVDTs. Figure 4.9 shows a comparison between LVDT and DIC vertical displacement results. These results show the very good agreement between the DIC and LVDT deflections. The slight discrepancies at higher loads are likely due to out-of-plane beam rotation. Digital image correlation was also applied to measure deformations of the concrete– GFRP direct bond shear tests. Figure 4.10 shows the typical test setup for the test series.

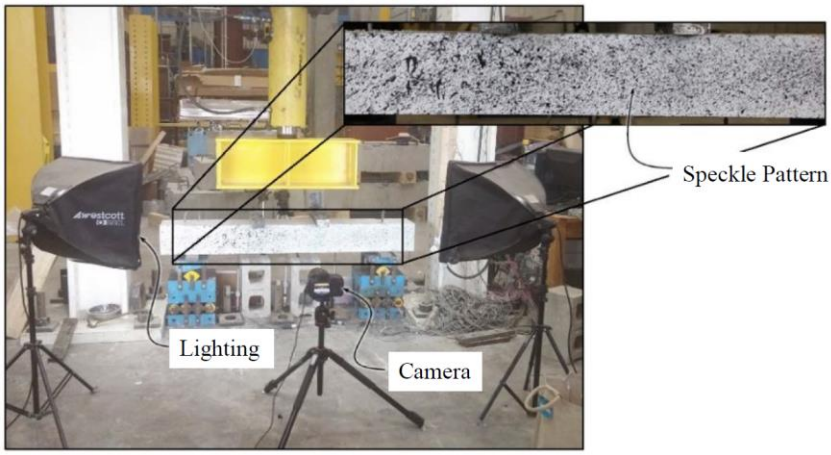


Figure 4.8. Digital image correlation test setup and beam speckle pattern.

Table 4.3. Bond shear test specimens

| Shear Direction | Sample | Oven Temperature (°C) | Bond Width (mm) | Bond Height (mm) | Bond Area ($mm^2$) |
|---|---|---|---|---|---|
| Parallel to fibres | A1 | 20 | 42 | 98 | 4085 |
| | A2 | 20 | 53 | 101 | 5292 |
| | A3 | 100 | 51 | 102 | 5184 |
| | A4 | 100 | 53 | 105 | 5618 |
| | A5 | 125 | 52 | 102 | 5268 |
| | A6 | 150 | 52 | 101 | 5321 |
| | A7 | 175 | 50 | 101 | 5060 |
| | A8 | 200 | 49 | 101 | 4999 |
| Perpendicular to fibres | B1 | 20 | 51 | 92 | 4720 |
| | B2 | 20 | 55 | 99 | 5477 |
| | B3 | 100 | 52 | 104 | 5366 |
| | B4 | 100 | 52 | 105 | 5476 |
| | B5 | 125 | 53 | 99 | 5231 |
| | B6 | 150 | 46 | 98 | 4473 |
| | B7 | 175 | 46 | 100 | 4576 |
| | B8 | 200 | 48 | 100 | 4765 |

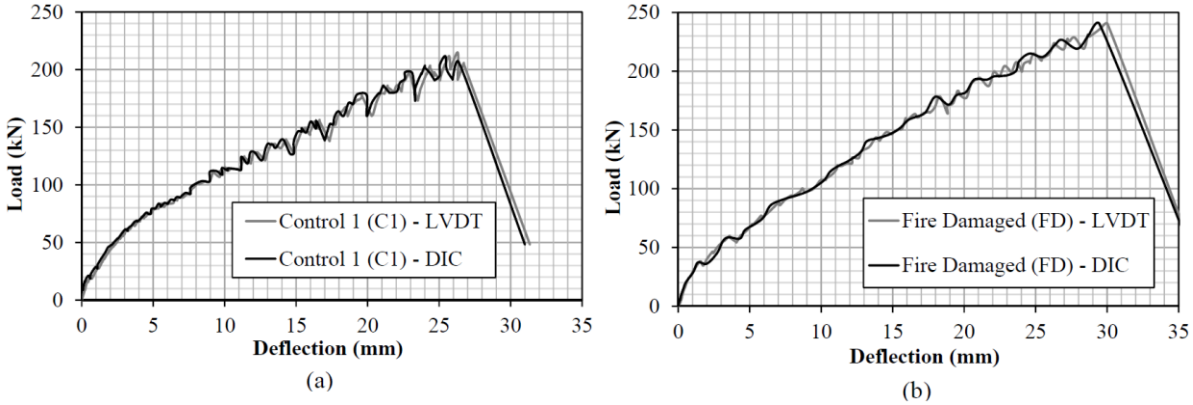


Figure 4.9. Comparison of LVDT and DIC midspan deflection response: (a) beam C1 and (b) beam FD.

Figure 4.10. Digital image correlation test setup for bond shear tests.

A MATLAB script is used to initiate the GeoPIV-RG software. Parameters for photo analysis are input, including an approximate point radius of 50 pixels, an analysis point radius of 25 pixels, a computational limit of 50 iterations, a correlation seed of 0.9, and a correlation limit of 0.9. These parameters influence the picture-to- picture point tracking accuracy. The first photo in the series is used as a baseline for future photos and the points of interest where relative displacements are measured are selected by the user. The GeoPIV-RG software creates acceptable centroids to track based on the selected points. The software runs through all pictures in the test series and tracks the chosen centroids. Relative centroid displacements are output in a MATLAB variable in units of pixels. Results are provided in both the vertical and horizontal directions. A reference image containing a known distance is used to convert pixels to displacements. In this case, the relative vertical displacement between the points selected represents the vertical displacement of the bond.

Figure 4.11 shows a typical point selection screen in GeoPIV-RG. This is the same screen used in the beam analysis to determine gap values. The points to be tracked are selected on this screen. In the gap analysis, one point is selected on the GFRP base plate at midspan and one point is selected on the concrete above the GFRP base plate to measure the differential displacement. For the bond shear tests, two points on opposite sides of the GFRP–concrete shear plane are selected.

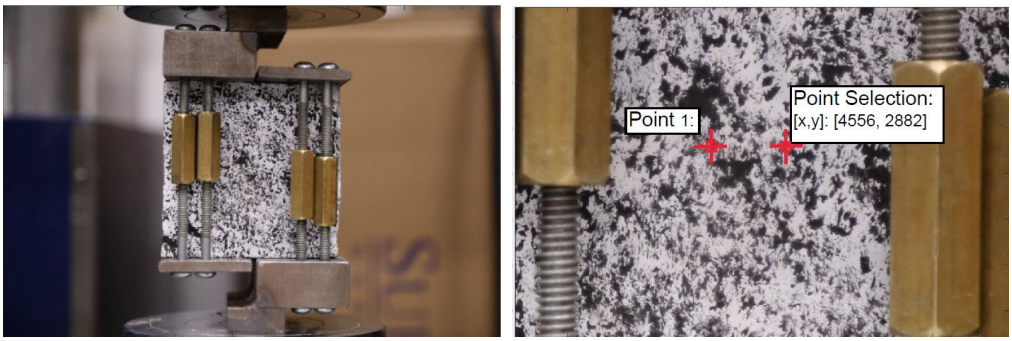

Figure 4.11. Point selection screen in GeoPIV-RG for a typical bond shear test.

## 4.4 Experimental Results

### 4.4.1 Load-Deflection Response

Beams C1 and C2 established a baseline for comparison and verified the effect of downscaling the width of GFRP stay-in-place reinforcement. Specimen C2 was twice the width and had twice the GFRP reinforcement area as C1 but about 10% more than double the ultimate capacity, verifying an approximately linear scaling of capacities with member width. The slight increase in C2 is attributed to concrete confinement by means of the two adjacent ribs. This could also be attributed to tension stiffening of concrete adjacent to the GFRP stay-in-place formwork, which has been observed by Honickman et al. (2009) and Nelson and Fam (2014b). Figure 4.12 and Table 4.4 show the load-deflection responses and key results for all test specimens. The most notable result is that the fire-damaged Beam FD had an approximately 13% higher ultimate capacity than the undamaged control C1. The increase in load carrying capacity is attributed to a concrete prestressing effect due to thermal expansion of the GFRP formwork. This hypothesis is discussed in more detail subsequently. All simulated damage tests had similar load-deflection behaviours except for Beam SD2, which failed at a much lower deflection. Despite having the smallest area of tensile reinforcement remaining, Beam SDF achieved the highest ultimate load and deflection. The damage inflicted on Beam SDF prevented the concentration of stresses at damage boundaries present in all other SD tests and likely delayed the onset of similar failure mechanisms.

Table 4.4. Summary of experimental beam results.

| Beam | Maximum Load (kN) | Maximum Deflection (mm) |
|---|---|---|
| C2 | 475 | 29.7 |
| FD | 240 | 30.0 |
| C1 | 212 | 25.7 |
| SDF | 75 | 27.9 |
| SD1 | 68 | 19.9 |
| SD3 | 62 | 24.2 |
| SD2 | 56 | 15.2 |

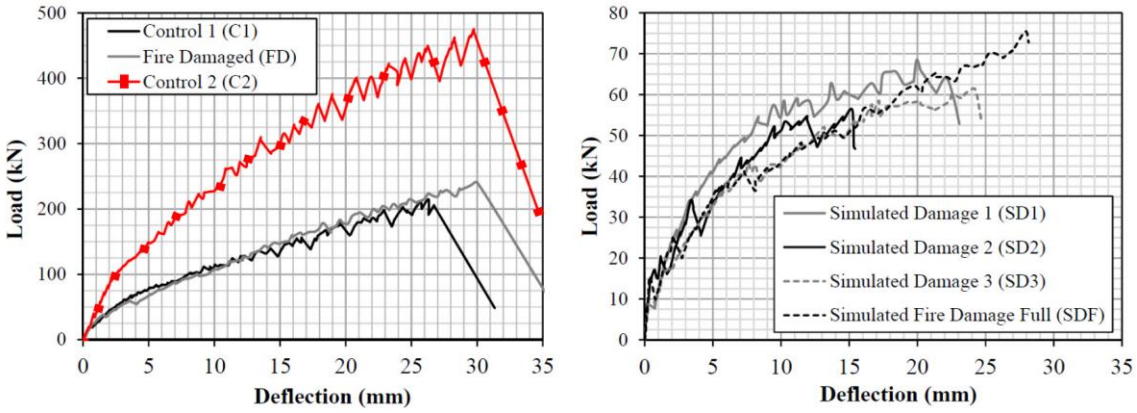


Figure 4.12. Beam midspan load-deflection responses: (a) control and fire damaged beams and (b) simulated damage beams.

### 4.4.2 Load-Slip Response

An important factor influencing the performance of GFRP stay-in- place formwork bridge decks is composite action between the formwork and the concrete. In practice, bond enhancement can be achieved through a variety of methods to help maintain composite action at higher loads. Some of the common methods include roughening the surface of the GFRP formwork, adhering silica crystals or coarse aggregates to the formwork surface or applying chemical adhesives prior to casting. In this study, no bond enhancement techniques were used such that the effect of fire on the GFRP could first be understood, avoiding introducing other complicating factors into the study. This was also relevant since one study showed adequate fatigue performance of this system without surface treatment up to five million loading cycles (Richardson et al. 2014).

A loss of composite action is characterized by slipping of the GFRP formwork relative to the concrete and, in more extreme cases, the formation of a vertical gap between the GFRP and concrete. Figure 4.13 illustrates the GFRP–concrete slip and gap phenomenon caused by loss of composite action and shows some of the GFRP–concrete slip observed in this study.

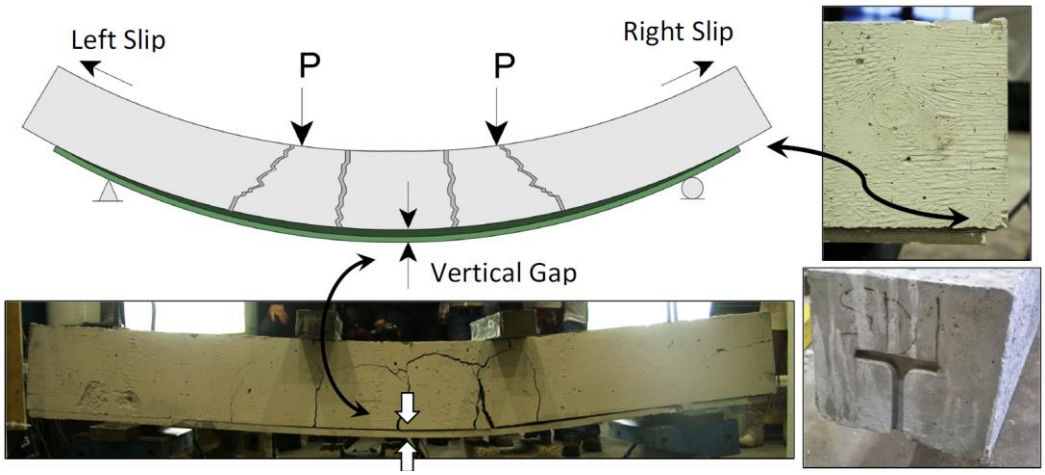


Figure 4.13. GFRP-concrete slip and gap behaviours. Specimen C1 is shown.

The relative GFRP–concrete slip for C1, C2, and FD was measured using DIC analysis to understand the GFRP–concrete bond relationship with load carrying capacity. Table 4.5 shows the results of the slip analysis. The slip phenomenon is quantified in terms of total GFRP–concrete slip (the sum of left and right slips). These values show that the total GFRP end slips at maximum load are similar between Beams C1, C2, and FD despite the damaged state of FD and the greater available bond area in C2. A larger ultimate midspan deflection would result in more relative GFRP–concrete slip due to a larger difference in curvature radii between the concrete and GFRP. Noting this, both Beams FD and C2 had larger ultimate deflections than C1 (approximately 30 mm, 30 mm, and 26 mm, respectively), meaning larger total slips should be observed in these specimens, which is not the case. The additional available bond area in C2 may have

resulted in better composite action than in C1. For a more relevant comparison of C1 and FD, the loads and deflections at which the slips are measured can be normalized, as shown in Table 4.6. The normalized values of 25 mm for deflection and 200 kN for load are arbitrary but were chosen at points closer to the ultimate load. When normalized, there is less total slipping in Beam FD than in C1 when compared at the same load or the same deflection, indicating better composite action in FD. A hypothesized concrete precompression effect due to GFRP heating in FD may have limited the ultimate total end slip. Alternatively, experimental variation between C1 and FD may have resulted in the discrepancies. Figure 4.14 shows the time-slip response for Beams C1 and FD.

Table 4.5. Summary of max relative GFRP-concrete slips for key specimens.

| Beam | Maximum Load (kN) | Maximum Slip Left (mm) | Maximum Slip Mid span (mm) | Maximum Slip Right (mm) | Total end slip (mm) |
|---|---|---|---|---|---|
| C1 | 212 | 4.6 | 1.8 | 11.0 | 15.6 |
| C2 | 475 | 7.9 | 0.2 | 7.6 | 15.6 |
| FD | 240 | 7.5 | 0.3 | 7.5 | 15.1 |

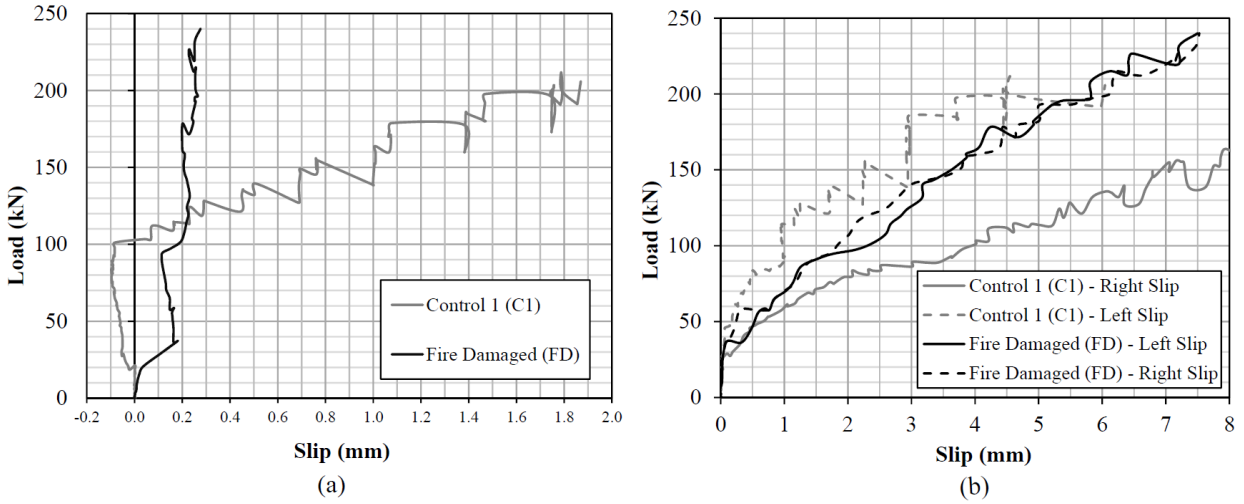


Figure 4.14. (a) Midspan horizontal GFRP-concrete slip and (b) left and right horizontal GFRP-concrete slip.

Table 4.6. Normalized total end slips for FD and C1.

| Condition | FD End Slip (mm) | C1 End Slip (mm) |
|---|---|---|
| Ultimate Load | 15.0 | 15.6 |
| Normalized for Deflection (25 mm) | 12.4 | 13.6 |
| Normalized for Load (200 kN) | 11.9 | 14.6 |

The vertical gap between the GFRP and concrete developed at midspan was also measured using DIC analysis to better understand the slip behaviours of Specimens C1 and FD. Specifically, points were selected on either side of the GFRP–concrete interface at midspan and were tracked as the gap formed. The vertical displacements recorded through DIC represent the vertical gap value, while horizontal values represent the slip. Figure 4.15 shows the values of the gap that formed between the top of the GFRP base plate and the

adjacent concrete at midspan for both beams. These results demonstrate a smaller vertical GFRP separation in Beam FD despite the inflicted fire damage, which implies a stronger GFRP–concrete bond at midspan due to heating and cooling when compared to C1. Although the values in Figure 4.15 are within the accuracy of the DIC software, the author acknowledges that variability between tests could have contributed to the differences discussed at such a small scale.

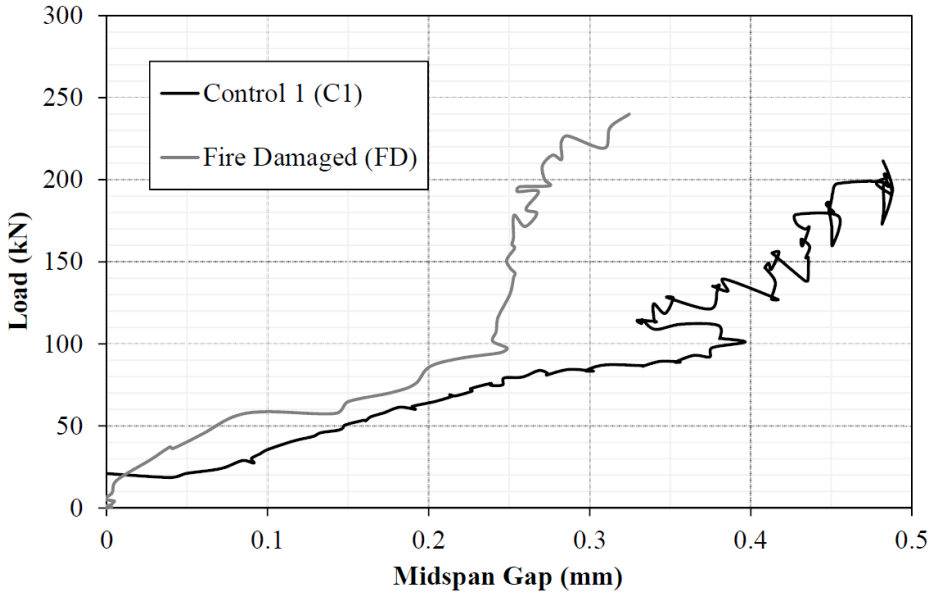


Figure 4.15. Vertical GFRP-concrete gap formation at beam midspan.

These data sets further describe better composite action at the midspan of Beam FD than in Beam C1. This indicates that there may be some level of strengthening, possibly due to the heating and cooling of the GFRP formwork, resulting in concrete prestressing. This theory is reinforced by the approximately 13% ultimate load increase in Beam FD compared to C1 and smaller crack widths in Beam FD described subsequently. A similar enhancement was observed by Gooranorimi (2016) in GFRP bars during a study on the performance of RC slabs reinforced with GFRP rebar and exposed to the ASTM E119 standard fire for 120 min. The peak rebar temperature was 115°C, which is similar to the peak interior temperature reached by the GFRP formwork in this study. The rebar was allowed to cool, removed from the slab, and tested mechanically. Results showed that the horizontal shear strength of the bars increased by roughly 15%, possibly due to resin post-curing (Gooranorimi 2016). Horizontal shear strength (shear in the direction of the fibres) is indicative of resin–fibre interface strength (Gooranorimi 2016). However, the strengthening in this study is not hypothesized to be a result of resin post-curing based on the results of the bond shear tests presented herein.

### 4.4.3 Direct Bond Shear Tests

The GFRP–concrete bond shear tests revealed information about the effect of elevated temperatures on the GFRP–concrete interface. In general, there was no evidence of a bond enhancement in direct shear due to resin post-curing or otherwise. There was a clear decrease in failure shear stress as bond temperatures increased. The DIC analysis monitored the bond deformation as shear loading increased. Due to the brittle failure of the test samples, recorded deformations are small but still within the accuracy of the DIC technology, as discussed earlier. Of particular interest was the relative displacement of the GFRP–concrete interface across the bond. Table 4.7 gives the ultimate loads and stresses for each sample and presents the relative displacements across the GFRP–concrete bond normalized by shear stress at failure. Based on the aforementioned data and physical deformities, Specimen A2 was believed to be defective, likely due to damage or issues encountered during casting, and was omitted from the associated plots. For temperatures at which two samples were tested, the results were averaged in the plots below. Figure 4.16 plots the relationship between heated temperature and ultimate shear stress, while Figure 4.17 plots the normalized relative GFRP–concrete displacement versus the bond temperature. These plots show that heating the GFRP-concrete interface decreases the ultimate bond shear stress and increases the relative bond deformation when tested in direct shear after the bond temperature has returned to ambient. Although a limited sample size was tested, the relationship between bond deformation and heated temperature appears to be nonlinear; however, additional testing may be required to further study the residual GFRP–concrete bond strength at elevated temperatures.

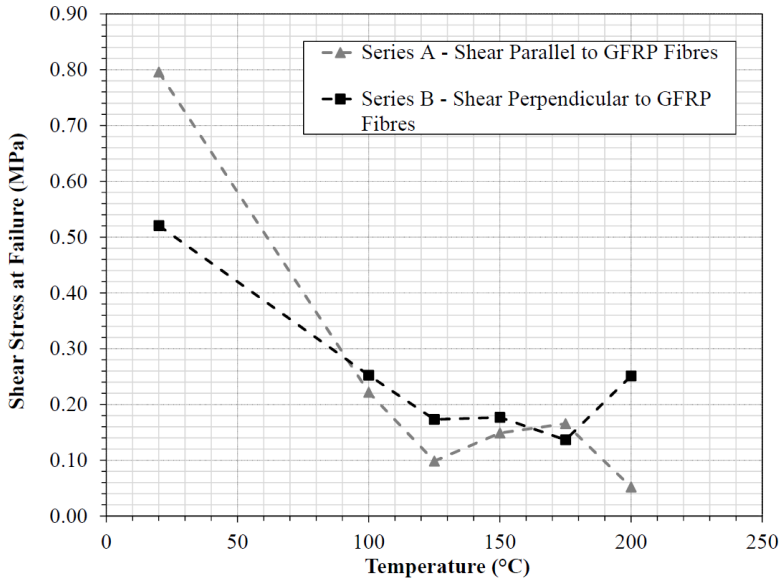


Figure 4.16. Ultimate bond shear stress versus heated temperature.

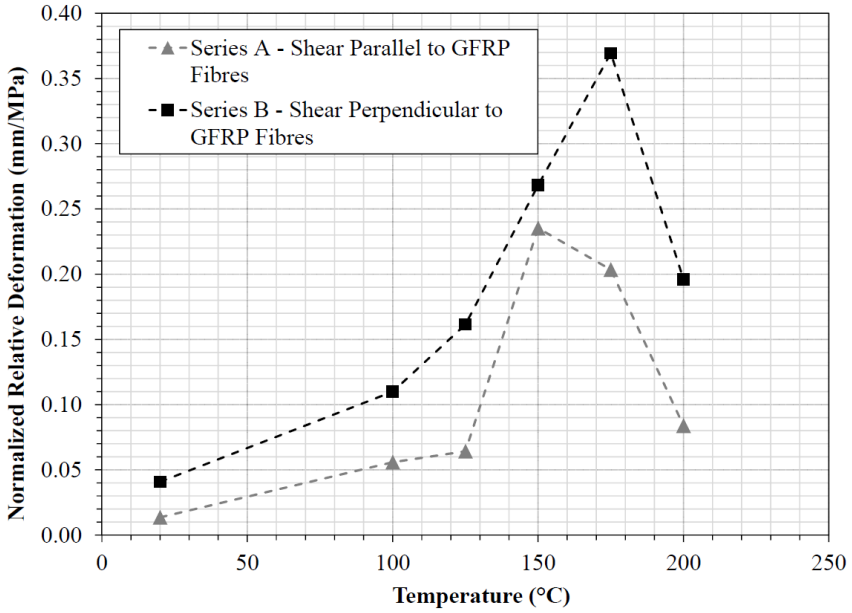


Figure 4.17. Normalized GFRP-concrete bond displacement versus heated temperature.

Table 4.7. Direct bond shear test results

| Shear Direction | I.D | Oven Temperature (°C) | Ultimate Load (N) | Ultimate Shear Stress (MPa) | Relative Displacement at Ultimate (mm) | Relative Displacement Normalized by Peak Shear Stress (mm/MPa) |
|---|---|---|---|---|---|---|
| Parallel to GFRP fibres | A1 | 20 | 3251 | 0.796 | 0.011 | 0.014 |
| | A2 | 20 | 504 | 0.095 | n/a | n/a |
| | A3 | 100 | 1233 | 0.238 | 0.018 | 0.075 |
| | A4 | 100 | 1156 | 0.206 | 0.008 | 0.036 |
| | A5 | 125 | 519 | 0.099 | 0.006 | 0.064 |
| | A6 | 150 | 792 | 0.149 | 0.035 | 0.235 |
| | A7 | 175 | 838 | 0.166 | 0.034 | 0.203 |
| | A8 | 200 | 260 | 0.052 | 0.004 | 0.084 |
| Perpendicular to GFRP fibres | B1 | 20 | 2595 | 0.550 | 0.003 | 0.006 |
| | B2 | 20 | 2692 | 0.491 | 0.037 | 0.076 |
| | B3 | 100 | 1034 | 0.193 | 0.007 | 0.034 |
| | B4 | 100 | 1709 | 0.312 | 0.058 | 0.185 |
| | B5 | 125 | 906 | 0.173 | 0.028 | 0.162 |
| | B6 | 150 | 791 | 0.177 | 0.047 | 0.268 |
| | B7 | 175 | 625 | 0.137 | 0.050 | 0.369 |
| | B8 | 200 | 1197 | 0.251 | 0.049 | 0.196 |

Based on these results, it is concluded that heating the GFRP– concrete interface decreases the bond strength in direct shear and reduces the bond stiffness. This does not exclude the potential for other strengthening

effects that could have influenced the largescale beam tests in this study, such as concrete prestressing due to formwork thermal straining, which may still be plausible.

### 4.4.4 Crack Behaviour

To better understand the effect of fire damage on load transfer to the GFRP stay-in-place formwork, DIC analysis was applied to measure flexural crack widths in Beams C1, FD, SD3, and SDF. Beams SD1, SD2, and C2 were omitted from the analysis because of their dissimilar damage regions. The widths of the most prominent flexural cracks were measured at the extreme concrete fibre in tension. Figure 4.18 shows the relationship between crack widths and applied load. This plot shows that, for the same applied load, Beam FD had smaller crack widths than Beam C1. Additionally, cracking initiated in Beam C1 and FD at approximately 20 and 80 kN, respectively. These results indicate better load transfer to the GFRP stay-in-place formwork in Beam FD than in Beam C1, despite the fire damage inflicted. Alternatively, smaller crack widths in Beam FD could indicate concrete precompression as a result of thermal straining. Despite having a damaged region similar to that of Beam FD, Beam SD3 experienced much wider cracks much earlier than other specimens. This is attributed to the hinge formation at the simulated damage boundary, where stress concentrations resulted in a premature GFRP web fracture and exacerbated concrete cracks. The lack of stress concentrations in the formwork of Beam SDF resulted in smaller crack widths than Beam SD3, despite a smaller area of tensile reinforcement.

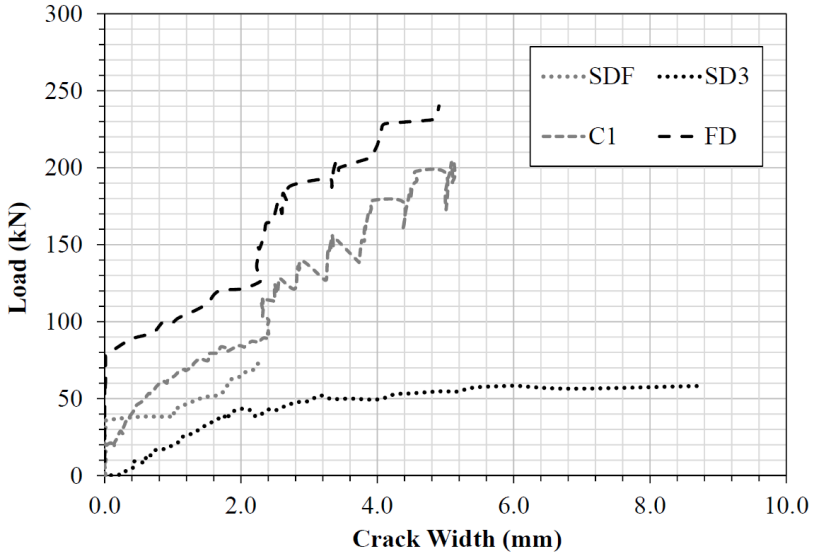


Figure 4.18. Flexural crack width at extreme concrete fibre in tension versus load.

### 4.4.5 Failure Modes

Two modes of failure were observed between all seven beam tests: (1) separation of the GFRP rib web from the base plate at beam ends in C1, C2, and FD and (2) fracture of the GFRP rib web in SD1, SD2, SD3, and SDF. Loss of composite action between the GFRP formwork and concrete preceded failure in

every test. In Beams C1, C2, and FD, partial composite action was maintained during loading, with occasional and large GFRP–concrete slips accompanied by a reduction in load. Even after large slips between the concrete and GFRP, the sustained load was able to re-establish and increase up until failure. Shear failure at the joint of the GFRP web and base plate initiated the separation of the GFRP base plate from the rib web at failure. The fracture length extended approximately from the support to the closest point load. This is shown in Figure 4.19.

(a)

(b)

Figure 4.19. (a) Beam C2 crack distribution and (b) separation of GFRP base plate from rib web.

Severe flexural cracking was observed in all SD specimens in regions where the GFRP base plate had been removed. Beyond the ultimate load, large portions of cracked concrete fell away from the SD beams and exposed the GFRP T-Up rib. Composite action was not maintained to the same degree as the control and fire-damaged specimens because of the reduced bond surface area. This yielded small and frequent GFRP slips and drops in load. Fracture of the GFRP T-Up rib web occurred at failure. The location of GFRP fracture was dependent on the location of GFRP base plate removal. Where a damage boundary was present, GFRP web fracture occurred at the boundary on the damaged side due to stress concentrations in the GFRP web. With no damage boundaries available in beam SDF, GFRP fracture occurred at approximately midspan. In Beam SD2, a GFRP fracture occurred just outside of the moment span at the damaged boundary. It is hypothesized that stress concentrations at the abrupt damage boundaries in Beam SD2 initiated failure earlier than SDF, which has no abrupt damage boundaries. This is reinforced by the flexural failure of the GFRP web at the damage boundary seen in Figure 4.20. Fire scenarios resulting in large char depths may cause similar stress concentrations if abrupt damage boundaries are present (such as where a GFRP stay-in-place formwork deck meets a bridge girder).

Although the shear resistance provided by the GFRP stay-in-place forms was not a focus of this study, some comparisons can be made with previous ambient temperature tests. One-way bending tests of a 1,220 × 400 × 150 mm concrete slab reinforced with an adhesively bonded, 9.5 mm thick GFRP plate (with no ribs) conducted by Honickman et al. (2009) yielded concrete shear failure and GFRP debonding at the midspan. By comparing these failure modes with those of Beams C1 and C2 in this study, it can be concluded that the GFRP T-Up ribs provide the concrete with ample shear resistance and help mitigate GFRP debonding at midspan.

(a)

(b)

Figure 4.20. (a) Beam SD1 crack distribution (post-failure) and (b) GFRP web fracture at a damage boundary.

### 4.4.6 Assessment of Simulated Damage

In general, the level of applied simulated fire damage was very conservative for the extent of damage experienced by Beam FD. However, removal of the entire thickness of GFRP plate may still be representative of a specimen inflicted with more severe fire damage depending on the level of concrete heating beyond the GFRP. Regardless of the accuracy of simulated damage in this study, the SD tests still give important information about the behaviour of damaged GFRP stay-in-place formwork. The control and simulated damage beams represent boundary conditions in terms of damage depth to the GFRP base plate. For a specific level of damage in the moment span, the corresponding failure mode changes from that of C1 to that of SD3. Beam FD demonstrated the same failure mode and general behaviour as C1 so it can be said that the fire damage sustained was insufficient to cause this change in failure mode, but a deeper char layer may induce the alternate failure mechanism.

One research goal was to determine whether the embedded T-Up ribs would bear additional load in the event of damage to the base GFRP plate. Figure 4.21 outlines the GFRP rib flange load-strain responses at midspan for all tests. Beam SD2 had all four strain gauges fail and is not shown on the plot. It is observed that there is a large increase in strain developed in the T-Up ribs in the SD tests when compared to C1 and FD. This is likely due to the larger curvatures developed in the SD GFRP formwork and reduced composite action that eventually led to GFRP fracture. Beam SDF had the highest capacity of all simulated damaged beams, suggesting it may be more beneficial to have a uniform region of damage instead of discrete damage boundaries. The strains in C1 and FD are of the same order of magnitude. The rib flange of Beam FD shows a decrease in a stiffness when compared to C1 due to the reduced area of GFRP reinforcement from fire damage and an extended zone of pyrolysis. The measured rib strains are compressive due to the loss of composite action between the GFRP formwork and the concrete. As demonstrated in Figure 4.22, as composite action is lost, a strain discontinuity is created between the strain distributions of the concrete and GFRP, denoted by $\varepsilon_{slip}$. For a full loss of composite action, the neutral axis of the GFRP is given by the centroid of the GFRP cross section and the reinforcement bends independently of the concrete. The strains developed in the T-Up ribs provide an important conclusion about the performance of GFRP stay-in-place formwork in fire conditions in that, for fire scenarios where the embedded ribs are undamaged (which is the vast majority of cases), the ribs provide a redundancy to the system.

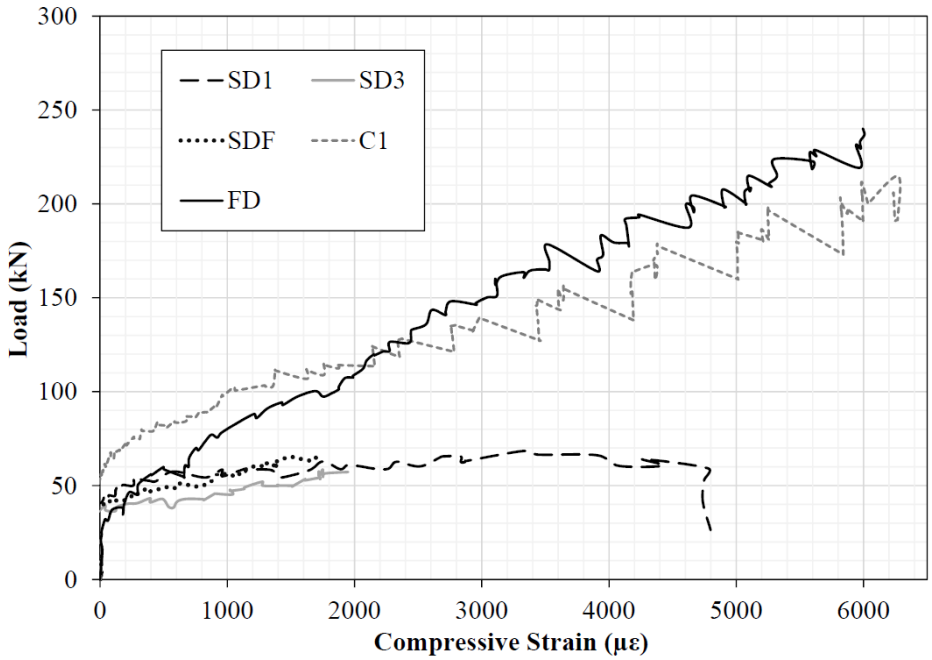

Figure 4.21. T-Up rib flange compressive strain response at midspan.

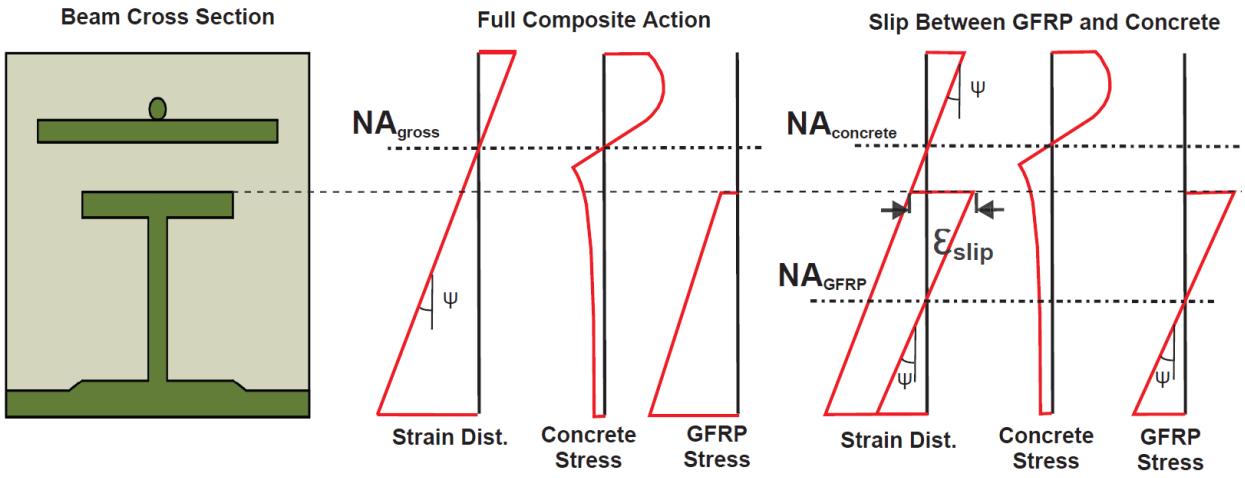


Figure 4.22. T-Up rib strain distribution due to GFRP-concrete slip. NA: neutral axis of cross-section. Adapted from Nelson and Fam 2014b.

### 4.4.7 Assessment of Fire Damage

Beam FD performed better than suggested by Gales et al. (2016c) under exposure to the pool fire. A char layer extended approximately 2 ± 0.5 mm or 15% into the exposed 13.7 mm thick GFRP base plate as measured in six locations across the damaged soffit. The small variation in char depth (0.5 mm) over the damaged region of Beam FD provides the author with confidence that heating was moderately uniform along the exposed region. The variations in char depth could be due to flame dispersion effects. It should be noted that the region directly beneath the char layer still contributes structurally to the member but may have undergone some level of chemical change, including pyrolysis during heating. This layer will have altered postfire mechanical properties based on chemical change from partial GFRP decomposition. Delamination of outer laminates occurred on the charred GFRP surface. The GFRP experienced flame-out almost immediately after the pool fire fuel was exhausted. This suggests that a more severe fire may be required to sustain a flame on the GFRP surface after flame-out. Figure 4.23 shows the delamination and charring of the base plate observed during the test.

Figure 4.23. Delaminated pyrolysis/char layer on GFRP base plate soffit.

## 4.5 Conclusions and Future Research

The goal of this project was to gain an understanding of the behaviour of GFRP stay-in-place T-Up structural formwork exposed to localized fire damage, within the context of concrete bridge deck applications. Fire damage was simulated in a series of bridge deck sections reinforced with GFRP formwork by physically removing the GFRP base plate. Comparisons were made to undamaged control beams and a beam damaged by a heptane pool fire. The effect of elevated temperatures on the GFRP–concrete bond was also investigated in direct shear. Further, the use of a pool fire as methodology for heating bridge structural members was examined.

### 4.5.1 Contributions to the State of the Art

This paper has presented first-stage research into the postfire performance of concrete beams reinforced with GFRP stay-in-place formwork intended for bridge deck construction. Despite the limitations outlined throughout this article, the information presented herein offers novel insights into a previously unexplored damage state for this specific structural system. Specifically, this manuscript has:

- conducted the first, to the knowledge of the author, high-temperature damage test on a GFRP stay-in-place formwork structural system that recorded GFRP surface temperatures exceeding 800°C, reported on the observed material and mechanical behaviours, and identified areas requiring future research, specifically, the potential for flexural strengthening resulting from low heating;
- examined and drawn conclusions about the influence of both minor-fire and severe physical damage on the mechanical behaviour of the GFRP system using four-point bending tests not considered in past mechanical research involving this structural configuration; and
- performed the initial study with a novel series of direct bond shear tests to further examine the effect of high temperatures on the concrete-GFRP interface which ruled out a bond strengthening phenomenon and gave badly needed information on the bond stiffness deterioration.

### 4.5.2 Limitations of the Heating Exposure Used in this Study

This study focused on the mechanical behaviour of GFRP stay-in-place formwork beams under a variety of damage states, including an arbitrary fire-damaged condition. The fire scenario presented in this paper represented the extent of the author's available resources and was used solely for the purpose of invoking a measurable postfire damaged state on the GFRP stay-in-place formwork system in order to study the mechanical response. The author by no means advocates such small-fire exposure in the context of bridge fire safety studies where realistic fires are orders of magnitude more severe than that presented herein, specifically with regard to the heat release rate and duration. It is also not the author's intention that the time–temperature data presented for the surface of the GFRP be interpreted as a realistic bridge fire

scenario; its inclusion is simply to provide context to the fire-damaged state of a specimen, not set a precedent for future tests. However, it is the author's opinion that the use of open-flame pool fires in structural fire testing, especially in connection with bridge fires where hydrocarbon pool fires are common, is an approach with merit when applied properly in scale and can yield behaviours not necessarily realized in other test methods. This paper is intended to act as a precursor to future studies where densely instrumented tests on appropriately scaled specimens with realistic hydrocarbon fires will be considered, coupled with well-controlled furnace tests that will both enable accurate modeling endeavors.

### 4.5.3 Future Work and Recommendations

The following topics were identified by the author as potential areas for future work:

- investigation of the bond behaviour of concrete and GFRP formwork in elevated temperatures at larger scales;
- investigation of concrete pre-compressive action as a result of GFRP formwork heating and cooling;
- simultaneous heating and loading of concrete–GFRP formwork systems to identify load-induced thermal straining effects (LITS) and creep effects;
- exposure of large-scale concrete–GFRP formwork systems to a variety of design fires including standard fires; and
- development of numerical models to account for secondary heating effects on concrete–GFRP formwork systems as well as full material characterization.

### 4.5.4 Conclusions

Conclusions from this test program are as follows:

1. The capacity increase present in fire-damaged beams when compared to the undamaged control is hypothesized to be a result of concrete precompression developed from the heating and cooling of the GFRP base plate.
2. There is no apparent strengthening effect from heating the GFRP–concrete bond and loading in direct shear. There is an evident and nonlinear decrease in bond shear stiffness as the heated bond temperature increased.
3. Removal of the full thickness of the GFRP base plate was an overly conservative approximation of the fire damage sustained by the specimen but may be accurate for more severe fires depending on the level of concrete heating.

4. The fire damage sustained was insufficient to reduce the ultimate load or change the failure mode of the specimen when compared to the undamaged control. The embedded T-rib is also protected from fire damage and provides redundancy to the system.
5. Despite a char thickness of about 15% of the base thickness, the GFRP base plate was able to protect the adjacent concrete from temperatures of over 100°C.
6. There is an approximately linear relationship between beam width and the ultimate load/strains developed in GFRP T-Up rib flanges at the scales studied, but confinement and tension stiffening may affect wider members with multiple ribs, causing about 10% increased strength per unit width.
7. It may be less detrimental to have symmetric and uniform areas of damage on the GFRP base plate when compared to abrupt or asymmetric damage boundaries due to the introduction of stress concentrations in the GFRP web.
8. The thermal thickness of GFRP base plates is a critical factor in fire resistance and prevents upscaling of small-scale GFRP stay-in-place formwork fire tests.
9. No sustained flaming was observed on the GFRP soffit after the pool fire was exhausted.
10. For the fire conditions studied, a stay-in-place formwork reinforced bridge deck would likely be repairable with minimal closure time due to the same level of flexural capacity.

This study was intended to direct the focus of future studies and provide an understanding of the effect of fire on GFRP stay-in-place formwork–concrete systems. More experiments of this nature should be conducted to confirm the conclusions drawn herein. These conclusions suggest that GFRP stay-in-place formwork hold great potential for civil engineering applications, but the performance and behaviour of GFRP materials at elevated temperatures must be better understood.

# Chapter 5: The Fire Performance of Unloaded Steel Stay-Cables for Bridge Infrastructure Subject to Pool Fires

## 5.1 Introduction

Not only are bridges critical infrastructure, these structures also constitute some of the most iconic civil engineering projects and most architecturally-pleasing designs. This is especially true for cable-supported structures like cable-stayed and suspension bridges as these structural systems allow for exceptionally long spans to be achieved. One of the main structural elements of these bridge types is the cable-stay. Cable-stays or strands are the primary support for bridge decks and transmit loads to either the bridge tower (in the case of cable-stayed bridges) or to the suspension cable (in the case of suspension bridges). These elements consist of configurations of individual high-strength and, typically, cold-drawn, steel wires. Note that the description of strand or stay-cable does not include suspension cables which refers to the very large diameter cables suspended between towers of a suspension bridges. Suspension cables are composed of large numbers of strands and/or wires and are not the focus of the research herein. Similarly, prestressing strands used in concrete construction are typically five or seven-wire spiral strands but are distinct from the cables used in bridges which are generally of much larger overall diameter. Wire ropes also do not fall into the category of cable-stay/strand. Wire ropes are composed of many strands wrapped around a central core element and are typically used in mechanical applications. In general, all elements described above are composed of individual wires at the smallest level. Stay-cables/strands are composed of configured around a central core, wire ropes are composed of multiple strands wrapped around a larger core (but are typically of smaller total diameter as they apply smaller wire sizes at the fundamental level), and suspension cables can vary in configuration but are often composed of many parallel wires to create a large diameter. The study herein focuses only on stay-cables/strands used in cable-supported structures.

Within the category of stay-cable or strand, herein referred to interchangeably as strand, cable, or stay-cable, there are three main configurations that are applied. The first are parallel strands which are composed of multiple parallel wires. Parallel strands are widely used in contemporary construction and provide the benefit of not wrapping wires around a core; this reduces the wire stresses created in manufacturing which allows higher cross-sectional strains to be attained and a wider elastic response to be developed (Gimsing and Georgakis 2011). Spiral strands are the second configuration which are composed of round wires coiled in consecutive layers around a core wire. Full locked-coil cables are the final configuration which are similar to spiral strands however the outer layers of the strand apply “Z-shaped” wires which enable interconnection between adjacent wires and reduces the overall void ratio of the cable cross-section.

Generally, full locked-coil strands have the densest steel cross-sections of the three configurations considered above (Gimsing and Georgakis 2011). Although the study herein does not consider parallel strand wires, it must be noted that the fire performance of these strands represents a knowledge gap in this topic.

Fires pose a risk to steel cable members due to the potential reduction of material properties (yield strength, modulus of elasticity, ultimate strength, and plastic (creep) performance) if elevated temperatures are reached. In a cable-supported bridge, fire hazards are generally limited to the potential fuel loads on the bridge deck but as Chen et al. (2018) discuss, fires can affect cables anywhere where combustible material can be found sufficiently close, such as in the applications of high-density polyethylene (HDPE) sheaths to encase strands and protect from corrosion. As structural cables can have exceptionally long spans and are part of complex cable systems, effects other than a loss of mechanical properties can occur from heating and have severe consequences. For example, thermal expansion, thermal bowing or thermal moment development, creep, and residual strain relief have the potential to cause critical effects in a cable-supported structure. These topics are not well studied and must be addressed to better understand the fire response of cable-supported structures like bridges.

### 5.1.1 Review of the Fire Performance of Steel Stay-Cable Members

In general, bridge fire research is understudied compared to other fields such as building fires. Moreover, the majority of bridge fire research has largely considered steel and concrete highway bridges due to their prevalence in highway networks. There exist many knowledge gaps pertaining to the fire performance of cable-supported bridges and, in particular, steel cable elements in general. To provide context to the research presented hereafter, this section will review existing literature on the study of the fire performance of steel strands, cables, wire ropes, and similar tension elements. Note that the literature reviewed in this section differs from that studied in Chapter 3 in that the research reviewed here has a specific focus on the response of the steel tension element to fire, not the overall cable-supported bridge structure.

In the past decade, there have only been a handful of studies that experimentally target the fire performance of steel cable members. One of the earliest modelling studies identified that unprotected stay-cables could reach critical temperatures very rapidly in a bridge fire scenario (Bennetts and Moinuddin 2009). Further studies have since confirmed the potential vulnerability of cable-stay elements to bridge fire hazards (see Liu et al. 2012, Gong and Agrawal 2016, Kotsovinos et al. 2016b). Major experimental studies on the topic began more recently with Fontanari et al. (2015) who explore the fire behaviour of steel wire ropes. Considering 60 mm diameter locked-coil strands (and later 26 mm and 80 mm strands) and six-strand Warrington-Seale wire ropes, those authors heated and simultaneously loaded the tension members using the ISO 834 standard fire heating curve. A finite element model (FEM) created in ANSYS was used to

model the results of the experiments and ultimately create a thermo-mechanical model for both elements considered. These authors present a nearly-linear increase in time-to-failure for the locked-coil strands with increasing diameter (between 26 mm to 80 mm). Based on the ISO 834 standard fire exposure, these authors show the 60 mm locked-coil cable had core wire temperatures of approximately 75°C, 225°C, 360°C, and 475°C, and exposed surface temperatures of approximately 280°C, 450°C, 550°C, and 625°C, for heating times of 5, 10, 15, and 20 minutes respectively (Fontanari et al. 2015).

To study the mechanical properties of galvanized steel cables after cooling post-fire, Jie et al. (2017) heat 20 mm diameter spiral strands to temperatures ranging from 100-1000°C and compare the effects of both air and water-cooling. Heating was conducted using a furnace and specimens were tested mechanically after cooling. The authors visually observed a variety of changes in the cables during testing including a loss of metallic lustre post-cooling from temperatures above 300°C and a flaking of the galvanized coating for temperatures above 800°C (Jie et al. 2017). Those authors note the observations could be useful in post-fire examinations of cable members in service. Jie et al. (2017) demonstrate a deterioration in cable mechanical performance post-fire with large decreases occurring for temperatures exceeding 400-500°C; in air-cooled specimens only, a large recovery in strength and deformation ability occurred between 750-1000°C. Both cooling methods demonstrated similar failure modes up to temperatures of 700°C when water cooling methods made the strands much more brittle (Jie et al. 2017). These authors define this 700°C as the critical temperature for water-cooling galvanized cable members. These authors note the fire performance of the anchorages exacerbated the stiffness reductions observed in the cable members. The fire performance of cable anchorages remains an unaddressed knowledge gap in the fire performance of cable-supported structures.

Chen et al. (2018) express concerns over the fire performance and extinguishment ability of bridge cable members due to their common encapsulation in flammable high-density polyethylene (HDPE) sheathes. The authors explore the combustibility and fire propagation of a replica sheath-cable system that contains a 250 mm diameter bundle of 73 unloaded spiral strands. A wall section was replicated to model the interface between the bridge pylon and cable member and assess fire transmission through the boundary. The fire load consisted only of the HDPE sheath encasing the strands; temperatures at the centre of the assembly were measured by K-type thermocouples and reached high temperatures (>500°C) from this fire load alone (Chen et al. 2018). This result has serious implications for cable systems protected by HDPE sheaths as a vehicle fires can produce critical temperatures without the added contribution and flame spread provided by the encapsulation. The authors later test extinguishing methods including the approved National Fire Protection Association (NFPA) dry powder procedure which failed to prevent re-ignition and did not cool internal temperatures as effectively as water extinguishment (Chen et al. 2018).

Du et al. (2018) apply a charge-coupled device camera (CCDC) to measure deformations of 15 mm spiral strands that are simultaneously heated and loaded in a tensile testing machine fitted with a furnace. A first test series considered unloaded cables allowed to freely expand under thermal expansion. Results of the unloaded tests indicate the cable thermal expansion approximately falls between the Eurocode equations for carbon and pre-stressing steel for temperatures up to 800°C (Du et al. 2018). The authors note a slight decrease in strain at 750°C which corresponds to a phase change in the steel microstructure. The second test series considered both loading and heating on the cables and found that the Eurocode method of determining the yield strength and rupture strain of cold-worked prestressing strands (EN 1992-1-2) was not conservative (Du et al. 2018).

Du et al. (2019) investigate the role of cavity radiation in the thermal modelling of steel spiral strands. Cavity radiation refers to the thermal radiation across air voids within the cable structure which is often neglected in simplified thermal models as the conduction through contact points between adjacent wires is assumed to be greater. The authors apply a concentric cylinder model separated by an air gap to quantify the role of cavity radiation to interior wire layers; numerical models for similarly sized cable and solid round bar cross-sections are compared. Cable cross-sections up to 63 mm in diameter are modelled and gradients between the outer wire layer and core wire are presented based on exposure to the ISO 834 standard fire. Two peaks in thermal gradients were observed: the first between 5-10 minutes where external wires heating rapidly and experienced a slower temperature rise and the second between 20-35 minutes corresponding to the change in specific heat between 700-800°C from a phase change in the steel microstructure (Du et al. 2019). The time ranges for these events were dependent on cable diameter with larger diameters experiencing longer delays. During the phase change between 700-800°C, cable temperatures plateaued, and the resulting cavity radiation slowed (Du et al. 2019). As the cables reached thermal equilibrium the thermal gradients approached zero. For 63 and 49 mm spiral strands, the maximum thermal gradient between core and external wires was approximately 155°C and 145°C respectively. The inclusion of cavity radiation led to both an increasing in the core wire heating rate and maximum temperature (Du et al. 2019).

Robinson et al. (2019) conduct steady-state testing of individual cold-drawn wires to evaluate material properties. The samples were heated between 20-700°C and results demonstrated a large reduction in elastic modulus and ultimate strength. These authors found degradation to be more severe than current models predict likely due to the relief of residual plastic strains that are created in manufacturing. Robinson et al. (2019) continue by testing two identical and non-commercial 61-wire strands in uniform heating and tension tests. The strands were created similarly to those done by Lugaresi (2017) and were composed of a

bundle of individual steel bars. The authors demonstrated strand failure at a temperature of 660°C at load of 430 MPa (Robinson et al. 2019).

Kotsovinos et al. (2020b) develop two-dimensional numerical models to calculate the thermal response of cable cross-sections considering both internal conduction and cavity radiation. The authors refer to the critical temperature for stay-cable members of 300°C suggested by PTI DC45.1-12 (PTI 2012) as a potential target for the protection of cable members, based on the acceleration of creep affects in prestressing steels beyond this temperature. These authors' model considers hexagonally-configured parallel-wire strands for the geometric simplicity and their prevalence in modern bridge construction. The thermal model is validated based on experimental results from 50 mm and 70 mm diameter steel spiral strands created by assembling commercially-available mild steel and heated non-uniformly by radiant heaters (Lugaresi 2017). A variety of fire exposures based on potential jet fire scenarios were considered in the modelling (Kotsovinos et al. 2020b). Results show that the critical temperature of 300°C could be exceeded as quickly as 60 seconds for some exposure levels, whereas fire protection could prolong this threshold to approximately 40 minutes. The model could qualitatively predict the redistribution of axial loads in internal wires as well as the development of moments resulting from thermal gradients. The authors conclude the lumped capacitance approach of modelling is not always conservative and should be approached with care (Kotsovinos et al. 2020b).

Sun et al. (2019) consider the post-fire performance of 14 and 20 mm diameter galvanized steel spiral strands. Eighteen tension tests were conducted after heating specimens to constant cross-sectional temperatures from ambient to 500°C in increments of 100°C. Strands were heated at various stress states and air-cooled. These authors observed melting of the galvanized coating at approximately 400°C which is confirmed by research from Ridge and Hobbs (2012) who determined a melting temperature of 380°C for the zinc alloy used in common cable sockets. Sun et al. (2019) conclude that the stress state during heating has negligible effect on mechanical properties except for fracture strain. Above 300°C, the strands began to lose yield strength, ultimate strength, stiffness, and fracture strain.

Kotsovinos et al. (2020a) presents a literature review of the state-of-the-art of research on the fire performance of structural cables. These authors review information pertaining to the fundamental fire performance of cable members with specific focus on material responses, thermal expansion, loading shedding between wires, creep and relaxation, and terminals. The authors note a lack of information pertaining to the thermal expansion of larger diameter cables in both experimental results and available code guidelines, and further indicate that temperatures of only 200°C could be critical in terms of second-order effects created by thermal expansion (Kotsovinos et al. 2020a). These authors continue by reviewing experimental research and note that only five studies have considered steel strands that exceed the diameter

of standard seven-wire strands used in prestressed concrete construction. Further, Kotsovinos et al. (2020a) indicate for three of those five studies, only one considered one-sided heating of the cables at a rate suitable for the development of large thermal gradients; this study was an earlier publication by the author of this thesis and this work being referred to by Kotsovinos et al. (2020a) is presented herein (Nicoletta et al. 2019a). Kotsovinos et al. (2020a) finally note that non-uniform heating of cable diameters greater than 80 mm has not yet been explored experimentally, nor has the potential for cable uncoiling, stress relaxation, thermal moments, nor creep. With respect to available modelling literature, Kotsovinos et al. (2020a) indicate that the majority of studies lack extensive validation due to the lack of experimental results on the thermal response of cable elements. These authors continue by reviewing industry standards for the fire protection of stay-cable elements presented by PTI DC45.1-12 (PTI 2012). This standard sets the critical temperature for stay-cable elements as 300°C which conservatively falls below the flashpoint of HDPE sheaths (330°C) and below the critical temperature for plastic deformations in steel varieties used in stay-cables (400°C). The test methods for this standard include a fire resistance test which must limit cable temperatures to 300°C for a minimum duration of 30 minutes and a loaded tension test in which a cable at 45% of its ultimate load must withstand a temperature of 300°C for 30 minutes (TI DC45.1-12). Kotsovinos et al. (2020a) identify potential limitations with this methodology as follows:

1) Separating the heating and loading of stay-cables into two separate phases is unconventional and no studies have confirmed this practice is representative;
2) This test procedure fails to consider the effects of thermal gradients as the strands are loaded at uniform temperatures;
3) There is a lack of research available to support a critical temperature of 300°C for stay-cable members although the value is assumed to be conservative; and
4) The guidelines do not adequately consider the fire performance of cable anchorages which is not well known.

These authors conclude by identifying eight areas related to the fire performance of structural cables which need further research.

The research presented in the subsequent section of this chapter targets three knowledge gaps not addressed in the literature and later identified by Kotsovinos et al. (2020a):

1) The development of experimental temperature profiles for large diameter structural strands (diameters > 80 mm) exposed to non-uniform heating;
2) The examination of the potential for cable uncoiling and other deformations related to heating; and

3) The thermal strain development on the surface of structural strands and the relationship between thermal moments and thermal strains.

Furthermore, the research presented herein also represents the first experimental study of stainless steel structural stands and the first study to apply novel optical measuring techniques for such an application. To conclude, there is a deficiency of experimental research targeting the fire performance of structural strands, especially of diameters greater than 80 mm. Current literature focuses more heavily on the fire performance of prestressing strands which may not be representative of the larger diameter strands used in bridge construction. This research attempts to further understand how structural cable behaviour changes with increasing diameter such that more directed research can be pursued in the future.

## 5.2 Experimental Methodology

The research herein attempts to better understand the high-temperature thermal response of unloaded steel structural strands. Specifically, steel strands are exposed to a pool-fire to induce a non-uniform, one-sided thermal response. A pool-fire is chosen for the following reasons:

1) The desire to inflict non-uniform and one-sided heating made the use of furnaces as an alternative unfavorable;

2) Although radiant heaters can inflict one-sided heating, the potential volatility of blocking agents and the potential uncoiling of cable members increased the risk of damaging equipment that would need to be placed directly adjacent to specimens; and

3) The use of pool fire exposure is conducive to the novel optical measurement techniques applied and described below.

The research program takes place in, first, a preliminary testing phase to adequately characterize the test procedures and scrutinize the initial experimental configuration, and later, a full testing phase.

### 5.2.1 Cable Specimens

A total of nine strand specimens were procured for the experiment presented herein. All specimens were supplied directly from three manufacturers and therefore represent commercially available cables that could be seen in cable-supported structures. The specimen diameters range from 22-140 mm and include both stainless and galvanized steel types, as well as locked-coil and spiral strand types. Table 5.1 provides information for each of the strands including the minimum cable strength grades and strand labelling which indicates the number of wires in each consecutive layer of the cable structure; wires indicated in brackets followed by “Z” refer to the Z-shaped wires used in the outer layers of locked-coil strands. The specimen naming convention uses the format *coil type – steel type – strand diameter* where *S* or *L* indicates spiral or

locked-coil strand types respectively, *GS* or *SS* indicates galvanized or stainless steel types respectively, and the final number indicates the nominal cable diameter in units of mm. Identical cables are followed by a letter after this nomenclature to further distinguish the specimens. For example, S-GS-74 refers to a 74 mm diameter, galvanized steel, spiral strand. Note that the steel type referred to as galvanized steel (GS) herein denotes the high-strength, cold-drawn steel used in cable elements that have been coated in a galvanizing alloy consisting of 95% zinc (Zn) and 5% aluminum (Al). Stainless steel specimens do not have this galvanizing alloy coating. Figure 5.1 provides accurately-scaled cross-sections for each of the specimens in Table 5.1. Manufacturer names have been removed to avoid potential product bias based on the results of this research.

Table 5.1. Description of cable specimens available for testing.

| Strand Type | Material | Nominal Diameter (mm) | Strand Labelling | Specimen Name | Specimen Length (m) | Nominal Strength (MPa) |
|---|---|---|---|---|---|---|
| Spiral | Galvanized Steel | 44[A] | 1+6+12+18+25 | S-GS-44 | 2 | 1720 |
| | | 74[B] | 1+6+12+18+24+30+36+33+39+45 | S-GS-74 | 1.5 | 1770 |
| | | 82[A] | 1+8+8+8/8+16+25+32+35+42+48 | S-GS-82 | 2 | 1720 |
| | Stainless Steel | 22[B] | 1+6+12+16 | S-SS-22 | 1.5 | 1670 |
| | | 50[B] | 1+6+12+18+25+32+42 | S-SS-50 | 1.5 | 1570 |
| Full Locked -Coil | Galvanized Steel | 70[B] | 1+6+12+18+24+(30+36+42) Z | L-GS-70 | 1.5 | 1570 |
| | | 100[C] | 1+6+6+12+18+24+30+(44+44+ 50+56) Z | L-GS-100-A/B | 1.5 | - |
| | | 140[B] | 1+6+12+18+24+30+(32+38+44+ 51+57+62+59) Z | L-GS-140 | 1.5 | 1570 |

A – Supplied by Manufacturer A, Canada
B – Supplied by Manufacturer B, Italy.
C – Supplied by Manufacturer C, Germany.

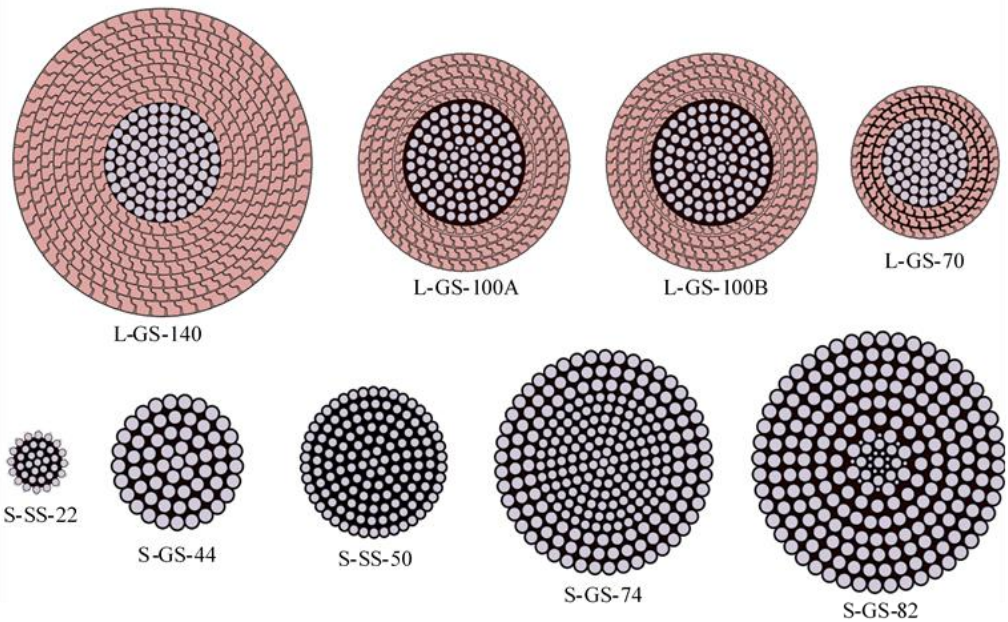


Figure 5.1. Relatively scaled cross-sections of cable specimens studied herein.

The steel compositions provided by the manufacturers are also tabulated in Table 5.2. Where ranges in values are presented in Table 5.2, multiple steel compositions were given for different wires of the cables. Note that the discrepancy between some compositions, especially in Carbon (C), Chromium (Cr), and Molybdenum (Mo) content, are reflective of the differences between stainless and carbon steel. Steel compositions and other information such as wire strengths were not available for strands L-GS-100A/B due to the manufacturer's reluctance to disclose otherwise proprietary information.

Table 5.2. Steel compositions from available wire certificates.

| Strand | C (%) | Mn (%) | Si (%) | P (%) | S (%) | Cr (%) | Mo (%) |
|---|---|---|---|---|---|---|---|
| L-SS-16* | 0.02- 0.02 | 0.46-1.54 | 0.0-0.5 | 0.02-0.03 | - | 16.6-16.7 | 2.02-2.05 |
| S-SS-22 | 0.02- 0.03 | 0.54-1.57 | 0.36-0.52 | 0.02-0.03 | - | 16.6-17.2 | 2.02-2.06 |
| S-SS-50** | ≤ 0.08 | ≤ 2.0 | ≤ 1.0 | ≤ 0.045 | ≤ 0.030 | 18-20 | - |
| S-GS-44 | 0.86 | 0.75 | 0.24 | 0.006 | 0.002 | 0.06 | - |
| S-GS-74 | 0.82- 0.85 | 0.63-0.74 | 0.20-0.24 | 0.01-0.02 | 0.004-0.017 | 0.04-0.08 | 0-0.01 |
| L-GS-70 | 0.83- 0.85 | 0.68-0.77 | 0.20-0.23 | 0.01-0.02 | 0.002-0.013 | 0.09-0.12 | 0-0.01 |
| L-GS-100A | Wire certificate not provided - proprietary | | | | | | |
| L-GS-100B | Wire certificate not provided - proprietary | | | | | | |
| L-GS-140 | 0.80- 0.86 | 0.63-0.81 | 0.19-0.26 | 0.01-0.01 | 0.002-0.016 | 0.06-0.28 | 0-0.01 |

*Strand could not be tested but is included as reference.
**Specific wire certificates were not provided but the material is identified as type 304 stainless steel which has the elemental compositions displayed.

In the context of fire, the elements with the greatest benefit towards fire performance are chromium and molybdenum. Specifically, the addition of chromium tends to reduce the thermal conductivity of the alloy while increasing the coefficient for thermal expansion (Cverna 2002). This is the primary source of stainless steel's superior high temperature properties when compared to other steels. Molybdenum further contributes to the high temperature strength of steel but slightly reduces the coefficient of thermal expansion in chromium-molybdenum-steel alloys (Cverna 2002). Therefore, stainless steel strands S-SS-22 and S-SS-50 are expected to have lower thermal conductivity and higher thermal expansion coefficients when compared to the other high-strength steel strands. Further, due to the lack of molybdenum, strand S-SS-50 is expected to undergo more thermal expansion than strand S-SS-22.

The fire performance of cable elements may be highly-dependent on manufacturing processes as they can directly influence the presence of residual strains in the system. Additionally, blocking compounds or blocking agents, substances used in the manufacturing of structural cables that act as lubricants and corrosion-inhibitors, are often found in structural cables, especially in cables of large diameter, and have not been considered in experimental or modelling research on the topic (Kotsovinos et al. 2020a). Table 5.3 presents blocking compound information for cables that have either been tested herein, were obtained by the author but not tested, or were not obtained by the author but had manufacturer documentation providing information indicating a blocking compound. Manufacturer C did not provide information

pertaining to the blocking compound in strands L-GS-100-A/B. Manufacturer A disclosed to the author a compound called TECTYL 4110 is used as a blocking agent in some applications (the specific applications of TECTYL 4110 were not disclosed nor was confirmation of its presence in the cable specimens acquired). According to material safety information on the substance, TECTYL 4110 is a petroleum-based rust-preventative and lubricating agent. It is hot-dip applied (heated above its melting point and pumped) over individual wires before entering the forming die to create a strand. TECTYL 4110 is flammable substance with a melting point of 76°C and a flashpoint of 232°C; note that this flashpoint is below the critical temperature of 300°C specified for the fire protection of cable members (Kotsovinos et al. 2020a).

A publicly-available technical document from Manufacturer B outlines some manufacturing details about full locked-coil strands (the information provided is believed to be relevant to other strand types as well). In terms of corrosion protection techniques, Manufacturer B lists the followings measures that can be taken in their products to enhance corrosion resistance: hot-dip galvanization (using 95 – 5 % zinc-aluminum alloy) of all wires, inclusion of a blocking agent called TENSOFILL (material information was requested but has not been provided), selection of interlocking Z-shaped wires for full locked-coil strands which is claimed to prevent the entry of external agents, application of wax or epoxy coatings after cable installation, and HDPE sheathing applied by hot extrusion. Pertaining specifically to the TENSOFILL blocking agent, the document specifies both spiral and locked-coil strands are filled in the "inner layers" with the substance which implies this agent may be applied differently than the TECTYL 4110 which is pumped over wires during stranding, not "filled" in inner layers specifically. The TENSOFILL agent is vaguely described as being made from Severe Atmosphere Corrosion Inhibitor (SACI 500) added to a zinc powder. Manufacturer C has publicly available information denoting the varying levels of blocking agent applications: the first is stranding which is used in the manufacture of the strands (TECTYL 4110 likely falls in this application level), the second is core closing which fills the cable to a certain internal layer (TENSOFILL likely falls in this application level), and the third is rope closing where the entire cable cross-section is filled with an agent. Figure 5.2 shows a drilling cable, S-GS-114, which was received by the authors but not tested due to concerns of the large quantities of blocking agent (confirmed by Manufacturer B to be ANTICORIT WRCP J207); it is assumed this cable is an example of a rope closing application of blocking agent.

Further in the documentation available from Manufacturer B, the process of pre-stretching is described. This process is used to remove initial inelastic deformation created by the helical winding of the cables and to "stabilize the elastic modulus". The pre-stretching equipment has a capacity of 5 MN and the process includes loading the cable in five cycles from 10% to 50-60% of the ultimate strength. The strands received by the author arrived wrapped with external confinement at both ends and at midspan to prevent the wires

from uncoiling. Through the research program, the author observed a strong tendency for the wires to unwind without adequate confinement, indicating some degree of prestressing on the strands.

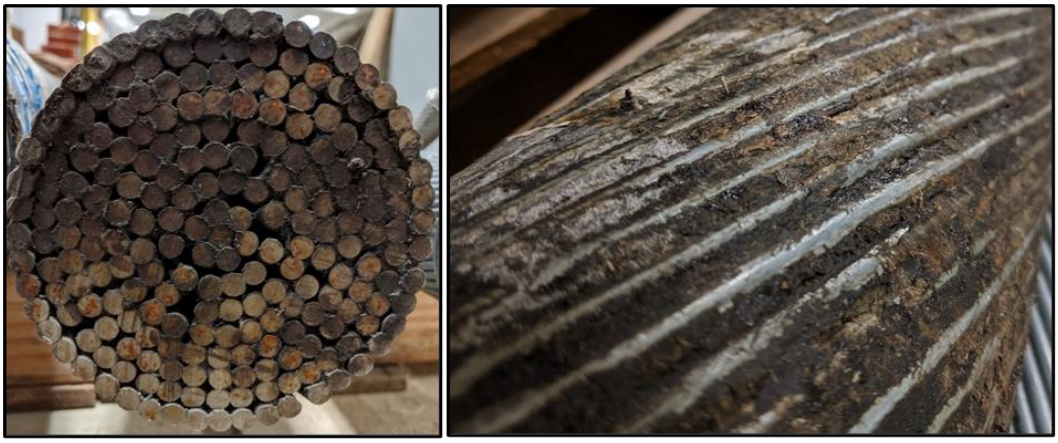

Figure 5.2. Cross-section and surface view of cable S-GS-114 demonstrating a rope closing level application of ANTICORIT WRCP J207 blocking agent.

Table 5.3. Blocking agent compound and assumed application levels for all cables either tested experimental or with documentation obtained by the author.

| Strand | Blocking Agent | Assumed Application Level | Flash Point (°C) |
|---|---|---|---|
| L-SS-16 | None Specified | | - |
| S-SS-22 | None Specified | | - |
| S-SS-50 | None Specified | | - |
| S-GS-44 | None Specified | | - |
| S-GS-74 | TENSOFILL | Core Closing | Unknown * |
| S-GS-82 | Assumed TECTYL 4110 | Core Closing | 232°C |
| S-GS-114 | ANTICORIT WRCP J207 | Rope Closing | Unknown |
| L-GS-70 | Assumed TENSOFILL | Core Closing | Unknown * |
| L-GS-100A/B | Unknown | Core Closing | Unknown |
| L-GS-140 | TENSOFILL | Core Closing | Unknown * |

*Note: Manufacturer B indicates TENSOFILL is a combination of SACI 500 and Zinc powder, however the manufacturer of SACI has no SACI 500 product listed and instead has SACI 5770A listed as a wire rope lubricating product (along with TECTYL 4110). SACI 5770A has a manufacturer listed flash point of 41°C in lieu of the specific material data for TENSOFILL.

### 5.2.2 Narrow-Spectrum Illumination and Optical Measurements

In addition to quantifying the thermal performance of steel strands, this research presents a novel application of optical measurement techniques. The core of the measurement technique is referred to as digital image correlation (DIC) which uses post-testing software analysis to determine deformations of test specimens based on photos taken during the experiment. DIC requires high resolution photos with high contrast to adequately track points on an object's surface. The camera used in the research herein was a 50-megapixel Canon EOS 5Ds Mark III DSLR camera with manual focus and no stabilization (see Gales and Green 2015); photos were taken at five second intervals for all tests. DIC also requires a clear and consistent view of the test target which, in the case of testing with open flames, can be difficult to achieve. Narrow-spectrum illumination provides a solution for this problem and enables an unobstructed view of test

specimens by selectively filtering light wavelengths that are not optically affected by flames (Smith and Hoehler 2018). By illuminating cable specimens with blue light of wavelength approximately 450 nm and fitting the DIC camera with a corresponding light filter, the visual obstructions created by flames are eliminated and the test can be observed as if no flames are present. This combination of light filtering and DIC has been successfully validated experimentally for timber members exposed to radiant heaters and gypsum encapsulation systems (Gatien et al. 2019, Chorlton et al. 2020).

### 5.2.3 Preliminary Testing

The preliminary testing phase served multiple functions. Namely, the selection of pool fire fuel and size, the characterization of the selected pool fire exposure in terms of average gas temperatures, and the overall experimental configuration in terms of the locations of instrumentation.

Pool fires are not commonly used by structural fire practitioners for testing and have extra considerations of fire dynamics to be understood, hence the author's attention to characterizing the fire properly herein. Three fuels were considered based on their varying suitability for optical measurement with narrow-spectrum illumination and DIC. Methanol, acetone, and kerosene pool fires were chosen for characterization based on their availability to the author. Kerosene was omitted qualitatively as its quality of combustion produced excessive smoke which interfered with the optical measurements beyond the corrective ability of narrow-spectrum illumination. Therefore, fuel properties for methanol and acetone are taken from the literature (Babrauskas 2016) and are available in Table 5.4.

Table 5.4. Fire properties for various liquid fuels considered for pool fires (Babrauskas 2016).

| Fuel | Max Theoretical Mass Burning Rate ($kg/m^2s$) | Extinction Coefficient * Mean Beam Length Corrector ($m^{-1}$) | Density ($kg/m^3$) | Heat of Combustion (MJ/kg) |
|---|---|---|---|---|
| Methanol | 0.015 (0.22 for diameters > 0.6 m) | 0 | 796 | 20.0 |
| Acetone | 0.041 | 1.9 | 791 | 25.8 |

Theoretical pool fire values are based on circular fuel containers; rectangular pans must be converted to an effective diameter through equation 5.1 in order to apply theoretical calculations (Quiel et al. 2015, Babrauskas 2016):

$$\text{if} \quad 0.5 \leq L_f / W_f \leq 2, \qquad D_{f,\,eff} = (4A_f / \pi)^{1/2} \qquad [5.1]$$

$$\text{else,} \qquad D_{f,\,eff} = (4\,[\,2{*}\min(L_f\,,\,W_f)^2\,] / \pi)^{1/2}$$

where $L_f$ and $W_f$ are the pan length and width respectively, $D_{f,\,eff}$ is the effective fire diameter, and $A_f$ is the pan fire area. In addition to the fuel type, a pan size was chosen to contain enough fuel to allow a fire duration of approximately 30 minutes and to expose a 500 mm length of the cable to flames. The theoretical

mass burning rate was used as an initial estimator for the quantity of fuel required to achieve a desired burn time of approximately 30 minutes. This theoretical mas burning rate is given by equation 5.2:

$$\dot{m}'' = \dot{m}''_{\infty} (1 - e^{-k\beta D_{f,\,eff}}) \quad [5.2]$$

where $\dot{m}''$ is the mass burning rate per unit area (kg/m$^2$s), $\dot{m}''_{\infty}$ is the theoretical maximum mass burning rate (kg/m$^2$s), and $k\beta$ is the product of the fuel's extinction coefficient (m$^{-1}$) and the mean beam length corrector (unitless), respectively. The theoretical mass burning rate can be used in equation [5.3] to estimate the theoretical maximum heat release rate (HRR) for a given fire size:

$$\dot{Q}_{f,\,max} = \dot{m}'' \, \Delta Hc \, A_f \quad [5.3]$$

where $\dot{Q}_{f,\,max}$ is the maximum theoretical heat release rate (kW) and $\Delta Hc$ is the fuel's heat of combustion (kJ/kg). Table 5.5 provides parameters for the pan sizes considered. In practice, this theoretical value is reduced based on the assumed quality of combustion (typically not less than 70% of the maximum).

Table 5.5. Pans considered for pool fire tests.

| Pan | Material | Width (mm) | Length (mm) | Depth (mm) | $L_f/W_f$ | Effective Diameter (m) (equation [5.1]) | Area (m$^2$) | Volume Capacity (L) |
|---|---|---|---|---|---|---|---|---|
| Rectangular 1 | Stainless Steel | 487 | 287 | 65 | 0.59 | 0.422 | 0.140 | 9.1 |
| Rectangular 2 | | 600 | 480 | 85 | 0.80 | 0.606 | 0.288 | 24.5 |

Preliminary fires in both pan sizes for methanol and acetone were conducted to estimate the mass burning rate for each and ultimately use these measurements to extrapolate the fuel necessary for a 30 minute fire. Measurements from these tests are presented in Tables 4.6 and 4.7. Note that the measured mass burning rate was calculated based on the volume of fuel and the duration to self-extinguishment; these values were intended only to inform fuel quantities later on and not to represent a characteristic fuel property. These tests enabled a comparison of the proposed optical measuring techniques for both fuel types (Figure 5.3).

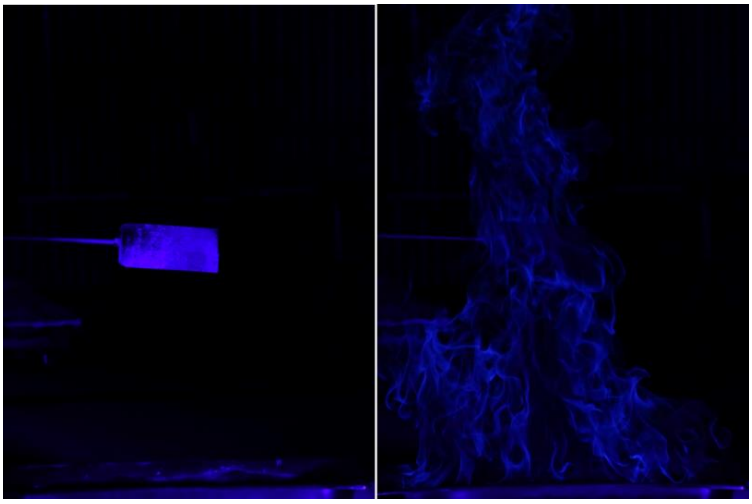

Figure 5.3. Side-by-side comparisons of blue-light filtering for: left) methanol; and right) acetone. A steel target is supported above the pan centre in both images.

Table 5.6. Measured mass burning rates for methanol.

| Pan | Fuel Volume (mL) | Burn Time (min.) | Calculated Mass Burning Rate ($kg/m^2 s$) | Theoretical Mass Burning Rate (equation [5.2]) ($kg/m^2 s$) |
|---|---|---|---|---|
| Rectangular 1 | 946 | 8.3 | 0.011 | 0.015 |
| | 946 | 8.8 | 0.010 | |
| Rectangular 2 | 1892 | 13.5 | 0.009 | 0.022 |

Table 5.7. Measured mass burning rates for acetone.

| Pan | Fuel Volume (mL) | Burn Time (min.) | Calculated Mass Burning Rate ($kg/m^2 s$) | Theoretical Mass Burning Rate (equation [5.2]) ($kg/m^2 s$) |
|---|---|---|---|---|
| Rectangular 1 | 946 | 4.6 | 0.019 | 0.023 |
| | 946 | 4.5 | 0.020 | |
| Rectangular 2 | 1892 | 5.3 | 0.016 | 0.028 |

As Figure 5.3 demonstrates, the optical measurement techniques were not suitable for this scale of acetone fire, likely because of the increasing amount of incomplete combustion found for larger diameter pool fires. Incomplete combustion results in soot production which blocks incident light from reaching the target specimen. Additionally, the higher mass burning rate of acetone yields that much more fuel would be needed in comparison to methanol. Based on these factors, methanol was chosen as the preferred fuel. The larger of the two rectangular pans was also chosen to accommodate more fuel if fire durations were to be updated later in the test series.

To adequately characterize the methanol pool fire using the selected pan, a series of three additional test fires were conducted. Table 5.8 provides the volume of methanol used for each test as well as the burn characteristics observed.

Table 5.8. Pool fire characterization data

| Test Burn | Volume (L) | Burn Out Time (min.) | Growth Period (min.) | Steady State Period (min.) | Decay Period (min.) | Volumetric Burn Rate (L/min.) |
|---|---|---|---|---|---|---|
| Methanol 1 | 6 | 16 | 0.7 | 9.3 | 6.0 | 0.375 |
| Methanol 2 | 11.3 | 29 | 0.6 | 21.8 | 6.6 | 0.391 |
| Methanol 3 | 14.3 | 34 | 0.8 | 28.8 | 4.7 | 0.417 |

A thermocouple tree consisting of seven K-type probe thermocouples was used in each test to measure temperatures with respect to the height above the pan base and choose an ideal height for the cables to be supported at. Figure 5.4 demonstrates the typical fire characterization configuration. Based on these results, a height of approximately 210 mm was selected as the cable height for the test program because this was the hottest region of the flame. Figure 5.5 provides the time-temperature histories for the three characterization tests at approximately a height of 210 mm. Note that, in the context of this study, the steady state gas time-temperature history refers to the period of fluctuation around an average maximum

temperature, not the growth or decay periods where temperatures increase or decrease with little fluctuation. This time-temperature information is updated with gas temperature information as the cable tests progress and are presented again in the following sections. Finally, a methanol fuel quantity of 14.3 L was chosen as it produced a fire duration greater than 30 minutes in the characterization tests. This volume was later revised to 16 L as the available fuel containers held 4 L of methanol. Based on equation 5.3, the maximum theoretical heat release rate of the chosen pool fire is approximately 122 kW.

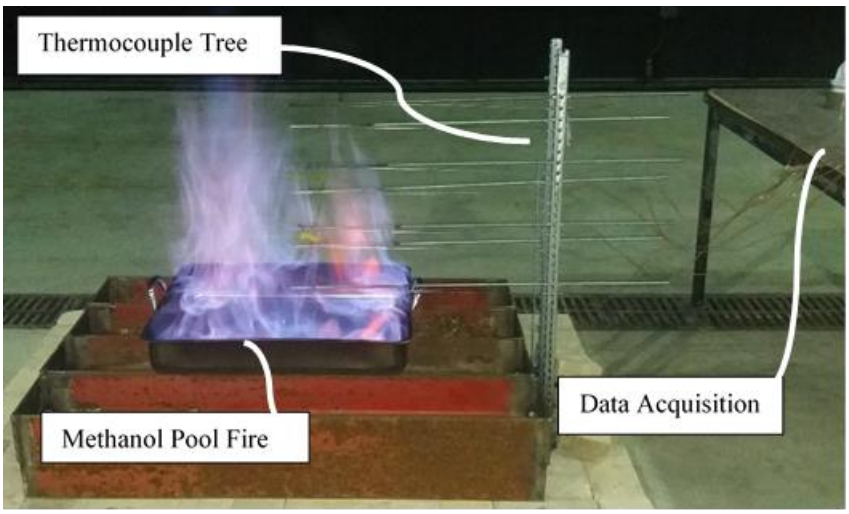


Figure 5.4. Typical fire characterization test configuration.

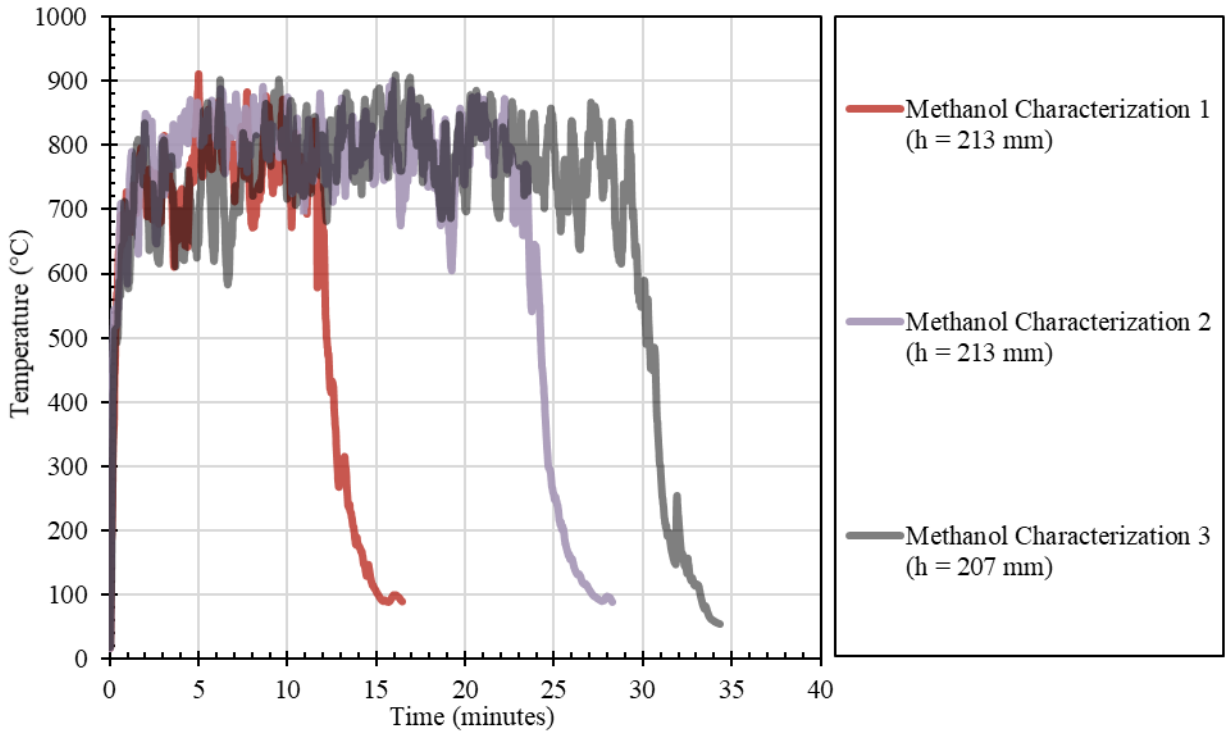


Figure 5.5. Methanol gas temperature-time histories at the selected height for cable heating.

### 5.2.4 Strand Heating

The preliminary testing phase concluded with the trial experiments of cables S-GS-44 and S-GS-82 which were procured separately from the other strands. Figure 5.6 shows the complete test configuration including the positioning of the optical measuring equipment and a sample DIC photo. The cables were supported by masonry blocks above the pool fire pan and were not restrained from thermal expansion. To ensure a localised heating effect, the centre 500 mm of cable length is exposed directly over the pool fire. This exposed length approximately corresponds with the shorter pan dimension of 490 mm and also ensures the transverse direction of the cable is sufficiently engulfed by the 600 mm pan dimension. Immediately outside of the exposed 500 mm region the cables are protected with mineral wool insulation to ensure the majority of applied heat directly affects on the exposed region. This was done such that the conduction into the insulated portion of the cable from solely the exposed region could be studied.

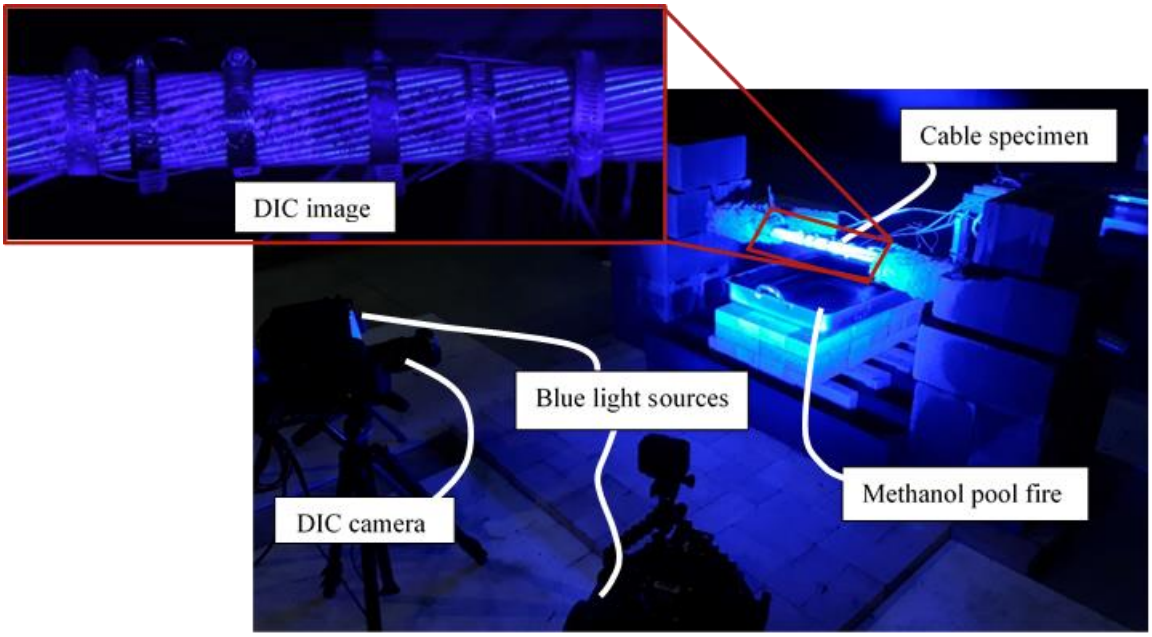


Figure 5.6. Typical digital image correlation and narrow-spectrum illumination test configuration.

In addition to the optical measurements intended to quantify cable deformations, multiple K-type probe thermocouples were installed into the cable specimens to monitor heat transfer. K-type thermocouples have a manufacturer-specified accuracy of the greater of 2.2°C or 0.75% of the measured temperature for temperatures above 0°C; the thermocouples used in this study had an operating temperature range of -200°C to 1250°C. Thermocouples were installed in four cross-sections along the cable length. Each cross-section contained three thermocouple probes, one on the soffit surface, one on the top surface, and one in contact with the core wire. Two thermocouple cross-sections were located 50 mm on either side of the cable centreline in the exposed region. The remaining two cross-sections were located a total of 500 mm on either side of the cable centreline in the insulated region (a total of 250 mm away from the edge of the fire-exposed

region). A final thermocouple was used to monitor gas temperatures directly below the cable. Table 5.9 provides the naming, location, and exposure of each thermocouple. The four locations of the thermocouple cross-sections are referred to as left, centre left, centre right, and right, with centre left and centre right indicating thermocouples in the fire-exposed region. For core temperature thermocouples, the core wires were accessed by milling 6 mm or 12 mm diameter holes (dependent on cable size – cables with diameter 100 mm or greater had to milled with 12 mm diameter holes based on the availability of machine tooling) through the top of the cable to half the total cable diameter. These holes were oriented at the top of the cable relative to the fire below. After the installation of the core thermocouples, the holes were stuffed with mineral wool insulation to ensure a separation between gas temperatures at the top of the cable and the core wire. The preliminary cables S-GS-44 and S-GS-82 assessed the effectiveness of the core hole insulation by comparing temperatures measured above the hole and at the core wire and found an adequate separation in temperature, thus validating this procedure. As a result of this validation however, temperature data for the top surfaces of these cables was not collected. For all other cables tested, thermocouples on the top of the cables measured the steel surface temperatures. Figure 5.7 demonstrates the difference in top surface temperature measurements between preliminary and main cable tests. Surface thermocouples were held in contact with the steel surface by metal ties and pipe clamps; the shielding provided by the pipe clamps was intended to limit some of the natural fluctuations in gas temperatures. For practical reasons, data recording concluded when the insulated regions appear to maximize on the data acquisition software; at this stage, both the fire-exposed and insulated regions are cooling, and no unexpected behaviours were anticipated.

Figure 5.7. (Left) preliminary thermocouple configuration to record temperature difference between core and gas temperature in tests S-GS-44 and S-GS-82; (right) thermocouple instrumentation at one cable cross-section showing the top surface and core thermocouple (soffit thermocouple not shown).

The specimen boundary conditions are indicated in Figure 5.8. The central 500 mm of each cable was exposed directly to the methanol pool fire and constituted the fire-exposed region of the cable. Here, the

thermal boundary is defined by convective and radiative heat transfer between the pool fire, the cable, and the surroundings. In the outer insulated regions, the thermal boundary is largely restricted to conduction through the mineral wool insulation and into the masonry support structure as well as through conduction along the cable member. The longitudinal conduction is assumed to be the dominant thermal boundary in the insulated region due to the low thermal conductivity of the mineral wool insulation. In this regard, cooling through radiation and convection is not facilitated except at the extents of the cable. There is not necessarily unrepresentative of a cable in situ as a HDPE sheath could combust in the fire exposed region while still providing a similar thermal boundary away from the heated zone. Structurally, the strands were prevented from translating out-of-plane and the individual wires were restrained at the ends of each cable through confining wire wrapping provided by the manufacturers. Pipe clamps were used to restrain broken wires near the holes milled in the cable which offer some degree of restraint in the fire-exposed region, however the degree of restraint is thought to be much less than that of the end restraints.

Table 5.9. Thermocouple locations and exposure conditions.

| Thermocouple Number | Location | Exposure | Abbreviation |
|---|---|---|---|
| 1 | Core Wire Right | Embedded | C_R |
| 2 | Cable Soffit Right | Insulated | S_R |
| 3 | Cable Top Right | Insulated | T_R |
| 4 | Core Wire Centre Right | Embedded | C_CR |
| 5 | Cable Soffit Centre Right | Exposed | S_CR |
| 6 | Cable Top Centre Right | Exposed | T_CR |
| 7 | Cable Top Centre Left | Exposed | T_CL |
| 8 | Cable Soffit Centre Left | Exposed | S_CL |
| 9 | Core Wire Centre Left | Embedded | C_CL |
| 10 | Cable Top Left | Insulated | T_L |
| 11 | Cable Soffit Left | Insulated | S_L |
| 12 | Cable Core Left | Embedded | C_L |
| 13 | Gas Temperature | Exposed | Gas |

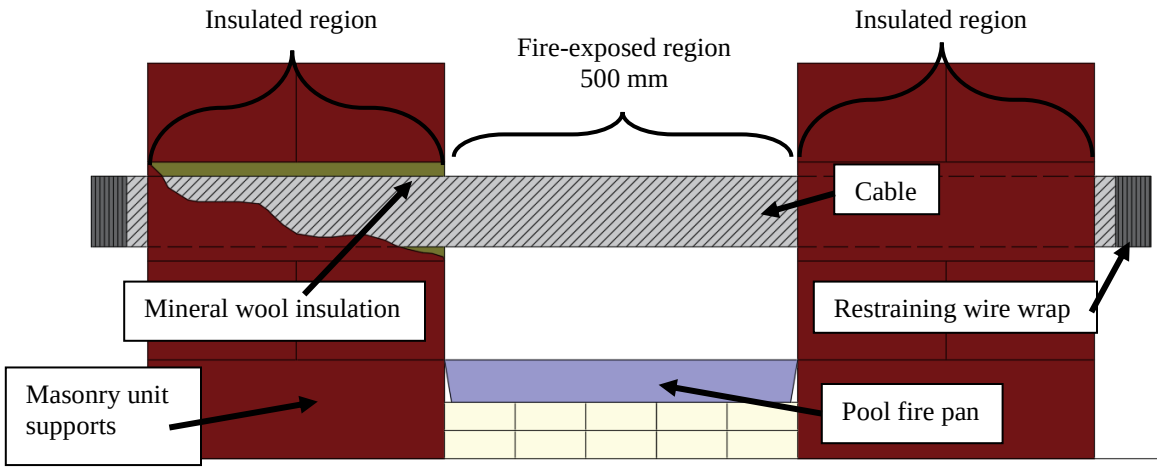


Figure 5.8. Boundary conditions for a typical cable specimen.

### 5.2.5 DIC Analysis

As described, DIC was used in conjunction with narrow-spectrum illumination to measure strand deformations during both the fire exposure and cooling phases of testing. To facilitate creating higher-contrast photos, black and white high-temperature automotive paints (brand name "VHT FlameProof Header Paint" rated for steel temperatures up to 1093°C) were used to speckle the cable surfaces. The DIC analyses were conducting using MATLAB R2019b and GeoPIV-RG, a freely-available MATLAB program that tracks chosen points between images and outputs coordinate data. This coordinate data can be used to calculate strain and displacements to a very high accuracy. The accuracy of the DIC method is dependent on the camera resolution but, with the analysis software above, can achieve values of up to 0.001 pixels (px) (Blaber et al. 2016). Measurements output from the DIC analysis are in units of pixels (px) and must be converted using the real-world length of a known object taken in the photos.

Of specific interest in these tests is the thermal strain development, cable deflection as result of thermally-induced moments (thermal bowing), residual strain recovery, and cable uncoiling. The thermal strain development is examined at two levels: the first level is global thermal strain which two tracks points on opposite sides of the cable midspan to calculate the longitudinal thermal expansion; the second level is wire thermal strain which tracks points on an individual wire to perform the same calculation. Also note that strictly the horizontal strain is calculated for both levels of analysis, not the vector combination of both horizontal and vertical strains as is intuitive for an inclined element with both horizontal and vertical components. The strain calculations are done in this way because the translation of the y-coordinates was greatly influenced by other deformations, such as rotation of wire layers and global deflections from bowing. When total strains were calculated, they were heavily influenced by the inflated y-coordinate movements and the more subtle movements in the x-coordinate were negligible. The x-coordinate

movement alone was found to be more representative of the thermal straining behaviour. Therefore, all strain values presented herein refer strictly to the x-coordinate deformations.

Multiple DIC analyses were conducted for each cable and analysis type (global or wire). For strain calculations, the initial analysis processed every photo consecutively. Due to signal noise arising from the mixing of hot and cold air between the camera and the cable specimens which created optical disruptions, the data required transformation to output final values. The signal noise proved to be a more significant problem for calculations with shorter gauge lengths, namely the wire strain analyses, as the optical disruptions constituted a larger fluctuation with respect to the total measurement. Additionally, the GeoPIV-RG program, originally intended for geotechnical applications, will experience analysis crashes if consecutive photos vary greatly or the points being tracked cannot be identified (due to some optical disruption or physical change at the point of interest). Table 5.10 identifies the input parameters required to perform a DIC analysis in GeoPIV-RG and includes some elaboration justify the selection of particular values.

Table 5.10. GeoPIV-RG parameters used in DIC analysis.

| Parameter | Description | Value | Justification |
|---|---|---|---|
| Approximate Radius | An estimate of the pixel radius of the point of interest to be tracked. | Varied based on selected point | These values are dependent on the specific point being tracked and as such varied between analyses |
| Centroiding Radius | A more refined radius that is used to calculate the centroid of the point of interested. | | |
| Tolerance | Represents how closely each image is tracked. | 0.00001 | Recommended by previous studies (Gatien et al. 2019, Nicoletta et al. 2019a) |
| Computational Limit | The number of iterations the program will use to find a point. | 100 | This value was chased based on trial and error. Too large of a value would waste analysis time by searching for a point that may have been disrupted during testing. |
| Correlation Seed | Provides the initial correlation tolerance for the analysis. | 0.9 | Recommended by previous studies (Gatien et al. 2019, Nicoletta et al. 2019a) |
| Correlation Limit | Sets the lower correlation tolerance for the analysis. | 0.8 | This value was chosen as a more lenient value than those suggested by previous literature (Gatien et al. 2019, Nicoletta et al. 2019a). This was necessary since, due to the degradation of point quality over the course of a test, points of interest did not retain their original shape nor centroid, so some correlation relaxation was required to minimize analysis crashes. A lower value was not selected so as to prevent false recognition of the wrong point. |

Due to analysis crashes occurring when points of interest were disrupted by deterioration or other factors, the aforementioned data transformation also included the task of splicing segments from failed analyses together.

To mitigate these effects, the following calculations were taken in MATLAB R2019b:

1. Output from the DIC analysis is loaded into MATLAB R2019b;

2. Engineering strain as a percentage is calculated based on horizontal coordinate information using equation 5.4:

$$\varepsilon_{x,i} = [\,(x_{2,i} - x_{1,i}) - (x_{2,0} - x_{1,0})\,] / (x_{2,0} - x_{1,0}) * 100 \quad [5.4]$$

where $x_1$ and $x_2$ represent the x-coordinates of the two points of interest, the subscript $i$ denotes the corresponding analysis image, and the subscript $0$ denotes the reference image coordinates. Note, in cases where the analysis crashed and splicing of data segments was required, the strain of a segment would be calculated relative to the start of that analysis, not to the original reference coordinates. This was done in case of small differences in gauge length between the reference images. The y-coordinate of tracked points was not applied to calculate cable thermal expansion because large displacements in the y-coordinate occurred during many tests as a result of wire movement, thermal bowing, and wire bulging. Therefore, the displacements in the y-coordinate were found to be unrepresentative of the true thermal strain development and were orders of magnitude larger than values determined by the x-coordinate alone. This entails that the combination of x and y-coordinate displacements to calculate the total thermal strain was weighted heavily by the erroneous thermal strain and unrealistic values were calculated and the y-coordinate was omitted for this calculation. As the longitudinal (x-direction) thermal strain was of specific interest, this omission was deemed appropriate by the author and produced reasonable calculated values.

3. Each data segment is passed through a standard deviation filter developed by the author to remove extreme outliers from the data set. In some cases, constructive or destructive interference based on the movement of hot and cold air in front of the target caused extreme jumps in coordinate values. The standard deviation filter operated by calculating a rolling average and standard deviation on a manually selected range of data. If a value was found to be outside of one standard deviation from the average of the surrounding data points, it is removed and replaced by the average of the surrounding points. The rolling average window size varied between analyses sets but stayed within the range of 1-5 surrounding data points. A window size of one was chosen for data sets that had no extreme outliers and resulted in no points being replaced. The threshold of one standard deviation for removal was chosen through trial and error as it was found more strict thresholds failed to replace obviously erroneous outliers. For a normally distributed range of signal disruptions, one standard deviation would correspond to over 40% of the data being replaced. However, since the data point density from analysing a photo every five seconds is high, and since the development of thermal strain is a continuous function, applying a small window size yields that the vast majority of values being replaced are extreme outliers, while adequate

data is largely unaffected. The standard deviation filter was applied consecutively five times for each data segment.

4. After the removal of outliers, data segments are spliced together. Splicing occurred by calculating the mean of a range of data points on both sides of a splice and modifying the posterior segment by the difference in means. This procedure was created by the author and operates under the assumption that the average of the boundary of two consecutive segments is equivalent to the average of the true, unsegmented data. This method was chosen instead of other methods such as equating the slope of adjacent segments because this would require curve fitting each data segment which was not always feasible due to the degree of signal noise. The range of data points used in calculating splicing averages was chosen by the author and varied depending on the data set. For example, data with extreme noise required a larger window size to adequately estimate the true average, and data with minimal noise required smaller window sizes. In general, the error associated with this method is higher for data with extreme noise, however, it is assumed that the error in this method for these data sets is contained by the error associated with the signal noise as will be described subsequently.
5. After splicing, the now-continuous data set is passed through a rolling average with a manually-selected window size that was dependent on the signal noise at this stage.

The majority of signal noise creating during the heating phase subsided after the fire was extinguished and air movement diminished. Therefore, the cooling phases for all tests were captured very accurately by the optical measurement system. For global and wire strain data sets, simplified DIC analyses were additionally run in reverse using similar points of interest and processing every 25 photos up until the exhaustion of the fire. This was performed to further quantify the cooling phase and provided a reliable cooling curve which could be used to estimate peak thermal strains as will be described later. To illustrate the process of data processing described above, Figures 5.9 and 5.10 show strain plots detailing the raw data, the filtered and spliced data, as well as a +/- two standard deviation error range on the calculated average value. The average of the reverse DIC analyses to estimate the cooling phase are presented as well. The standard deviation error range was calculated based on a rolling standard deviation of the raw data set before any processing was completed; therefore, this error range represents the maximum spread of the raw data as calculated directly from the DIC output before correction. Deflection calculations were also performed by tracking the midspan of the cables. This analysis considered every ten photos but were not processed as the strain values were. As shown in Figures 5.9 and 5.10, the optical disruptions for the wire strain analysis are much more severe than those in the global strain analysis due to the smaller gauge length. Despite this, the cooling phase of the wire strain analysis is still useful to estimate what the peak thermal strain in the wire was the

moment the fire was exhausted. Therefore, herein only the global strain analysis plots will be presented but the maximum thermal strains developed for both analysis types are provided.

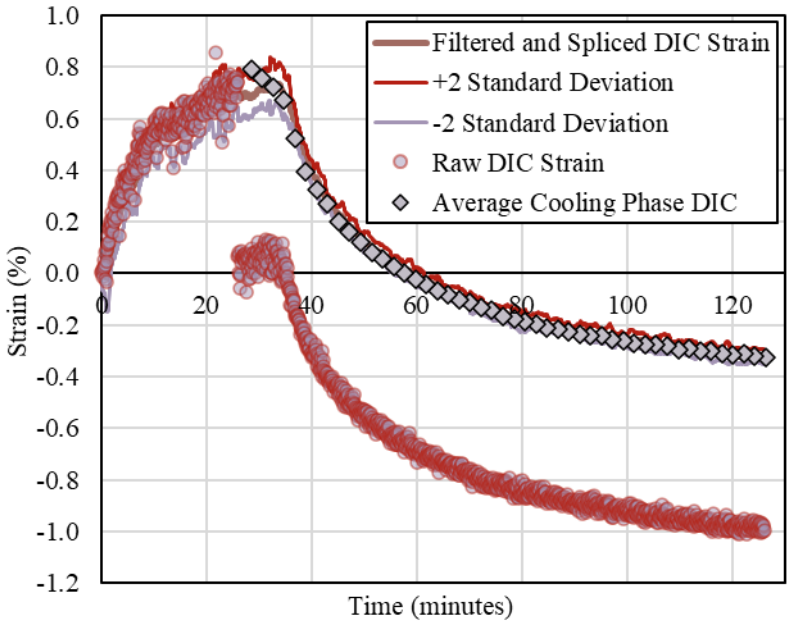


Figure 5.9. Post-processing DIC results for a typical global cable strain analysis. Shown here are the results for cable S-SS-50.

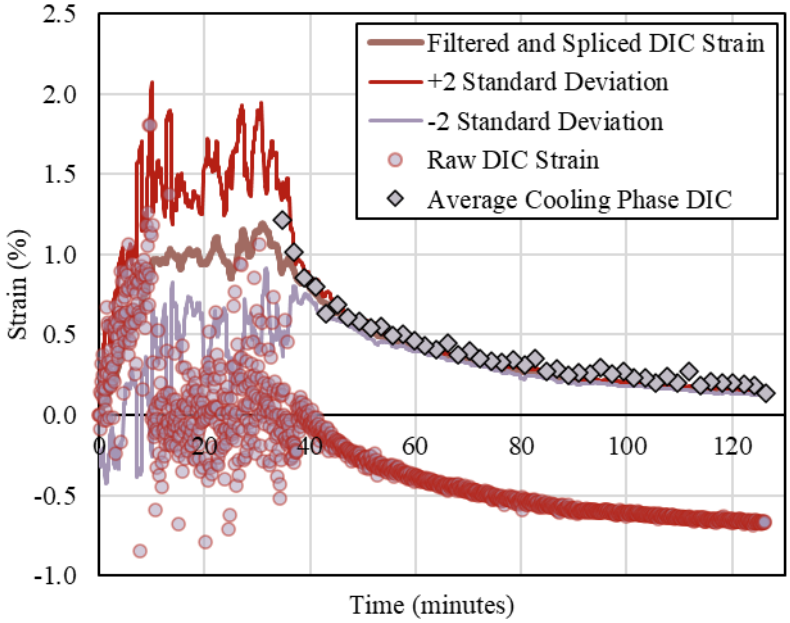


Figure 5.10. Post-processing DIC results for a typical wire cable strain analysis. Shown here are the results for cable S-SS-50.

## 5.3 Results

The numerical results for thermal strain development and heat transfer are presented below. The collective results for each cable will be discussed followed by a comparative analysis considering cable diameter, coil type, and steel type. First, to compare the fire exposures between tests, Figure 5.11 provides an envelope

of gas temperatures versus height above the pan base determined from the initial three methanol characterization pool fires. The enveloped represents the +/- one standard deviation in steady state gas temperatures as determined by a rolling standard deviation. The points represent the average steady state gas temperature calculated from each cable test; the error bars on each point also represent +/- one standard deviation.

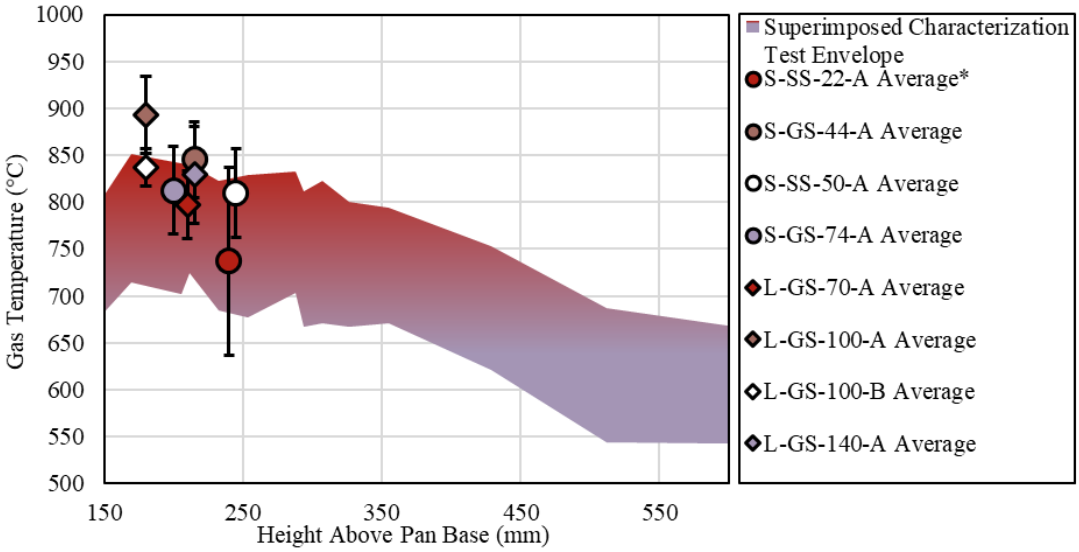


Figure 5.11. Average steady state gas temperatures versus height with ±1 standard deviation in temperature for cable and fire characterization tests. *Thermocouple became unstable and increased variability; this is not necessarily a reflection of a lower fire exposure.

### 5.3.1 Comparison of Strand Heat Transfer

The temperature development within a strand is of importance for the thermo-structural response of a cable-supported structure as the material properties directly depend on this behaviour. This section examines the heat transfer recorded by the thermocouples positioned in the fire-exposed and insulated regions of each strand. Here, comparisons will be made between cables of varying diameter, coil type, and steel composition. Table 5.11 provides the maximum recorded temperatures for key locations in the strand structure. Note that thermocouple instrumentation was placed symmetrically around the centre of the pool fire and therefore values presented represent the average values for the same location on both sides of a strand.

Table 5.11. Maximum temperatures in critical regions for each cable test.

| Cable | Steady State Fire Time (min.) | Exposed Region | | | | Insulated Region | |
|---|---|---|---|---|---|---|---|
| | | Soffit Temp. (°C) | Top Surface Temp. (°C) | Core Temp. (°C) | Time to Max. Core Temp.(min.) | Core Temp. (°C) | Time to Max. Core Temp. (min.) |
| S-SS-50 | 32 | 692 | 552 | 582 | 33 | 43 | 112 |
| S-SS-22 | 27 | 721 | 586 | 596 | 10 | 42 | 77 |
| S-GS-44 | 26 | 776 | N/A | 612 | 27 | 82 | 72 |
| S-GS-74 | 34 | 540 | 462 | 450 | 39 | 79 | 94 |
| L-GS-70 | 34 | 578 | 505 | 488 | 37 | 82 | 98 |
| L-GS-100A | 33 | 501 | 430 | 408 | 37 | 73 | 104 |
| L-GS-100B | 32 | 450 | 482 | 418 | 37 | 72 | 108 |
| L-GS-140 | 32 | 465 | 338 | 238 | 42 | 67 | 143 |

In general, intuitive trends such as decreasing surface and core temperatures with increasing cable diameter are present. The time to maximum core temperatures also increased with increasing diameter with the exception of the two stainless steel strands (S-SS-22 and S-SS-50) which have a reduced thermal conductivity when compared to the galvanized steel strands. This resulted in longer times to reach a maximum temperature for areas heated primarily through conduction such as the exposed core and all insulated regions. Compared to a similarly-sized spiral strand (S-GS-74), strand L-GS-70 developed slightly hotter temperatures in the exposed region due to a smaller void ratio which enabled more conduction through the cross-section. This relative temperature increase was reduced in the insulated region where temperatures between S-GS-74 and L-GS-70 were more normalized.

To consider the effect of increasing cable diameter on heat transfer, Figure 5.12 compares the temperature development of strands L-GS-70, L-GS-100B, and L-GS-140 in both the exposed and insulated regions. Here, the role of increasing cable diameter can be clearly observed where a decrease in maximum temperature occurs for larger strands. An increase in the time to maximum core temperature is also observed for larger diameters as the conduction path to the core is correspondingly larger and there is more latent heat in the structure after the fire is exhausted. Additionally, the temperature gradients between the core, soffit, and top are greater for the larger diameter strands which has implications for thermal deformation effects which are largely dependent on temperature differential. The insulated regions shown in Figure 5.12 more clearly illustrate the effect of increasing diameter where L-GS-70 reaches a maximum approximately 40 minutes before L-GS-140. Also of interest in the insulated region is the effect of cross-sectional temperature normalization which reduces the temperature gradients between the core, soffit, and top to below 10°C for all strands at a length of 250 mm past the exposed-insulated boundary. To consider the role of strand diameter in spiral strands, Figure 5.13 compares the heat transfer in strands S-GS-44 and S-GS-74. Similarly to the locked-coil comparison, S-GS-44 and S-GS-74 experience a reduced temperature

maxima for a larger strand diameter and a normalization of insulated temperatures in both cases. Figure 5.14 provides a similar diameter comparison for the stainless steel strands S-SS-22 and S-SS-50. Here it can be seen that strand S-SS-22 achieves steady state exposed temperatures, denoted by the plateau in core, soffit, and top temperatures approximately 10 minutes into the fire exposure. Strand S-SS-50 achieves a similar plateau after approximately 22 minutes of fire exposure. In this comparison, there is little difference in maximum exposed temperatures nor exposed temperature gradients with varying diameter; the greatest distinction between strands S-SS-22 and S-SS-50 is the time to reach maximum exposed temperatures. This response is consistent with both strands reaching steady state temperatures in the exposed region before the fire was exhausted. A steady state response such as that shown in Figure 5.14 is characterized by the stabilization of the thermal boundary and internal temperatures and will occur earlier in smaller diameter strands due to a correspondingly small thermal inertia. The response of the insulated regions of strands S-SS-22 and S-SS-50 demonstrates larger temperature gradients than previous tests. This is attributed to the lower thermal conductivity of stainless steel which plays an important role in the internal temperature distribution.

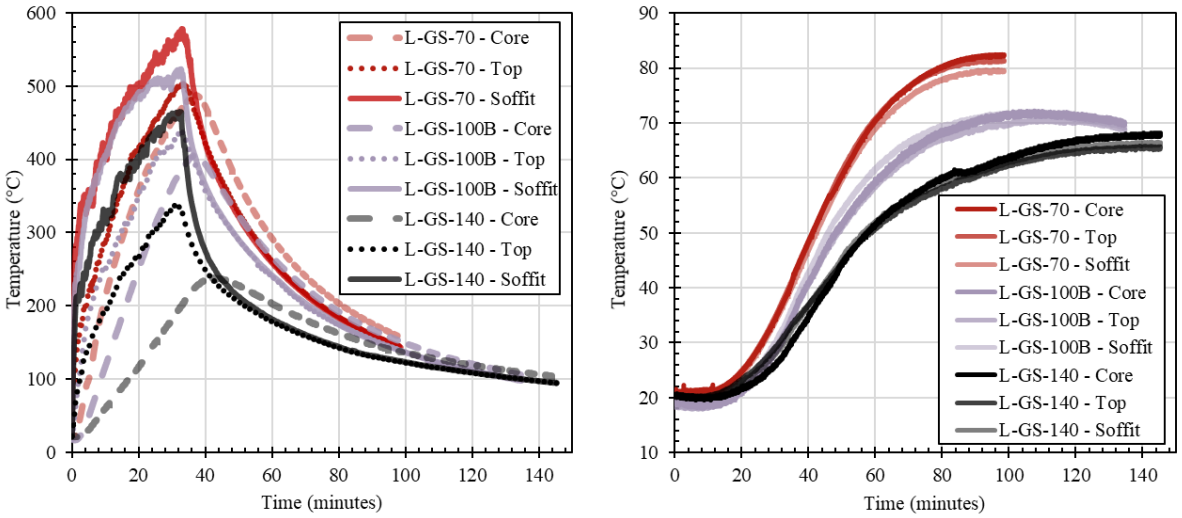


Figure 5.12. Comparison of average core, soffit, and top temperatures between locked-coil, galvanized steel strands of varying diameter for the (left) fire-exposed and (right) insulated regions.

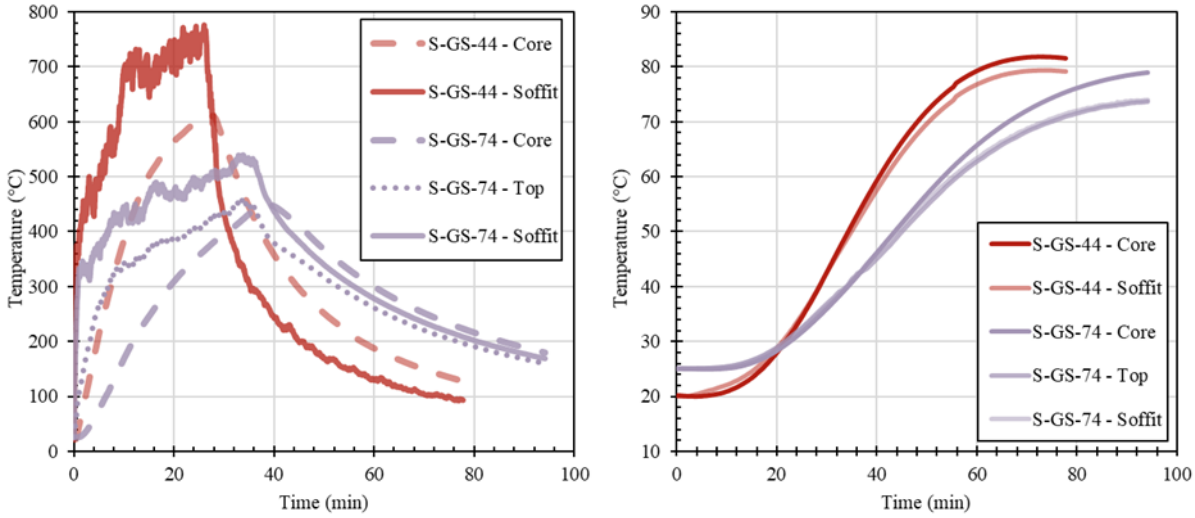


Figure 5.13. Comparison of average core, soffit, and top temperatures between spiral coil, galvanized steel strands of varying diameter for the (left) fire-exposed and (right) insulated regions.

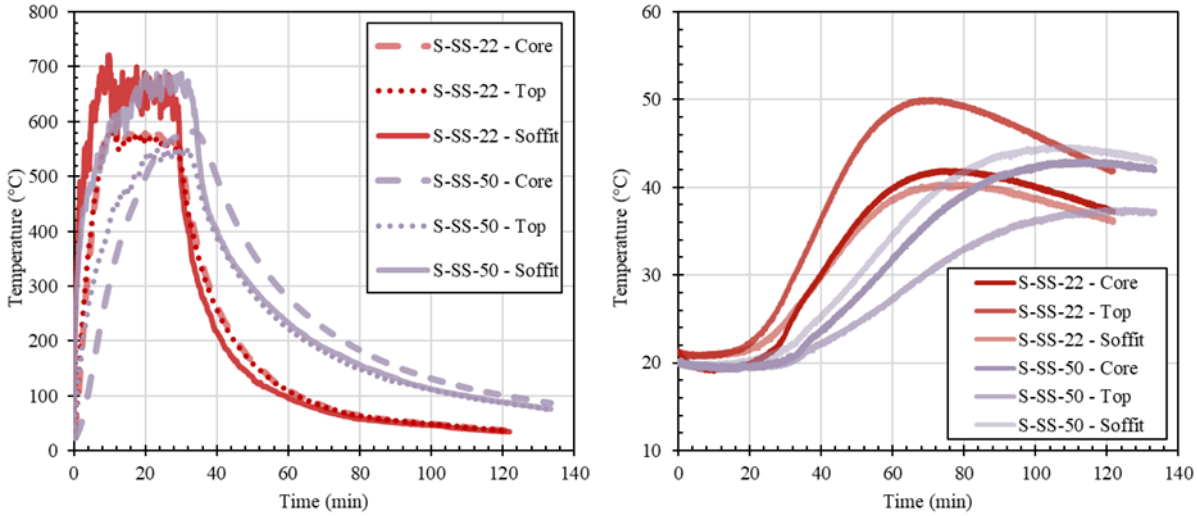


Figure 5.14. Comparison of average core, soffit, and top temperatures between spiral coil, stainless steel strands of varying diameter for the (left) fire-exposed and (right) insulated regions.

Figure 5.15 presents the results of strands S-GS-74 and L-GS-70 to compare the effects of coil type on heat transfer. Despite a similar fire exposure, the spiral coil strand reaches lower maximum temperatures in the fire-exposed and insulated regions. Additionally, the heating rate for S-GS-74 appears to slow after approximately 10 minutes compared to L-GS-70. These behaviours are attributed to the greater steel area in the locked-coil strand and the high level of inter-wire contact provided by the outer Z-shaped wires. These two effects both enable more paths for conduction from the outer wires layer and reduced the interior air voids available to insulate the strand. The increased conductive heat transfer in L-GS-70 is demonstrated more explicitly by the temperature development in the insulated region. Here, temperatures in the core, soffit, and top increase more quickly and to larger maxima than those of S-GS-74. For both strands, the insulated temperatures are normalized and do not create the gradients seen in the fire-exposed region.

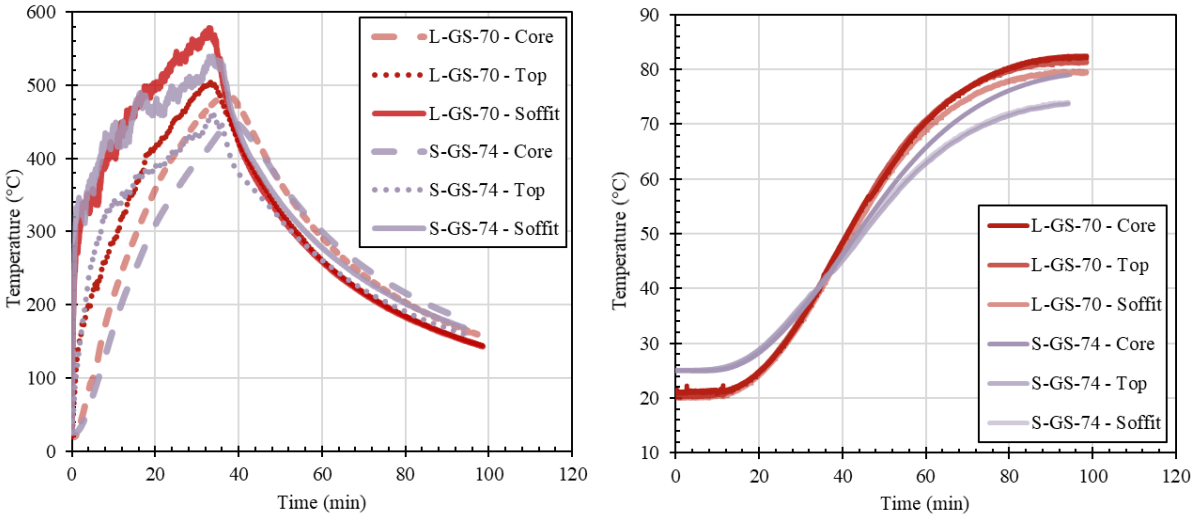


Figure 5.15. Comparison of average core, soffit, and top temperatures between similarly sized, galvanized steel, locked-coil and spiral strands for the (left) fire-exposed and (right) insulated regions.

Figure 5.16 compares the heat transfer measured in strands S-GS-44 and S-SS-50 to quantify the effect of steel type. The fire-exposed time-temperature histories of both strands appear relatively similar in terms of heating rate, maxima, and temperature gradients. Strand S-SS-50 achieved slighly lower temperatures despite experiencing a longer fire duration (32 minutes versus 26 minutes). This is attributed to a combination of the slightly larger diameter of strand S-SS-50 as well as the reduced thermal conductivity of stainless steel which limited heat transfer within the cable. The important role of thermal conductivity is shown in the response of the insulated region of both strands where the maximum temperatures developed by strand S-SS-50 are greatly reduced than those of S-GS-44. Additionally, the normalization of insulated temperatures is observed to a lesser extent in strand S-SS-50 again due to the reduced thermal conductivity.

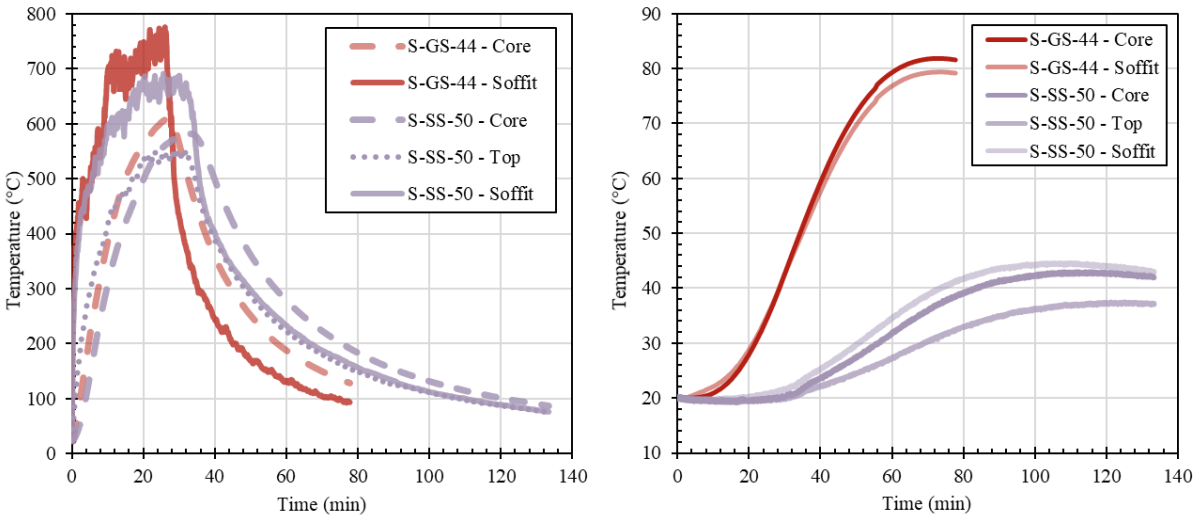


Figure 5.16. Comparison of average exposed core, soffit, and top temperatures between similarly sized stainless and galvanized steel, spiral coil strands for the (left) fire-exposed and (right) insulated regions.

Figure 5.17 compares the heat transfer response of identical strands L-GS-100A and L-GS-100B to assess the repeatability of the fire exposure. Note that the test of L-GS-100A required the activation of emergency ventilation which reduced gas temperatures near the strand for approximately five minutes between 10 and 15 minutes into the test. Despite this discrepancy, the behaviours of L-GS-100A and L-GS-100B are very similar in terms of temperature maxima in the exposed and insulated regions. The exposed core and insulated temperatures were particularly unaffected by the ventilation introduced during the testing of L-GS-100A, owing to the thermal inertia of the strand and that the ventilation likely had a greater impact on the reading of the thermocouples which are sensitive to changes in convective heat transfer. This implies the disruption to the external surface thermocouples may not represent the same severity of thermal disturbance to the strand as the change recorded is largely a result of the convective heat transfer only, and not necessarily as severe of a change in radiative heat transfer, for example.

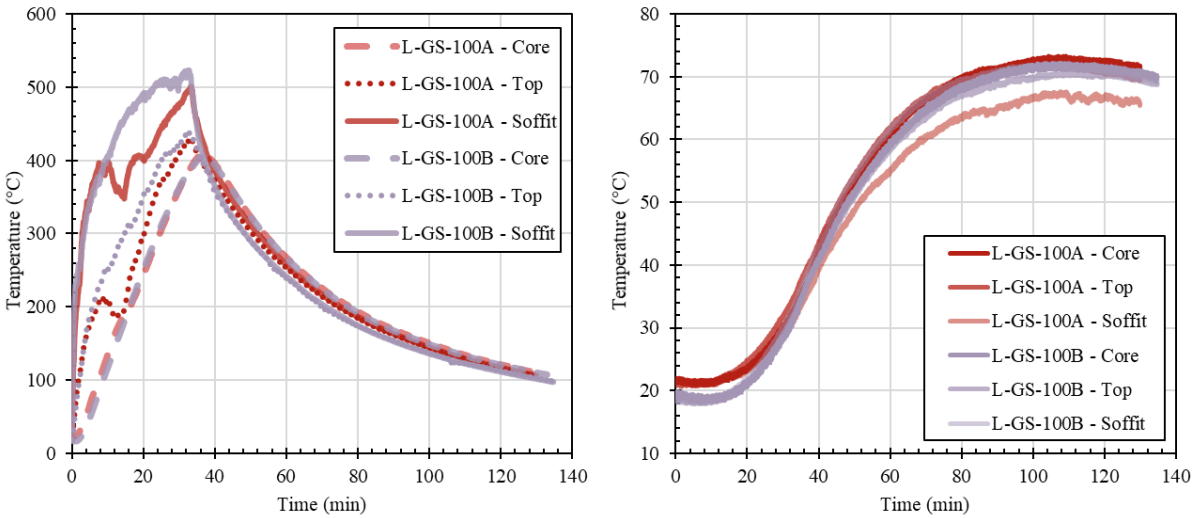


Figure 5.17. Comparison of average exposed core, soffit, and top temperatures between identical strands (L-GS-100) for the (left) fire-exposed and (right) insulated regions

To make some general conclusions about the heat transfer response of the strands investigated, it was shown that increasing cable diameter reduces the overall temperature maxima developed in both the fire-exposed and insulated regions of the cable. Furthermore, the temperature maxima of interior or insulated regions of larger-diameter strands occur later than those of smaller diameters due to the increased thermal inertia. Generally, larger-diameter strands were found to achieve steady state temperatures later, if at all, and had larger thermal gradients in the fire-exposed region when compared to smaller-diameter strands. In the insulated regions, temperature gradients between the core, soffit, and top were diminished regardless of strand diameter, indicating temperature normalization can occur in as little as 250 mm from the edge of the heated zone for all galvanized steel strands. The reduced thermal conductivity of the stainless steel strands S-SS-22 and S-SS-50 developed relatively large thermal gradients, especially in the insulated region, considering that both strands approached or reached steady state temperatures during testing. The thermal

conductivity of the stainless steel strands decreased the conduction to the insulated region compared to a similarly-sized galvanized steel strand, highlighting the important implications of material properties on the thermal response. The effect of full locked-coil stranding versus spiral stranding increased the maximum temperatures and heating rate developed because the full locked-coil strand had less thermal insulation resulting from a smaller proportion of air voids and provided a more effective conduction path through the interlocking Z-shaped outer wires. The facilitation of thermal conduction resulted in hotter insulated temperatures in the locked-coil strands. An important implication from these results is the normalization of cross-sectional temperatures after a short conduction path. This implies that modelling efforts need only consider the fire-exposed region plus a small boundary area in two or three-dimensional heat transfer modelling and cable portions heated only through conduction can be modelled by one-dimensional heat transfer. The mechanism for this temperature normalization is a combination of both inter- and intra-wire thermal conduction, where adjacent wires transfer heat to the interior of the cable structure and individual wires transfer heat around the strand circumference as they spiral around the core wire. Based on this result, future work should assess if heat transfer in parallel-strand wires normalize in a similar manner despite applying helically wrapped wires.

### 5.3.2 Overall Strand Thermal Response

The following series of figures represent the superimposed plots of exposed cable temperatures, horizontal and vertical translations of the points of interest used in global strain calculations, the midspan cable deflection, and the calculated global strain. Also presented are the thermal gradients between the soffit and the core, the soffit and the top, and the top and the core thermocouples. This configuration was chosen to help explain variations in each parameter. Strand behaviour is discretized into various stages to represent specific thermal deformation actions occurring in each. The “points” referred to in the horizontal and vertical translation plots represent the two points of interest used in the DIC analysis and subsequent global strain calculation; therefore, “Point 1” refers specifically to the point chosen on the left side of the strand relative to the camera, and “Point 2’ refers to the point chosen on the right side of the strand. The points of interest were taken at the maximum possible gauge length based on the quality of point contrast maintained through the test duration. The translations of these points were included to aid in understanding the movements occurring on the cable surface and the correlation to the calculated strain values.

To reiterate, the specimen naming convention uses the format *coil type – steel type – strand diameter* where *S* or *L* indicates spiral or locked-coil strand types respectively, *GS* or *SS* indicate galvanized or stainless steel types respectively, and the final number indicates the nominal diameter in units of mm. Identical cables are followed by a letter after this nomenclature to further distinguish the specimens. Figure 5.18 presents the thermal response of cable S-SS-50.

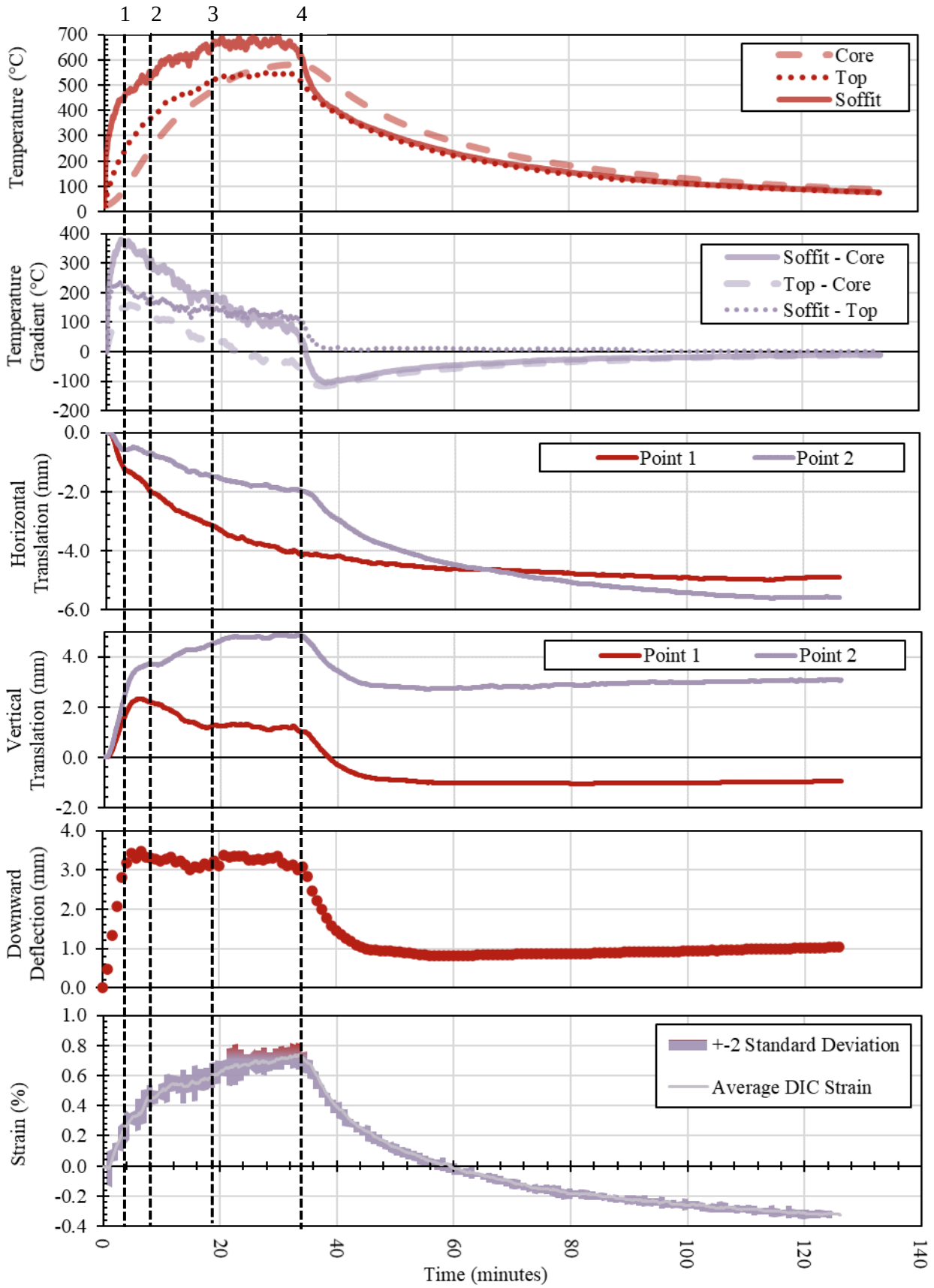


Figure 5.18. Thermal response of cable S-SS-50.

**Stage 0-1:** Cable temperatures rapidly increase corresponding to an increase in strain and downward deflection. At point 1, the thermal gradients in the cable peak which causes an abrupt stop in deflection development. This is due to thermal bowing, an induction of moment in the cable caused by a temperature differential; the greater the temperature differential, the more deflection is induced.

**Stage 1-2:** Top and soffit temperatures change in slope as cable temperatures increase. This change in heating rate is reflected in the thermal strain in this stage which also experiences a decrease in slope. In this stage, downward deflection has plateaued, corresponding to the plateau of the soffit-top thermal gradient. The vertical translation of points of interest begins to separate in this stage, corresponding to wire displacement created by rotation of the surface layer.

**Stage 2-3:** Soffit and top temperatures experience another reduction in slope which again is matched in the strain development. The midspan deflection decreases slightly as the top-soffit gradient is reduced.

**Stage 3-4:** Soffit and top temperatures plateau as the external wire layers reach a steady state. This causes the thermal gradient to plateau once more with the midspan deflection responding similarly. Strain continues to increase at the same rate as more of the internal cable structure is heated. This behaviour is noteworthy as it indicates the calculated strain is not only that of the external wires, and some interaction with lower wire layers may be present through a frictional effect.

**Stage 4 onward:** Point 4 represents the exhaustion of the pool fire which causes all parameters to enter to the cooling phase. Note that the core temperature peaks slightly after the cooling phase begins due to the delay in heat transfer to the core. The downward deflection reverses as a negative thermal gradient is developed with cooling. Also note that none of the deformation values return to zero, indicating a release of residual strains as a result of heating. This residual deformation for the strain and translations can also be attributed to the non-ambient temperature of the cable at the end of analysis; however this does not explain the residual deflection which is governed by the temperature gradient and at the end of the analysis as equalized. Both the relief of residual strains and the non-ambient cable temperatures play a role in these residual values.

Figure 5.19 presents the thermal response of cable S-SS-22 which takes place in four identified stages.

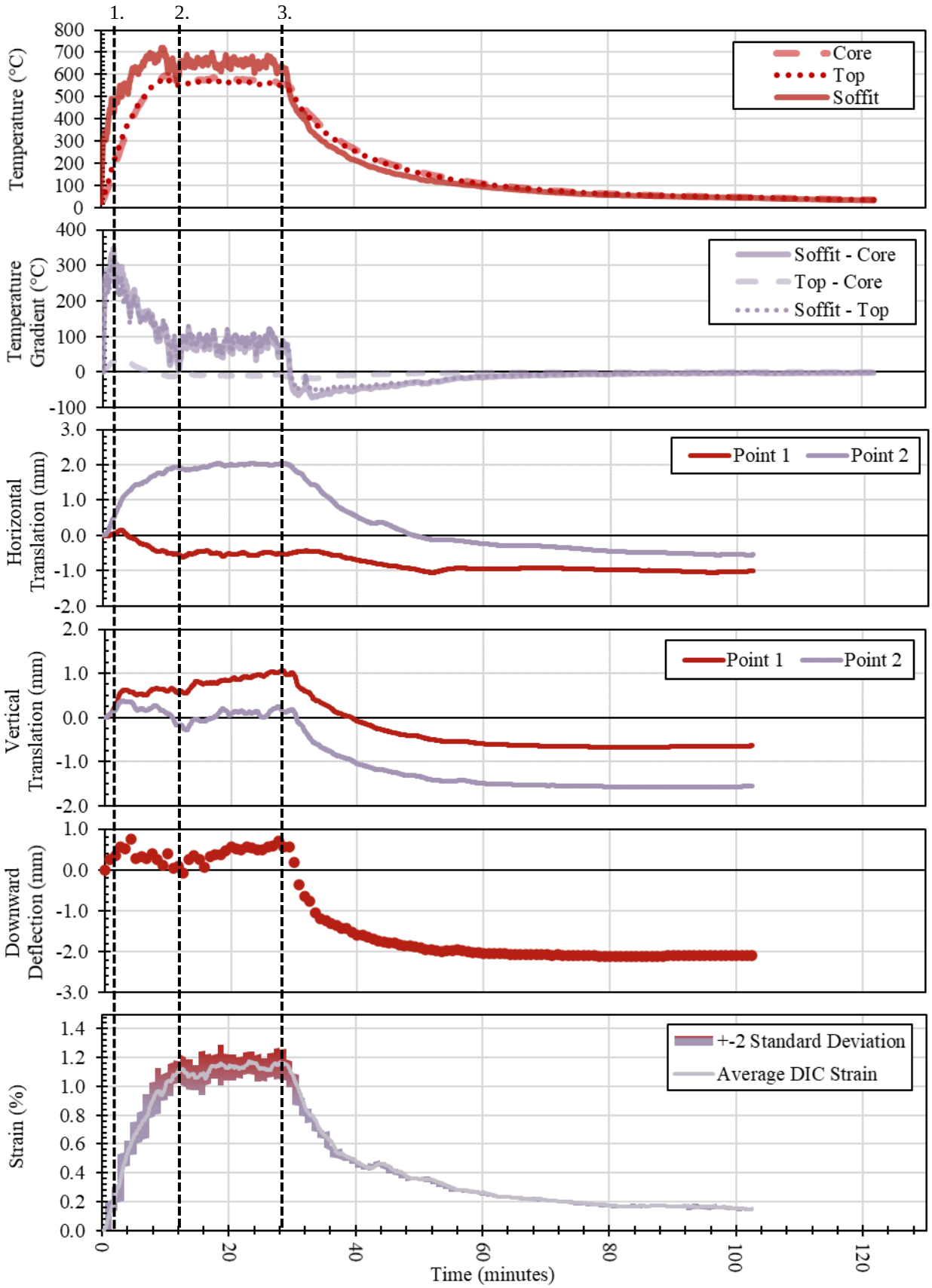


Figure 5.19. Thermal response of cable S-SS-22.

**Stage 0-1:** Soffit temperatures increase rapidly and establish the peak thermal gradient between the top and soffit. Downward deflection increases with the thermal gradient. Since the thermal gradient stabilizes relatively quickly for this small-diameter strand, the magnitude of the deflection is minimized.

**Stage 1-2:** Soffit temperature slope decreases while top and core temperatures are unchanged. Thermal gradients decrease dramatically in this stage as the small-diameter strand approaches thermal equilibrium. This decrease is shown in the midspan deflection where the thermal bow decreases correspondingly. Small magnitudes of cable unwinding occur here as the vertical translation of the points of interest separates. By Stage 2, the separation of vertical translation has subsided.

**Stage 2-3:** Soffit, core, and top temperatures plateau as the system enters thermal equilibrium. Minor deflection continues as a result of vertical wire movements on the cable surface. Strain development also plateaus here to match temperature equilibrium.

**Stage 3 onward:** The pool fire is exhausted, and the cooling phase begins. The downward deflection is reversed as a negative thermal gradient is developed. The residual deflection is not accompanied by a residual strain because the residual strain associated with manufacturing a small-diameter strand is minimal compared to larger diameters which require more deformation. Therefore, the residual downward deflection is believed to be a result of residual strains from cable spooling which predominantly deforms wires on the top and bottom of the strand which were not visible to the DIC camera and therefore not unquantified by the strain plots.

Figure 5.20 demonstrates the existing strand curvature for cables S-SS-22 and S-SS-50. Cable S-GS-44 also had a noticeable bow before testing as a result of spooling. Figure 5.21 provides the thermal response for strand S-GS-44.

Figure 5.20. Pre-testing cable bow for stands S-SS-22 and S-SS-50.

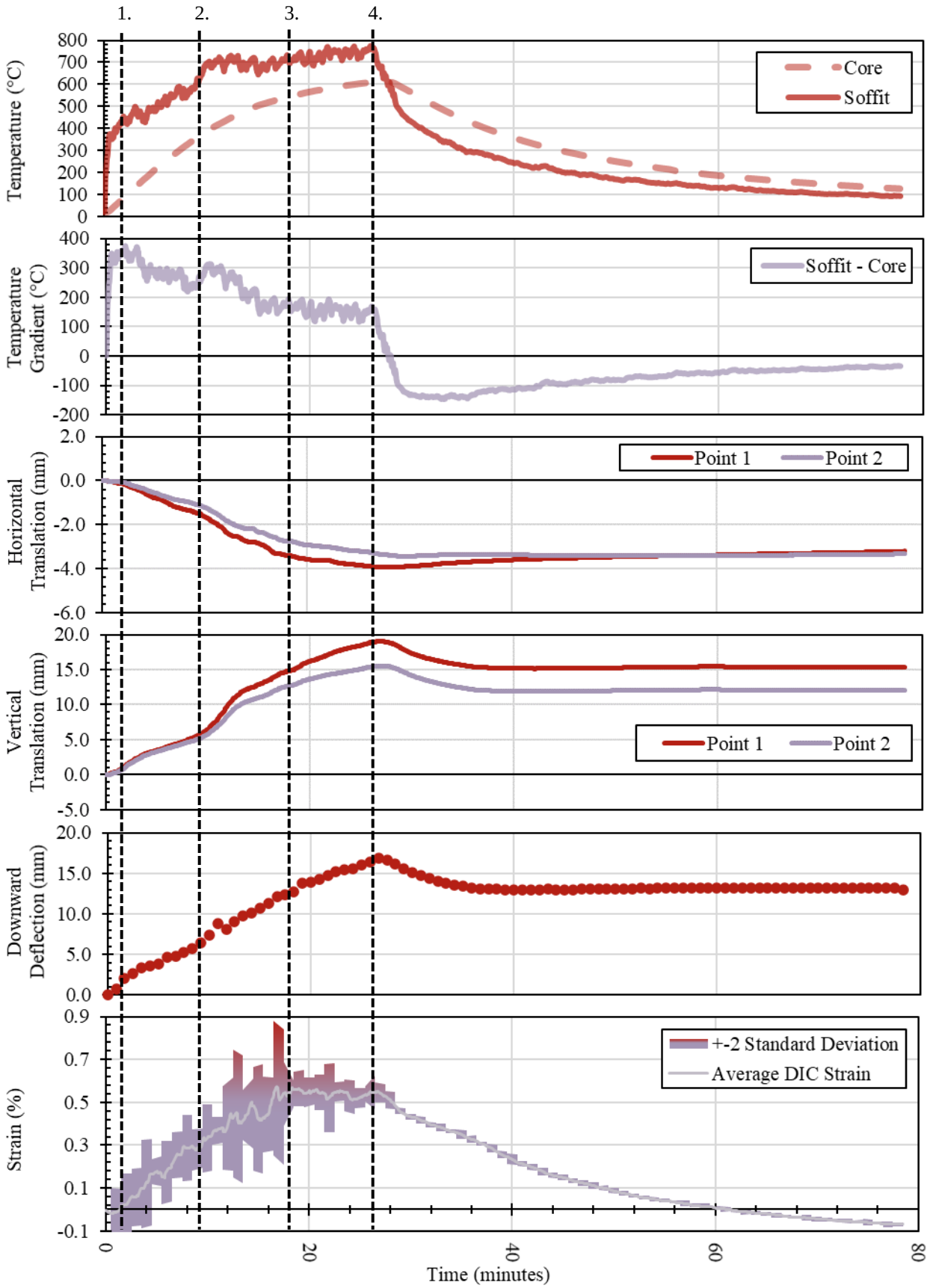


Figure 5.21. Thermal response of strand S-GS-44.

**Stage 0-1:** Thermal gradient between the soffit and core peaks. Temperature data of the top surface was not collected for this preliminary cable and so information about the soffit-top thermal gradient is unknown. Based on the top temperature trend for previous tests, the temperature of the top likely follows a profile in between those of the soffit and core.

**Stage 1-2:** The thermal gradients begin to decrease as more of the cable is heated. Both strain and midspan deflection inflect slightly as soffit temperatures begin to increase more slowly.

**Stage 2-3:** Soffit temperatures and thermal gradient begin to plateau. Strain development begins to slow as temperatures approach equilibrium. Downward deflection continues likely because the soffit-top gradient is yet to plateau. Vertical point of interest translation begins to separate indicating some unwinding is occurring.

**Stage 3-4:** Strain plateaus as soffit temperatures finish equalizing. The separation of vertical translations is increasing while midspan deflection begins to peak.

**Stage 4 onward:** The cooling phase begins, and some deflection is recovered as negative thermal gradients are created. Strain decreases and some residual strain recovery is made apparent. Again, there is a distinction between the residual deformations in the midspan deflection and thermal strain where the strain associated with the pre-test bow of strand S-GS-44 is recovered but is not shown in the DIC analysis.

Figure 5.22 demonstrates the thermal response of cable S-GS-74.

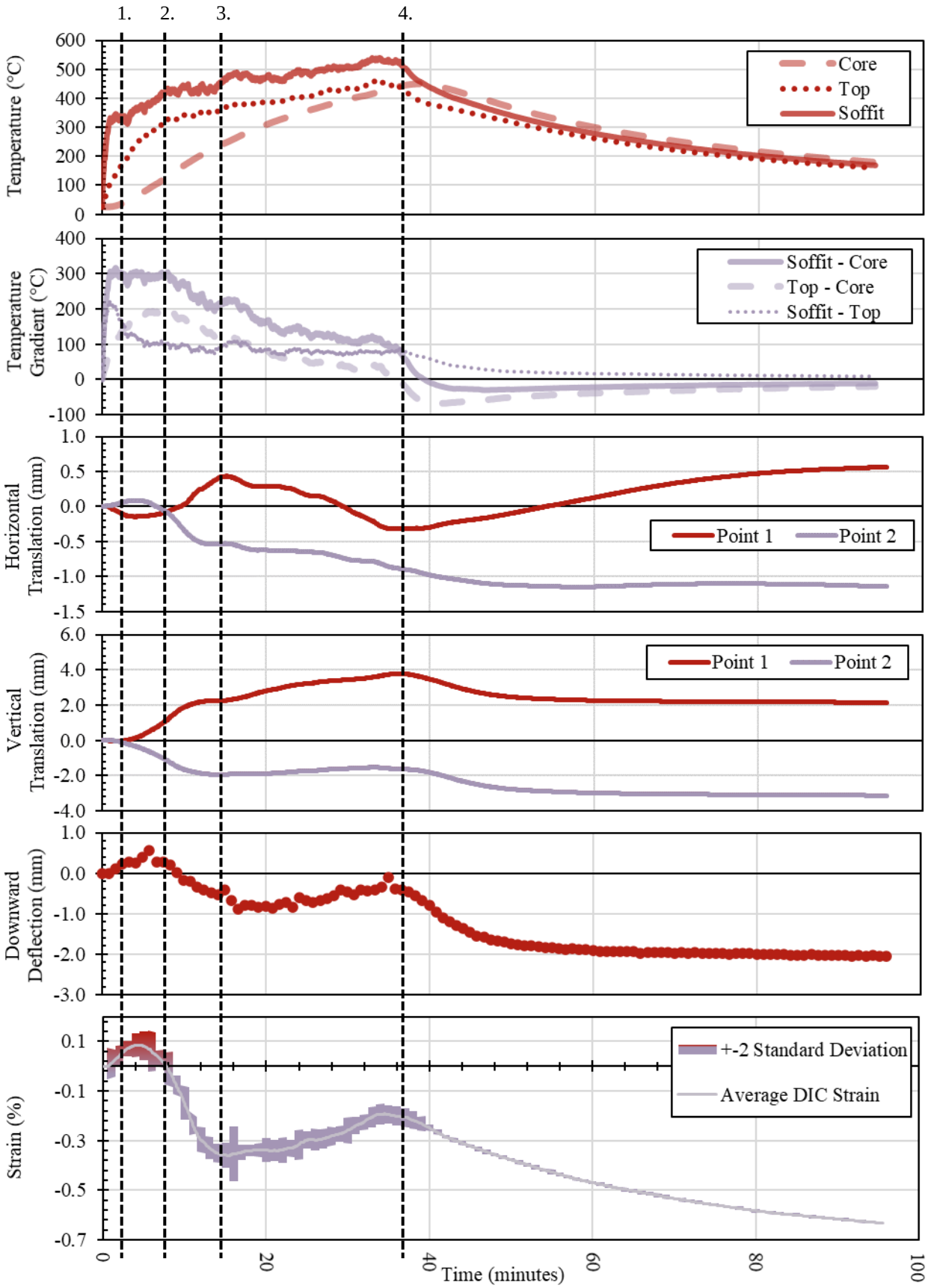


Figure 5.22. Thermal response of strand S-GS-74.

**Stage 0-1:** Soffit temperatures increase rapidly, creating a peak in thermal gradients between the soffit and core, and between the soffit and top. The soffit-top gradient quickly begins to decrease as top temperatures increase. This results in only a slight increase in downward deflection in this phase.

**Stage 1-2:** A point of inflection occurs for both the strain and downward deflection. Vertical translations of the points of interest also begin to separate, indicating uncoiling is occurring. The downward deflection remains relatively consistent as the thermal gradients plateau. The increase in soffit temperatures begins to slow which should yield a slower, but still increasing, strain development. Instead, the strain reaches a maximum and begins to decrease, closely following the behaviour of the downward deflection. The mechanism operating in this stage is the result of two thermal gradients: the circumferential and wire-longitudinal gradients. The wire longitudinal gradient results in a torsional effect where wires with lay angles that pass through the soffit force the expansion of higher portions of the same wire. Due to the lay angle of the wires, higher wire segments are forced upwards from the expansion of the longitudinal lower segments at the soffit. This vertical component of longitudinal wire expansion causes segments of adjacent wire to rotate relative to the core wire. This effect occurs circumferentially around the strand, but the driving force is the expansion caused by the hotter soffit wires. Therefore this is highly-dependent on the lay angle and direction of the strand and implies that wires will be "pushed" from the soffit along the direction they are laid, and the vertical component of this expansion causes the wire layer to rotate. Figure 5.23 demonstrates this mechanism in action. This behaviour is reaffirmed by the occurrence of bulging, resulting from restrained thermal expansion of individual wires on the left-side of strand S-GS-74, for example. Since this effect occurs on both sides of the cable, the strand rotation is more pronounced at the insulated boundaries and very limited at midspan since there is no equal-and-opposite effect to counteract the rotation. Although some wire rotation was present in the smaller-diameter strand tests, this effect relies on a longitudinal thermal gradient in individual wires which is greater for larger cables. This behaviour is corroborated by the by the vertical translation of the points of interest which show an upward translation for the right-side point of interest and a downward translation for the left-side point of interest. Ultimately, this rotation of surface wires forces the points of interest inward horizontally, which creates the strain reversal seen in this stage.

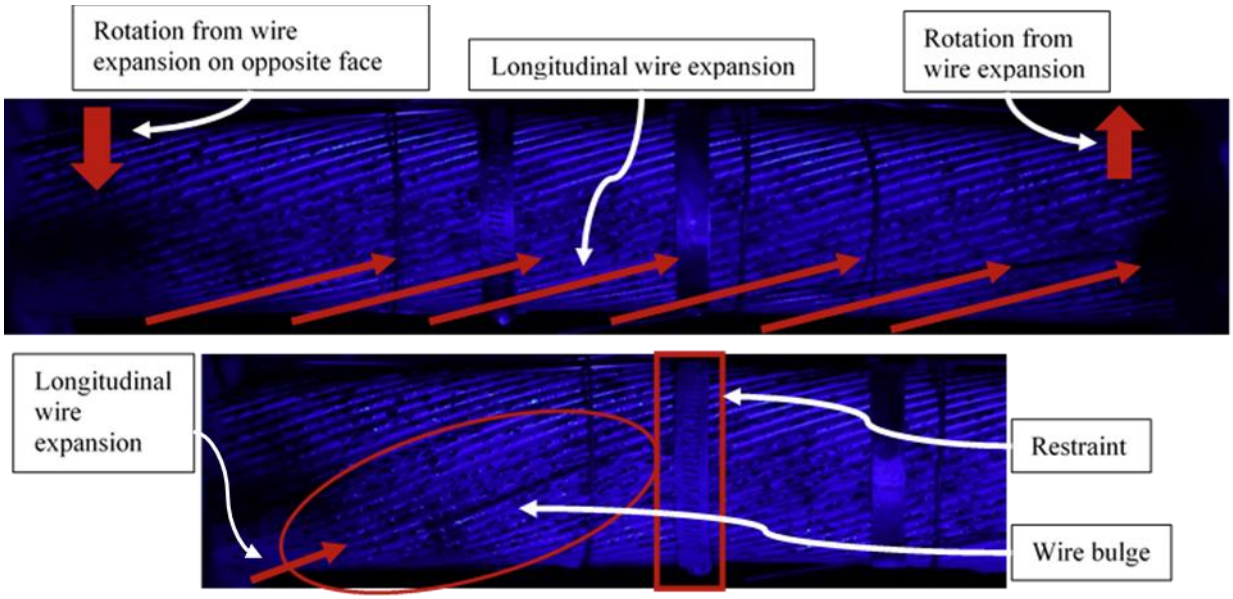


Figure 5.23. Thermal torsion and wire bulging from individual wire thermal expansion in strand S-GS-74. Top photo was taken at ignition and the bottom photo was taken 14 minutes after ignition.

**Stage 2-3:** In this stage, the deflection continues to decrease slightly as temperature gradients reduce. Strain decreases dramatically as the thermal torsion effect accelerates. Vertical translation continues to separate in this stage, confirming the rotation of the cable ends. The soffit-top temperature gradient remains relatively constant, while the soffit-core and top-core gradients decrease. This is reflected by a slight rebounding of downward deflection. Note that the deflection behaviour in this strand is less directly dependent on the soffit-top temperature gradient as internal and adjacent wires contribute more as strand diameter increases.

**Stage 3-4:** In this stage, wire rotation has ended, and the vertical translations stabilize and move in unison. As there are no more surficial deformations, the stage marks the resumption of expected cable heating without other complicating factors, yielding an increase in thermal strain and a slight increase in downward deflection. This small increase in deflection without an increase in thermal gradient is attributed to cable thermal dilation and further heating of interior wires not represented by the measured temperatures.

**Stage 4 onward:** The cooling phase begins and yields a large reversal in deflection resulting from the negative thermal gradients associated with cooling as well as a decrease in thermal strain. Note that the apparent residual strain may not entirely represent the actual magnitude of residual strain recovered due to the deformations associated with thermal torsion.

Figure 5.24 provides the thermal response for cable L-GS-70.

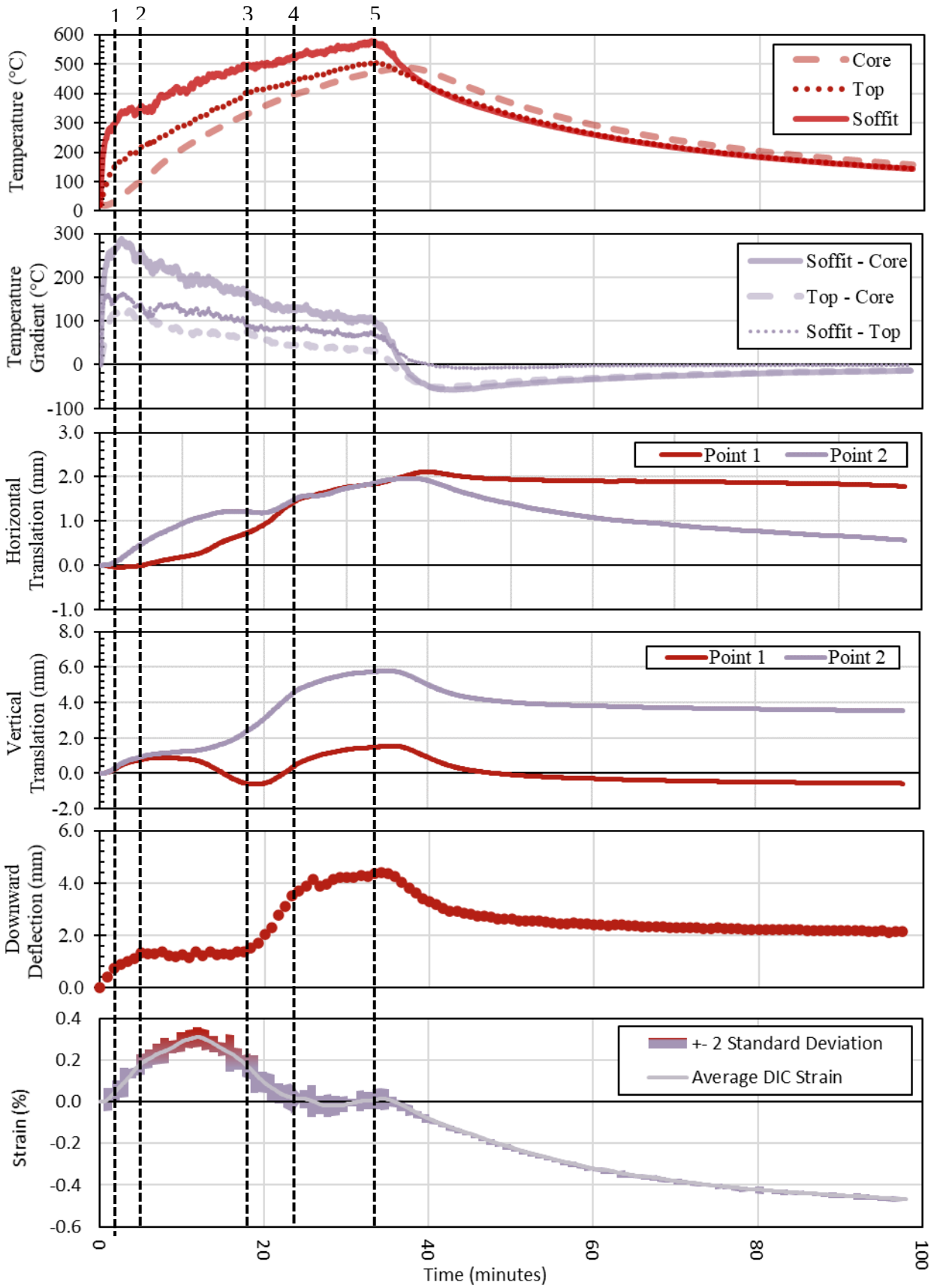


Figure 5.24. Thermal response of strand L-GS-70.

**Stage 0-1:** Strain and downward deflection increase as temperatures increase and thermal gradients peak.

**Stage 1-2:** Soffit temperature slope decreases along with all thermal gradients as internal temperatures increase. Strain development slows as a separation of vertical translations forms, indicating the beginning of thermal torsion development. Downward deflection reaches a plateau as thermal gradients decrease.

**Stage 2-3:** Thermal torsion accelerates the rotation of the strand extents. This stage is similarly denoted by an upward rotation of the left-most point of interest and a downward rotation of the right-most point of interest. Note that the direction of rotation is reversed compared to cable S-GS-74 because the lay angle of the wires relative to the DIC camera is opposite in this test. The rotation of the points of interest result in a horizontal inward movement and rapid decrease in apparent horizontal strain.

**Stage 3-4:** In this stage, thermal torsion effects subside, and thermal strain development resumes as expected. A rapid increase in downward deflection occurs as top surface temperatures exceed 400°C.

**Stage 4-5:** Heating continues as thermal strains continue to increase. Downward deflections slow dramatically and approach a maximum as thermal gradients stabilize.

**Stage 5 onward:** The cooling phase begins.

Figure 5.25 provides the thermal response of strand L-GS-100A.

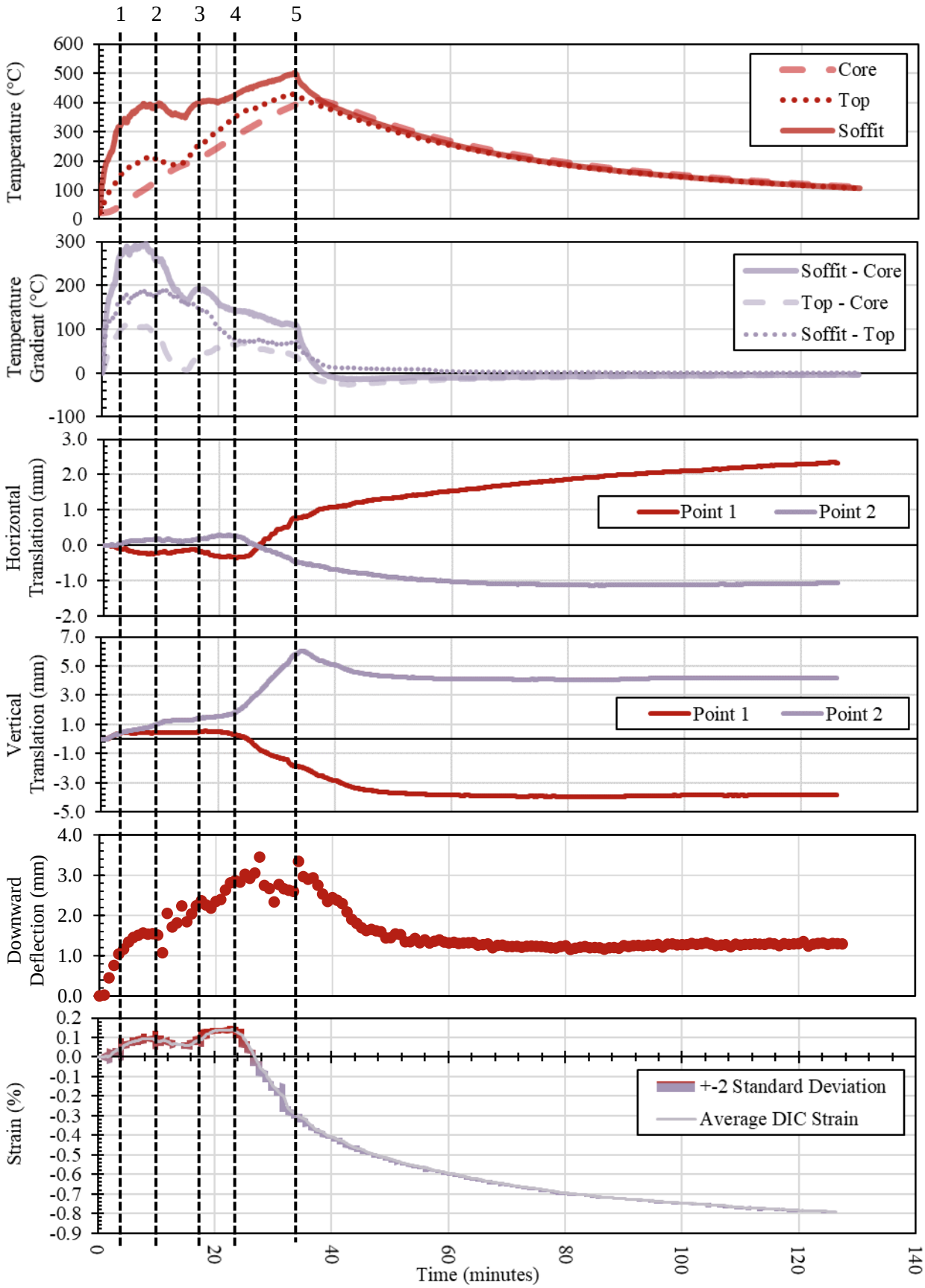


Figure 5.25. Thermal response of strand L-GS-100A.

**Stage 0-1:** Deflection and strain increase as strand temperatures rise and thermal gradients peak.

**Stage 1-2:** The deflection plateaus in response to a sustained maximum in thermal gradient. Thermal strain continues to increase. There is a slight separation in vertical translations likely from some minor independent wire movements, but thermal torsion has not yet begun severely.

**Stage 2-3**: Due to smoke production from the combustion of a blocking agent, a ventilation unit was activated which directed hot gases away from the strand. This process cooled the cable, resulting in a decrease in surface temperatures and strain. Downward deflection in this stage continues to increase however as the top-soffit gradient is relatively unaffected and other internal gradients continue to develop. There is little separation of vertical point translation at this stage indicating thermal torsion has not yet begun

**Stage 3-4:** The ventilation is deactivated and heating resumes, yielding a further increase in strain and downward deflection.

**Stage 4-5:** The vertical separation of point translations increases dramatically, with the left-most point rotating upwards and the right-most point rotating downwards. This thermal torsion corresponds similarly to the wire lay direction as indicated in previous tests and results in a large decrease in apparent thermal strain. The downward deflection plateaus in this stage as thermal gradients equalize.

**Stage 5 onward:** The cooling phase begins before the effects of thermal torsion have subsided, resulting in an apparent continuous decrease in thermal strain from stages 4 onward. However, as indicated by the separation of vertical translations, the thermal torsion ends as cooling begins, indicating this portion of the strain decrease is in fact from cooling, not further torsion. Therefore, for very large diameter cables, deformation effects such as thermal torsion may not always occur or subside if the fire exposure insufficient in heat or duration.

Figure 5.26 gives the thermal response of strand L-GS-100B.

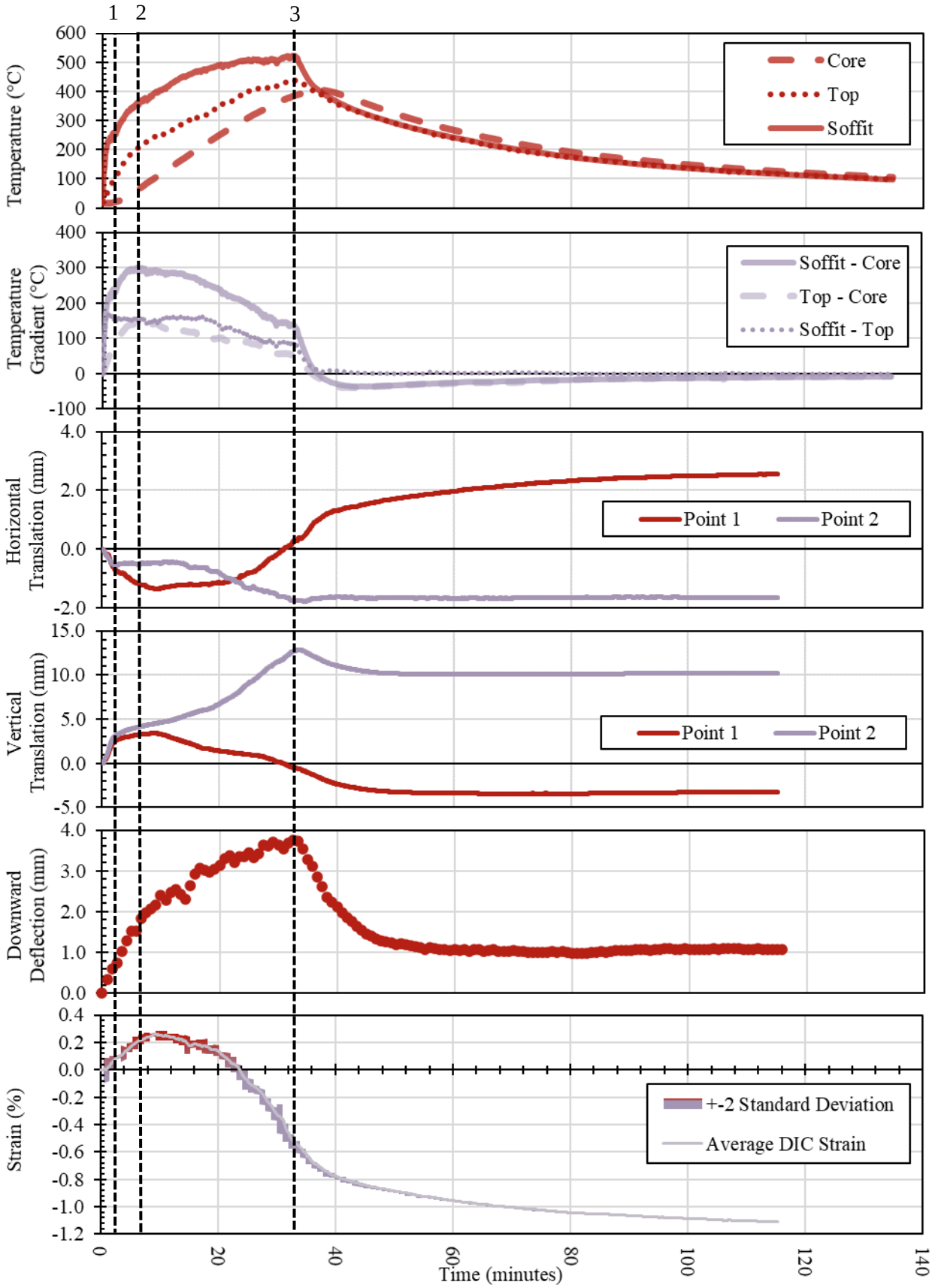


Figure 5.26. Thermal response of strand L-GS-100B.

Strand L-GS-100B is identical to strand L-GS-100A however an effort was made in this test to avoid activating the ventilation unit used previously.

**Stage 0-1:** Downward deflection and strain increase as thermal gradients are developed and the strand is heated.

**Stage 1-2:** Soffit temperature slope decreases and thermal gradients plateau. Downward deflection increases unabated as gradients elsewhere in the cable develop. A slight separation of vertical translations is observed however thermal torsion has not yet accelerated; this creates a point of inflection in strain development despite an overall increase.

**Stage 2-3:** Top temperature slope decreases, and thermal gradients begin to decrease slightly. The downward deflection responds with a decrease in slope but continues to increase. The separation of vertical translations begins to accelerate, indicating thermal torsion is occurring. The rotational direction of the left and right points of interest matches those of strand L-GS-100A as the lay angle relative to the camera is the same in both tests. The thermal torsion is marked by a decrease in strain development, leading to a maximum, then followed by a sharp drop that continues until cooling.

**Stage 4 onward:** The cooling phase begins, and downward deflection reverses as negative thermal gradients are developed. The thermal torsion effect subsides as indicated by the lack of vertical point translation divergence. Strain begins to decrease as result of cooling. Similarly, to strand L-GS-100A, note that only a portion of the overall strain decrease is a result of cooling, with the early phase starting at point 3 resulting from thermal torsion.

The thermal response of strand L-GS-140 is given in Figure 5.27.

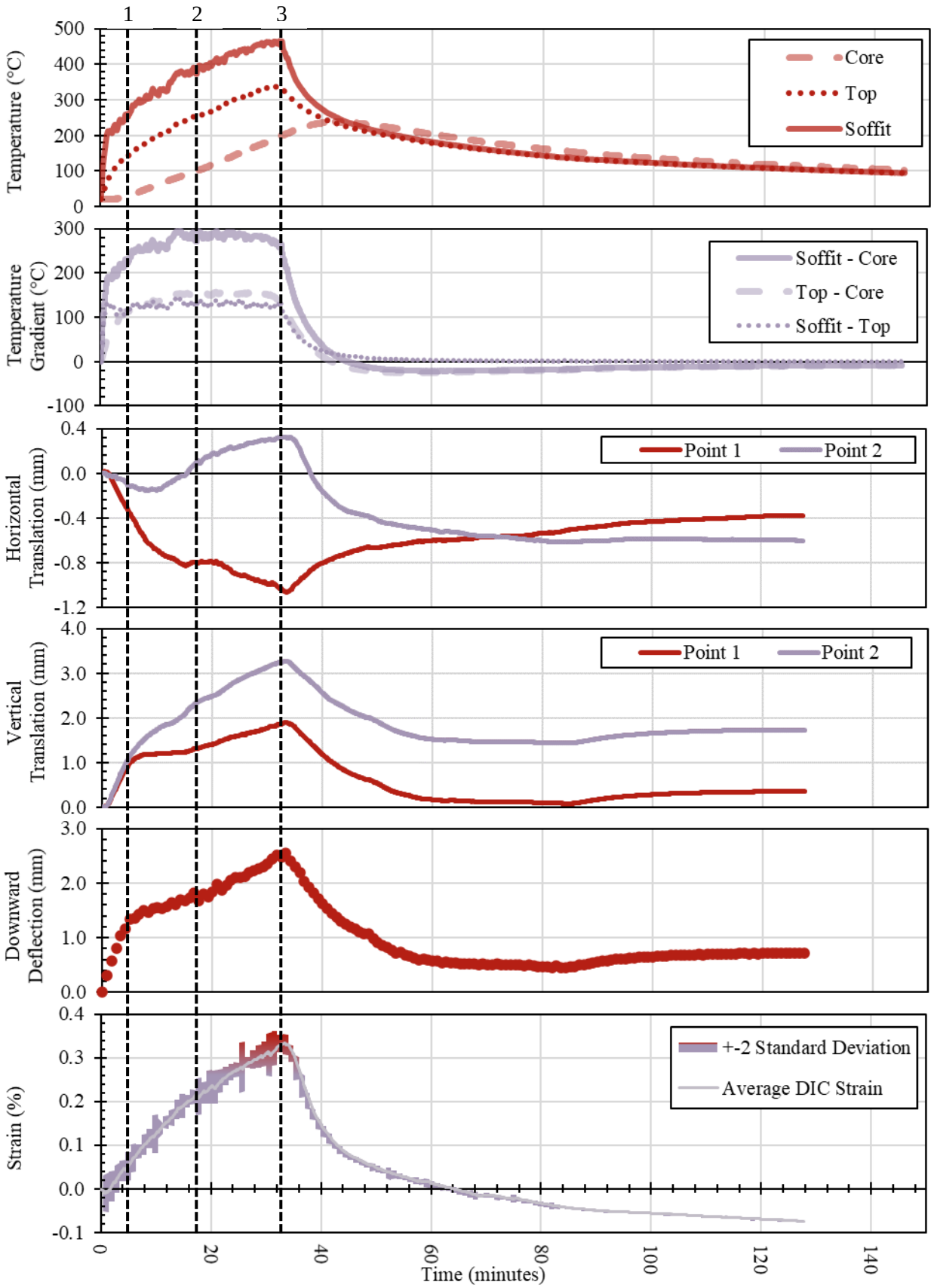


Figure 5.27. Thermal response of strand L-GS-140.

**Stage 0-1:** Peak thermal gradients are developed as downward deflection increases rapidly and thermal strain is induced.

**Stage 1-2:** A slight separation of vertical translations occurs in this phase however the effects of thermal torsion are not evident in other metrics. Strain continues to increase. Downward deflection decreases in slope as thermal gradients plateau. In this stage, the core, soffit, and top are heating at relatively the same rate.

**Stage 2-3:** Downward deflection accelerates slightly as additional thermal gradients are developed in the strand. Thermal strain development begins to slow as more of the strand is heated. There are marginal separations of vertical translation but still no indication of thermal torsion occurring.

**Stage 3 onward:** The cooling phase begins and a recovery in downward deflection occurs along with a decrease in thermal strain. No thermal torsion effects were observed in this test because of the large lay angle of the wires of strand L-GS-140. For this strand, wires at the soffit span to the top of the cable outside of the heated zone; specifically, within the 500 mm fire-exposed length, no wire spans from the soffit to the top of the cable, indicating that the thermal torsion mechanism requires a wire to at least complete half of a circumferential rotation. Coupled with the relatively lower temperatures sustained in strand L-GS-140, thermal torsion had a negligible impact on the deformational behaviour.

The influence of wire helical span on the effects of thermal torsion implies that, for a smaller-diameter cable where wires may complete a full strand rotation multiple times within the observed length, thermal torsion will similarly not occur as the longitudinal expansion is met by the equal and opposite expansion of the reverse cable face. Similarly, large thermal gradients do not develop in smaller-diameter strands, and so thermal expansion is more uniform, and rotation is not as great. Figure 5.28 illustrates how the large helical span of the wires of strand L-GS-140 could not greatly contribute to thermal torsion.

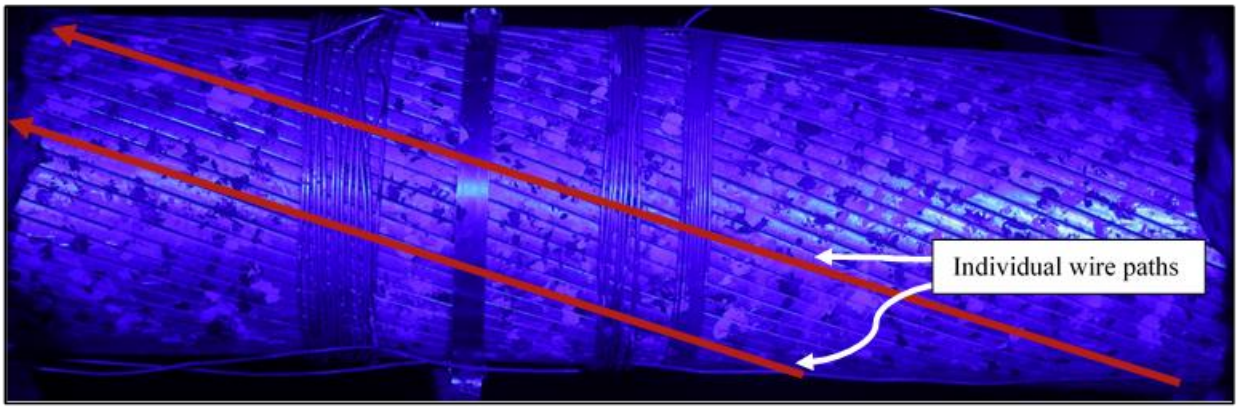


Figure 5.28. Illustrated span of the wires of strand L-GS-140.

The thermal torsion phenomenon is dependent largely on the temperatures driving wire thermal expansion and the helical span of the wires. If either of these components are not present, thermal torsion will not

occur or the effect may be negligible. Table 5.12 attempts to identify the conditions at the onset, demarcated by the separation of vertical point of interest translations, and the termination of thermal torsion. Note that, for L-GS-100A, thermal torsion initiated before the activation of the ventilation unit, stopped, then resumed after temperatures had recovered once again. The temperatures recorded in Table 5.12 for L-GS-100A represent those at the earliest onset of thermal torsion. Based on the proposed mechanism, the core temperature likely has less influence over thermal torsion than the soffit and top temperatures but are included for reference. A gradient is required for thermal torsion to exist as, for a uniformly heated cross-section, wire elongation will occur omnidirectionally, it is only when a driving thermal gradient occurs can wire elongation cause the twisting mechanism. For this reason, the occurrence of thermal torsion is limited in smaller-diameter strands like S-SS-22, S-SS-50, and S-SS-44. Further, the wire helical span must complete one half-rotation within the region of interest, or the torsion will not be observed, as was the case for L-GS-140.

Table 5.12. Onset and termination of thermal torsion observations.

| Strand | Thermal Torsion Onset | | | Thermal Torsion Termination | | |
|---|---|---|---|---|---|---|
| | Soffit Temperature (°C) | Top Temperature (°C) | Core Temperature (°C) | Soffit Temperature (°C) | Top Temperature (°C) | Core Temperature (°C) |
| S-SS-22 | Torsion not observed | | | | | |
| S-SS-50 | 550 | 375 | 250 | 650 | 510 | 480 |
| S-GS-44 | Torsion not observed | | | | | |
| S-GS-74 | 325 | 180 | 40 | 450 | 360 | 250 |
| L-GS-70 | 350 | 210 | 100 | 500 | 400 | 475 |
| L-GS-100A* | 325 | 160 | 50 | 500 | 425 | 380 |
| L-GS-100B* | 360 | 200 | 75 | 500 | 425 | 380 |
| L-GS-140 | Torsion not observed | | | | | |

*Thermal torsion concluded when the fire was exhausted.

For the galvanized steel strands, the onset of thermal torsion appears to occur approximately at a soffit temperature between 320-360°C and a top temperature between 160-210°C. This corresponds to a top-soffit gradient of approximately 145-165°C. Similarly, the soffit-top gradient corresponding with the termination of thermal torsion is approximately 75-100°C. Note that the top and soffit thermocouples are more representative of the thermal boundary condition of the steel surface and therefore the initial gradients observed do not necessarily reflect the true gradients between the top and soffit wires. Therefore, the effect of thermal torsion is not immediate as the soffit wires need time to heat; this stage is not captured by the surface thermocouples. Figure 5.29 attempts to generalize the behaviour of the strands studied herein into five stages. Although more testing is required to more consistently determine the onset of thermal torsion, the general framework is applicable to the strands examined in this research. Note that, based on the phenomenon observed experimentally, thermal torsion can occur in either spiral or locked-coil cables.

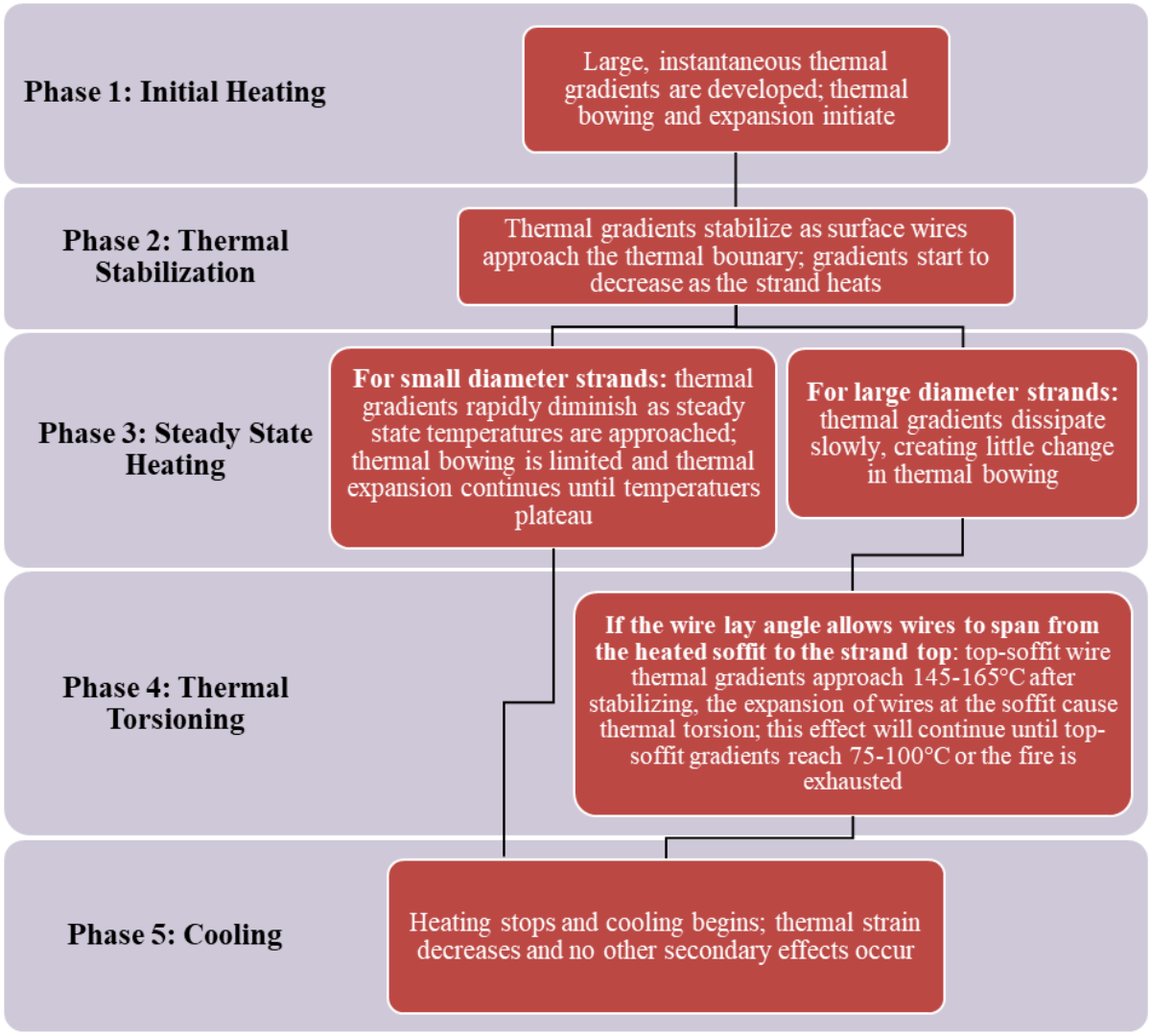


Figure 5.29. Generalized strand behaviour based on severe non-uniform heating from below.

### 5.3.3 DIC Strain Comparison

As explored in the previous section, the effects of thermal torsion make the direct comparison of strand thermal expansion impractical as different strands experience different deformations that may not correspond directly to a single phenomenon. Therefore, the comparisons herein will only consider portions of thermal strain development identified as uninfluenced by thermal torsion or other secondary effects. Some portions of the individual wire strain profiles may be truncated to remove erroneous data resulting from optical disruptions remaining immediately after the fire is exhausted. Additionally, maximum thermal strains herein are estimated based on the strain recovered during the cooling phase only in order to avoid the complicating factors associated with secondary deformations during heating. The maximum thermal strain values are calculated based on the average and standard error of multiple DIC analyses conducted in reverse from the end of the test until the beginning of cooling to avoid the signal noise observed in the

heating phase. These values are presented in Table 5.13 with the average temperature of the exposed strand region at the end of data collection. The calculated values are compared to the thermal expansion equations provided by Eurocode 2 Part 1-2 for prestressing steel and Eurocode 3 Part 1-11 for the wires of steel tension members (CEN 2004, CEN 2006):

For prestressing steel: $$\varepsilon_{th}(\theta) = -2.016 \times 10^{-4} + \theta \times 10^{-5} + 0.4 \times 10^{-8} \times \theta^2 \quad [5.5]$$

For steel wires: $$\varepsilon_{th}(\theta) = \theta \times 12 \times 10^{-6} \quad [5.6]$$

For stainless steel wires: $$\varepsilon_{th}(\theta) = \theta \times 16 \times 10^{-6} \quad [5.7]$$

where $\varepsilon$ is the thermal strain (unitless) and $\theta$ is the steel temperature (°C). Note here that equation 5.5 is intended for use in the fire design of prestressed concrete structures and has an effective temperature range from 20°-1200°C (CEN 2004). Equations 5.6 and 5.7 are based only on the coefficients of thermal expansion presented in Eurocode 3 Part 1-11 and so their effectiveness for temperatures far exceeding operational ranges is unknown (CEN 2006). The calculated values for the wire thermal strain are also presented in Table 5.13 although, as described earlier, the inherent error present in these wire values make a comparison difficult without considering the full DIC analysis, and therefore these values are included only for reference to the global strain values.

Table 5.13. Comparison of critical strain parameters. DIC values are presented with the standard error from multiple trials.

| Cable | Analysis Type | Maximum DIC Thermal Strain (%) | Average Exposed Region Temperature at End of Analysis (°C) | Estimated Thermal Strain at End of Analysis (%) (based on equations 5.5, 5.6) |
|---|---|---|---|---|
| S-SS-50 | Global | 0.96 ± 0.04 | 86 | 0.09 |
| | Wire | 0.96 ± 0.03 | | |
| S-SS-22 | Global | 0.98 ± 0.03 | 47 | 0.03 |
| | Wire | 0.99 ± 0.08 | | |
| S-GS-44 | Global | 0.62 ± 0.02 | 149 | 0.09 |
| | Wire | 0.60 ± 0.05 | | |
| S-GS-74 | Global | 0.44 ± 0.01 | 170 | 0.15 |
| | Wire | 0.56 ± 0.06 | | |
| L-GS-70 | Global | 0.50 ± 0.02 | 111 | 0.13 |
| | Wire | 0.55 ± 0.04 | | |
| L-GS-100A | Global | 0.51 ± 0.01 | 120 | 0.09 |
| | Wire | 0.51 ± 0.09 | | |
| L-GS-100B | Global | 0.57 ± 0.06 | 107 | 0.10 |
| | Wire | 0.44 ± 0.01 | | |
| L-GS-140 | Global | 0.37 ± 0.02 | 97 | 0.09 |
| | Wire | 0.59 ± 0.07 | | |

For stainless steel strands, the cooling phase of the DIC strain output is presented with the thermal strain determined by equation 5.7 in Figure 5.30. The DIC strain is adjusted to compensate for the estimated thermal strain remaining in the cable; this adjustment normalizes the curve to the end value of the curve created by equation 5.7 to better compare the maximum strain value and the strain development. The same procedure is done for all other strand strain calculations with normalization to equation 5.5 instead. The temperatures input into the relevant thermal strain equations are taken as the average of the soffit and top surface temperatures.

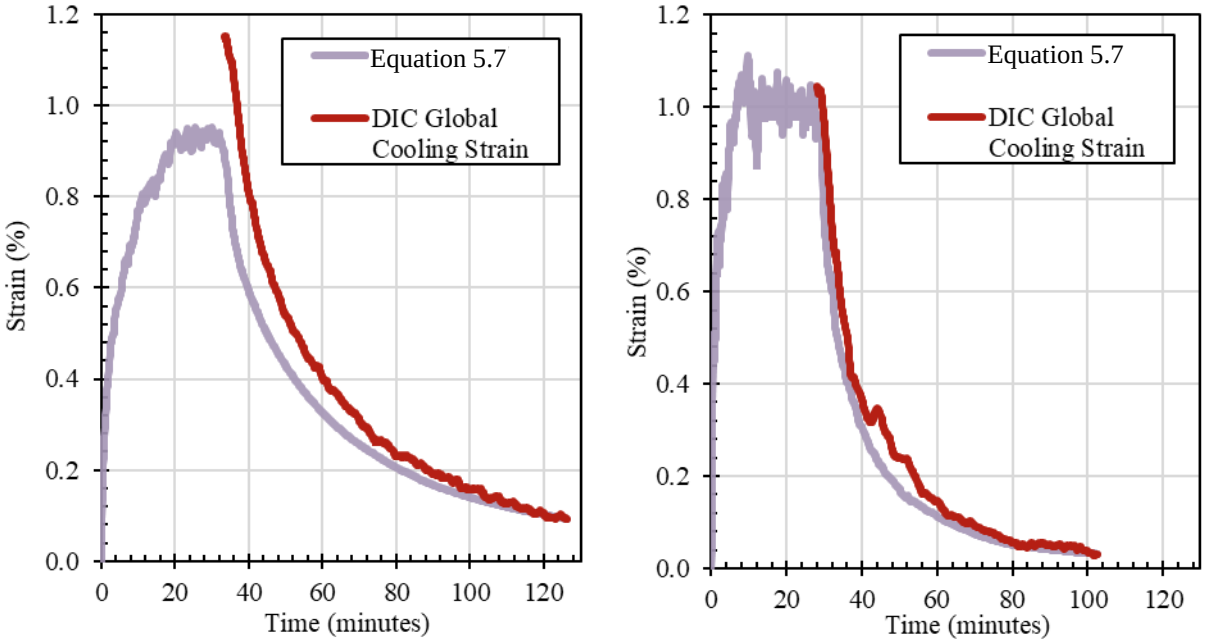


Figure 5.30. Global cooling phase DIC and Eurocode thermal strain development using the average soffit and top temperatures for strands (left) S-SS-50 and (right) S-SS-22.

As Figure 5.30 demonstrates, the maximum thermal strain and rate of thermal contraction of strand S-SS-22 are accurately predicted by equation 5.7. The maximum strain reached by S-SS-50 exceeds the predicted thermal strain and contracts more quickly than predicted based on the average soffit and top surface temperatures. This discrepancy could be attributed to the different steel compositions between strands S-SS-50 and S-SS-22. Specifically, the lack of molybdenum and higher chromium content in strand S-SS-50 is responsible for the increase in maximum thermal elongation. Low molybdenum content was found to have a similar effect on steel studied by Wan et al. (2012).

Figure 5.31 presents the estimated thermal strains from equations 5.5 and 5.6 and the DIC cooling phase strain for strands S-GS-44 and S-GS-74. Similarly, the average of the top and soffit temperatures was used in equations 5.5 and 5.6. Note that top surface temperature measurements were taken during the test of S-GS-44 and so the strains predicted by equations 5.5 and 5.6 over predict the measured strain. Despite this, there is fair agreement between the Eurocode equations for thermal strain and the measured DIC strain in

strand S-GS-44. For S-GS-74, quality of the Eurocode prediction for the maximum thermal strain is similar although the rate of contraction is slightly overestimated due to persisting internal cable temperatures which do not decay as quickly as external surface temperatures.

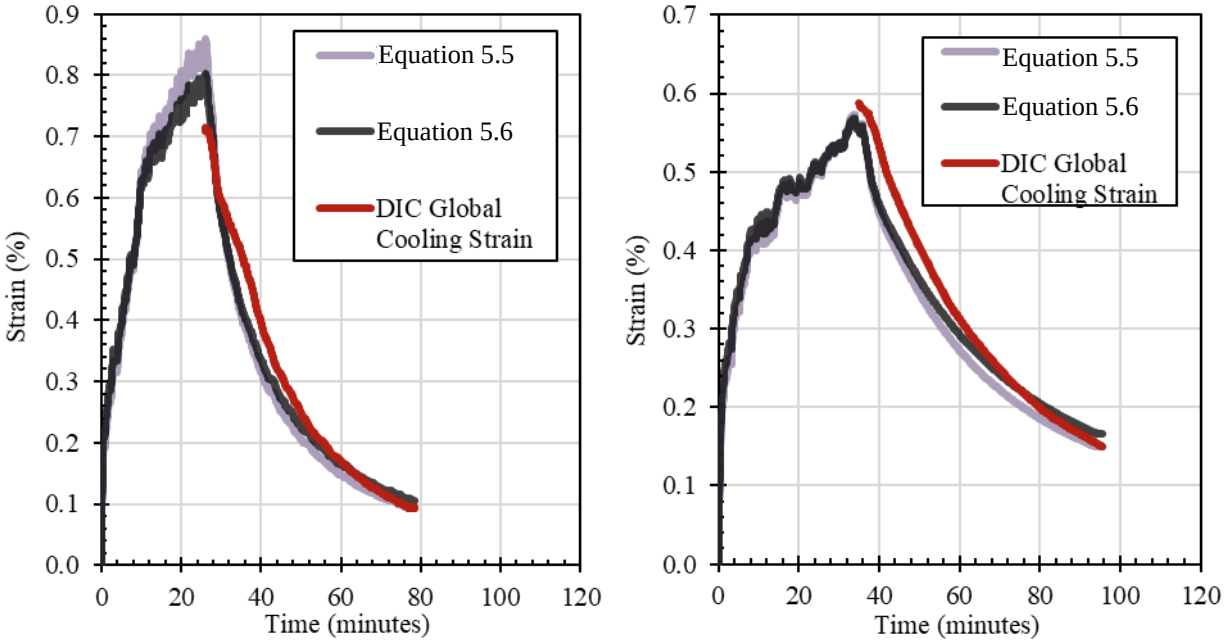


Figure 5.31. Global cooling phase DIC and Eurocode thermal strain development for strands (left) S-GS-44 and (right) S-GS-74.

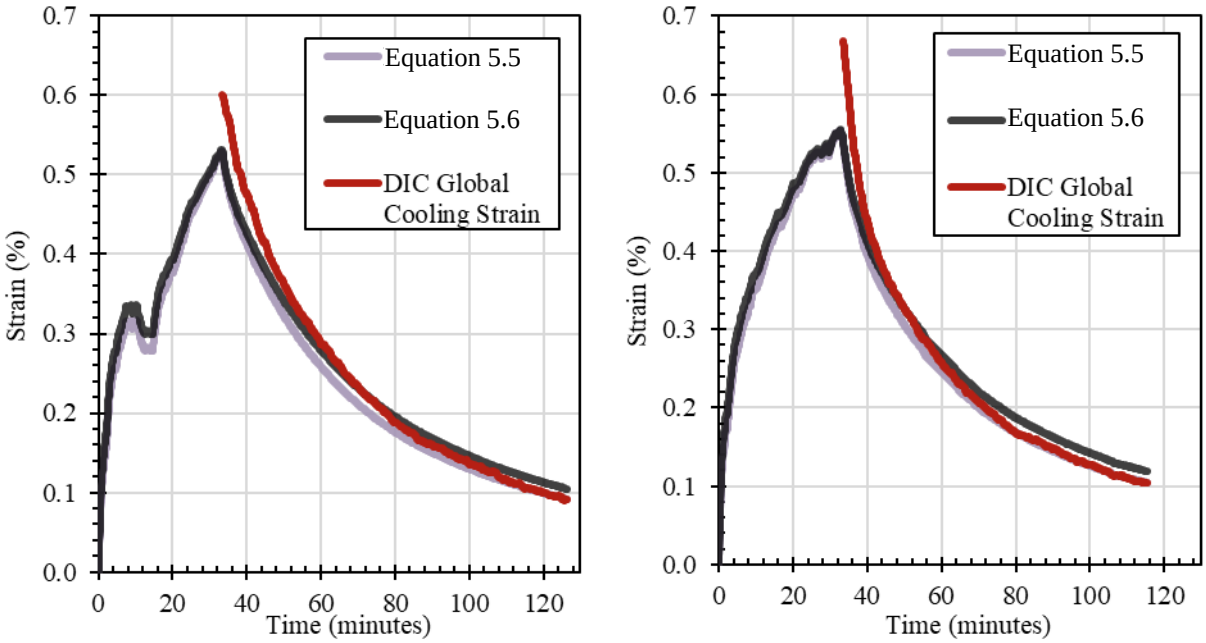


Figure 5.32 Global cooling DIC and Eurocode thermal strain development for strands (left) L-GS-100A and (right) L-GS-100B.

Figure 5.32 compares the Eurocode predicted and DIC measured thermal strains for strands L-GS-100A and L-GS-100B. In both strands, the rate of contraction is well matched by equations 5.5 and 5.6, however the maximum thermal strains are underestimated. The underestimation is especially true for L-GS-100B

which did not have ventilation activated as L-GS-100A did and therefore underwent a longer duration of heating. In lieu of major differences in steel composition, the discrepancy in maximum thermal strain is partially attributed to the average top and soffit temperatures used in equations 5.5 and 5.6. For larger diameter cables with larger temperature gradients through the cross-section, this average temperature may be less representative of the temperatures responsible for the thermal expansion measured by the DIC analysis.

Figure 5.33 provides the DIC cooling phase thermal strain with the Eurocode predicted strain values for strands L-GS-70 and L-GS-140. Equations 5.5 and 5.6 accurately predict the maximum thermal strain for strand L-GS-70 despite marginally overestimating the rate of contraction. Like strands L-GS-100A and L-GS-100B, the Eurocode prediction underestimates the maximum thermal strain of L-GS-140.

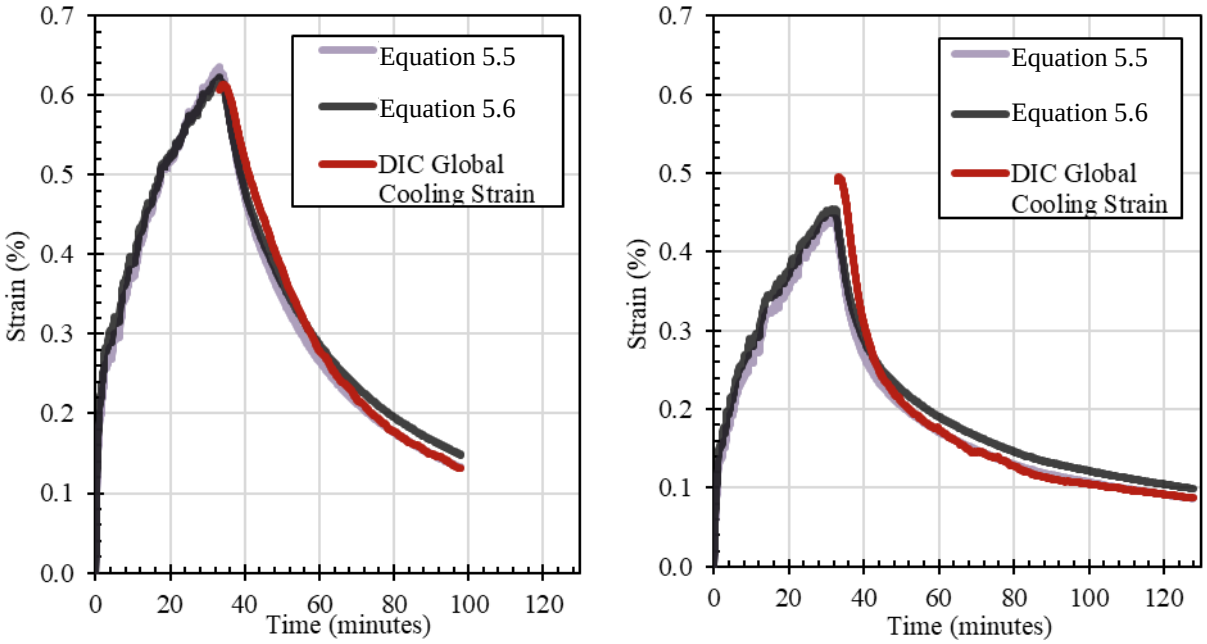


Figure 5.33. Global cooling phase and Eurocode thermal strain development for strands (left) L-GS-70 and (right) L-GS-140.

In general, the stainless steel strands S-SS-22 and S-SS-50 achieved the highest thermal strains due to the greater coefficient of thermal expansion stainless steel has compared to galvanized steel. Of these two strands, S-SS-50 had the largest thermal expansion relative to the temperatures developed in the cable due to the lack of molybdenum in the steel used. For this reason, equation 5.7 was found to be inaccurate in estimating the thermal strains of S-SS-50. Equations 5.5 and 5.6 could approximately predict the thermal strains for the non-stainless steel strands but often overestimated the rate thermal contraction as the average top and soffit temperatures do not consider the internal heat of the cables. For the larger diameter strands L-GS-100A, L-GS-100B, and L-GS-140, equations 5.5 and 5.6 underpredicted the maximum thermal strain more severely as result of the decreasing ability for the average of the top and soffit strand temperatures to

represent the strand at large diameters. The maximum measured DIC thermal strain was found to decrease with increasing diameter with strand S-GS-44 yielding the largest and L-GS-140 yielding the smallest magnitudes. This distinction is a result of the maximum temperatures developed in the strands decreasing with increasing diameter. Despite this general trend, a plateau occurs between these diameters where maximum thermal strain varied approximately between 0.6-0.7%. This plateau is attributed in part to a similar plateau in maximum strand temperatures, as shown in Figure 5.34 for the non-stainless steel strands. The temperature similarities between strands of diameter 70-100 mm induced similar levels of thermal strain. Due to with the assumed presence of a variable steel compositions for L-GS-100A/B when compared to the other galvanized steel specimens, the thermal strains in these cables were higher than those in L-GS-70 and S-GS-74. This discrepancy based on the unknown steel composition of L-GS-100A/B can be confirmed if the steel composition from this manufacturer is determined. The difference in strain between L-GS-100A and L-GS-100B is the thermal exposure difference resulting from the activation of ventilation in the test of L-GS-100A. Although the maximum temperatures were recovered in this case, the reduced degree of heating meant less expansion of interior wires which failed to contribute as greatly as in L-GS-100B.

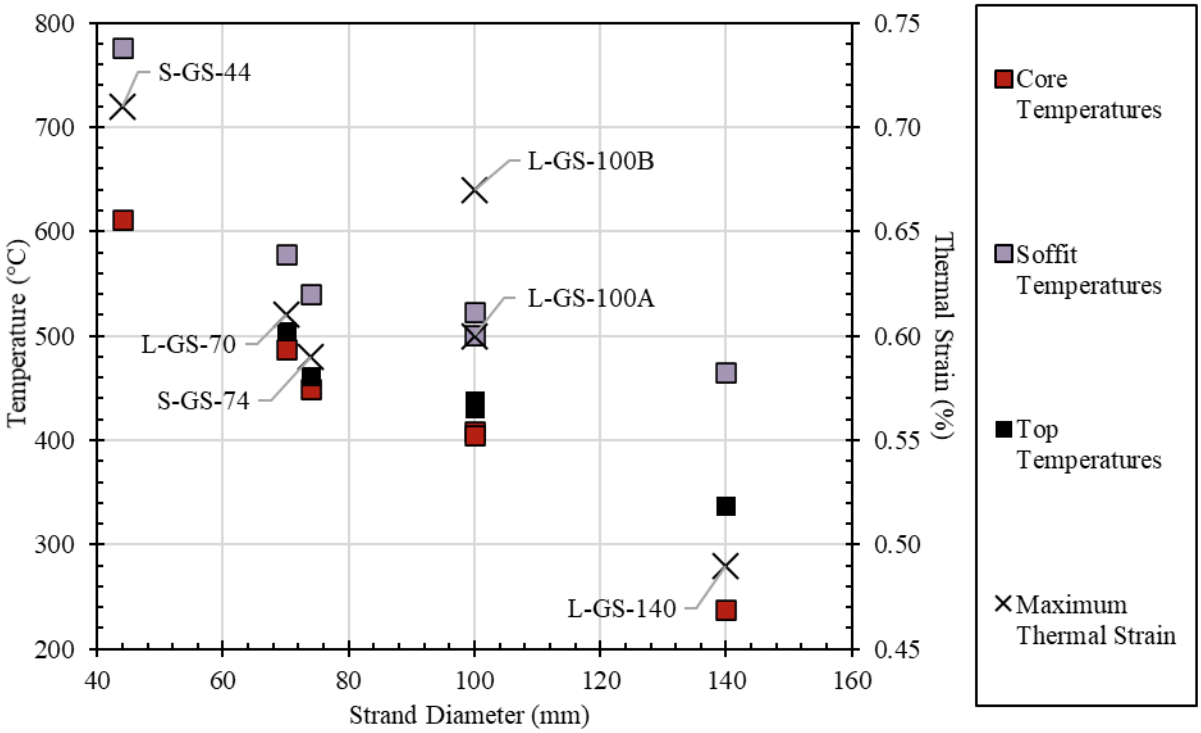


Figure 5.34. Maximum temperature and thermal strain information for all galvanized steel cables.

As demonstrated in Figure 5.34, between 70-100 mm in strand diameter, the difference in maximum temperatures is within approximately 50°C for any of the top, soffit, and core measurements. However, between strands L-GS-100A/B and L-GS-140, there is a greater decrease in core and top temperatures

specifically. Additionally, the temperature gradient for a strand diameter of 140 mm is greater than that for the other strand diameters tested. This rapid increase in apparent thermal resistance arises from the parabolic increase in cable mass given by a linear increase in cable diameter. For example, given the same air void ratio, strand L-GS-70 has approximately one-quarter the mass of L-GS-140 despite having half of the diameter. This increase in mass has multiple effects on heat transfer, first, that the heat capacity of the assembly increases based on the mass of material requiring thermal energy and, second, that the larger cross-sectional dimension provides more paths for conduction throughout the cable and therefore less heat transfer directly to the core and other interior locations. The same rapid decrease in temperature is not shown by the soffit temperatures as it represents the boundary temperature between gas temperatures and the strand. With increasing diameter, the soffit temperatures are expected to approach the temperature of the boundary layer for an infinitely-sized cable (relative to the fire exposure) which may be approximated by a non-infinite cable diameter within the realm of practical strand sizes. The implication on thermal strain development is that applying the average temperature of the cable top and soffit for use in thermal strain equations becomes less valid with increasing cable diameters as the boundary layer becomes less representative of the internal temperature development.

Based on Figure 5.34, the development of thermal strains appears to not to be directly affected by locked-coil or spiral strand varieties. Although S-GS-74 had a maximum thermal strain slightly below that of L-GS-70, it also had proportionately lower temperature maxima, implying that the difference between coil types directly affects the heat transfer, then indirectly affects the thermal strain development.

### 5.3.4 Cable Physical Change Observations

In addition to the thermal deformations and temperature developments studied herein, a number of material degradation effects were observed during testing. An important effect was the combustion of the aforementioned blocking agents, observed in tests L-GS-70, S-GS-74, S-GS-82, L-GS-100A, L-GS-100B, and L-GS-140 to varying degrees. The most severe instances of blocking agent combustion were observed in L-GS-100A and L-GS-100B, as displayed in Figure 5.35. In these tests, the mineral wool insulation used to shield core thermocouples in the exposed region initiated a wicking action of the liquified agent inside the strand, create a mechanism for it to expel from the strand and ignite on the exterior.

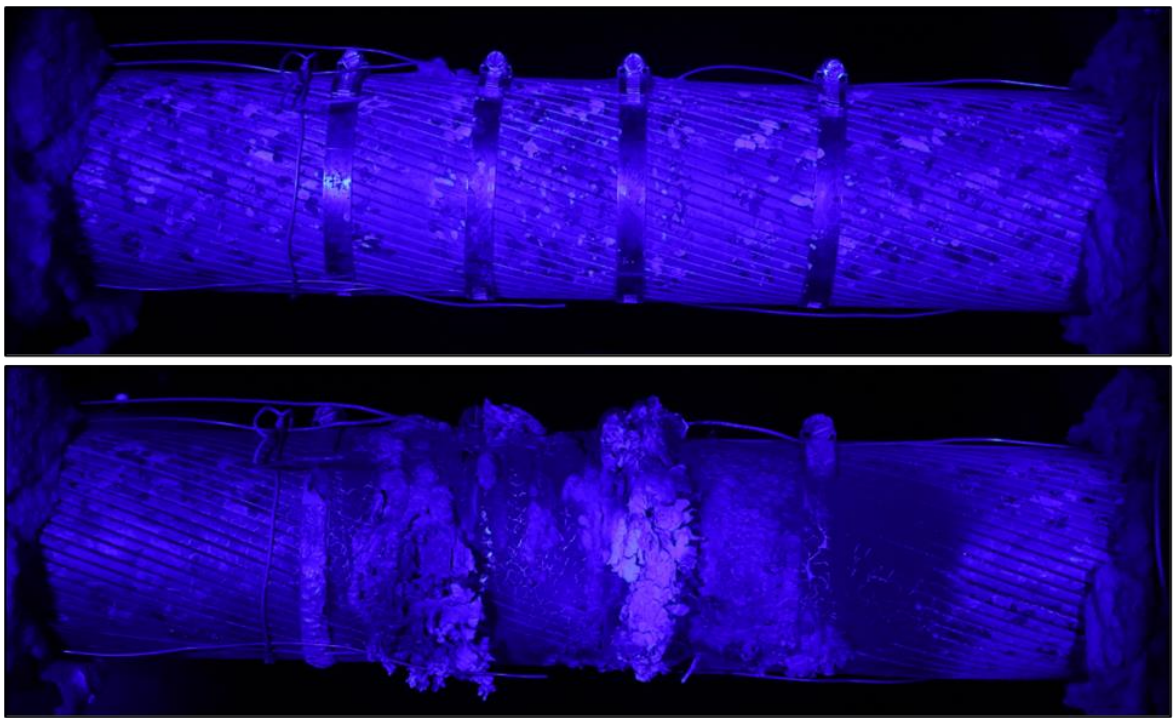

Figure 5.35. Before (top) and after (bottom) the combustion and spilling of flammable blocking compound in cable L-GS-100A.

Although it is assumed the mineral wool insulation enabled the blocking agent to wick out of the cable structure, this was not observed in strand L-GS-140 which instead released smoke from the internal structure after the pool fire was exhausted, as seen in Figure 5.36, indicated a smouldering of the internal blocking agent. This phenomenon was observed to some degree for all strands identified as utilising a blocking agent in Table 5.3 and, for strands S-GS-74 and S-GS-82, the lack of interlocking locked-coil wires allowed the liquefied agent to drip out of the cable structure directly into the pool fire, thus contributing fuel to the heat source.

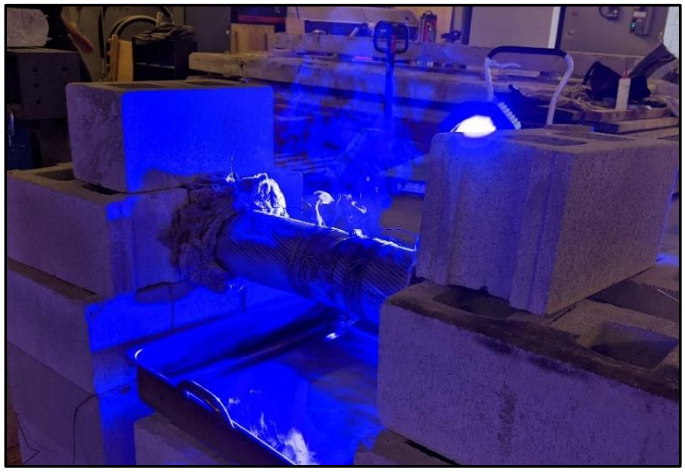

Figure 5.36. Smoldering of the blocking agent in strand L-GS-140.

The deterioration of the galvanized coating was also observed in all non-stainless steel strands. As indicated by Ridge and Hobbs (2012), the zinc-aluminum alloy used in galvanization melts at approximately 380°C. The known melting point of this coating allows for the observation of a propagation front as demonstrated in Figure 3.36. In more severe instances, such as in the test of S-GS-74, the galvanization coating melted and collected at the bottom of the strand where it re-solidified and created cracks during cooling (Figure 5.37).

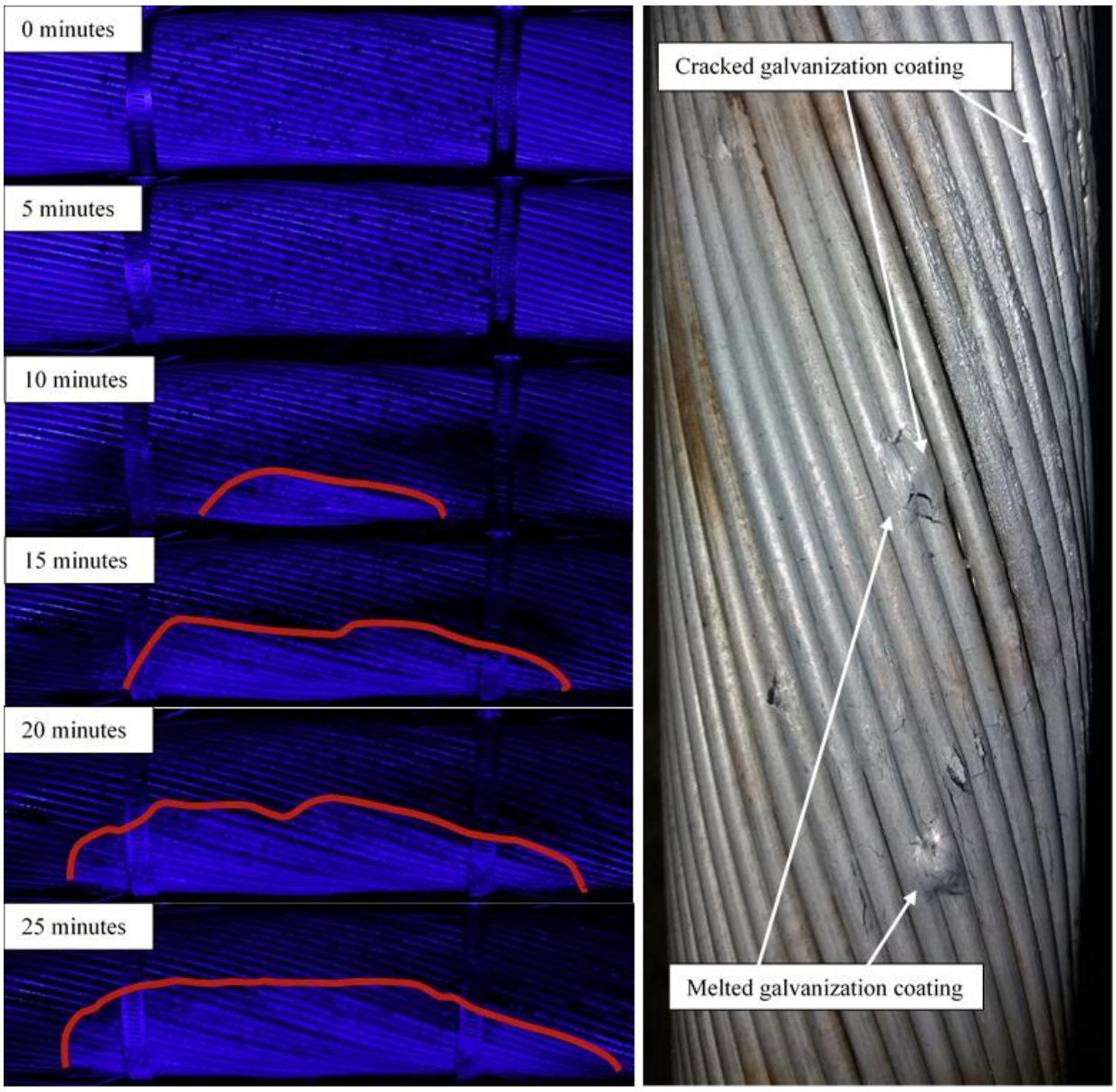


Figure 5.37. (Left) Propagation of galvanization deterioration observed in strand S-GS-82; (right) re-solidification and cracking of the zinc-aluminum alloy coating on the soffit of strand S-GS-74.

Although these deterioration effects may not have direct implications on the mechanical response of a cable-supported structure, these results are important for the general fire protection of tension members. Primarily, the fire protection of cable members is generally done to limit steel from reaching a predefined critical

temperature of 300°C, which, to the knowledge of the author, exceeds the flashpoint of the known blocking agents present in the cables tested in this study. Further, based on the flashpoint of commonly-used HDPE sheaths of 330°C which could easily be exceeded if an internal blocking agent were to ignite, the critical temperature of 300°C for the fire protection of steel stay-cables is not conservative. Additionally, for stay-cables without fire protection, temperatures of 380°C could readily be reached by even a small vehicle fire on a bridge, thus initiating the deterioration of the galvanization layer. As galvanization is done to improve corrosion resistance, any fire-exposed strand, regardless of material degradation, would likely need to be replaced or repaired to ensure its corrosion performance is not compromised. Therefore, the fire protection of bridge cable-stays must consider the secondary degradation effects studied here. Additionally, stay-cables are typically associated with an air void ratio to represent the voids within the cable structure. Specific research may be required to identify if the presence of a blocking agent in these voids alters the thermal response versus a strand with no blocking agent.

## 5.4 Conclusions

The research presented herein sought to quantify the thermal response of steel stay-cables exposed to non-standard, localised heating. Thermocouples on the surface and core wires of the strand monitor the thermal response of the fire exposure while digital image correlation and narrow-spectrum illumination enable the optical measurement of surface strains, thermal bowing, and other deformational effects. Cross-sectional temperature data in fire-exposed and insulated regions of the cable enable a quantification of heat transfer through the strand. Results are presented for eight structural strands of diameters varying between 22 and 140 mm, spiral and full locked-coil types, and stainless and galvanized steel alloys after exposure to an approximately 30 minute methanol pool fire of dimensions 0.6 m x 0.49 m.

While the results of this experimental program are valuable, context towards some limitations in this test series should be discussed. First, the fire exposure studied herein should not be considered representative of a full-scale bridge fire event. However, the author argues that the scale of the experiments herein appropriately matches the scale of the fire exposure applied. The data from these experiments can be used to explore how fire exposure affects cable members in general, which could later be extrapolated to anticipated in-situ scenarios. Second, the boundary conditions of the cables examined do not necessarily represent the boundary conditions of an in-service cable in a structure largely due to the lack of tension in the member. The implications of the lack of tension, specifically towards the presence of interwire forces, are discussed further in Chapter 6. Despite the unloaded nature of the tests herein, the temperature development is still considered valid as heat transfer is largely independent of the stress state of the cable. The thermal deformational effects observed are more heavily influenced by the cable stress state due to the simultaneous mechanical deformation of a cable under tension. However, this test series provides an

excellent opportunity to separate the thermal and mechanical responses of a cable in simultaneous heating and tension in future tests, as the sole effect of non-uniform heating is now quantified for a variety of cable types. Therefore, future work will be able to use the information from this thesis to better understand loaded cables in similar fire exposures. Finally, limitations of the DIC methodology must be discussed. Mainly, the DIC applied for this test series relies on analyzing two-dimensional images of three-dimensional phenomenon. While the strain data calculated herein is accurate, the methodology applied does not fully consider the three-dimensional nature of the cables examined. Therefore, future work could study how three-dimensional effects occur in similar scenarios. Future work could also examine the inherent variability between tests due to the nature of pool fire exposure and how these variations may or may not affect results.

The novelty of the research presented herein is reinforced by the following considerations. This is the first experimental study to consider stay-cables of diameter greater than 80 mm in non-uniform heating and the first to consider stainless-steel structural strands in non-uniform heating. The results identified the previously unknown mechanism of thermal torsion which induces rotational effects on the wires of structural cables. Further, this research is the first to consider the secondary deformation effects associated with non-uniform cable heating and the first to consider the role of blocking agents used in cable manufacturing. Finally, this research presented a novel application of digital image correlation coupled with narrow-spectrum illumination. The important conclusions found by this research are presented below:

1. The thermal responses of stay-cables are intuitive to some degree in non-uniform heating: smaller-diameter strands heat faster and more uniformly while larger-diameter strands undergo larger thermal gradients and remain cooler for the same fire exposure. A smaller-diameter strand will also reach steady state temperatures more readily. The maximum core temperatures take longer to occur in larger-diameter strands and often occur after fire exposure has ended.

2. There is only a small difference in the temperature development in similarly sized full locked-coil and spiral strands (< 50°C). The reduced proportion of air voids in locked-coil strands reduces some inherent insulation and results in hotter maximum temperatures being developed. The interlocking outer wires of full locked-coil strands also provide a better path for thermal conduction which contributes to hotter overall temperatures, especially in non-fire-exposed regions of the cable which are heated primarily through longitudinal conduction.

3. In general, stainless steel stay-cables perform more favorably in regards to heat transfer under the fire exposure studied based on the lower thermal conductivity of the metal which resulted in slightly reduced maximum temperatures in the fire-exposed region when compared to a similarly-sized galvanized steel strand. The lower thermal conductivity also resulted in greatly reduced maximum

insulated temperatures achieved through conduction and more temperature variation across the insulated cross-section (approximately 42°C maximum for the stainless steel cable versus 82°C for the similarly sized galvanized cable).

4. Cross-sectional temperatures in the insulated region of galvanized cables become uniform a short distance outside of the heated region for all strand diameters tested (up to 140 mm). Therefore, thermal modelling of these tension elements can likely simplify heat transfer effects to one-dimensional processes outside of the fire-exposed region.

5. The combination of digital image correlation and narrow-spectrum illumination proved viable for measuring thermal deformations. However, for shorter gauge lengths, the accuracy of this technique diminishes as the fluid interaction of hot and cold air between the camera and the target introduces a signal noise in the output. Despite this, the presented method for treating the signal noise proved reliable for the majority of instances.

6. The deformation behaviour of stay-cables can have secondary components such as thermal bowing which was observed in strands with large temperature gradients. Thermal torsion, a rotational effect owing to the differential thermal expansion of soffit wires, was observed and characterized based on the tests the phenomenon was observed in. Thermal torsion created apparent strain reversals based on the movement of surface wires which complicated the heating phase strain development in some tests.

7. Despite the disruptions to strain calculations created by thermal torsion, the cooling phases for all tests remained unobstructed by secondary effects. The cooling phase thermal strain contraction was sufficient to estimate the maximum thermal strain developed in all strands. Relevant Eurocode equations could reproduce the measured thermal strains with some accuracy, however this accuracy diminished with larger-diameter strands ($\leq$ 100 mm) as the measured thermal boundaries became less representative of the heat transfer within the cable. Some discrepancies from the Eurocode equations were found for various steel alloys.

8. The combustion of blocking agents within the cable structure did not have a discernable effect on the heat transfer nor thermal strain development of the strands tested. However, the interaction of blocking agents with high-temperatures creates the potential for these substances to provide additional fuel to a fire or create a smouldering fire within the cable structure. This is a concern as the flashpoint for the blocking agents examined in this study are below the critical temperature used in the fire protection of stay-cable members. The level fire protection should be sufficient so as to prevent the combustion of blocking agents present in the element.

9. Based on the combustion of blocking agents observed in this thesis, current guidance for the fire protection of cable members limiting maximum temperatures to 300°C is unconservative, as the flashpoint of blocking agents can be below this temperature.

10. The zinc-aluminum alloy galvanization layer was observed to deteriorate and melt on fire-exposed cable surfaces. Similarly to the blocking compound combustion scenario, fire protection should be sufficient so as to prevent the deterioration of this layer, else a fire-exposed element may require replacement based on temperatures lower than would otherwise be structurally severe.

Despite the conclusions presented herein, knowledge gaps persist with respect to the fire performance of steel structural cables. Namely, the effects of simultaneous heating and loading in a similar manner to the study presented herein have not been examined nor have the effects of thermal bowing or thermal torsion. Additionally, the mechanism for load shedding to interior wires is not well known for large diameter structural cables. Moreover, to support modelling endeavours, more experimental data on the thermal response is required for a wide variety of cable coil types, diameters, and alloys under a wide variety of uniform and non-uniform heat exposures. Finally, the fire performance of cable anchorages may be critical in dictating the fire response of cable-supported structures however a very limited number of studies have considered this aspect. Future work beyond this research program could examine the changes in cable steel microstructure post-fire to estimate the maximum temperatures developed for each wire. This could prove valuable as a forensic method after testing to assess the accuracy of thermocouple measurements. Ultimately, the research presented here aims to contribute to the greater goal of developing the fire resilience of bridge infrastructure to better protect the communities, people, and economies they serve.

# Chapter 6: Implications for the Thermal Modelling of Steel Stay-Cables

## 6.1 Introduction

While Chapter 5 of this thesis focuses primarily on the experimental fire performance of steel stay-cables, the ultimate goal of this experimental research is to develop tools for practitioner use that can sufficiently represent the expected thermal behaviour. These tools can take the form of analytical or computational solutions such that specific phenomena can be accounted for in design. This chapter explores the thermal modelling of steel stay-cable members first by reviewing existing models from the literature and later by discussing how the experimental results from Chapter 5 can be applied. An outline of experimental results and their implications on the existing and future models of cable members exposed to fire is presented. Of specific interest is not only the modelling of cable members, but also that of steel members exposed to localized heating in general. Relevant experimental results to be considered in future studies are discussed in five categories: the behaviour of fully locked-coil cables, longitudinal heat transfer in cable members, cable thermal deformations and interwire friction, and general topics associated with cable fire performance.

## 6.2 Modelling of Cables and Other Steel Members Exposed to Heating

Specific work towards the modelling of stay-cable members is limited although the increasing number of experimental studies in the last five years has produced models capable of calculating heat transfer through a cable's cross-section. While important to the overall cable behaviour, also of interest is the longitudinal heat transfer under localized fire exposure which may hold similarities to other non-cable steel members exposed to localized heating. This section will review modelling studies these two key areas: the thermal response of stay-cables and the general thermal response of steel members exposed to localized heating.

### 6.2.1 Modelling of Steel Stay-Cables Exposed to Localized Heating

Bennetts and Moinuddin (2009) present one of the first modelling attempts of a stay-cable exposed to a uniform fire. These authors consider a stay-cable cross-section as concentric lumped masses separated completely by air gaps, where larger-diameter strands have more concentric layers to represent more wire layers. Two cases are considered, an insulated and uninsulated case with and without the presence of a mineral wool exterior layer respectively, for a variety of fire exposures. The thermal boundaries are assumed to be consistent around the cable and reflect the convection and radiation from hot gases from various vehicle fires. Although this method ignores conduction between concentric layers which may increase heat transfer to internal layers, it is one of the first studies to consider the radiation between wire layers that occurs in cable void spaces.

Main and Luecke (2010) create a three-dimensional thermo-mechanical model of a parallel-wire strand and treat the cable structure as an exterior layer composed of a paint, wire-wrap layer, and a corrosion inhibiting paste, surrounding a solid metal interior representative of the steel wire structure. This approach therefore does not consider the role of air voids in the cable structure. Various heating exposures, including non-uniform heating with boundary gas temperatures of 800°C, were studied to determine specific wire temperatures which later informed the same model in a thermo-mechanical setting based on material properties determined from experimental tests. Unique to this study is the consideration of cracked wires which are assigned different mechanical properties based on damage levels created by corrosion.

Conversely to Bennetts and Moinuddin (2009) and similarly to Main and Luecke (2010), Liu et al. (2012) apply commercial software ANSYS to model a stay-cable cross-section by considering no internal discretization of wires or voids. This solid tube model was used to determine the temperature development in the cable cross-section during uniform exposure to a tanker truck fire, represented by a uniform convective and radiative thermal boundary with a predefined time-temperature curve.

The first experimentally validated modelling effort in the context of the thermal behaviour of steel stay-cables was presented by Fontanari et al. (2015). These authors consider a 60 mm diameter full locked-coil strand in addition to a six-strand rope consisting of six 38 mm strands wrapped around a polymeric core. Experimental furnace heating tests were conducted for both member types at ambient and elevated temperatures (considering uniform heating to the ISO 834 standard fire curve) to produce data on each member's heat transfer response. Specific mechanical tests were also conducted on individual wires from both member types to determine high-temperature mechanical properties. A parametric thermal finite element model in ANSYS was validated based on the furnace tests and other available data and considered the specific contact area between adjacent wires in the heat transfer analysis. This model was used to produce a time-temperature history for all elements which was later applied to the thermo-mechanical model to inform material properties based on the experimental wire tests. The developed model was found to replicate the experimental results with good accuracy and this methodology is suggested by the authors to be the basis for thermo-mechanical cable models moving forward.

Sloane (2017) applies a similar approach to Main and Luecke (2010) and uses a three-dimensional model considering a homogenous steel cylinder with no air voids. The three-dimensional heat transfer model is used to inform a two-dimensional mechanical model considering both temperature dependent and independent thermal properties (for example, thermal conductivity, heat capacity). This comparison yielded that the use of temperature-independent thermal properties in modelling leads to higher cable temperatures and therefore provides a conservative estimate while reducing analysis complexity and computational time for the specific modelling case studied (Sloane 2017). Sloane and Betti (2019) expand upon the

methodology of Sloane (2017) by refining the two-dimensional analytical solution to enable non-uniform and angular heating toward a cable member represented by a solid cylinder.

Du et al. (2019) develop analytical equations to consider the role of cavity radiation in the heat transfer of a steel cable cross-section and make a comparison to a similarly sized solid steel bar. The developed analytical equations found that the cable member, approximated to a concentric cylinder model separated by an air gap, developed slightly warmer temperatures than the solid bar due to an increased external surface area for heat transfer and a reduced outer layer density. These authors develop ABAQUS models for both a parallel-wire strand and a similarly-sized solid bar under exposure to the ISO 834 standard fire to assess the role of cavity radiation and validate the analytical equations; it was found there was good agreement between the methods (Du et al. 2019).

Most recently, Kotsovinos et al. (2020b) developed an analytical approach that considers both wire-to-wire conduction and cavity radiation in a two-dimensional cross-sectional thermal analysis. The developed analytical approach was applied in an ABAQUS thermo-mechanical model to investigate the effect of cross-sectional heat transfer on load shedding between wires under non-uniform heating. This model was idealized such that out-of-plane wire movements were restrained, in addition to the thermal dilation of the cable and rotation of individual wires. Thermal moment development based on the elongation of wires was permitted and monitored. These authors conclude that lumped capacitance models which consider no internal wire/void discretization are and less accurate than the analytical developed analytical approach for some thermal exposures. Additionally, potentially critical effects such as the development of thermal moments and wire load shedding are indicated as phenomena that may not typically be reproduced in the modelling efforts of cable members which can be dangerous.

These studies outline the development of the thermal modelling of steel cable members to present. While a large portion of modelling research on this topic has focused on the applicability of assumptions like lumped capacitance versus wire discretization, only a portion of these models have begun to consider the complex effects that occur in the thermo-mechanical response of cable members. For example, load shedding from heated wires to cooler wires has been predicted numerically (Fontanari et al. 2015, Kotsovinos et al. 2020b), but this has not been studied in the context of interwire friction which has been theorized to limit cable longitudinal thermal expansion (Wright et al. 2013) and potentially induce further tensile loads to adjacent, cooler wires. Additionally, in the case of localized heating, out-of-plane wire movements associated with wire bulging has not been reproduced through modelling, nor has the role of blocking agents within cable air cavities. These secondary thermal deformation behaviours are yet to be realized in the thermo-mechanical modelling of cable members, as many require extremely detailed, three-dimensional models;

these deformation effects have also not been quantified in terms of their effect on the mechanical performance of heated cables.

### 6.2.2 Modelling of Isolated Steel Members Exposed to Fire

Existing research on the modelling of cable members has focused primarily on the heat transfer through the complex cross-section of a cable. However, for localized heating scenarios, longitudinal heat transfer in a cable member may also be important in determining thermal deformations that may not be realized in a two-dimensional, cross-sectional model. This section will briefly explore modelling work on isolated steel members to examine the considerations taken by researchers and any possible applicability to the case of heated cable members.

Sjöström et al. (2012) apply experimental results of a full-scale steel column exposed to a large diameter pool fire to compare temperature measurements to gas temperature calculations from the Eurocode. These authors then develop a heat transfer model in TASEF and apply a calculated adiabatic surface temperature as the flame temperature boundary condition and note the occurrence of thermal moment development in the cross-section due to asymmetric heating; it is concluded however that for a hollow circular column, internal heat transfer will disperse temperatures more quickly than other shapes.

Lange and Boström (2015) conduct a round robin study on the calculation of the fire performance of a loaded steel beam exposed to the ISO 834 standard fire in a furnace. After the first stage of modelling submissions for which the beam temperatures and heat exposure information was not provided, the temperature development in the beam was well-replicated with the exception of beam regions closer to the concrete cover where submission results varied based on the assumptions made to account for its presence. Deflection predictions in general were found to be conservative and over-estimated the measured values. The second submission stage provided participants with the measured furnace and steel temperatures had a reduced variation in the times-to-failure determined by the models, although the average response is still conservative. Overall, Lange and Boström (2015) indicate the variability in responses was greater than anticipated and that it is unclear what aspect of the modelling submissions yielded the conservative nature of the results. Later, Lange and Boström (2017) explain that the conservativity is not a result of the assumed mechanical properties related to the strength of the steel nor the assumed thermal exposure as both sets of values were obtained experimentally, independent of factors of safety. These authors highlight the importance considering this inherent variation between modelling tools for design purposes as not all of the participants' responses were conservative in both stages, and the variability between modelling applications should be accounted for when considering a design. Lange and Boström (2017) conclude the need for a standard determination of failure criteria as these are not necessarily established for modelling applications whereas they are controlled for fire testing laboratories.

In the context of the modelling of cable members, the discussions provided by Lange and Boström (2017) are relevant as the failure criteria for cable members exposed to fire has been defined seemingly arbitrarily based on a critical temperature of 300°C for both modelling and experimental studies (Kotsovinos et al. 2020a). Little work has addressed the precise failure mechanisms and, in turn, the failure criteria of cable members. Therefore, it is prudent that the failure criteria for cable members under thermal exposure be reviewed by the research community and disseminated so as to enable comparisons between bodies of work. It is the author's opinion that the state of the modelling of cable members is not advanced sufficiently to warrant a round robin modelling series and that a number of unaddressed topics should be examined by research first, as will be discussed in the subsequent section.

## 6.3 Modelling Implications Based on the Experimental Fire Performance of Steel Stay-Cables

The experimental results presented in Chapter 5 yield some behaviours pertaining to the fire performance of steel cable members that should be investigated through future studies and which may have implications towards the results of existing models. This section will explore these experimental results in the context of the thermal modelling of steel stay-cables and inform a methodology towards applying them.

### 6.3.1 Experimental Results to Consider in Modelling Endeavors

The first modelling feature to be addressed is the use of lumped capacitance which ignores wire discretization and therefore does not directly consider the presence of air voids nor wire-to-wire contact. This approach was found to yield lower temperatures than models accounting for wire discretization by both Du et al. (2019), who considered the case of concentric cylinders separated by an air gap compared to full wire structure, and Kotosovinos et al. (2020a), who considered the case of a solid bar compared to the full wire structure. These authors consider spiral and parallel-wire strand types, but the lumped capacitance approach has yet to be assessed for use in the modelling of fully locked-coil strands that have much denser exterior layers of Z-shaped wires surrounding an interior spiral strand type. As the interface between Z-shaped wires provides more contact area than round wires, including between adjacent layers of Z-shaped wires, a lumped capacitance approach for these wire types may be appropriate and should be explored in modelling. Experimentally, locked-coil strands were found to reach slightly higher temperatures than similarly sized spiral strands which contradicts the modelling findings of Du et al. (2019) and Kotsovinos et al. (2020b) which predicted lower temperatures for greater use of lumped capacitance. Therefore, a partial approach where outer Z-shaped wires are modelled as a lumped thermal capacitance surrounding an inner, discretized spiral strand should be taken to assess if this approach still produces conservative results for the case of a locked-coil strand (see Figure 6.1). It is also hypothesized that, in the case of non-uniform heating,

radial and circumferential conduction in the locked-coil cable layers normalizes temperatures and that the thermal boundary for the interior spiral strand may be more uniform than the external boundary condition. This has implications on the potential load shedding within locked-coil strands as the normalization of temperatures within the locked-coil layer will result in more uniform expansion and degradation of steel material properties, therefore less individual wires may reach extreme temperatures within the cross-section, potentially improving the thermo-mechanical performance of the system.

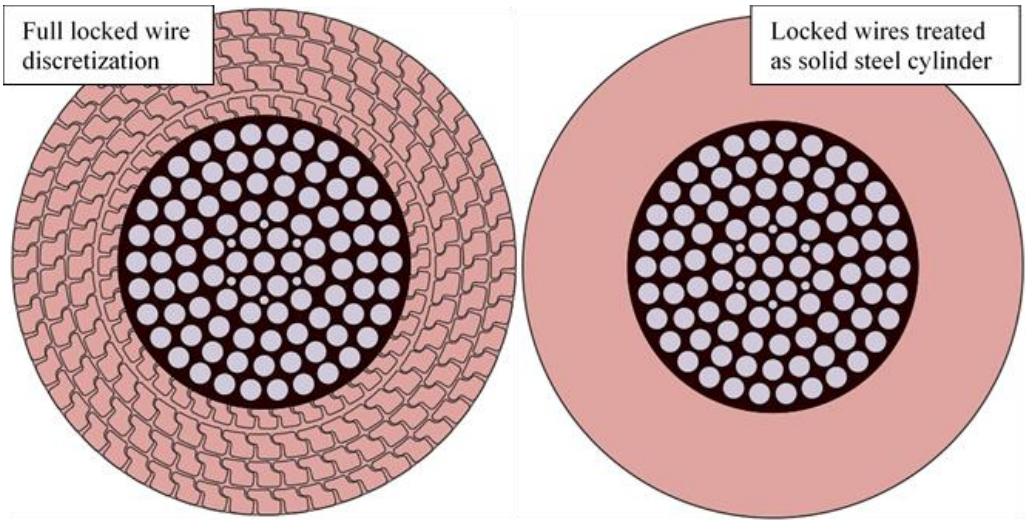


Figure 6.1 Proposed partial lumped-capacitance model (right) compared to a full discretization model (left) for a locked-coil cable.

Another important experimental result is the longitudinal normalization of cross-sectional temperatures outside of the heated length in stay-cable members exposed to fire. In the majority of tests in Chapter 5, the cross-sectional temperatures at the top, core, and bottom of the strands 250 mm beyond the edge of the 500 mm heated region were normalized to within 10°C for the duration of the heating and cooling phases and for strand diameters of up to 140 mm. Although still greatly normalized compared to temperatures in the exposed region, the two stainless steel spiral strands considered had larger gradients outside of the exposed length than the galvanized steel strands. This is attributed to the reduced thermal conductivity of the stainless-steel strands and suggests the longitudinal normalization of temperatures is primarily driven by radial and longitudinal interwire conduction. Modelling efforts should examine the longitudinal conduction in cable members to establish a boundary beyond which heat transfer can be simplified to one-dimensional which would assist in limiting computational resources for complex three-dimensional models (see Figure 6.2).

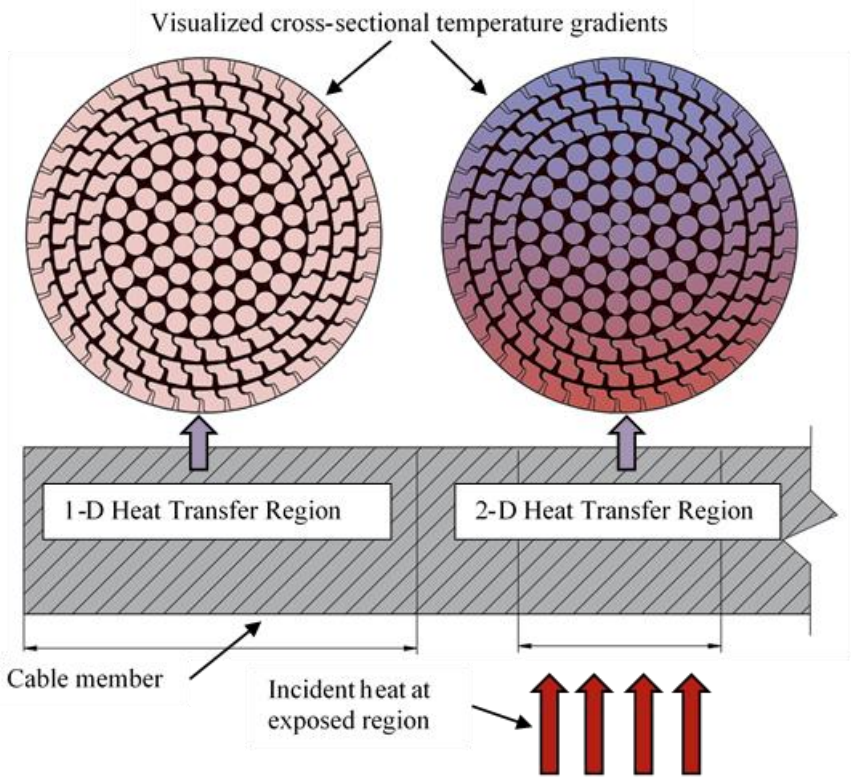


Figure 6.2 Visualization of the normalization of cross-sectional temperatures and the proposed modelling strategy based on the experimental results of Chapter 5.

The parameters controlling longitudinal thermal conduction should also be explored in modelling studies. For example, it is expected that the normalization effect is assisted by the helical rotation of wires and that conduction along individual wires may be greater than conduction along the longitudinal path of the overall cable as transmitted through wire-to-wire contact. This would imply that cross-sectional temperature normalization is less apparent in parallel-wire strands due to the lack of helical wire rotation relative to the core wire.

Assumptions of interwire friction and its effects have been made previously in the literature (Main and Luecke 2010, Wright et al. 2013) but further investigation into the validity or general behaviour of this phenomenon has not been pursued yet. These past assumptions of interwire friction have assumed great frictional interwire forces in stay-cable members based on the presence of clamping apparatuses and the tendency for a bundle of wires to tighten under tension, however experimental results in Chapter 5 yield the potential for contradictory thermal deformations such as thermal torsion and the associated wire bulging. Thermal torsion was observed in some stages of heating and is characterized by the thermal elongation of individual wires originating from the heated side of the cable. This behaviour results in the rotational movement or apparent “unwinding” of individual wires at regions away from the heated cable face. This effect is dependent on the occurrence of a sufficient thermal gradient between the top and bottom cables faces, otherwise a counteracting expansion originating at the top of the cable negates the effect. The

rotational direction of thermal torsion is dependent on the lay length and direction of wire layers. Although this phenomenon was observed experimentally in unloaded cables, the potential for thermal torsion to occur in loading strands is unquantified due to the assumed interwire frictional forces restraining the movement. Even if the wire displacement associated with thermal torsion is inhibited, this process would still serve to more rapidly shed loads from heated wires. There is much to study regarding the phenomenon of thermal torsion, mainly if interwire friction restrains the observed displacements and, if so, how might the effect accelerate load shedding, especially from wires that wrap around the member. More specifically, future research could examine what longitudinal portion of an individual wire is disengaged from contributing mechanically and at what helical wire span interwire friction can mechanically reengage an adjacent wire through friction. These processes are complex and would be very difficult to model numerically as three-dimensional analyses would be necessary with very specific boundary conditions to enable out-of-plane wire movements without introducing other complicating factors.

Related to the phenomenon of thermal torsion is the bulging effect of a thermally expanding wire meeting an area of high clamping force. This was observed experimentally in Chapter 5 where wire movement from thermal torsion was resisted by a clamp and caused out-of-plane bulging (see Figure 6.3). As any out-of-plane wire movement likely entails that a wire is no longer supporting load in tension, this effect should also be studied in cables under load to assess if a similar effect occurs and how the effect may accelerate load shedding. Additionally, if the interwire friction predicted previously is sufficient, a cooler region of a cable member (in which all wires of the cable cross-section are engaged mechanically) may act as a clamped region compared to a locally heated cable length. If thermal expansion from a heated region is sufficient to overcome interwire friction, thermal torsion may occur along a wire until a cooler cable cross-section which has not yet overcome interwire friction halts the process, and the wire bulges. These highly complex interactions associated with thermal torsion may be better suited to examination in specific experimental settings or very simplified numerical models. For example, only a single layer of wrapped wires could be modelled while interior wires are replaced by a solid steel cylinder to investigate these deformational effects.

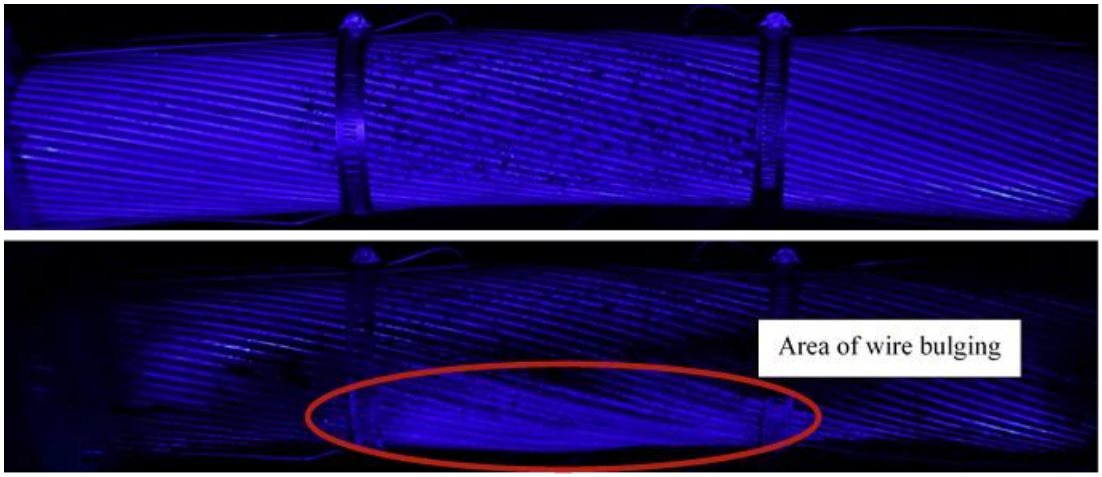

Figure 6.3. Wire bulging occurring on exposed surface wires between clamped areas. The cable shown is S-GS-82.

Interwire friction assumes no wire can move independently from the others (Main and Luecke 2010) which has led to the assumption that the global thermal expansion of the cable is governed by the thermal expansion of the coldest wire (or more realistically, coldest wire layer) (Wright et al. 2013). While this assumption could be valid along the fire-exposed length of the cable where temperature gradients in the cross-section exist, the temperature uniformity of cable cross-sections away from the heated region will still contribute to the global thermal elongation of a cable and therefore must be considered in structural models. Therefore, ignoring longitudinal conduction and temperature normalization outside of a fire-exposed cable region may yield unconservative elongation calculations by failing to consider thermal elongation that is not inhibited by interwire friction.

General topics that require attention include the effect of blocking agents on internal heat transfer (blocking agent presence in air voids) and the high-temperature properties of high-strength carbon and stainless steels. The addition of blocking agents into a thermal model of stay-cables exposed to fire would be extremely complex as it has been observed that these substances smolder within the cable structure and can potentially liquefy and drip onto the cable surface or into a fire below. Therefore, this assessment will require experimental attention, potentially through a comparison of the thermal response of identical cables with and without blocking agents to determine any major changes to internal temperature development. Additionally, as suggested by Kotsovinos et al. (2020a), more experimental data on the high-temperature material properties of steel types used in steel cables is needed, as was reinforced by the variability in thermal strain response between the two stainless steel cables tested in Chapter 5 due to different steel compositions. Further, the experimental observations of the deterioration of galvanizing alloy could be explored more thoroughly and may potentially lead to post-fire assessment strategies or could more accurately inform critical temperatures for cable fire protection.

### 6.3.2 Future Modelling Agenda and Strategy Based on Experimental Results

The discussion in the previous section is intended to discuss how the experimental results in Chapter 5 could potentially influence future models of the fire performance of stay-cable members. This section will briefly summarize the modelling agenda associated with important experimental results and will suggest approaches for modelling the experiments in Chapter 5. Table 6.1 presents major experimental conclusions and observations that the author has deemed important for consideration in future modelling efforts. Note that a similar set of conclusions are presented by Kotosovinos et al. (2020) based on their review of relevant literature on the topic of the thermo-mechanical performance of cable members; these areas of future work should also be reviewed by the interested reader, whereas the areas for future work presented herein are based solely on the experimental results discussed in this thesis.

Based on the experiments outlined in Chapter 5, the cables with the most complex behaviours were L-GS-100A and L-GS-100B as they exhibited thermal torsion, blocking agent combustion, and were assumed to have a different steel composition (based on the assumed different coefficient of thermal expansion compared to other tests). Conversely, the most simplified thermal responses were from smaller-diameter cables S-GS-44, S-SS-22, and S-SS-50 which saw limited secondary thermal deformation effects.

Table 6.1 Areas of interest to be targeted by future modelling or experimental research.

| Area of Interest | Topic to Consider |
|---|---|
| Full locked-coil cables | 1. Modelling efforts should determine if the lumped capacitance assumptions are valid in the case of multiple layers of interlocking Z-shaped wires and how the thermal boundary for the interior spiral strand of a locked-coil cable may become more normalized than external boundary conditions.<br><br>2. A similar procedure to that of Kotosovinos et al. (2020b) could be applied to assess the degree of load shedding and thermal moment development in locked-coil cables, and if the reduction of these effects based on improved thermal conduction in the locked-coil layer could potentially improve fire performance. |
| Longitudinal heat transfer | 3. A modelling study on the longitudinal heat transfer in cable members should be conducted to identify at what distance outside and under what conditions cross-sectional cable temperature gradients normalize. This can be used to simplify cable models to a single dimension of heat transfer for localized heating studies.<br><br>4. The effect of helical wire rotation on the longitudinal heat transfer of a cable should be investigated to consider what portion of temperature normalization is attributed to longitudinal heat transfer in individual wires or to wire-to-wire conduction (and cavity radiation). |
| Thermal deformations and interwire friction | 5. The phenomenon of thermal torsion should be investigated more thoroughly and for the case of loaded cable members. This may be better suited for experimental studies at this stage. Ultimately, the effects of thermal torsion on load shedding behaviour and any potential interaction with interwire frictional restraints should be targeted. |

| Area of Interest | Topic to Consider |
|---|---|
| | 6. Similarly to the previous point, wire bulging due to clamping forces should also be investigated in the context of interwire friction in loaded cables. The effect of cooler cable regions preventing wire thermal expansion and initiating bulging can also be examined. This is also perhaps best suited for an experimental study.<br><br>7. While thermal expansion of surface wires was observed and measured experimentally in Chapter 5, global cable elongation should be studied in the context of interwire friction. Specifically, the degree of cable elongation in a locally heated region where cross-sectional gradients are large should be compared to elongation away from the heated zone where gradient are normalized. Both components of thermal elongation must be considered in a thermo-mechanical model. |
| General topics | 8. Further investigation into the role of blocking agents is critically needed, as, based on the flashpoints of some substances studied in Chapter 5, their presence in a cable likely renders the assumed critical temperature for fire protection of 300°C unconservative. Additionally, experimental research should examine how the potential smoldering of blocking agents in the cable structure affects the overall thermal response.<br><br>9. The variation of steel types used in the manufacturing of cable members should be studied in terms of their high-temperature material properties in the temperature ranges a potential bridge fire scenario could produce (greater than 800°C). This should be performed for both stainless and carbon steel types.<br><br>10. The deterioration of galvanizing alloys on the surface of wires could also be examined more thoroughly and its potential effect on the heat absorption on a cable's surface should be studied. For example, examining how thermal conduction through a zinc-aluminum surface layer could affect wire-to-wire conduction or how melting of the galvanization could fill air voids, may be topics of interest. |

## 6.4 Summary

This chapter served as a review of the experiments performed in Chapter 5 in the context of past modelling endeavors of steel cable and other isolated steel members from the literature. Studies involving the modelling of cable members were reviewed and modelling implications were discussed. Although the level of complexity associated with each topic was briefly discussed, care should be taken to determine the correct level of analysis required to develop tools for the fire design of cable members. Analytical or modelling solutions should follow the "consistent crudeness" paradigm discussed in Chapter 3 such that complex phenomenon are analyzed with sufficiently complex means. Therefore, future researchers considering this topic must assess the complexity of the topics discussed herein to best select the level of analysis detail and, ultimately, the intricacy of the implemented design solution. To conclude, a total of ten areas of interest were identified within four subcategories related to the thermo-mechanical performance of steel stay-cables. These topics include the assumptions and behaviour of full locked-coil cables, longitudinal heat transfer in cable members, thermal deformations and interwire friction, and other general areas of discussion such as the role of blocking agents, high-temperature material properties, and galvanization coatings. These recommendations for future work are informed directly from experimental

results and are believed to be necessary topics of study for future experimental or numerical literature on the topic of the fire performance of steel cable members.

# Chapter 7: Conclusions and Recommendations

## 7.1 Summary

As performance-based fire designs become more standard in Canada and globally, structural fire engineers will require more knowledge on a variety of structural configurations for a range of fire exposures such that safe and efficient designs can be developed. This is especially true for bridges and cable-supported structures which, over the past decade, have only begun to be targeted by research and have historically had no guidance or code requirements promoting thermo-structural designs for fires. The knowledge gaps in the thermo-structural behaviour of these structures hinders architectural advancement and fails to develop the fire resilience of critical infrastructure. The goal of this thesis has been to experimentally test the fire behaviour of the steel cable members used in cable-supported bridges and structures to help better understand how these elements could affect the high temperature response of a global structure. This thesis has provided valuable data relevant to the heat transfer of steel cables exposed to fire, identified previously undocumented cable deformational behaviours, and provided context in the larger scheme of bridge fire safety engineering. Ultimately, the work in this thesis serves to help further develop the design capacity for practitioners apply cable elements and thereby facilitates the development of fire resilient structures in Canada and globally.

A brief introduction into the practice of structural fire engineering was presented in Chapter 2 to help provide context to the reader who may be unfamiliar with fire safety principles. With specific commentary towards steel structures and cable-supported bridges, this chapter provides a simplified overview of the effects of fire on steel in terms of the microstructural changes and mechanical property losses at elevated temperatures. An introduction into the fires applied as thermal boundaries for structural engineering applications is provided and discussions of the European and Canadian practices of fire safety engineering as well as contemporary issues facing this field are supplemented. Finally, the general methodologies for contemporary structural fire engineering practice and specific implications for bridge structures in this context are discussed.

Chapter 3 established knowledge gaps through a literature review of bridge fire research and discussed a framework for bridge fire research moving forward. This literature considered a variety of categories under the topic of bridge fire safety. First, a review of the determination of bridge fire risks and hazards reviewed best practices for quantifying the likelihood and severity of various bridge fire events as well as how to account for the critical nature of specific bridge fire events in design. The modelling of bridge fire scenarios examined the tools applied in establishing plausible thermal boundaries for bridge structures exposed to fire. Finally, the thermo-mechanical responses of steel, composite steel and concrete, cable-supported,

concrete, and polymer-reinforced bridges to fire were reviewed through literature pertaining to the structural analysis of each respective bridge type for the fire load case. To conclude, knowledge gaps for each category were presented and a guideline for developing the fire resilience of bridges in Canada was put forth.

Chapter 4 explored the use of an open-air pool fire to inflict fire damage to bridge structural members. In this chapter, a GFRP stay-in-place formwork beam was exposed to a pool fire and compared in flexure post-fire to identical members with simulated fire damage. An additional study of the bond shear strength between the GFRP and concrete found a decrease in bond performance with increasing temperature exposure. Although some limitations were present, such as the relatively small heat release rate when compared to a bridge fire event, the pool fire exposure was useful in invoking a thermo-mechanical response and highlighted a potential for future test programs to apply this chapter's methodology.

The experimental fire performance of unloaded steel stay-cables was considered in Chapter 5 in addition to a literature review of existing experimental research examining the behaviour of cable members at elevated temperatures. This experimental program examined the temperature and thermal deformation development of multiple steel strands in a variety of diameters, steel types, and configurations. In this chapter, multiple steel stay-cables were exposed to non-uniform and localized heating through the use of a methanol pool fire. A novel application of narrow-spectrum illumination coupled with digital image correlation enabled a calculation of cable surface strains which were compared to code-suggested values. A unique deformational behaviour referred to as thermal torsion was observed and quantified in this program. Ultimately, comparative conclusions were made about the role of spiral versus full locked-coil cable types, cable diameter, steel type.

Chapter 6 reviewed existing models of the thermo-structural performance of cable members in the literature and presented discussions on how the results of Chapter 4 could be applied towards tools for practitioner use and future model development. Four areas of interest, the performance of full locked-coil cables, longitudinal heat transfer, thermal deformations and interwire friction, and general topics, were explored in the context of the fire performance of cables and future work was suggested for each area.

## 7.2 Conclusions

The following conclusions are made based on the experimental testing and discussion presented in this thesis:

1. The thermal responses of stay-cables are intuitive to some degree in non-uniform heating in that cable diameter is inversely proportional to heating rate, maximum temperature, and thermal gradient, especially for core wires.

2. There is a small difference (<50°C) in the maximum temperature developed in similarly sized full locked-coil and spiral strands due to the reduced insulation increased conduction ability of the denser locked-coil layers. This results in greater temperatures developed in non-fire-exposed regions of a cable.

3. In general, stainless steel stay-cables perform more favorably in regard to heat transfer under the fire exposure studied based on the lower thermal conductivity of the metal. This resulted in slightly reduced maximum temperatures in the fire-exposed region when compared to a similarly-sized galvanized steel strand and greatly reduced (45°C versus 85°C maximum temperatures) insulated temperatures.

4. Cross-sectional temperatures in the insulated region of galvanized cables become uniform only a short distance outside of the heated region for all strand diameters tested which can have benefits for modelling heat transfer in cables exposed to localized fires.

5. The combination of digital image correlation and narrow-spectrum illumination proved viable for measuring thermal deformations however, for shorter gauge lengths, the accuracy of this technique diminishes as the fluid interaction of hot and cold air between the camera and the target introduces a signal noise in the output.

6. The deformation behaviour of stay-cables can have secondary components, such as thermal bowing which was observed in strands with large temperature gradients. Thermal torsion, a rotational effect owing to the differential thermal expansion of soffit wires, was observed and characterized.

7. The cooling phase thermal strain contraction was sufficient to estimate the maximum thermal strain developed in all strands. Relevant Eurocode equations could reproduce the measured thermal strains with some accuracy, however this accuracy diminished with larger-diameter strands (≤ 100 mm) as the measured thermal boundaries became less representative of the heat transfer within the cable. Some discrepancies in the Eurocode equations were found for various steel alloys.

8. The combustion of blocking agents within the cable structure did not have a discernable effect on the heat transfer nor thermal strain development of the strands tested. However, the interaction of blocking agents with high-temperatures creates the potential for these substances to provide additional fuel to a fire or create a smouldering fire within the cable structure.

9. Based on the combustion of blocking agents observed herein, current guidance for the fire protection of cable members limiting maximum temperatures to 300°C is unconservative, as the flashpoint of blocking agents can be below this temperature.

10. The zinc-aluminum alloy galvanization layer was observed to deteriorate and melt on fire-exposed surfaces. This should be considered in design as the galvanization layer is important to the inhibition of corrosion and should be undamaged for a cable to continue in service after a fire.

## 7.3 Research Recommendations

As identified from the literature in Chapter 3, the following topics for future work could be considered:

1. There is a lack of statistical data on all aspects of bridge fires in many jurisdictions which should be addressed by robust bridge fire reporting system. A study from the economic perspective of bridge fire resilience considering indirect losses could also be enlightening. Appropriate tools should be developed to assist designers in establishing the credibility of a fire scenarios and how to mitigate fire hazards. Residual strength assessment and repair strategies are not well developed and could be enhanced through research, as many tests rely on qualitative observations.

2. There is a need to firmly establish what a realistic fire exposure entails with respect to bridge infrastructure. It is the author's opinion that a realistic bridge fire should consider rapid initial temperature rise, realistic variations in temperature that have the potential to create thermal shock phenomena, a cooling phase, and a localized area of fire exposure (except in the case of short-span bridges where care must be taken to ensure uniform fire exposure is realistic). Specific research could examine what proportion of bridge fire exposure constitutes a "localized fire" based on the sizes of potential vehicle fires, the predicted containment of spilled hydrocarbon fuels, or in general the characteristics of a given fire scenario.

3. More experimentation is needed to study aspects of steel girder behaviour under hydrocarbon fire exposures such as the effect of extreme localized heating, the global bridge response under non-uniform heating in the transverse span direction, the post-fire strength and deformation recovery, and the effect of rapid localized steel quenching from firefighting methods. Localized behaviour in steel box girders is also an understudied topic. Experimental research into the influence of structural steel compositions is needed.

4. There is a lack of experimentation focusing on the fire performance of concrete bridge elements. many concrete bridges in service are disrepaired with large portions of exposed steel reinforcing and reduced cross-sections due to spalling. Specific research could examine the vulnerability of aged and disrepaired bridges to fire exposure and suggest retrofits to reduce fire risk.

5. High temperature interactions between FRP-reinforcements and concrete in bridge applications are not well understood especially in novel applications such as stay-in-place formwork. The influence of

exposed and flammable GFRP reinforcements contributing to fire severity is also a concern in some applications.

6. Specific experimental research should consider timber bridges which have had very little attention in the context of bridge fire safety. Of interest is the fire response of timber trestles which typically apply many small-sized members, covered bridges which make use of mid-sized members, and, more recently, prestressed timber bridges which apply massive members.

7. Information is needed concerning the thermal expansion of steel cables of varying configurations like locked-coil, parallel, and spiral structural strands, the risk of cable uncoiling as a result of thermal expansion and loss of tension, the influence of lubricants and stopping agents, and the global structural response of cable-supported systems in terms of load shedding to adjacent unheated cables.

Based on the applications of experimental results discussed in Chapter 5, the following topics for future work could be considered:

8. Modelling efforts should determine if the lumped capacitance assumptions are valid in the case of full locked-coil cables and how the thermal boundary for the interior spiral strand of a locked-coil cable may change based on this consideration.

9. A modelling study on the longitudinal heat transfer in cable members should be conducted to identify at what distance beyond the fire-exposed region and under what conditions cross-sectional cable temperature gradients normalize, as well as to establish the main mechanisms behind longitudinal heat transfer in cables.

10. Secondary thermal deformations such as wire bulging and thermal torsion require further experimental study to assess any significant effects these phenomena may have on the mechanical performance of a cable in fire.

11. A study into the presence and implications of interwire frictions should be conducted for cables exposed to fire while in tension.

12. Specific research should be conducted into the effects associated with blocking agent combustion in cable members, namely if combustion can occur through fire protection and the resulting thermal implications of a smoldering fire within the cable structure.

13. Steel grain microstructural analysis could be a very useful forensic tool in experimental studies such as that of Chapter 4 and should be considered in future work to further establish maximum steel temperatures in cable structures.

# Bibliography

AASHTO (American Association of State Highway and Transportation Officials). 2015. LRFD Bridge Design Specifications. Washington, DC.

Adelzadeh, M., Hamzeh H., and Green, M. 2014. Numerical Study of FRP Reinforced Concrete Slabs at Elevated Temperature. Polymers, MDPI AG, 6(2): 408-422. DOI: 10.3390/polym6020408.

Alnahhal, W. I., Chiewanichakorn, M., Aref, A. J., and Alampalli, S. 2006. Temporal Thermal Behaviour and Damage Simulations of FRP Deck. J. Bridge Eng., 11(4): 452-464. DOI: 10.1061/(ASCE)1084-0702(2006)11:4(452).

Alos-Moya, J., Paya-Zaforteza, I., Garlock, M. Loma-Ossorio, E., Schiffner, D. and Hospitaler, A. 2014. Analysis of a Bridge Failure due to Fire Using Computational Fluid Dynamics and Finite Element Models. Eng. Struct., 68(2014), 96-110. DOI: 10.1016/j.engstruct.2014.02.022.

Alos-Moya, J., Paya-Zaforteza, I., Hospitaler, A., and Rinaudo, P. 2017. Valencia Bridge Fire Tests: Experimental Study of a Composite Bridge under Fire. J. Constr. Steel Res., 138(2017), 538-554. DOI: 10.1016/j.jcsr.2017.08.008.

Alos-Moya, J., Paya-Zaforteza, I., Hospitaler, A., and Loma-Ossorio, E. 2019. Valencia Bridge Fire Tests: Validation of Simplified and Advanced Numerical Approaches to Model Bridge Fire Scenarios. Advances in Eng. Software, 128(2019), 55-68. DOI: 10.1016/j.advengsoft.2018.11.003.

Ann, H., Choi, Y., Lee, J. H., Jang, Y. I., and Kong, J. S. 2019. Semiquantitative Fire Risk Grade Model and Response Plans on a National Highway Bridge. Advances in Civ. Eng., (2019). DOI: 10.1155/2019/5154309.

ASCE. 2018. Structural Fire Engineering. LaMalva, K.J. ed. American Society of Civil Engineers (ASCE) Fire Protection Committee. DOI: 10.1061/9780784415047.

ASTM. 2014. Standard Test Methods for Determining Effects of Large Hydrocarbon Pool Fires on Structural Members and Assemblies. ASTM E-1529-14a. West Conshohocken, United States.

ASTM. 2016. ASTM E119-16a. Standard Test Methods for Fire Tests of Building Construction and Materials. ASTM International. West Conshohocken, PA.

Atalioti, A., Rein, G., Kotsovinos, P., and Sadowski A.J. 2017. Computational Study of the 2D Thermal Response of High-Strength Structural Steel Cables under Various Heating Regime. International Conference of Applications of Structural Fire Engineering (ASFE), Manchester, United Kingdom.

Au, A. 2016. Re-Testing of a Fire Damaged Bridge. CSCE Resilient Infrastructure Conference, CSCE, London, Canada.

Aziz, E. M., and V. Kodur. 2013. An Approach for Evaluating the Residual Strength of Fire Exposed Bridge Girders. J. Constr. Steel Res. 88: 34–42. DOI: 10.1016/j.jcsr.2013.04.007.

Aziz, E. M. 2015. Response of Fire Exposed Steel Bridge Girders. Ph. D Thesis. Michigan State University.

Aziz, E. M., V. Kodur., Glassman J. D., and Garlock, M. 2015. Behaviour of Steel Bridge Girders under Fire Conditions. J. Construct. Steel Res., 106(2015), 11-22. DOI: 10.1016/j.jcsr.2014.12.001.

Babrauskas V. 2016. SFPE Handbook of Fire Protection Engineering: Heat Release Rates, Springer, New York, NY.

Bai, Y., T. Keller, J. R. Correia, F. A. Branco, and J. G. Ferreira. 2010. Fire Protection Systems for Building Floors made of Pultruded GFRP Profiles — Part 2: Modeling of Thermomechanical Responses. Compos. Part B, 41(8), 630–636. DOI: 10.1016/j.compositesb.2010.09.019.

Beneberu, E., and Yazdani, N. 2018. Performance of CFRP-Strengthened Concrete Bridge Girders under Combined Live Load and Hydrocarbon Fire. J. Bridge Eng., 23(7). DOI: 10.1061/(ASCE)BE.1943-5592.0001244.

Beneberu, E., and Yazdani, N. 2019. Residual Strength of CFRP Strengthened Prestressed Concrete Bridge Girders after Hydrocarbon Fire Exposure. Eng. Struct., 184(2019), 1-14. DOI: 10.1016/j.engstruct.2019.01.057.

Bennetts, I., and Moinuddin, K. 2009. Evaluation of the Impact of Potential Fire Scenarios on Structural Elements of a Cable-Stayed Bridge. J. Fire Prot. Eng., 19(2), 85-106. DOI: 10.1177/1042391508095091.

Beyler, C.L. 2002. SFPE Handbook of Fire Protection Engineering: Fire Hazard Calculations for Large, Open Hydrocarbon Fires. NFPA, Quincy, USA.

Bisby, L., Gales, J., and Maluk, C. 2013. A Contemporary Review of Large-Scale Non-Standard Structural Fire Testing. Fire Sci. Rev., 2(1), 1. DOI: 10.1186/2193-0414-2-1.

Blaber, J., S. A. Stanier, W. A. Take, and D. J. White. 2016. Improved Image-Based Deformation Measurement for Geotechnical Applications. Can. Geotech. J. 53 (5), 727–739. DOI: 10.1139/cgj-2015-0253.

Boles, R., M. Nelson, and A. Fam. 2015. Durability of Bridge Deck with FRP Stay-In-Place Structural Forms under Freeze-Thaw Cycles. J. Compos. Constr., 19 (4). DOI: 10.1061/(ASCE)CC.1943-5614.0000531.

Braxtan, N. L., Whitney, R., Wang, Q., and Koch, G. 2015. Preliminary Investigation of Composite Steel Box Girder Bridges in Fire. Bridge Struct., 11(3), 105-114. DOI: 10.3233/BRS-150089.

Byström, A., J. Sjöström, U. Wickström, D. Lange, and M. Veljkovic. 2014. Large Scale Test on a Steel Column Exposed to Localized Fire. J. Struct. Fire Eng., 5 (2), 147–160. DOI: 10.1260/2040-2317.5.2.147.

Cabova, K., Ryjacek, P., Hrasky, O., Kolpasky, L., Vujtech, J. and Wald, F. 2016. Fire Test of FRP Members Applied to Railway Bridge. In 9th Structures in Fire, Princeton, USA, 784-790.

CEN (Committee of European Normalisation). 2002. EN 1991-1-2-2002. Eurocode 1: Actions on Structures - Part 1-2: Actions of Structures Exposed to Fire. Eurocode 1, Brussels, Belgium.

CEN (European Committee for Standardization). 2003. EN1991-2-2003. Eurocode 1: Actions on Structures - Part 2: Traffic Loads on Bridges. Eurocode 1, Brussels, Belgium.

CEN (European Committee for Standardization). 2004. EN1992-1-2-2004. Eurocode 2: Design of Concrete Structures - Part 1-2: General Rules—Structural Fire Design. Eurocode 2, Brussels, Belgium.

CEN (Committee of European Normalisation). 2005. EN 1994-1-2-2005, Eurocode 4: Design of Composite Steel and Concrete Structures - Part 1-2: General Rules - Structural Fire Design. Eurocode 4, Brussels, Belgium.

CEN (European Committee for Standardization). 2006. EN1993-1-11-2006. Design of Steel Structures–Part 1-11: Design of Structures with Tension Components. Eurocode 3, Brussels, Belgium.

Chen, C., Chen, J., Zhao, X., and Shi, C. 2018. Experimental Investigation on Combustion Characteristics of Steel Cable for Cable-Stayed Bridge. J. Therm. Anal. Calorim., 134(3), 2317-2327. DOI: 10.1007/s10973-018-7689-6.

Choi, J., Haj-Ali, R., and Kim, H. S. 2012. Integrated Fire Dynamic and Thermo-mechanical Modeling of a Bridge under Fire. Struct. Eng. and Mech., 42(6), 815-829. DOI: 10.12989/scs.2010.10.2.129.

Chorlton, B., Forrest, B., Gales, J., and Weckman, B. 2020. Performance of Type X Gypsum Board on Timber to Non-Standard Fire Exposure. Fire Mat., 1(16). DOI: 10.1002/fam.2822.

Chung, P., Wolfe, R. W., Ostrom, T. and Hida, S. 2008. Accelerated Bridge Construction Applications in California – a Lessons Learned Report. USA: California Department of Transportation (CALTRANS).

Correia, J. R., F. A. Branco, J. G. Ferreira, Y. Bai, and T. Keller. 2010. Fire Protection Systems for Building Floors made of Pultruded GFRP Profiles. Part 1: Experimental Investigations. Compos. Part B, 41 (8), 617–629. DOI: 10.1016/j.compositesb.2010.09.018.

Correia, J. R., M. M. Gomes, J. M. Pires, and F. A. Branco. 2013. Mechanical Behaviour of Pultruded Glass Fibre Reinforced Polymer Composites at Elevated Temperature: Experiments and Model Assessment. Compos. Struct., (98), 303–313. DOI: 10.1016/j.compstruct.2012.10.051.

Correia, J. R., Y. Bai, and T. Keller. 2015. A Review of the Fire Behaviour of Pultruded GFRP Structural Profiles for Civil Engineering Applications. Compos. Struct., (127), 267–287. DOI: 10.1016/j.compstruct.2015.03.006.

CSA (Canadian Standards Association). 2014a. CAN/CSA-S6-14. Canadian Highway Bridge Design Code. Rexdale, Canada.

CSA (Canadian Standards Association). 2014b. CAN/CSA-S16-14. Design of Steel Structures. Mississauga, Canada.

Cui, C., Chen, A., and Ma, R. 2020. Stability Assessment of a Suspension Bridge Considering the Tanker Fire Nearby Steel-Pylon. J. Constr. Steel Res., 172(2020), DOI: 10.1016/j.jcsr.2020.106186.

Cverna, F. 2002. ASM Ready Reference: Thermal Properties of Metals. ASM International.

de Melo, M., Wheatley, R., Gibbin, N., Gonzalez-Quesada, M., and Harwood, K. 2014. Assessment and Repair of a Fire-Damaged Pre-Stressed Concrete Bridge. Struct. Eng. Int., 24(3), 408-413.

Del Prete, I., A. Bilotta, and E. Nigro. 2015. Performances at High Temperature of RC Bridge Decks Strengthened with EBR-FRP. Compos, Part B, (68), 27–37. DOI: 10.1016/j.compositesb.2014.08.011.

Destrebecq, J., E. Toussaint, and E. Ferrier. 2011. Analysis of Cracks and Deformations in a Full Scale Reinforced Concrete Beam using a Digital Image Correlation Technique. Exp. Mech., 51 (6), 879–890. DOI: 10.1007/s11340-010-9384-9.

Dotreppe, J. C., Majkut, S., and Franssen, J. M. 2005. Failure of a Tied-Arch Bridge Submitted to a Severe Localized Fire. IABSE Symposium Report, International Association for Bridge and Structural Engineering, 90(7), 15-22.

Drysdale, D. 2011. An Introduction to Fire Dynamics. 3rd ed. Chichester, UK: John Wiley & Sons.

Du, Y., Peng, J. Z., Liew, J. R., and Li, G. Q. 2018. Mechanical Properties of High Tensile Steel Cables at Elevated Temperatures. Contr. Build. Mat., 182(2018), 52-65. DOI: 10.1016/j.conbuildmat.2018.06.012.

Du, Y., Sun, Y. K., Jiang, J., and Li, G. Q. 2019. Effect of Cavity Radiation on Transient Temperature Distribution in Steel Cables under ISO834 Fire. Fire Saf. J., 104(2019), 79-89. DOI: 10.1016/j.firesaf.2019.01.002.

Fam, A., R. Boles, and M. Robert. 2016. Durability in a Salt Solution of Pultruded Composite Materials used in Structural Sections for Bridge Deck Applications. J. Bridge Eng., 21 (1). DOI: 10.1061/(ASCE)BE.1943-5592.0000768.

Flint, G., Lamont, S., Lane, B., Sarrazin, H., Lim, L., Rini, D. and Roben, C., 2013. Recent Lessons Learned in Structural Fire Engineering for Composite Steel Structures. Fire Tech., 49(3), 767-792.

Flint, G., Kotsovinos, P., Panev, Y., and Woodburn, P. 2017. Quantified Fire Risk Assessment for the Design of Bridges Against Fire. In CONFAB 2017: 2nd International Conference on Structural Safety under Fire & Blast Loading. September 2017, London, United Kingdom.

Fontanari, V., Benedetti, M., Monelli, B. D., and Degasperi, F. 2015. Fire Behaviour of Steel Wire Ropes: Experimental Investigation and Numerical Analysis. Eng. Struct., 84, 340-349. DOI: 10.1016/j.engstruct.2014.12.004.

Gales, J., Bisby, L., and Maluk, C. 2012. Structural Fire Testing – Where Are We, How Did We Get Here, and Where Are We Going? 15th International Conference on Experimental Mechanics. Porto, Portugal. 22.

Gales, J., and M. Green. 2015. Optical Characterization of High Temperature Deformation in Novel Structural Materials. 14th International Conference on Fire and Materials, 626–640. London: Grayson Franks Ltd.

Gales, J., Hartin, K. and Bisby, L. 2016a. Structural Fire Performance of Contemporary Post-Tensioned Concrete Construction. Springer, New York. DOI: 10.1007/978-1-4939-3280-1.

Gales, J., Robertson, L., and Bisby, L. 2016b. Creep of Prestressing Steels in Fire. Fire Mater., 40(7), 875-895.

Gales, J., N. Nagy, and B. Weckman. 2016c. Improving Fire Safety of Glass Fibre Reinforced Polymers for Bridge Infrastructures. Interflam. Egham, UK: Royal Holloway College. 747–752.

Garlock, M., Paya-Zaforteza, I., Kodur, V., and Gu, L. 2012. Fire Hazard in Bridges: Review, Assessment and Repair Strategies. Eng. Struct., 35(89), 89-98. DOI: 10.1016/j.engstruct.2011.11.002.

Gatien, S., Young, T., Hoehler, M.S. and Gales, J., 2019. Application of Narrow-Spectrum Illumination and Image Processing to Measure Surface Char Formation in Lateral Ignition and Flame Spread Tests. Fire Mat., 43(4), 358-364. DOI: 10.1002/fam.2706.

Gibson, A. G., Y. S. Wu, J. T. Evans, and A. P. Mouritz. 2006. Laminate Theory Analysis of Composites under Load in Fire. J. Compos. Mater., 40 (7), 639–658. DOI: 10.1177/0021998305055543.

Gimsing, N. J., and Georgakis, C. T. 2011. Cable Supported Bridges: Concept and Design. John Wiley & Sons, New York.

Giuliani, L., Crosti, C., and Gentili, F. 2012. Vulnerability of Bridges to Fire. 6th International Conference on Bridge Maintenance, Safety, and Management, 8-12.

Glassman, J. D., and Garlock, M. E. M. 2014. Post-Fire Strength Assessment of Steel Bridges Based on Residual Out-of-Plane Web Deformations. Structures Congress, Boston, United States, 335-344.

Glassman, J. D., Boyce, V., and Garlock, M. E. M. 2019. Effectiveness of Stiffeners on Steel Plate Shear Buckling at Ambient and Elevated Temperatures. Eng. Struct., 181(2019), 491-502. DOI: 10.1016/j.engstruct.2018.12.012.

Godart B.F., Berthellemy J., and Lucas J.P. 2015. Diagnosis, Assessment and Repair of the Mathilde Bridge Close to Collapse during a Fire. Struct. Eng. Int. 25(3), 331-338. DOI: 10.2749/101686615X14210663188691.

Gong, X., and Agrawal, A.K. 2015. Numerical Simulation of Fire Damage to a Long-Span Truss Bridge. J. Bridge Eng., 20(10). DOI: 10.1061/(ASCE)BE.1943-5592.0000707.

Gong, X., and Agrawal, A. K. 2016. Safety of Cable-Supported Bridges During Fire Hazards. J. Bridge Eng., 21(4). DOI: 10.1061/(ASCE)BE.1943-5592.0000870.

Gooranorimi, O. 2016. Investigation of Bond, Microstructure and Post-Fire Behaviour of GFRP Reinforcement for Concrete. Ph.D. Dissertation, Dept. of Civil, Architectural, and Environmental Engineering, Univ. of Miami.

Heskestad, G., and Hamada, T. 1993. Ceiling Jets of Strong Fire Plumes. Fire Saf. J., 21(1), 69-82. DOI: 10.1016/0379-7112(93)90005-B.

Honickman, H., M. Nelson, and A. Fam. 2009. Investigation into the Bond of Glass Fibre-Reinforced Polymer Stay-in-Place Structural Forms to Concrete for Decking Applications. Transp. Res. Rec., 2131 (1), 134–144. DOI: 10.3141/2131-13.

Hu, J., Carvel, R., Sanad, A. and Usmani, A. 2016. New Design Fires for Performance Based Engineering of Highway Bridges. Structures in Fire, Princeton, US.A., 9, 768-775.

Hu, J., Usmani, A., Sanad, A., and Carvel, R. 2018. Fire Resistance of Composite Steel & Concrete Highway Bridges. J. Construct. Steel Res., 148(2018), 707-719. DOI: 10.1016/j.jcsr.2018.06.021.

Ingberg, S. 1916. Fire Tests of Building Columns. NFPA Quarterly, 253–260.

Jeanneret, C., Gales, J., Kotsovinos, P., and Rein, G. 2019. Acceptance Criteria for Unbonded Post-Tensioned Concrete Exposed to Travelling and Traditional Design Fires. Fire Tech., 1-24.

Jie, L., Hongbo, L., and Jiadi, L. 2017. Post-Fire Mechanical Properties of Galfan-Coated Steel Cables with Extruded Anchorages. J. Tianjin Uni., 50, 7-17. DOI: 10.11784/tdxbz201704074.

Kim, M. O., Kim, K. W., Yun, J. H., and Kim, M. K. 2020. Fire Risk Assessment of Cable Bridges for Installation of Firefighting Facilities. Fire Saf. J., 115(2020). DOI: 10.1016/j.firesaf.2020.103146.

Kodur, V., Gu, L., and Garlock, M. E. M. 2010. Review and Assessment of Fire Hazard in Bridges. Transp. Res. Rec., 2172(1), 23-29. DOI: 10.3141/2172-03.

Kodur, V., Aziz, E., and Dwaikat, M. 2012. Evaluating Fire Resistance of Steel Girders in Bridges. J. Bridge Eng., 18(7). 633-643. DOI: 10.1061/(ASCE)BE.1943-5592.0000412.

Kodur, V. K., Aziz, E. M., and Naser, M. Z. 2017. Strategies for Enhancing Fire Performance of Steel Bridges. Eng. Struct., 131(15), 446-458. DOI: 10.1016/j.engstruct.2016.10.040.

Kotsovinos, P., Flint, G., Walker, G. and Lane, B. 2016a. Qualitative Assessment of the Fire Hazard Beneath Bridges. 14th Interflam. Egham, UK: Royal Holloway College. 4-6.

Kotsovinos, P., Walker, G., Flint, G., and Lane, B. 2016b. Assessing the Fires on the Deck of Cable Stayed Bridges. Structures in Fire, Princeton, United States, 9.

Kotsovinos, P., Judge, R., Walker, G., and Woodburn, P. 2020a. Fire Performance of Structural Cables: Current Understanding, Knowledge Gaps, and Proposed Research Agenda. J. Struct. Eng., 146(8). DOI: 10.1061/(ASCE)ST.1943-541X.0002703.

Kotsovinos, P., Atalioti, A., McSwiney, N., Lugaresi, F., Rein, G., and Sadowski, A. J. 2020b. Analysis of the Thermomechanical Response of Structural Cables Subject to Fire. Fire Tech., 56(2), 515-543. DOI: 10.1007/s10694-019-00889-7.

Kragh, E., Narasimhan, H., and Jensen, J. L. 2020. Fire Protection of Bridge Cables. Struct. Eng. Int., 1-4. DOI: 10.1080/10168664.2020.1716653.

Kukay, B., Todd, C., Jahn, T., Sannon, J., Dunlap, L., White, R., and Dietenberger, M. 2016. Evaluating Fire-Damaged Components of Historic Covered Bridges. USDA Forest Service, Forest Products Laboratory, General Technical Report, FPL-GTR-243, 243, 1-40.

LaMalva, K., Bisby, L., Gales, J., Gernay, T., Hantouche, E., Jones, C., Morovat, A., Solomon, R. and Torero, J. 2020. Rectification of "Restrained vs Unrestrained". Fire Mater., 44(3), 341-351.

Lange, D., and Boström, L. 2015. Round Robin on Calculations: Steel Beam with Standard Fire Exposure. SP Technical Research Institute of Sweden.

Lange, D., and Boström, L. 2017. A Round Robin Study on Modelling the Fire Resistance of a Loaded Steel Beam. Fire Saf. J., 92, 64-76. DOI: 10.1016/j.firesaf.2017.05.013.

Liu, Y. J., Ning, B., and Wang, Y. 2012. Study on Thermal and Structural Behaviour of a Cable-Stayed Bridge under Potential Tanker Truck Fires. App. Mech. Mater., 238(2012), 684-688. DOI: 10.4028/www.scientific.net/AMM.238.684

Liu, Y. S., and Lou, G. B. 2016. Safety Evaluation of a Large-Span Double-Deck Cable-Stayed Steel Bridge under Fire. Maint., Saf., Safety, Risk and Resil. of Bridges and Bridge Netw., 1(2-3), 4283-4293. DOI: 10.1002/cepa.487.

Lugaresi, F. 2017. Thermal Response of Structural Spiral Strands Subject to Fire. BEng Thesis, University of Edinburgh, UK

Ma, R., Cui, C., Ma, M., and Chen, A. 2019. Performance-Based Design of Bridge Structures under Vehicle-Induced Fire Accidents: Basic Framework and a Case Study. Eng. Struct., 197(2019). DOI: 10.1016/j.engstruct.2019.109390.

Main, J. A., and Luecke, W. E. 2010. Safety Assessment of Parallel Wire Suspension Bridge Cables under Thermal Effects. US Department of Commerce, National Institute of Standards and Technology.

Mamlouk, M.S. and Zaniewski, J.P., 2016. Materials for Civil and Construction Engineers. Pearson Education, Incorporated.

Morgado, T., J. R. Correia, A. Moreira, F. A. Branco, and C. Tiago. 2015. Experimental Study on the Fire Resistance of GFRP Pultruded Tubular Columns." Compos. Part B, 69, 201–211. DOI: 10.1016/j.compositesb.2014.10.005.

Morgado, T., N. Silvestre, and J. R. Correia. 2018a. Simulation of Fire Resistance Behaviour of Pultruded GFRP Beams—Part I: Models Description and Kinematic Issues. Compos. Struct., 187, 269–280. DOI: 10.1016/j.compstruct.2017.12.063.

Morgado, T., N. Silvestre, and J. R. Correia. 2018b. Simulation of Fire Resistance Behaviour of Pultruded GFRP Beams—Part II: Stress Analysis and Failure Criteria. Compos. Struct., 188, 519–530. DOI: 10.1016/j.compstruct.2017.12.064.

Mueller, K., Marjanishvili, S. and Quiel, S. 2016. Resilient Bridge Design Framework to Extreme Fire Loading. Structures in Fire, Princeton, US.A., 9, 751-758.

Nahid, M. N. 2015. Computational Study of Highway Bridges Structural Response Exposed to a Large Fire Exposure. Ph. D. Thesis, Virginia Tech.

Nahid, M. N., Sotelino, E. D., and Lattimer, B. Y. 2017. Thermo-Structural Response of Highway Bridge Structures with Tub Girders and Plate Girders. J. Bridge Eng., 22(10). DOI: 10.1061/(ASCE)BE.1943-5592.0001029.

Nariman, N. A. 2018. Thermal Fluid-Structure Interaction and Coupled Thermal-Stress Analysis in a Cable Stayed Bridge Exposed to Fire. Frontiers of Struct. and Civ. Eng., 12(4), 609-628. DOI: 10.1007/s11709-018-0452-z.

Naser, M. Z. and V. K. R. Kodur. 2015. A Probabilistic Assessment for Classification of Bridges Against Fire Hazard. Fire Saf. J., 76, 65-73. DOI: 10.1016/j.firesaf.2015.06.001.

Nelson, M., and A. Fam. 2013. Structural GFRP Permanent Forms with T-Shape Ribs for Bridge Decks Supported by Precast Concrete Girders." J. Bridge Eng., 18 (9), 813–826. DOI: 10.1061/(ASCE)BE.1943-5592.0000418.

Nelson, M., and A. Fam. 2014a. Full Bridge Testing at Scale Constructed with a Novel FRP Stay-in-Place Structural Forms for Concrete Deck. Constr. Build. Mater., 50, 368–376. DOI: 10.1016/j.conbuildmat.2013.09.056.

Nelson, M., and A. Fam. 2014b. Modeling of Flexural Behaviour and Punching Shear of Concrete Bridge Decks with FRP Stay-in-Place Forms using the Theory of Plates. J. Eng. Mech., 140 (12). DOI: 10.1061/(ASCE)EM.1943-7889.0000813.

NFPA. 2007. Guide for the Evaluation of Fire Risk Assessments. NFPA 551, National Fire Protection Association (NFPA), Quincy, United States.

NFPA. 2008. Vehicle Fire Trends and Patterns. National Fire Protection Association (NFPA), Quincy, United States.

NFPA. 2014. Standard for Road Tunnels, Bridges, and other Limited Highways. NFPA 502, National Fire Protection Association (NFPA), Quincy, United States.

Nicoletta, B., Smith, M., and Gales, J. 2018. Toward Fire Resilience in Canadian Bridge Infrastructure. CSCE Conference for Short and Medium Span Bridges, Quebec City, Canada.

Nicoletta, B., Woods, J., Gales, J., and Fam, A. 2019a Postfire Performance of GFRP Stay-in-Place Formwork for Concrete Bridge Decks. J. Compos. for Constr., 23(3), DOI: 10.1061/(ASCE)CC.1943-5614.0000941.

Nicoletta, B., P. Kotsovinos, and J. Gales. 2019b. Experimental Thermal Performance of Structural Steel Stay-Cables in Fire: Preliminary Progress. 15th Interflam. Egham, UK: Royal Holloway College.

Nicoletta, B., Kotsovinos, P., and Gales, J. 2020a. Review of the Fire Risk, Hazard, and Thermomechanical Response of Bridges in Fire. Can. J. Civ. Eng., 47(4), 363-381. DOI: 10.1139/cjce-2018-0767.

Nicoletta, B., Gales, J., Kotsovinos, P. 2020b. The York-Arup Cable Experiments: Implications for the Fire Design of Cable-Supported Bridges. IABSE 2020 Conference. New Zealand.

Nicoletta, B., Gales, J., Kotsovinos, P. 2020c. Experimental Fire Performance of Unloaded stay-cables for Bridge Infrastructure. IABSE 2020 Conference. New Zealand.

Noble, C. R., Wemhoff, A. P., and McMichael, L. D. 2008. Thermal-Structural Analysis of the MacArthur Maze Freeway Collapse. ASME 2008 Heat Transfer Summer Conference. American Society of Mechanical Engineers, 511-519.

Payá-Zaforteza, I., and Garlock, M. E. 2012. A Numerical Investigation on the Fire Response of a Steel Girder Bridge. J. Construct. Steel Res., 75(2012), 93-103. DOI: 10.1016/j.jcsr.2012.03.012.

Peris-Sayol, G., Paya-Zaforteza, I., Alos-Moya, J., and Hospitaler, A. 2015. Analysis of the Influence of Geometric, Modeling and Environmental Parameters on the Fire Response of Steel Bridges Subjected to Realistic Fire Scenarios. Comp. Struct., 158(2015), 333-345. DOI: 10.1016/j.compstruc.2015.06.003.

Peris-Sayol, G., Balasch-Parisi S, Paya-Zaforteza, I., and Alós-Moya, J. 2016. Analysis of the Factors that Influence the Maximum Adiabatic Temperatures in I-girder Bridges. Structures in Fire, Princeton, United States, 9, 743-750.

Peris-Sayol, G. and Payá-Zaforteza, I. 2017. Bridge Fires Database. Accessible at www.researchgate.net.

Peris-Sayol, G., Alós-Moya, J., Paya-Zaforteza, I., and Balasch-Parisi S. 2017. Detailed Analysis of the Causes of Bridge Fires and their Associated Damage Levels. J. Perform. Constr., Facil., 31(3). DOI: 10.1061/(ASCE)CF.1943-5509.0000977.

Pettersson, O., Magnussen, S.E. and Thor, J. 1976. Fire Engineering Design of Steel Structures, Swedish Institute of Steel Construction.

Platt DG, Elms DG, and Buchanan AH, 1994. A Probabilistic Model of Fire Spread with Time Effects. Fire Saf. J., 22 (4), 367-398. DOI: 10.1016/0379-7112(94)90041-8.

PTI DC45.1-12. 2012. Recommendations for Stay-Cable Design, Testing, and Installation. Post-Tensioning Institute, Farmington Hills

Quiel, S., Yokoyama, T., Bregman, L.S., Mueller, K., and Marjanishvili, S. 2015. A Streamlined Framework for Calculating the Response of Steel-Supported Bridges to Open-Air Tanker Truck Fires. Fire Saf. J., 73(2015), 63-75. DOI: 10.1016/j.firesaf.2015.03.004.

Quiel S., Zhu Z., Mueller K., Carlton A. and Marjanishvili, S. 2016. Performance-Based Prioritization of Fire Mitigation for Highway Bridges. Structures in Fire, Princeton, United States, 9, 776-783.

Quiquero, H., Smith, M. and Gales, J. 2018. Developing Fire Safety Engineering as a Practice in Canada. Canadian Journal of Civil Engineering, 45(7), pp.527-536.

Rackauskaite, E., Hamel, C. and Rein, G. 2016. Improved Travelling Fires Methodology - iTFM. Applications of Structural Fire Engineering.

Richardson, P., M. Nelson, and A. Fam. 2014. Fatigue Behaviour of Concrete Bridge Decks Cast on GFRP Stay-in-Place Structural Forms. J. Compos. Constr., 18 (3). DOI: 10.1061/(ASCE)CC.1943-5614.0000432.

Ridge, I., and R. Hobbs. 2012. The Behaviour of Cast Rope Sockets at Elevated Temperatures. J. Struct. Fire Eng. 3 (2): 155–168. DOI: 10.1260/2040-2317.3.2.155.

Robertson, L. and Gales, J. 2016. Post Fire Guidance for the Critical Temperature of Prestressing Steel. 14th Interflam. Egham, UK: Royal Holloway College. July 4-6, 2016.

Robinson, J. A., A. Brugger, and R. Betti. 2019. Experimental Study of High Temperature Performance of Steel Suspension Bridge Wires. IABSE Congress. Zürich, Switzerland.

Scheer, J. 2010. Failed Bridges: Case Studies, Causes and Consequences, John Wiley & Sons, USA.

Shokri, M. and Beyler, C.L. 1989. Radiation from Large Pool Fires. J. Fire Prot. Eng., 4(1), 141-150. DOI: 10.1177/104239158900100404.

Sjöström, J., Byström, A., Lange, D., and Wickström, U. 2012. Thermal Exposure to a Steel Column from Localized Fires. SP Technical Research Institute of Sweden.

Sloane, M. J. D. 2017. Fire Effects on Suspension Bridge Main Cables: Methods for Determining Both Temperature and Strain Distributions Within an Exposed Cable. Ph. D. Thesis, Columbia University.

Sloane, M. J. D., and Betti, R. 2019. Heat Transfer on a Disk: A Closed-Form Solution for Suspension Bridge's Main Cables Exposed to Fire. J Eng. Mech., 145(3), DOI: 10.1061/(ASCE)EM.1943-7889.0001573.

Smith, C.M. and Hoehler, M.S., 2018. Imaging Through Fire using Narrow-Spectrum Illumination. Fire Tech., 54(6), 1705-1723.

Smith, M., and Gales, J. 2017. Operational Resilience and Performance-Based Fire Design. CSCE Annual Conference 2017, Vancouver, British Columbia, Canada.

Smith, M., Gales, J. 2018a. Connection Behaviour in Contemporary Canadian Buildings Subjected to Real Fires. 12th International Performance-Based Codes and Fire Safety Design Methods Conference, Honolulu, Oahu. April 25-27, 2018.

Smith, M., Gales, J., and Frater, G. 2018b. Structural Fire Design in Canada Using Annex K. Canadian Society for Civil Engineering 2018 Conference, Fredericton, Canada. June 13-16, 2018.

Song, C., Zhang, G., Hou, W., and He, S. 2020. Performance of Prestressed Concrete Box Bridge Girders under Hydrocarbon Fire Exposure. Advances in Struct. Eng., 23(8), 1521-1533. DOI: 10.1177/1369433219898102.

Stern-Gottfried, J. and Rein, G. 2012. Travelling Fires for Structural Design-Part II: Design Methodology. Fire Saf. J., 54, 96-112.

Stoddard R. 2004. Inspection and Repair of a Fire Damaged Prestressed Girder Bridge. International Bridge Conference, Pittsburgh, United States.

Sun, G., Li, X., Xue, S., and Chen, R. 2019. Mechanical Properties of Galfan-Coated Steel Cables at Elevated Temperatures. J. Constr. Steel Res., 155(2019), 331-341. DOI: 10.1016/j.jcsr.2019.01.002.

Tolstrup, J., Giuliani, L., Narasimhan, H., Jensen, J. L., and Jomaas, G. 2019. Experimental Study of Epoxy Coatings for Fire Protection of Bridge Cables. ce/papers, 3(3-4), 653-658. DOI: 10.1002/cepa.1116.

Usmani, A. S., Rotter, J. M., Lamont, S., Sanad, A. M., and Gillie, M. 2001. Fundamental Principles of Structural Behaviour under Thermal Effects. Fire Saf. J., 36(8), 721– 744. DOI: 10.1016/S0379-7112(01)00037-6.

Verbruggen, S., S. De Sutter, S. Iliopoulos, D. G. Aggelis, and T. Tysmans. 2016. Experimental Structural Analysis of Hybrid Composite-Concrete Beams by Digital Image Correlation (DIC) and Acoustic Emission (AE). J. Nondestr. Eval., 35 (1), 1–10. DOI: 10.1007/s10921-015-0321-9.

Wan, R., Sun, F., Zhang, L., and Shan, A. 2012. Effects of Mo on High-Temperature Strength of Fire-Resistant Steel. Mat. Des., 35, 335-341. DOI: 10.1016/j.matdes.2011.09.009.

Wang, Y., and Liu, M. 2016. Buckling Instability Behaviour of Steel Bridge under Fire Hazard. Math. Probl. in Eng. DOI: 10.1155/2016/8024043

Wardhana, K., Hadipriono, F. 2003. Study of Recent Building Failures in the United States. J. Perform. Constr. Facil., 17(3), 151-158. DOI: 10.1061/(ASCE)0887-3828(2003)17:3(151).

Whitney, R., Braxton, N. L., and Alsayed, H. 2018. Recommendations for Improving Fire Performance of Steel Bridge Girders. Structures Congress. Fort Worth, Texas.

Woodworks. 2019. Ontario Wood Bridge Reference Guide. Canadian Wood Council.

Woodworth, M.A., 2013. Fire Hazard Assessment for Highway Bridges with Thermal Mechanical Modeling. Ph. D. Thesis, Virginia Tech.

Woodworth, M., Hansen, E., McArthur, C., and Abboud, N. 2015. Protection of Cable-Stay Bridges from Accidental and Man-Made Fire Hazards: A Rational Physics-Based Approach to Analysing Vulnerabilities and Mitigations. Structures Congress, Portland, United States, 24-37.

Wright, W., Lattimer, B., Woodworth, M., Nahid, M., and Sotelino, E. 2013. Highway Bridge Fire Hazard Assessment Draft Final Report. Virginia Polytechnic Institute and State University, Blacksburg, VA.

Xiang, K., Wang, G. H., & Liu, H. X. 2013. Damage Assessment of One Prestressed Concrete Bridge after Fire. Appl. Mech. and Mater., 256-259, 2729-2734. DOI: 10.4028/www.scientific.net/AMM.256-259.2729.

Yanagisawa, N., Imagawa, Y., Ohyama, O., Rutner, M., and Kurita, A. 2017. Fire Safety of Bridges–Methodology Supporting Design and Forensic Evaluation. Steel Constr., 10(1), 2-9. DOI: 10.1002/stco.201710002.

Yanes-Armas, S., J. de Castro, and T. Keller. 2016. System Transverse In-Plane Shear Stiffness of Pultruded GFRP Bridge Decks. Eng. Struct., (107), 34–46. DOI: 10.1016/j.engstruct.2015.11.003.

Yanes-Armas, S., J. de Castro, and T. Keller. 2017. Rotational Stiffness of Web-Flange Junctions of Pultruded GFRP Decks. Eng. Struct, 140, 373–389. DOI: 10.1016/j.engstruct.2017.03.003.

Zhang, G., He, S. H., Guo, H. J., and Hou, W. 2012. Deflection for Pre-Stressing Concrete Thin-Wall Box Girders Bridge under Action of Multi-Span Loads Exposed to Fire. Appl. Mech. and Mater., 205, 2188-2191. DOI: 10.4028/www.scientific.net/AMM.204-208.2188.

Zhang, G., Kodur, V., Xie, J., He, S., and Hou, W. 2017. Behaviour of Prestressed Concrete Box Bridge Girders under Hydrocarbon Fire Condition. Procedia Eng., 210(2017), 449-455. DOI: 10.1016/j.proeng.2017.11.100.

Zhang, G., Kodur, V., Yao, W., and Huang, Q. 2019. Behaviour of Composite Box Bridge Girders under Localized Fire Exposure Conditions. Struct. Eng. and Mech., 69(2), 193-204. DOI: 10.12989/sem.2019.69.2.193.

Zhang, G., Kodur, V., Song, C., He, S., and Huang, Q. 2020a. A Numerical Model for Evaluating Fire Performance of Composite Box Bridge Girders. J. Constr. Steel Res., 165(2020). DOI: 10.1016/j.jcsr.2019.105823.

Zhang, Y., Fang, Z., Jiang, R., Xiang, Y., Long, H., and Lu, J. 2020b. Static Performance of a Long-Span Concrete Cable-Stayed Bridge Subjected to Multiple-Cable Loss during Construction. J. Bridge Eng., 25(3). DOI: 10.1061/(ASCE)BE.1943-5592.0001529.

Zobel, H., Karwowski, W., Wróbel, M., and Mossakowski, P. 2016. Łazienkowski Bridge Fire in Warsaw–Structural Damage and Restoration Method. Archives of Civ. Eng., 62(4), 171-186. DOI: 10.1515/ace-2015-0104.